THE HONG KONG
POLYTECHNIC UNIVERSITY
香港理工大學
Pao Yue-kong Library
包玉剛圖書館

Copyright Undertaking

This thesis is protected by copyright, with all rights reserved.

By reading and using the thesis, the reader understands and agrees to the following terms:

1. The reader will abide by the rules and legal ordinances governing copyright regarding the use of the thesis.
2. The reader will use the thesis for the purpose of research or private study only and not for distribution or further reproduction or any other purpose.
3. The reader agrees to indemnify and hold the University harmless from and against any loss, damage, cost, liability or expenses arising from copyright infringement or unauthorized usage.

If you have reasons to believe that any materials in this thesis are deemed not suitable to be distributed in this form, or a copyright owner having difficulty with the material being included in our database, please contact lbsys@polyu.edu.hk providing details. The Library will look into your claim and consider taking remedial action upon receipt of the written requests.

Pao Yue-kong Library, The Hong Kong Polytechnic University, Hung Hom, Kowloon, Hong Kong

http://www.lib.polyu.edu.hk

The Hong Kong Polytechnic University

Department of Health Technology and Informatics

Ultrasonic Characterization of Transient and Inhomogeneous Swelling Behavior and Progressive Degeneration of Articular Cartilage

by

WANG QING

A thesis submitted in partial fulfillment of the requirements for the Degree of Doctor of Philosophy

December 2006

Pao Yue-kong Library
PolyU • Hong Kong

CERTIFICATE OF ORIGINALITY

I hereby declare that this thesis is my own work and that, to the best of my knowledge and belief, it reproduces no material previously published or written, nor material that has been accepted for the award of any other degree or diploma, except where due acknowledgement has been made in the text.

_____ (Signed)

Wang Qing (Name of student)

Abstract of thesis titled

"Ultrasonic Characterization of Transient and Inhomogeneous Swelling Behavior and Progressive Degeneration of Articular Cartilage"

Submitted by WANG QING
for the Degree of Doctor of Philosophy
at The Hong Kong Polytechnic University
in December 2006

Articular cartilage is the soft connective tissue that covers the bony ends in diarthrodial joints providing good distribution of the load on the bone and good lubrication for joint movement. However, many factors may result in the degeneration of articular cartilage and then lead to osteoarthritis (OA). Swelling is an electrochemical mechanical property of articular cartilage and plays an important role in weight bearing and joint lubrication. The overall aim of this study is to use high-frequency ultrasound to characterize the transient and inhomogeneous swelling properties and progressive degeneration of articular cartilage *in situ*.

In this study, an ultrasound swelling measurement system (USMS) was developed. 95 full-thickness cartilage-bone specimens were prepared from fresh mature bovine patellae for different tests. The osmotic free shrinkage and swelling behavior was induced by changing the concentration of bathing saline solution from 0.15 M to 2 M and then back to 0.15 M. The hydration behavior in 0.15 M saline was monitored by the USMS after the specimen was dehydrated in the air for 45 minutes. The progressive degeneration of articular cartilage was induced by trypsin digestion. Swelling tests,

histological assessments and acoustic measurements were performed for both normal and trypsin-digested cartilage specimens. Moreover, the aggregate moduli at different layers were extracted from the swelling strains detected by the USMS using a newly-developed bi-layered triphasic model.

A good repeatability of the present ultrasonic measurement for the shrinkage-swelling behavior was obtained (n = 10, ICC > 0.8, CV% < 10%). The USMS successfully detected the progressive penetration of trypsin through the cartilage tissue. The digestion speed slowed down from the initial rate of 0.62 ± 0.16 μm/s to 0.04 ± 0.02 μm/s when the digestion front reaching the deep region (approximately 70% of the full thickness).

It was demonstrated that the cartilage specimens might experience an "overshoot-relaxation" behavior during the swelling-shrinkage test. The absolute peak shrinkage strain (0.010 ± 0.005, n = 50) was significantly ($p < 0.001$) larger than the peak swelling strain (0.003 ± 0.003). The non-uniformity of the swelling strains at different depths was observed. The degenerated cartilage specimens (n = 30) showed weaker shrinkage, swelling and hydration behaviors.

Using the triphasic model, it was demonstrated that the region near the bone, for the normal specimens, had a significantly higher aggregate modulus (Ha_1 = 18.5 ± 15.5 MPa, $p < 0.001$) in comparison with the middle zone and the surface layer (Ha_2 = 7.6 ± 11.6 MPa and Ha_3 = 3.6 ± 3.3 MPa, respectively). The predicted normalized thickness of the deep layer h_1 was 0.67 ± 0.22. For the specimens with 30-minute trypsin

digestion, the values decreased to Ha_1 = 11.1 ± 10.1 MPa, Ha_2 = 6.7 ± 16.9 MPa, Ha_3 = 1.9 ± 2.8 MPa, h_1 = 0.55 ± 0.24.

It was found that the acoustic parameters of the degenerated specimens had insignificant changes in comparison with the normal specimens. Moreover, the correlations among swelling, acoustic and biochemical parameters were obtained.

In summary, the USMS proposed in this study has been successfully used to measure the transient and inhomogeneous swelling behavior and to track the trypsin penetration, which simulated the progressive degeneration of the OA-like articular cartilage *in situ*.

Keywords: Ultrasound, Articular cartilage, Proteoglycans, Osmotic shrinkage-swelling, Dehydration-hydration, Triphasic modeling, Trypsin-digestion, Osteoarthritis, Ultrasound tissue characterization, Depth-dependence, Swelling strain, Aggregate modulus.

PUBLICATIONS ARISING FROM THE THESIS

Journal Papers

1. Niu HJ, **Wang Q**, Zheng YP. 2007. Extraction of modules of articular cartilage using four-parameter triphasic model and transient ultrasound method. *Chinese Science Bulletin*. 52(1): 41-46.

2. **Wang Q**, Zheng YP. 2006. Non-contact evaluation of osmosis-induced shrinkage and swelling behavior of articular cartilage *in situ* using high-frequency ultrasound. *Instrumentation Science and Technology*. 34: 317-334.

3. **Wang Q**, Zheng YP. 2006. Quantitative analysis of shrinkage and swelling behavior of articular cartilage using high-frequency ultrasound. *Chinese Journal of Biomedical Engineering*. 25(5): 571-579.

4. **Wang Q**, Zheng YP, Niu HJ, Mak AFT. 2007. Extraction of mechanical properties of articular cartilage from osmotic swelling behavior monitored using high-frequency ultrasound. *Journal of Biomechanical Engineering*. 129(3): 413-422.

5. Zheng YP, Patil S, **Wang Q**. 2006. Ultrasound speed in articular cartilage under different bathing saline concentration. *Key Engineering Materials*. 321-323: 972-977.

6. Zheng YP, Lu MH, **Wang Q**. 2006. Ultrasound elastomicroscopy using water jet and osmosis loading: Potentials for assessment for articular cartilage. *Ultrasonics*. 44(Supplement 1): e203-e209.

7. **Wang Q**, Zheng YP, Qin L, Mak AFT. 2006. Ultrasonic measurement of dimension-dependence of swelling behavior of bovine articular cartilage. *Biorheology*. (Submitted).

8. **Wang Q**, Zheng YP, Huang QH, Leung G, Lam WL, Guo X, Lu HB, Qin L. Ultrasonic assessment of progressive proteoglycan depletion of articular cartilage. *Ultrasound in Medicine and Biology*. (Submitted).

9. **Wang Q**, Zheng YP, Huang QH, Leung G, Lam WL, Guo X, Lu HB, Qin L, Mak AFT. Altered osmotic swelling behavior of proteoglycan-depleted bovine cartilage using high frequency ultrasound. *Physics in Medicine and Biology*. (Submitted).

10. **Wang Q**, Zheng YP. Dehydration-induced hydration behavior of normal and degenerated articular cartilage *in situ* monitored using high-frequency ultrasound. *Biorheology*. (To be submitted).

11. **Wang Q**, Zheng YP, Niu HJ. Changes in mechanical properties of trypsin-digested articular cartilage extracted from osmotic swelling behavior monitored using high-frequency ultrasound. *Journal of Biomechanics*. (To be submitted).

Book Chapters

1. **Wang Q**, Zheng YP. Ultrasound measurement of swelling behaviors of articular cartilage *in situ*. (Accepted by BIOMECHANICS SYSTEMS. WORLD SCIENTIFIC PUBLISHERS multi-volume International MRW (Major Reference Work)).

2. Zheng YP, **Wang Q**. Ultrasonic characterization of dynamic depth-dependent biomechanical properties of articular cartilage. (Accepted by Advanced Bioimaging Technologies in Assessment of Quality of Bone and Scaffold Materials – Techniques and Applications of nanoCT and microCT, pQCT/QCT and MRI and their Applications-).

Conference Proceedings

1. Ling HY, **Wang Q**, Zheng YP, Lau KT. A fibre bragg grating temperature sensor for monitoring saline solution temperature *in situ* during ultrasonic measurement of shrinking-swelling behaviour of articular cartilage. *Proceedings of Biomedical Engineering Conference on Biomedical Engineering in Education, Research and Industry*, Hong Kong, China. September 21-23, 2006, pp10-14.

2. Niu HJ, **Wang Q**, Zheng YP. Extraction of modulus from the osmotic swelling of articular cartilage measured using ultrasound. *3rd International Conference on the Ultrasonic Measurement and Imaging of Tissue Elasticity*, Lake Windermere, Cumbria, UK. October 17-20, 2004. pp115.

3. **Wang Q**, Zheng YP. Ultrasonic measurement of dimension-dependence of swelling behavior of bovine articular cartilage. *5th World Congress of Biomechnics*, Munich, German. July 29-August 4, 2006.

4. **Wang Q**, Zheng YP. Ultrasonic characterization of dynamic depth-dependent biomechanical properties of articular cartilage. *Proceedings of 2005 International Symposium on Quality of Bone and Scaffold Biomaterials Evaluated by microCT, pQCT and MRI*. Hong Kong, China. October 17-18, 2005. pp31.

5. **Wang Q**, Zheng YP. Evaluation of osmosis-induced deformation of articular cartilage using ultrasound biomicroscopy imaging. *Proceedings of ISB XXth Congress - ASB 29th Annual Meeting*, Cleveland, Ohio, USA. July 31 – August 5, 2005. pp440.

6. **Wang Q**, Zheng YP. Osmotic-induced shrinkage and swelling behaviors of normal bovine patellar articular cartilage *in situ* monitored by ultrasound. *3rd International Conference on the Ultrasonic Measurement and Imaging of Tissue Elasticity*, Lake Windermere, Cumbria, UK. October 17-20, 2004. pp116.

7. **Wang Q**, Zheng YP. *In situ* ultrasound measurement of the transient free swelling behavior of articular cartilage. *2nd World Conference for Chinese Biomedical Engineers*, Beijing, China. September 27-29, 2004.

8. **Wang Q**, Zheng YP. Study on transient osmotic-induced hydration of articular cartilage by high-frequency ultrasound. *Proceedings of Biomedical Engineering Conference on Integrating Science and Technology in the Healthcare Industry*, Hong Kong, China. September 23-25, 2004, pp135-140.

9. Zheng YP, Lu MH, **Wang Q**. Noncontact Ultrasound Elastomicroscopy. *World Congress on Ultrasonics merged with Ultrasonics International, WCU/UI'05,* Beijing, China. August 28 – September 1, 2005. pp11.

10. Zheng YP, **Wang Q**, Lu MH, Patil S, Choi APC, Cheung J. Ultrasound characterization of articular cartilage. *1st International Conference on Advanced Nondestructive Evaluation*. Jeju, Korea. Nov 6 – 9, 2005.

ACADEMIC AWARDS

2004	1st Runner-up in Best Student Papers Competition at Biomedical Engineering Conference on Integrating Science and Technology in the Healthcare Industry, Hong Kong, China. 2004

ACKNOWLEDGEMENTS

This study was carried out in the Department of Health Technology and Informatics (earlier named Jockey Club Rehabilitation Engineering Centre), The Hong Kong Polytechnic University during 2003-2006. I would like to express my sincere thanks to people who helped and encouraged me. Without their supports, this thesis would never have come out.

First of all, my deepest and most sincere thanks to my supervisor, Dr. Yong-Ping Zheng. I am very grateful for the opportunity given to me to study under his professional and dynamic guidance. His insight, care and encouragement were extremely helpful throughout the project. He was always available to discuss questions and share his knowledge and expertise. His valuable comments and enthusiasm on the study had been important for me to complete this study. I also wish to express my sincere thanks to my co-supervisor, Prof. Arthur F.T. Mak, for his supports in my study concerning the use of Biomaterials Laboratory and sharing his immense knowledge of electrochemomechanics of articular cartilage.

I would like to thank Prof. Daniel Chow and Dr. Raymond Tong for assessing my confirmation report and providing valuable comments and suggestions to my study. I also want to address my gratitude to Prof. Ling Qin, Dr. Hong-Bin Lu and Ms. Xiao-Hong Yang of the Department of Orthopaedics and Traumatology, the Chinese University of Hong Kong, and Dr. Xia Guo, Ms. Trish Lam and Ms. Xiao-Yun Wang of the Department of Rehabilitation Sciences for their kind help and guidance in enzyme digestion and histological analysis. I owe my deep thanks especially to Dr. Gina Leung

and Ms. Brenda Cheung for sharing their knowledge and expertise in histological theory and practice and the use of Biomedical Science Laboratory. I also wish to thank Dr. Mo Yang, Mr. Jin-Jiang Yu and Mr. Brain Pow for the use of the microscopy system. I would like to issue my thanks to Mr. Kung-Chee Chen and Mr. Chi-Fai Tin for the use of the devices in the workshop for specimen preparation in my study.

I would also like to acknowledge all my fellow students and colleagues who had contributed in my research study. Sincere thanks are given to Mr. Qing-Hua Huang, Ms. Tracy Lu, Dr. Hai-Jun Niu, Mr. Yan-Ping Huang, Mr. James Cheung, Dr. Jun Shi, Mr. Sushil Patil, Dr. Xin Chen, Dr. Yong-Jin Zhou, Dr. Carrie Ling, Mr. Jun-Feng He, Mr. Cong-Zhi Wang, and Mr. Pong-Chi Choi for their invaluable cooperation and support in software development and specimen preparation, as well as their friendly attitude and sincere encouragement. Special thanks are given to Ms. Sally Ding for her valuable help in editing my research reports and thesis.

I am deeply thankful to my parents who have been a great source of support and encouragement throughout my life. This thesis is specially consecrated to my mother, who always cared for my study but passed away in the second year of my study. My brother, sister and boy friend deserve my sincere thanks as well for their kind care and support during the last three years.

Finally, the Research Grant Council of Hong Kong (PolyU5199/02E, PolyU 5245/03E) and The Hong Kong Polytechnic University are gratefully acknowledged to support this project.

TABLE OF CONTENTS

LIST OF ABBREVIATIONS & SYMBOLS

3D	Three-dimensional
A/D	Analog-to-digital
AIB	Apparent integrated backscatter
CV	Coefficient of variation
BUA	Broadband ultrasonic attenuation
DMMB	Dimethyl-methylene blue
EDTA	Ethylenediamine-tetra-acetic acid
FCD	Fixed charge density
FFT	Fast fourier transform
GAG	Glycosaminoglycan
IA	Integrated attenuation
IBS	Integrated backscatter coefficient
ICC	Intraclass correlation coefficient
IRC	Integrated reflection coefficient
LL	Lateral lower
LSE	Least square error
LU	Lateral upper
ML	Medial lower
MU	Medial upper
OA	Osteoarthritis
OCT	Optical coherence tomography
PG	Proteoglycan
PVDF	Polyvinylidene fluoride
RF	Radio frequency
ROI	Region of interest
rRMSD	Relative root mean square difference
UBM	Ultrasound biomicroscopy
UMME	Ultrasound measurement of motion and elasticity
USMS	Ultrasound swelling measurement system
ϕ	Diameter or width of specimen

l	Length of specimen
E	Young's modulus
ε	Strain
Ha	Aggregate modulus
p	Fluid pressure
π	Donnan osmotic pressure
c^F	Fixed charge density
c^*	Eelectrolyte concentration of external bathing solution
c_0^F	Reference fixed charge density
ϕ_0^w	Reference water volume fraction
κ	Permeability
ν	Poisson's ratio
R^2	Correlation coefficient
h	Thickness of cartilage
β	Attenuation slope
f_c	Centroid frequency
c_s	Ultrasound speed in saline solution

LIST OF FIGURES

LIST OF TABLES

CHAPTER 1 INTRODUCTION

1.1 Research Background and Significance

1.1.1 Knee joint and articular cartilage

The knee is one of the major weight bearing joints of the body. It consists of two articulating joints, i.e. the tibio-femoral joint and the patello-femoral gliding joint, which are associated with femur, tibia and patella (Fig. 1.1). The large round ends of the femur, the flat top of the tibia, and the posterior surface of the patella are covered by articular cartilage.

The patella is the largest sesamoid bone in the body. The primary functional role of the patella is knee extension. The proximal patella bears the tensile forces transferred from quadriceps muscles. The anterior patella bears both tension and compressive forces.

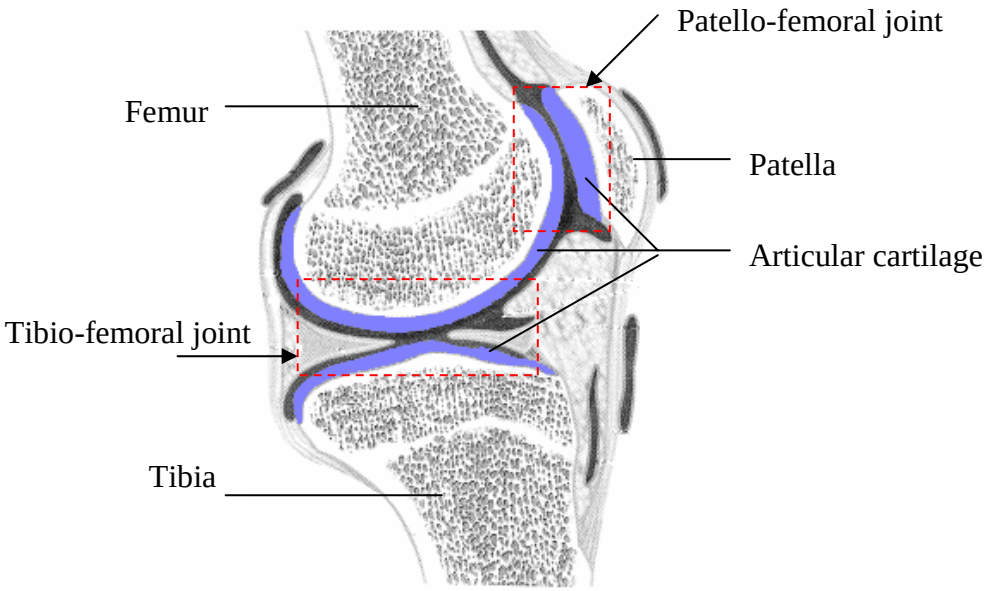

Fig. 1.1 Diagram of a midsagittal section of the knee joint (Saladin, 2005).

There are three broad classes of cartilaginous tissues in the body: hyaline cartilage, fibro-cartilage, and elastic cartilage (Mow et al., 2005). Articular cartilage is the most common hyaline cartilage and mainly consists of the organic composite proteoglycan-collagen matrix and water content. Functionally, articular cartilage provides joints with excellent lubrication and wearing characteristics, and maintains a smooth efficient force-bearing system for the body. Normal or healthy cartilage looks white, has a smooth surface and has an ability to withstand the large load. When there is an external load on the joint, articular cartilage deforms (or behaves the variations in dimension and hydration) to respond to the tensile, shear, and compressive stresses.

Articular cartilage has been found to be a multi-phasic hydrated mixture mainly composed of proteoglycan (PG) (5–10%), collagen (10–20%), and water (60–80%) (Mow et al., 2005). According to its structure, articular cartilage can be roughly separated into three zones: superficial, middle and deep, occupying approximately 10-20%, 40-60%, and 30% of the total tissue thickness, respectively (Fig. 1.2). It has been found that in the superficial part, collagen fibrils orientate tangentially to the surface, randomly in the middle zone, and perpendicularly to the cartilage-bone interface in the deep layer (Fig. 1.2c) (Mow et al., 2005). In addition, the changes in the cellular shape correspond to the orientation of collagen fibres. Cells are in an elliptic shape in the surface zone while the long axis is parallel to the surface. With depth increasing, chondrocytes tend to be round. In the deep zone, chondrocytes arrange together in lines perpendicular to the cartilage-bone interface (Fig. 1.2a).

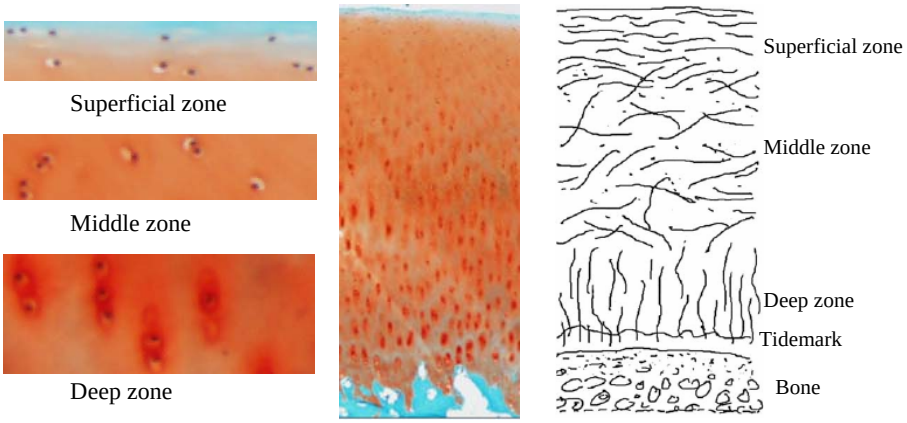

Fig. 1.2 (a-b) Histology of normal articular cartilage stained with safranin O and fast green; (a) The enlarged images at different layers of (b); (c) Schematic of the layered structure of articular cartilage (Mow et al., 2005).

Moreover, it has been discovered that the inhomogeneous distributions of cartilage components are depth-dependent (Mow and Guo, 2002). The collagen content is highest in the superficial zone and lower in the middle and deep zone. The fibrils at the surface zone play a structurally important role in limiting the swelling behavior of cartilage (Setton et al., 1998). The PGs composed of a core protein bonded with glycosaminoglycan (GAG) chains, enmesh in collagen network. They are highly distributed in the middle layer. Collagen network and PGs construct the solid matrix of articular cartilage. The interactions between these macromolecules significantly contribute to the complex mechanism of articular cartilage. The amount and the spatial distribution of the interstitial water in the cartilage layer depend largely on the following three factors: the PG concentration and the correspondingly induced swelling pressure, the orientation of collagen network, and the biomechanical properties of the matrix (Mow et al., 2005). Therefore, its distribution is also non-uniform along the depth direction (Mow and Guo, 2002; Shapiro et al., 2001; Torzilli et al., 1990). The

interstitial water makes the collagen-PG matrix swollen and being a strong solid matrix (Mankin et al., 2000). Since water can diffuse freely between the tissue and the bathing solution, exudation and imbibition of the interstitial fluid (i.e. shrinkage and swelling of cartilage) play an important role while the load is applied on and removed from the tissue (Lai et al., 1991; Maroudas, 1976a). Because articular cartilage has no blood vessels, the fluid component also provides a transition path for nutrients and waste products (Mow and Hung, 2001). The degree of hydration of articular cartilage becomes an index of the balance between the total swelling pressure and the strong tensile force within collagen network (Mankin et al., 2000; Maroudas, 1976a). The increasing water content causes an increase in the permeability and a decrease in the strength and stiffness of the matrix. More detailed review on articular cartilage will be introduced in Chapter 2.

1.1.2 Swelling behavior of articular cartilage

Swelling, an electrochemical mechanical coupling phenomenon of articular cartilage, arises from the interactions between the fixed negative charges on the PGs and the mobile ions (Lai et al., 1991; Maroudas, 1976a). Mainly, two force resources give rise to the swelling pressure within cartilage (Lai et al., 1991; Mow et al., 2005). One is the ion imbalance which creates a substantial pressure in the interstitium higher than the ambient pressure in the bathing solution. This part of swelling pressure is known as the Donnan osmotic pressure. The other is the charge-to-charge repulse force known as the chemical-expansion pressure. This pre-swollen state under biological conditions (Setton et al., 1998; Wang et al., 2002) plays a significant role in the biomechanical behavior of articular cartilage (Maroudas, 1976a; Narmoneva et al., 1999) and protects joints from

heavy loading (Mankin et al., 2000). With the increasing concentration of the external bathing solution, the difference between the internal and external ion concentration decreases and thus the overall swelling pressure is reduced (Lai et al., 1991; Maroudas, 1979). Therefore, the tissue merged in the hypertonic solution (2 M saline) is regarded as the reference configuration of zero swelling pressure (Eisenberg and Grodzinsky, 1985; Narmoneva et al., 1999).

In the physiological condition, normal cartilage does not show any swelling behavior due to the balance between the collagen tension and the swelling pressure (Eisenberg and Grodzinsky, 1985; Lai et al., 1991; Maroudas, 1976a; Maroudas et al., 1986). Therefore, swelling of cartilage is sensitive to the damage of collagen fibrils (Setton et al., 1994; Zhu et al., 1993). The changes in the swelling behavior of articular cartilage reflect the changes in the proteoglycan concentration, fixed charge density (FCD), water volume fraction, and the intrinsic mechanical properties of the cartilage solid matrix (Eisenberg and Grodzinsky, 1985, 1987; Flahiff et al., 2002; Lai et al., 1991; Maroudas, 1976a; Mow and Guo, 2002; Narmoneva et al., 1999). The triphasic model regarded as an electrochemomechanical swelling theory provides a more accurate description of the tissue composition and the thermodynamic foundation and the potential complex mechanical chemical electrokinetic mechanism for cartilage swelling, deformation, and viscoelasticity (Lai et al., 1991).

1.1.3 Degeneration of articular cartilage and osteoarthritis

Proper functions of articular cartilage, however, can be only maintained when the tissue retains its normal structure and composition. Factors such as aging, wear and tear,

excessive weight-bearing stress, a sudden knee injury, and genetic factors affecting collagen and PG formation may give rise to cartilage degeneration. Untreated injuries will lead to further degeneration, and even result in osteoarthritis (OA). Since OA is induced by cartilage damage, not by inflammation, OA is generally regarded as "wear-and-tear arthritis" different from rheumarthritis.

"*Osteoarthritis is a group of overlapping distinct diseases, which may have different etiologies but with similar biologic, morphologic, and clinical outcomes. The disease processes not only affect the articular cartilage, but involve the entire joint, including the subchondral bone, ligaments, capsule, synovial membrane, and periarticular muscles…*"

The above determination of OA (Flores and Hochberg, 2003) demonstrates that OA is a symptom-complex musculoskeletal disease. It is noted that the degeneration of articular cartilage occurs in the early stage of OA and is a base for the further damage of other components in the joint. Clinically, a longtime knee pain, limitation in joint movement and age (> 38) are selected as diagnosis criteria (Flores and Hochberg, 2003). However, the late-stage damages including cartilage depletion (Fig. 1.3), bone exposition, knee pain and joint immobility cannot be reconverted. The severe OA increasingly costs a huge amount of financial expense and affects the life quality of people. OA has been regarded worldwide as one of the most common forms of musculoskeletal disease, which ranks fourth and eighth in health problems for female and male (Murray and Lopez, 1996). Nonpharmacological treatment and drug therapy cost high, e.g. the most cost-effective hip or knee replacement operation will be a cost per DALY (disability-adjusted life year) of more than US$4800 (Brooks, 2003). A recent research indicated that osteoarthritis cost $989 annually and ranked second in 1-year disease-specific costs

(Fenter et al., 2006). Although many researchers have made plenty of efforts, the definitive resolution still awaits further research. Therefore, it is quite important to find an assessment method of early OA.

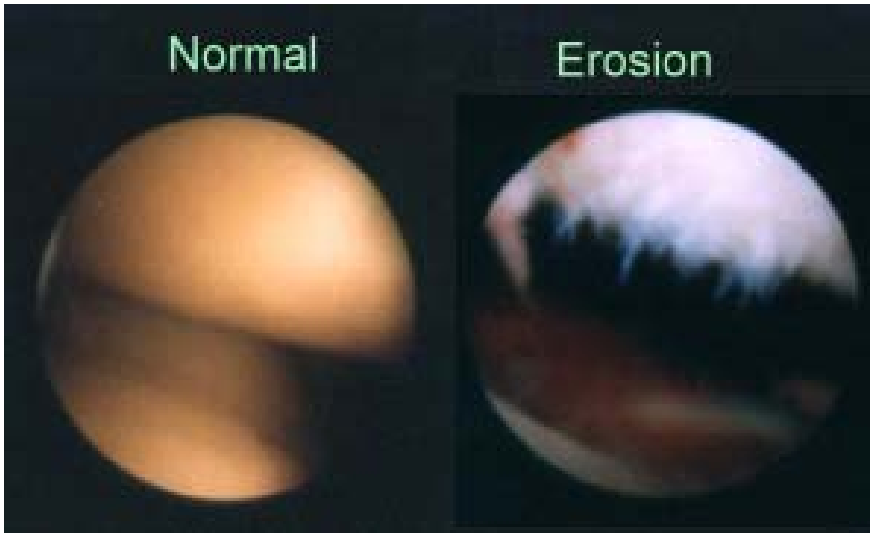

Fig. 1.3 Arthroscopic view of normal and damaged articular cartilage (www.pt.ntu.edu.tw).

There are many previous studies putting efforts on the investigations on the cartilage degeneration to avoid the severe OA and to save the huge amount of financial expenses. The increase of tissue hydration, the loss of PGs, and the damage of collagen fibrils are indicated to be the earliest signs of cartilage degeneration during OA (Armstrong and Mow, 1982; Martini, 2004; Torzilli et al., 1990). The PGs of the OA tissue tend to be much less aggregated and more easily extracted, and the collagens tend to be disorganized (Mow and Hung, 2001). The quantification of these swelling effects on articular cartilage can be used to characterize the degenerative changes associated with OA in early studies using water-gain weighting (Maroudas, 1976a) and optical

microscopy method (Narmoneva et al., 1999), and recent studies using MRI (Calvo et al., 2004) and finite element modeling (Wilson et al., 2004).

1.1.4 Significance of the study

First of all, various types of ultrasonic information including A-mode signals, M-mode images, and B-mode biomicroscopic images could be provided using the focused high-frequency ultrasound to monitor the transient inhomogeneous swelling behavior and progressive degeneration of articular cartilage *in situ*. Secondly, the ultrasonic transient deformation mapping could probe what happens inside the cartilage tissue during swelling in a real-time non-contact and non-destructive way. Thirdly, the proposed transient ultrasonic monitoring of enzyme digestion provided a method for the dynamic quantification of tissue degeneration. Furthermore, the study analyzed not only the swelling behavior of articular cartilage but also the acoustic parameters such as reflection coefficient, frequency spectrum and attenuation and thus provided more comprehensive information for cartilage assessment. Finally, the results of this study could be a foundation for further research on articular cartilage and the studies of other biological tissues, as well as biomaterials of which the transient and inhomogeneous properties are concerned.

1.2 Objectives of the Study

Many methods including water-weighting, optical, mechanical, and MRI and their combined approaches have been employed to investigate the swelling behavior of articular cartilage in the literatures. However, these methods have their own limitations

in quantification of swelling behavior of articular cartilage, which will be discussed in details in Chapter 2.

The primary objective of this study is to develop an ultrasound swelling measurement system (USMS) to explore the transient inhomogeneous swelling of articular cartilage *in situ*. This system can provide a non-contact, non-destructive method to real-time display A-mode ultrasound signals, M-mode images and B-Mode biomicroscopic images. It is expected that this ultrasound system can provide reliable quantitative information of the osmosis-induced swelling behavior of articular cartilage, including the swelling strain, shrinkage strain, hydration strain, as well as the acoustic coefficients of ultrasound attenuation, backscatter, and reflection, etc.

The second objective is to provide a novel method to monitor and evaluate the progressive degeneration of articular cartilage during the trypsin digestion. In this study, the experimental OA was induced via enzyme digestion and the ultrasound system was used to detect the progressive degeneration and swelling behavior of the degenerated cartilage. The parametric analysis was performed in comparison with that of the normal samples.

The third objective of this study is to establish an improved layered triphasic model to extract the aggregate modulus (*Ha*) and the free swelling strain pattern of full-thickness cartilage based on the ultrasound-measured data.

1.3 Outline of the Dissertation

Following the introduction chapter, Chapter 2 begins with a review of previous studies on the relationship between the mechanical properties and the complex compositions and structure of articular cartilage. The origin and contribution of swelling behavior of articular cartilage is then introduced and followed by a detailed review of the various methods of measuring the mechanical, acoustic, swelling or combined properties of articular cartilage. The effects of OA on the mechano-acoustic properties and swelling behavior of articular cartilage are reviewed in this chapter.

In Chapter 3, the methodology of this study is systematically introduced. Following specimen preparation, the 3D USMS set-up for the experiments is presented. Feasibility studies were performed to prove the reliability and validity of this novel approach in the measurement of swelling behavior of articular cartilage. Then, the experimental protocols for the ultrasonic characterizations of the transient and inhomogeneous swelling behavior of articular cartilage are described in details. Experimental OA model was induced by enzyme digestion in this study. The real-time dynamic degeneration progress was monitored using the USMS. Microscopic, histological, biochemical and acoustic analyses for both the normal and degenerated samples were performed. The theoretical bi-layered triphasic model was built up. Finally, the related data processing and data analysis are included.

Chapter 4 presents the results of the experimental studies and modeling analysis. According to the methodology chapter, the results of feasibility test, ultrasonic

characterization of swelling, acoustic parameters and modeling prediction are reported one by one.

In Chapter 5, systematic discussions on the experiment set-ups and the results are provided. The results of this study are compared with the results of related previous studies and the possible explanations for our findings are given. Meanwhile, the limitations of the methods are discussed and further improvements are suggested.

Chapter 6 summarizes the findings of this study and the potentials of using this ultrasound system in other research fields. Suggestions on future research directions are highlighted.

CHAPTER 2 LITERATURE REVIEW

2.1 Articular Cartilage

Articular cartilage covers the articulating bony ends in diarthrodial joints to reduce the load on the bone and provide a frictionless and smooth surface for movement lubrication. Without it, it is hard to imagine how the skeleton can bear the weight of the body and conduct the movement. Proper functions, however, can work only if the cartilage tissue retains its normal structure. It has been found that the exact composition and structure of articular cartilage depend greatly on anatomy location, depth, and age, as well as the pathological state of the tissue (Fung, 1993; Mow et al., 2005; Mow and Hung, 2001). The complex hydrated-charged nature and magic functions of articular cartilage have attracted tremendous research interests.

2.1.1 Composition, structure and mechanical properties

Chondrocytes, PGs, collagens and water are the major components of articular cartilage. Their distributions depend on depth and consequently they consist of the layered structure of articular cartilage. The composition-structure-function relationship determines the mechanical properties of articular cartilage.

2.1.1.1 Composition

Chondrocytes and Extracellular Matrix

Articular cartilage can be regarded to consist of chondrocytes and extracellular matrix (ECM) (Mow et al., 2005). ECM (95% of the total wet weight) is primarily composed of water, collagen fibres, PGs, and other minor components, such as growth factors,

lipids, enzymes and adhesives (Mow et al., 2005). Chondrocytes occupy a small proportion of the total volume. However, the cells are important in the control of matrix turnover throughout production of collagens, PGs, and enzymes for cartilage metabolism. Previous studies seemed to ignore their contributions on the mechanical properties of articular cartilage. In recent years, the relationship between chondrocytes and their ambient environment has become a focused research area. Wang et al. (2002) observed the environment of chondrocytes under a compressive force and osmotic loading using microscopy. They found the depth-dependent inhomogeneity of stiffness, strain and FCD of the intrinsic tissue. Using micropipette aspiration, Alexopoulos et al. (2005) found that the mechanical properties of cell-perimatrix were similar to ECM while Guilak and Mow (2000) obtained a contrary result that the stress and strain of cell-perimatrix were obviously higher than those of ECM using a multi-scale biphasic finite element model.

Proteoglycan and Collagen

PGs are enmeshed and reinforced by a network of collagen fibres. The cartilage matrix mainly consists of these two components and is swollen with water (Mow et al., 2005). PGs are bio-macromolecules, produced by chondrocytes and secreted into the matrix, with a half-life period of three months. A single PG aggrecan molecule consists of a protein core to which numerous GAG chains are bounded by sugar bonds. The aggregating PGs are strongly electronegative. These negatively charged groups (SO_3^- and COO^-) are quantified as the fixed charge density (FCD) (Lai et al., 1991; Maroudas, 1976a). They contribute to the origin of articular cartilage swelling mechanism, as discussed in section 2.2. The size, structural rigidity, and complicated molecular

conformation of PGs contribute to the electrochemical mechanical behaviour of articular cartilage (Mow et al., 2005). It was discovered that the mechanical parameters of the PG-degraded tissue including shear modulus (Zhu et al., 1993), compressive modulus (Qin et al., 2002; Zheng et al., 2001) and swelling modulus (Flahiff et al., 2004; Narmoneva et al., 2001) greatly reduced but the superficial swelling strain increased (Flahiff et al., 2004; Narmoneva et al., 2001).

Collagen fibres contribute to the mechanical properties of articular cartilage, i.e. provide the stiffness and the elastic energy storage capability (Zhu et al., 1993). The fibrils like a network and horizontally spread in the superficial part of the tissue. In the middle zone, collagen fibres are randomly arranged with a lower density but attached with the high concentration of PGs. Collagen fibres at the deep zone are bundled together, orientated vertically to the interface between the cartilage and the calcified cartilage, and tightly attached to the underlying bone tissue (Hunziker et al., 1997; Mow and Hung, 2001). This zone distributes loads and resists compression. Therefore, the depth-dependent orientation of collagen fibres is greatly responsible for the mechanical properties of articular cartilage.

Interstitial water

Generally, articular cartilage, a hydrated tissue, contains more water than other cartilages (Martini, 2004). The interstitial water distributes non-uniformly and plays an important role in controlling the mechanical behaviour of articular cartilage. The fluid contributes to allow the deformation via shifting in and out of the tissue in response to stress. It has been demonstrated that the decrease or increase of water content has an

effect on the permeability, strength, stiffness and Young's modulus. When the water content of the OA cartilage increases, the permeability increases. In contrast, the strength, stiffness (LeRoux et al., 2000; Lyyra et al., 1999) and modulus (Flahiff et al., 2004; Laasanen et al., 2003a; Narmoneva et al., 2002; Qin et al., 2002; Saarakkala et al., 2003; Toyras et al., 1999; Zheng et al., 2001) of the OA cartilage were all found to decline.

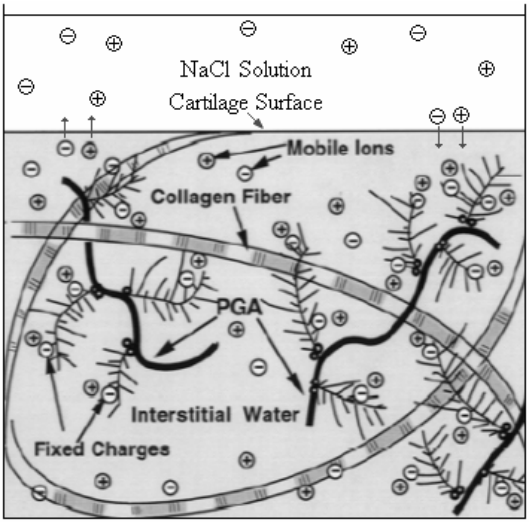

Fig. 2.1 Ultra-scale diagram of the charged-hydrated soft tissue equilibrated with NaCl solution (Lai et al., 1991).

Mobile Ions

In the ultrastructural view, mobile ions are dissolved in the interstitial water and can freely move with the interstitial fluid by convection or shift through the interstitial fluid by diffusion. A part of cations is attracted by the fixed negative charges on the PGs, creating a substantial Donnan osmotic pressure, one of the causes of the cartilage swelling (Fig. 2.1) (Lai et al., 1991). Since Myers et al. (1984) proposed the ionic strains of the continuum theory, ions have been regarded as the third phase of articular cartilage in the triphasic theory in addition to solid and fluid phases (Lai et al., 1991). In

1997, a quadriphasic theory, an extension of the triphasic theory, proposed that the ion phase could be divided into two independent phases, i.e. cation phase and anion phase (Huyghe and Janssen, 1997). However, this theory has not been widely applied.

2.1.1.2 Layered structure

The cartilage tissue can be roughly divided into three layers, i.e., surface, middle, and deep layer (Fig. 1.2c). Each layer contributes the individual role to the properties of intact articular cartilage.

Surface layer (or superficial zone)

The surface layer is the thinnest layer but forms a smooth surface for articular cartilage. In this layer, PG content is lower but collagen and water contents are highest (Mow et al., 2005; Shapiro et al., 2001; Wang et al., 2002). Collagen fibres are horizontally arranged to form a dense network. Therefore, the surface layer can resist the shear stress during the joint motions (Mow and Guo, 2002) and limit the swelling stress (Eisenberg and Grodzinsky 1985; Lai et al., 1991; Maroudas 1976a; Maroudas et al., 1986).

Middle layer (or transitional zone)

The middle layer occupies more than half of the whole cartilage layer. It plays an important role in mechanical function (transform the shearing forces to the compressive forces) and swelling behavior due to the orientation of collagen fibres and the highest PG content (Mow et al., 2005; Narmoneva et al., 2001).

Deep layer (or radial zone)

The deep layer occupies approximately one third of full thickness and contains a high content of collagen and PGs but a low content of water. It has been found that this layer is stiffer than the upper two layers (Chen et al., 2001; Narmoneva et al., 2001), probably because collagens are packed to bundles and a calcified cartilage zone is formed beneath the deep layer. Its stiffness ranges between the stiffness of the cartilage and the bone (Mente and Lewis, 1994). It provides a tight junction between the cartilage layer and the bone tissue and thus resists the stresses (Hunziker et al., 1997). Therefore, it has been demonstrated that there is a difference between the *ex situ* behaviors and properties and the *in situ* ones (Mow and Schoonbeck, 1984; Setton et al., 1998; Skaggs et al., 1994).

2.1.1.3 Inhomogeneity and anisotropy of mechanical properties

Based on the layered composition-structure-function relationship, the mechanical properties (including tension, compression, shear, viscoelasticity, and swelling) of articular cartilage are inhomogeneous, depth-dependent and anisotropy. The zonal variations of the mechanical properties of articular cartilage have been measured in tension (Guilak et al., 1994; Roth and Mow, 1980; Verteramo and Seedhom, 2004; Woo et al., 1976) and in compression (Chen et al., 2001; Setton et al., 1994) using carefully excised tissue slides at different depths. It should be noted that the overall integrity of articular cartilage could not be protected during these measurements. The nonhomogeneous deformation distribution within the full-thickness cartilage layer was theoretically predicted (Mow et al., 1980; Wang et al., 2001). In the 1990's, the inhomogeneity of the mechanical properties of articular cartilage was directly measured

using a confocal microscope (Guilak et al., 1995) and a video microscope (Schigagl et al., 1996, 1997). A new optical method was developed for the investigation of the nonuniform strain distribution within the cartilage layer during free-swelling induced by varying the concentration of the bathing saline solution (Narmoneva et al., 1999, 2001). Their results demonstrated that the strain distribution of cartilage was significantly depth-dependent. However, the strain map was measured along one side of the excised specimen in the optical methods. It is not clear whether the depth-dependent material properties of articular cartilage obtained in such a 'destructive' way would be the same as those in its natural intact state. Associated with compression or indentation, ultrasound has been used to facilitate the direct measurement of the depth-dependent mechanical properties of articular cartilage, such as the transient Poisson's ratio (Fortin et al., 2000), and the compressive strain (Zheng et al., 2002). Cohn et al. (1997a, 1997b) extended the elastography technique (Ophir et al., 1991, 1999) to an elastic ultrasound microscope system. A 2D ultrasound elastomicroscopy system was developed to map deformations of articular cartilage (Zheng et al., 2004b). During the recent years, the inhomogeneous swelling of cartilage was investigated using osmotic loading combined with optical imaging (Narmovena et al., 1999) and ultrasound (Wang and Zheng, 2006; Wang et al., 2006; Zheng et al., 2006a).

2.1.2 Degeneration of articular cartilage and osteoarthritis

2.1.2.1 Spontaneous osteoarthritis changes

Generally, the normal functions of articular cartilage can last for decades. However, factors including aging, cumulative wear and tear, constant pounding of joints, overwork, excessively weight-bearing stress, and genetic factors may result in the

damage of articular cartilage. If the progressive pathological changes start, untreated injuries may lead to OA with symptoms such as the loss of the cartilage tissue and even worse the exposition of the bone across the joint causing pain, swelling, immobility, and finally the loss of the joint functions.

At present, it is clearly indicated that the macromolecular degradation catalyzed by proteolytic enzymes happened at the early- and mid-stages of cartilage degeneration (Sandy, 2003). The component-level changes including the increase of tissue hydration, the loss of PGs, and the damage of collagen fibres are indicated to be the earliest signs of cartilage degeneration during OA (Armstrong and Mow, 1982; Martini, 2004; Sandy, 2003; Torzilli et al., 1990). Moreover, the swelling behavior of articular cartilage may also serve as an indicator of OA because the damage of collagen network and the resultant decrease of PGs result in the alteration of cartilage swelling (Bank et al., 2000). However, the early signs are not easily detected.

The spontaneously degenerated human articular cartilage is relatively difficult to obtain and the degeneration level is not easy to control. In addition, little information on the progressive degeneration can be provided. Animal model of spontaneous OA has significant utility for OA study due to its similarities to the human disease. Generally, there are two typical methods to experimentally induce the pathological changes. One is enzyme digestion and the other is surgery. The experimental methods will be reviewed in the following section.

2.1.2.2 Experiment-induced cartilage degeneration

The proper proteinases have been experimentally applied in the animal model of OA. A recent research suggested that the early stage of OA pathogenesis was characterized by a series of proteinase-involved tissue destruction (Sandy, 2003). The macromolecular degradations are catalyzed by proteinases. The OA-like cartilage can be obtained using digestion by enzymes to deplete one or two components in articular cartilage. Trypsin and chondroinase ABC are widely used to digest the PGs although trypsin has been reported to cleave a minor amount of collagen (Harris et al., 1972). Collagenase is used to damage collagen fibres. Table 2.1 lists the enzymes used in previous studies. Using histological evaluation, the PG depletion could be quantified using safranin O and fast green staining (Kiviranta et al., 1987; Leung et al., 1999; Rosenberg, 1971). It was found that the area fraction of safranin O staining decreased rapidly in the first half hour of trypsin digestion with a concentration of 0.25% (Qin et al., 2002). The changes in collagen fibrils could be observed using scanning electron microscope (SEM) (Laasanen et al., 2005; Saarakkala et al., 2004) or polarized light microscope (Arokoski et al., 1996; Cherin et al., 2001; Kiraly et al., 1997; Nieminen et al., 2002).

Table 2.1 List of various enzymes used in the literatures for the degeneration of articular cartilage.

Authors (Year)	Specimen	Enzyme	Protocol	Digested composition	Parametric measurement
Bank et al. (2000)	Human femoral cartilage (ϕ=6mm)	0.5mg/500μl α-chymotrypsin	37˚C 12 hours	Collagen	Instantaneous deformation; Swelling increased.
Basser et al. (1998)	Human femoral cartilage (middle layer, ϕ=7mm)	1mg/ml trypsin	room temperature 5 hours	PG	PG loss did not affect stiffness of collagen network.
DiSilvestro and Suh (2002)	Bovine patellar articular cartilage plug	0.25% trypsin	37˚C 15 minutes	PG	Biphasic proviscoelastic parameters: E and ν decreased, but κ increased.
Hattori et al. (2005a)	Pig cartilage (ϕ=5mm)	30U/ml collagenase	37˚C 1, 2, 4, 8, 16, and 24 hours	Collagen	Magnitude of echo decreased; Aggregate modulus decreased
Joiner et al. (2001)	Human and bovine articular cartilage (ϕ=3mm, h=1.5mm)	0.3% papain	37˚C 12 hours	PG	Sound speed decreased; Attenuation increased.
Lyyra et al. (1999)	Bovine patellar articular cartilage plug	30U/ml collagenase	37˚C 48 hours	Collagen	Stiffness decreased; Related to PG depletion in surface layer.
		50µ g/ml trypsin	37˚C 24 hours	PG	
		0.1U/ml chondroitinase ABC	37˚C 24 or 48 hours	PG	
Nieminen et al. (2002)	Cylindrical bovine cartilage-bone specimen (ϕ=9mm)	30U/ml collagenase	37˚C 6 hours	Collagen	Reflection coefficient decreased; Attenuation decreased; Speed decreased.
		200µ g/ml (0.02%) trypsin	37˚C 4 hours	PG	Reflection coefficient decreased; Attenuation increased; Speed decreased.
Pellaumail et al. (2002)	Rat patellar articular cartilage	1000U/ml hyaluronidase	37˚C 6 hours	PG	AIB and IRC: no significant difference between control and degenerated specimens.
Qin et al. (2002)	Cylindrical bovine cartilage-bone specimen (ϕ=3mm)	0.25% trypsin	0.5, 1, and 3 hours	PG	Percentage area with safranin O staining reduced with digestion time.
Saarakkala et al. (2004); Laasanen et al. (2002, 2003b); Toyras et al. (2002)	Bovine cartilage-bone plug (ϕ=16mm; ϕ=4mm; ϕ=9mm)	30U/ml collagenase	37˚C 44 hours	Collagen	Reflection coefficient decreased; Surface roughness increased.
		1mg/ml trypsin	37˚C 1, 1.5, or 4 hours	PG	Reflection coefficient decreased; The relationship between reflection coefficient and creep rate and between dynamic and equilibrium modulus were reported.
		0.1U/ml chondroitinase ABC	37˚C 44 hours	PG	
Suh et al. (2001)	Bovine patellar articular cartilage (1cm×1cm×1cm)	1mg/ml trypsin	37˚C 20 minutes	PG	Sound speed decreased.
Zheng et al. (2004a)	Cylindrical bovine cartilage-bone sample (ϕ=6.35mm)	1mg/ml trypsin	20˚C 6 hours	PG	Swelling of cartilage decreased; The trypsin front in the tissue was detected.

Many experimental models of the degenerated tissue have been obtained using external operations, including repetitive loading, surgical damage of ligaments or menisci, and intra-articular drug injection. These models evolve chronically (a few of weeks) to induce OA lesions *in vivo* by a surgery, such as transection of the anterior cruciate ligament (ACL) and meniscectomy (Batiste et al., 2004; Calvo et al., 2004; Laurent et al., 2006; Song et al., 2006). Joint immobilization is another method to induce the degeneration in the cartilage tissue (Narmoneva et al., 2002). These methods usually cause a change in joint mechanics, which consequently leads to an alteration of the loading on articular cartilage. Murphy et al. (1999) revealed that surgical model produced only mild pathology. Acute cartilage damage is often induced by intra-articular injection of chemical reagents and biological mediators, such as mono-iodo-acetic acid (MIA) or papain (Cherin et al., 1998; Laurent et al., 2003; Saied et al., 1997) and collagenase (Hattori et al., 2005a).

Animal models, such as rat, rabbit, canine, pig, and bovine model, are able to conveniently provide a control on time course, an access to cartilage tissue, and a quantification assessment using various techniques. They contribute to the investigation of the insights of the pathology of OA. However, since OA is a complex disease, it is not expected that a single model could mimic all aspects of the human OA.

2.2 Swelling Behavior of Articular Cartilage

2.2.1 Origins of swelling

As a result of the physicochemical forces, swelling is often defined as the ability of articular cartilage to alter (gain or lose) in dimension, weight and hydration when an

osmotic loading exerts on the tissue (Mankin et al., 2000). During the past three decades, the mechanism of swelling and the development of methods to quantify swelling have been of great interests.

The swelling behavior of articular cartilage is considered as an electrochemical mechanical coupling phenomenon of cartilage (Lai et al., 1991). This interesting electrochemomechanical phenomenon is attributed to the interactions between the fixed negative charges and mobile ions. Two force resources give rise to a swelling pressure within articular cartilage (Lai et al., 1991; Mow et al., 2005). One is the imbalance of ions caused by the fixed negative charges, which attract counter-ions to create a substantial pressure in the interstitium higher than the ambient pressure in the bathing solution. This part of swelling pressure is known as the Donnan osmotic pressure (π), which is related to the fixed charge density (c^F) and the electrolyte concentration (c^*) of the external bathing solution and thereby can be adjusted by the ion concentration of the bathing solution. The other is the charge-to-charge repulse force generated by the charged groups fixed on the PGs, known as the chemical-expansion pressure. This swelling pressure balances with the collagen tension, so no swelling behavior can be detected under normal conditions (Eisenberg and Grodzinsky, 1985; Lai et al., 1991; Maroudas, 1976a; Maroudas et al., 1986). The pre-swollen state of articular cartilage plays an essential role in the biomechanical functions (Setton et al., 1998; Wang et al., 2002). When external forces are exerted on articular cartilage, the swollen cartilage carries forces like a cushion (Mankin et al., 2000).

When the cartilage tissue is bathed in a hypertonic salt solution (with a high concentration of salt ions), the difference of the ion concentration between the cartilage matrix and the bathing solution decreases. In other words, the Donnan osmotic pressure reduced. As a result, the tissue shrinks and loses water. In contrast, when the cartilage tissue is bathed in a hypotonic salt solution (with a low concentration of salt ions), the difference of the ion concentration increases. The tissue swells and gains water. The variations in dimension and hydration can be measured during these procedures (Lai et al., 1991; Mow et al., 2005; Myers et al., 1984; Sun et al., 1999). It has been reported that the swelling strain distribution is inhomogeneous throughout the thickness of articular cartilage (Lai et al., 1991; Maroudas 1976a, 1976b; Narmoneva et al., 1999, Wang et al., 2002; Wang and Zheng, 2006). Moreover, it is noted that the effects of osmotic loading within the ECM are different from the effects the practical mechanical loading conditions achieved in the laboratory (Mow et al., 1999). Therefore, the study on cartilage swelling induced by osmotic loading is useful to provide the insight understanding of articular cartilage.

2.2.2 Swelling behavior

Osmosis-induced swelling

Osmotic loading technique by varying the concentration of the bathing saline solution is a simple and useful method to induce and investigate mechanical-combined swelling (Eisenberg and Grodzinsky, 1985, 1987; Grodzinsky et al., 1981; Guilak et al., 1994; Mow and Schoonbeck, 1984; Myers et al., 1984; Wang et al., 2002) and free-swelling behaviour of articular cartilage (Narmoneva et al., 1999, 2001; Setton et al., 1998; Wang and Zheng, 2006). Generally, the concentration of NaCl solution is altered

between 2 M, 0.15 M, and 0.015 M. The solution containing 0.15 M NaCl is regarded as physiological saline; the 0.015 M NaCl solution as hypotonic solution and the 2 M saline as hypertonic solution. In the early studies, the water gains of different zones of articular cartilage were weighted to indirectly qualify the swelling behavior while the *ex situ* samples were at equilibrium in saline solutions with different concentrations (Maroudas, 1976a; Maroudas et al., 1986; Mow and Schoonbeck, 1984). In addition, integrated with tension and compression, the isometric swelling phenomena of cartilage strips with a fixed length were examined by changing the bathing ionic concentration (Eisenberg and Grodzinsky, 1985, 1987; Grodzinsky et al., 1981; Guilak et al., 1994; Mow and Schoonbeck, 1984). Recently, the equilibrium swelling strain of the full-thickness cartilage was optically measured (Narmoneva et al., 1999) and the transient swelling and shrinkage strains were obtained using ultrasound (Wang and Zheng, 2006).

To study swelling, the state equilibrating in 2 M NaCl solution is usually regarded as the reference configuration of zero swelling pressure (Eisenberg and Grodzinsky, 1985; Narmoneva et al., 1999). The reference inhomogeneous distribution of water volume fraction ϕ_0^w and PG-associated negative FCD (c_0^F) are generally required by the estimation of swelling pressure (Lai et al., 1991). ϕ_0^w can be measured by calculating the wet and dry weight of cartilage slices (Flahiff et al., 2002; Narmoneva et al., 1999, 2001, 2002) or by MRI (Shapiro et al., 2001). c_0^F can be determined by a compression microscopy method (Wang et al., 2002) and the DMMB dye-binding assay (Narmoneva et al., 1999).

Intrinsic inhomogeneity

The intrinsic inhomogeneity of the swelling behaviour is determined by the heterogeneous composition and micro-structural organization of the cartilage tissue. Since the early 1980's, it has been discovered that the cartilage tissue dimensionally swells when the concentration of the external solution is changed. In Myer's study (1984), the dimensional swelling measured by stereomicroscope and tension device showed that the osmosis-induced contractions of the superficial, middle and deep zone varied and the largest contraction occurred at the deep zone of the cartilage layer. It is suggested that the gradient of swelling pressure from the surface to the deep well protects articular cartilage from fatigue (Maroudas, 1976a). However, the cartilage layer had to be cut into slices in the previous studies and thereby lost the integrity of the full-thickness cartilage layer.

Recently, with the decrease of the ion concentration of the bathing solution, the matrix-dependent anisotropy of the residual swelling of the *ex-situ* intact cartilage layer was studied by evaluating the changes in curvature, stretch and area (Setton et al., 1998). The non-uniformity of the swelling strains at different zones was also optically observed in 2D swelling-induced residual strains at the cut surface of the cartilage-bone samples (Narmoneva et al., 1999, 2001). The finding that the deep zone had compressive strains while the middle and superficial zones had the tensile strains (Narmoneva et al., 1999) may be explained by the constraint of collagen network in the surface layer and the support of the subchondral bone layer. When articular cartilage was degenerated, the OA cartilage showed a more obviously inhomogeneous change in hydration and swelling strain (Maroudas, 1976a; Narmoneva et al., 2001). However,

many previous studies only investigated the equilibrated swelling of articular cartilage, and thus failed to address its transient inhomogeneity.

2.2.3 Theoretical models

Since the 1970's, a variety of analytical or numerical models, from the linear elasticity models to multi-phasic models, have been established to describe the mechanical properties of articular cartilage. With the deeper understanding of the composition and structure of articular cartilage, the models have been challenged and improved. Currently, the biomechanical properties of articular cartilage have been well understood using biphasic theory. And the triphasic models can reasonably describe the electrochemomechanism of cartilage swelling. To provide a clear review, the summary of the models and their limitations is presented in Table 2.2. Among various theories, biphasic theory and triphasic theory have been widely accepted and applied in studies on articular cartilage.

Articular cartilage has been viewed as a biphasic material, composed of solid phase (PG-collagen matrix) and fluid phase (water and the dissolved ions) (Mow et al., 1980). The biphasic mixture theory has been applied in various experimental and theoretical studies (reviewed by Mow et al., 2005; Mow and Guo, 2002). In view of the porosity and viscoelasticity of articular cartilage, the biphasic poroviscoelastic model of articular cartilage was proposed (Disilvestro and Suh, 2002; Mak, 1986; Mak et al., 1987). Although the assumption of the homogeneous tissue could be accepted for the measurement of the aggregate modulus H_a, the parameters such as strain, stress, and pressure inside the inhomogeneous tissues obviously differ from those of homogeneous

materials. The possible reason is that the biphasic pressure does not include the FCD (osmotic) effects (Mow et al., 1998).

Table 2.2 Summary of different theoretical models of articular cartilage.

Authors (Year)	Model	Features			Limitations
		Solid Matrix	**Fluid Flow**	**Ions**	
Hayes et al. (1972)	Linearly elastic	Linearly elastic, isotropic, and homogeneous material	/	/	Unable to describe the time-dependent behaviors such as creep and stress-relaxation behaviors.
Hayes and Bodine (1978) Parsons and Black (1977)	Viscoelastic	Viscoelastic solid matrix	/	/	Unable to describe the effects of interstitial fluid.
		Creep and stress-relaxation behaviors			
Mow et al. (1980)	Biphasic	Incompressible, nondissipative PG-collagen solid matrix	Incompressible, nondissipative interstitial fluid	/	Solid matrix is linearly elastic, homogeneous, and isotropic; Did not include the FCD (osmotic) effects.
			Elastic stress fluid pressure		
Mak (1986)	Biphasic poroviscoelastic	(same as above) Viscoelastic in shear and bulk	(same as above)	/	Solid matrix is linearly elastic in bulk deformation; Did not include the FCD effects.
Myers et al. (1984)	Thermoelastic analogy	(same as Mow's model)	(same as above)	Ion-induced strain	Ions were not modeled as a dependent phase.
Lai et al. (1991)	Triphasic	(same as above)	(same as above)	Ion phase of cations and anions	The PG-collagen solid matrix was assumed to be homogeneous; a homogeneous distribution of FCD; uniform modulus and Poisson's ratio.
		Donnan equilibrium ion distributions, the dimensional swelling effects, Donnan osmotic pressures, and kinetics of swelling.			
Huyghe and Janssen (1997)	Quadriphasic	(same as above)	(same as above)	Divited into two mono-valent ion phases: cation (+) and anion (-).	Assumed that deformation is incompressible and isothermal; The mixture as a whole is assumed locally electroneutral.
Gu et al. (1998)	Multi-electrolytes mixture theory (n+2 model)	Charged solid phase	Non-charged solvent phase	*n* ion species	Only increase the number of species.

Triphasic theory models articular cartilage as triphasic material, composed of solid phase (PG-collagen matrix), fluid phase (water) and ion phase (Lai et al., 1991). Taking

into account the ion concentration and the electrical potential effects, triphasic theory provides the thermodynamic foundation and the complex mechanical chemical electrokinetic mechanism for cartilage swelling, deformation, and viscoelasticity. Therefore, triphasic theory can describe the electrochemomechanism of swelling more comprehensively than any other former theories. Using this theory, Narmoneva et al. (2001) and Flahiff et al. (2002) developed the triphasic theoretical formulation of articular cartilage in a free-swelling configuration to determine the stiffness at different layers and the thickness-averaged uniaxial modulus which ranges from several to over 20 MPa. A recent study established a micro-scale (molecular-level) triphasic model using finite element modeling to describe the electric field of the chondrocytes and their vicinity while a macro-scale model is used to describe the cartilage layer (Wang et al., 2002). This method may offer a way to better understand the intrinsic properties of articular cartilage at multi-scale.

By changing the salt concentration of the bathing solution, a combination of electrostatic forces and hydration forces may lead to osmosis-induced swelling or shrinking deformations of articular cartilage (Lai et al., 1991). It has been found that hydration forces are a dominant swelling factor in the mineral porous media (Huyghe and Janssen, 1997). The flow-dependent and flow-independent viscoelastic behaviors, swelling behaviors, and electrokinetic behaviors of the charged-hydrated soft tissues have been well described using the triphasic theory (Lai et al., 1991; Mow et al., 1998, 2005; Sun et al., 1999). However, with reviewing of the investigations of the interactions between FCD and the physiochemical properties of articular cartilage, the equivalence of mechanical loading and osmotic pressure in the triphasic theory was

highly restrictive (Mow et al., 1999). One of the limitations of triphasic theory for soft hydrated tissue (e.g. cartilage) is the neglect of the electrical flux, geometric non-linearity and hydration forces (Huyghe and Janssen, 1997; Lai et al., 1991). Although many studies have been conducted, some theories are overlapped or even contradictory. Therefore, further research is needed.

In Lai's model (1991), the cartilage solid matrix was assumed to have homogeneous elastic material properties with uniform aggregate modulus *Ha* and Poisson's ratio ν_s. However, the multilayered structure and the non-uniform distribution of components determine the inhomogeneous material properties of articular cartilage. Narmoneva et al. (2001) developed a partial inhomogeneous bi-layered triphasic model to predict the non-uniform material properties of the normal and degenerated tissues.

2.3 Evaluation Techniques for Articular Cartilage

2.3.1 Mechanical methods

Since articular cartilage is a weight-bearing tissue, its mechanical properties have been the original interest in the research area of articular cartilage. Tension, compression and shear tests have been usually designed to study the species- and location-dependence (site-dependence) (Laasanen et al., 2003a; Lyyra et al., 1999; Treppo et al., 2000) and inhomogeneity and anisotropy (refer to section 2.1.1.3). Fig. 2.2 shows schematics of the experiment set-up of the unconfined and confined compression, indentation, and tension tests. The unconfined and confined compression and tension are suitable for the *in-vitro* testing because the cartilage sample must be removed from the anatomical

location. Indentation using an indenter to compress the tissue can be applied for *in-vivo* testing.

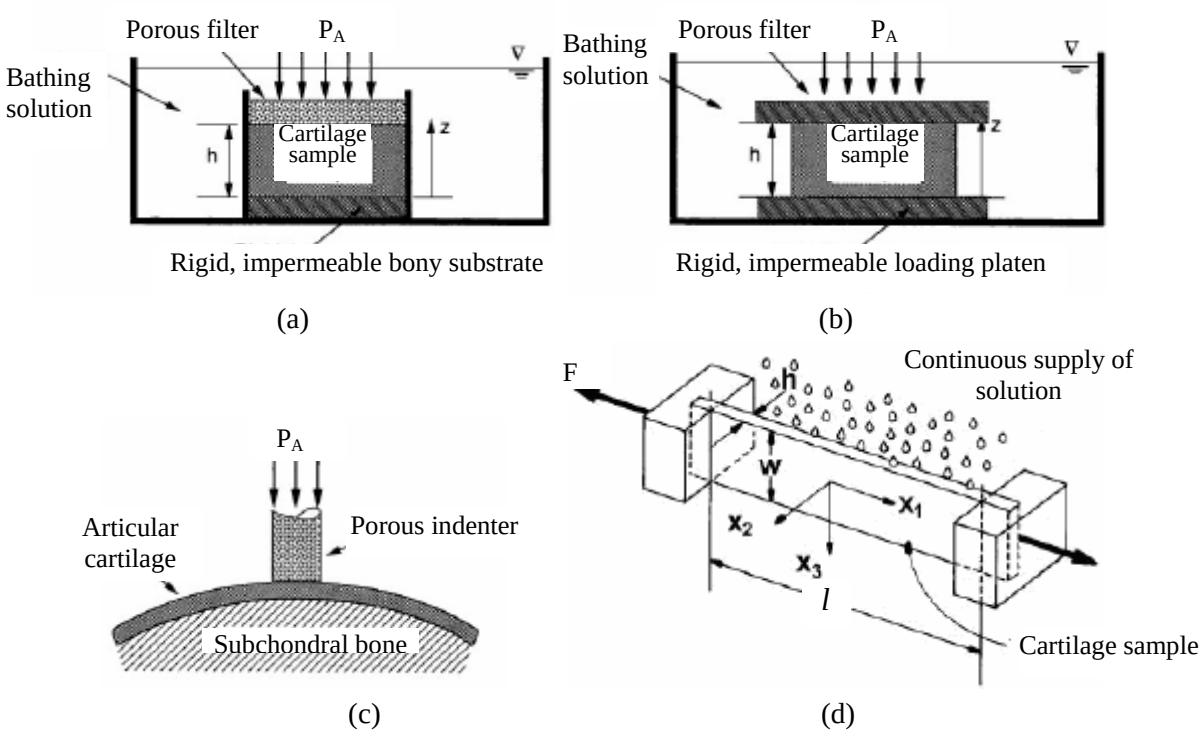

Fig. 2.2 Schematics of (a) confined compression configuration, (b) unconfined compression, (c) indentation (Mow and Guo, 2002), and (d) tension (Myers et al., 1984).

Ultrasound techniques combined with compression and indentation have recently been applied to measure the mechanical properties, such as modulus, Poisson's ratio, and the creep rate (Cherin et al., 2001; Fortin et al., 2003; Joiner et al., 2001; Suh et al., 2001; Toyras et al., 1999; Zheng et al., 2001, 2002, 2004b). A recent study introduced an ultrasonic indentation method using water flow as an indenter (Lu et al., 2005). The ultrasound pulses penetrate the tissue from the lateral side or along the depth direction. However, ultrasound indentation has seldom been used in the swelling tests. The swelling behavior of articular cartilage has been tested using tension and the osmotic loading by the change of the concentration of the external bathing solution (Guilak et al., 1994; Myers et al., 1984) (Fig. 2.2d). The swelling-induced deformation can be

measured using the sensors. The relationship between the electromechanical stress and the ion concentration was investigated during swelling process in tension (Grodzinsky et al., 1981; Guilak et al., 1994). However, these aforementioned mechanical-swelling methods can only measure the restricted swelling of articular cartilage, which may lose some characteristics of the *in-situ* or *in-vivo* cartilage swelling. Swelling induced by the osmotic loading instead of external forces is called as free swelling, which has been investigated using ultrasound, optical imaging, etc.

2.3.2 Ultrasound techniques

Ultrasound technique provides a noninvasive visualization of articular cartilage. Not only traditional A-mode, B-mode, and M-mode signals have been widely used in the research on articular cartilage, but ultrasound biomicroscopic (UBM) image with a high resolution reaching the order of micrometer has been applied (Cherin et al., 2001; Foster et al., 2000; Laasanen et al., 2006; Saarakkala et al., 2006; Saied and Laugier, 2004; Toyras et al., 2002; Wang and Zheng, 2005; Zheng et al., 2004b).

2.3.2.1 Free swelling

Ultrasound techniques have been mainly applied in studies on both acoustic and mechanical characterizations of cartilage in last two decades, which are described in details in next section. Tepic et al. (1983) first probed the hydration process of the dehydrated cartilage using ultrasound. Our previous study with a small number of specimens has demonstrated that it is feasible to use high-frequency ultrasound to monitor the transient behavior of articular cartilage during the free swelling or shrinkage process induced by the concentration change of the bathing saline solution as well as the

progressive enzyme digestion (Zheng et al., 2004a). In our recent study, the quantitative ultrasonic characteristics of the transient changes of normal bovine patellar cartilage under the osmotic loading were introduced (Wang and Zheng, 2006). In comparison with water-gain weighting and optical imaging, ultrasound can provide the transient and depth-dependent swelling of the intact cartilage tissue *in situ*. However, not enough effort has been made in this research field.

2.3.2.2 Acoustic properties of articular cartilage

Ultrasound is defined as sound with a frequency above the upper limit of normal human hearing, typically 20 KHz (Meire and Farrant, 1995). Medical ultrasound is sound with a frequency ranging from 2 MHz to 100 MHz. Generally, high frequency ultrasound applied in clinical practice has a frequency of more than 7.5 MHz. In comparison with low frequency ultrasound, high frequency ultrasound has a higher resolution, but a less propagation depth in tissues. For example, 40 MHz ultrasound can only propagate several millimeter (Kremkau, 1998). Since the thickness of bovine patellar cartilage is approximately 1.5 mm, high frequency ultrasound can be applied.

The acoustic parameters (including sound speed, attenuation coefficient, reflection coefficient, backscatter coefficient, etc.) additionally provide more comprehensive information for cartilage assessment. During the last decade, ultrasound has been widely used in studies on articular cartilage from small and/or large animal models (such as rat, canine, porcine and bovine) to human subjects. Table 2.3 lists a summary of ultrasound methods applied in the literatures in the last two decades.

Table 2.3 Studies on articular cartilage using ultrasound in the last two decades.

Authors (Year)	Mode	Frequency (MHz)	Specimens	Parameters
Adam et al. (1998)	A	12.5	Human knee cartilage (2-5 mm)	Accuracy and reproducibility of thickness measurement
Agemura et al. (1990)	A; Laser	100	Bovine articular cartilage (ϕ = 2 mm; and slices (patellar groove)	Attenuation coefficient; sound speed at different depth and orientation
Cherin et al. (1998, 2001); Pellaumail et al. (2002); Saied et al. (1997)	A, B	50; 55	Rat patellae cartilage (with aging/aged or immature/mature)	Reflection, backscatter coefficients; thickness
Disler et al. (2000)	B	5-12	Porcine and human knee articular cartilage	Accuracy and reliability of grading defects
Forster et al. (1990)	A	25	Dog skin	Attenuation coefficient
Fortin et al. (2003)	A Unconfined compression	50 (focused)	Human humeral head cartilage (ϕ=1.65mm, h=1.00mm)	Dynamic deformation; Poisson's ratio
Hattori et al. (2004, 2005a,b); Kuroki et al. (2004)	A	10	Human articular cartilage; pig and rabbit cartilage	Echo magnitude and duration
Joiner et al. (2001)	A	30	Human and bovine articular cartilage (ϕ=3mm, h=1.5mm)	Sound speed; attenuation coefficient
Jurvelin et al. (1995)	A	10	Canine and bovine knee articular cartilage (10mm×10mm×5mm)	Thickness
Laasanen et al. (2002, 2003a)	A	10.5	Bovine knee joint (patello-femoral groove, medial femoral condyle, and medial tibial plateau, ϕ=4mm)	Reflection and dynamic modulus
Lefebvre et al. (1998)	B 3D	50	Rat knee patellar articular cartilage	3D ultrasonic reconstruction
Nieminen et al. (2002)	A	29.4 (focused)	Bovine patellar cartilage (ϕ=9mm)	Attenuation and reflection coefficients
Patil et al. (2004); Zheng et al. (2006b)	A	50 (focused)	Bovine patellar cartilage	Depth- and concentration-dependent ultrasound speed
Saarakkala et al. (2004, 2006); Laasanen et al. (2006)	B	20 (focused)	Bovine patellar cartilage; Porcine femoral cartilage	Reflection coefficient
Senzig et al. (1992)	A	25	Bovine femur articular cartilage (ϕ=4mm)	Attenuation coefficient

Table 2.3 continued

Authors (Year)	Mode	Frequency (MHz)	Specimens	Acoustic parameters
Suh et al. (2001)	A	10	Bovine patellar cartilage (1cm×1cm×1cm)	ultrasound speed; accuracy of thickness measurement
Toyras et al. (1999,2002)	A or B, C D, F, M	22	Bovine patellar cartilage (ϕ=6mm)	Reflection coefficient; ultrasound speed
Toyras et al. (2003); Saarakkala et al. (2003)	A indentation	10.5	Bovine knee joint (different anatomical locations, ϕ=4mm)	Ultrasound speed; thickness; dynamic modulus; Young's modulus
Wang and Zheng (2005)	A, UBM	40 (focused)	Bovine patellar cartilage (ϕ=6.35mm)	Swelling strains; Ultrasound biomicroscopy imaging
Wang and Zheng, (2006); Zheng et al. (2004a)	A, M	50 (focused)	Bovine patellar cartilage (ϕ=6.35mm)	Shrinkage and swelling strains; Progressive degeneration of articular cartilage
Zheng et al. (2004b, 2006a)	A, UBM; Confined compression	50 (focused)	Bovine patellar cartilage (ϕ=6.35mm, with a thin bone layer); mouse skin	Elastomicroscopy of displacement and strains
Zheng et al. (2001, 2002, 2005)	A, M; Confined compression	50 (focused)	Bovine patellar cartilage (ϕ=6.35mm, with a thin bone layer)	Depth-dependent strains; Equilibrium compression modulus; transient deformation

Ultrasound speed in cartilage

Ultrasound speed is an important parameter in the quantitative measurement of articular cartilage. However, it depends on many factors, such as temperature, density of the medium, intensity of pressure, etc. Some studies on articular cartilage assumed ultrasound speed as different constants (Fortin et al., 2003; Joiner et al., 2001; Jurvelin et al., 1995; Laasanen et al., 2003a; Modest et al., 1989; Myers et al., 1995; Toyras et al., 2002; Zheng et al., 2001, 2002), which ranged from 1654 to 1765 m/s. Other studies found the inhomogeneity of ultrasound speed in articular cartilage (Agemura et al., 1990; Patil et al., 2004; Yao and Seedhom, 1999) and doubted the validity of results measured using ultrasound (Lee and Bouffard, 2001; Yao and Seedhom, 1999). The uncertainty of ultrasound speed in the tissue is still in controversy. However, ultrasound techniques

have been widely used in research on articular cartilage and demonstrated to be acceptable (Adam et al., 1998; Disler et al., 2000; Jurvelin et al., 1995; Laasanen et al., 2002; Mann, 2001; Modest et al., 1989; Wang and Zheng, 2006). Moreover, Nieminen et al. (2002) believed that a constant ultrasound speed could be accepted in the measurement of the cartilage thickness based on their results that there was a mild difference in the averaged sound speed in the full-thickness cartilage.

Ultrasound measurement of cartilage thickness

The thickness of cartilage layer is an important index for assessing OA since thinning of the cartilage layer is one of signs of OA. Generally, the thickness measured using ultrasound is calculated by the equation, $h = c \times T / 2$, where c is the speed of ultrasound in articular cartilage, T is the flight time of ultrasound echoes for a round trip in the tissue. The possible variation in ultrasound speed may affect the ultrasonic measurement of cartilage thickness. In current, since the variation of ultrasound speed is acceptable, ultrasound has been used in measuring the thickness of the cartilage layer. Many previous studies demonstrated that ultrasound techniques *in vitro* provided highly accurate and reproducible measurements of the cartilage thickness (Adam et al., 1998; Disler et al., 2000; Jurvelin et al., 1995; Mann, 2001; Modest et at., 1989). Deformation of the tissue induced by compression or osmosis loading was measured using ultrasound (Wang and Zheng, 2006; Zheng et al., 2002, 2004a).

Attenuation coefficient

Ultrasound attenuation describes the propagation property of ultrasound in medium. In the normal cartilage, attenuation is frequency-dependent (Agemura et al., 1990; Joiner

et al., 2001; Nieminen et al., 2002; Senzig et al., 1992; Wells, 1993). Integrated attenuation values of approximately 2.8-6.5 dB/mm for bovine cartilage have been measured in the frequency range of 10-40 MHz (Senzig et al., 1992), while the mean values ranged from 9.79 to 11.49 dB/mm at the frequency range of 18.8-40.0 MHz (Nieminen et al., 2002) and the values of approximately 100 dB/mm were reported at 100 MHz (Agemura et al., 1990). It was revealed that ultrasound attenuation positively correlated with compressive stiffness (Jurvelin et al., 1995) and was strongest under high stresses during joint motion (Senzig et al., 1992). Agemura et al (1990) found that attenuation coefficient significantly increased when the collagen intermolecular cross-links were cleaved.

Reflection coefficient

Reflection coefficient may be regarded as a quantitative analysis parameter assessing the acoustic energy level reflected from the interfaces (ranging from -21 to -24dB, measured by Cherin et al., 1998, 2001). It has been found that ultrasound reflection coefficient of the cartilage surface is site-dependent in indentation test (Laasanen et al., 2003a) and specifically sensitive to the degeneration of collagen network (Laasanen et al., 2002; Nieminen et al., 2002; Toyras et al., 1999). However, no association was proposed between the reflection coefficient and GAG concentration (Laasanen et al., 2003a). In the view of cartilage structure, collagen fibres arranged parallel to the surface to form a network seem to play a significant role in reflection.

Backscatter coefficient

Backscatter coefficient is another important parameter for quantifying the level of acoustic energy backscattered by the internal structure and composition of articular cartilage (Cherin et al., 1998, 2001; Pellaumail et al., 2002). It was revealed that collagen fibrils played a more important role in ultrasound backscattering properties than PGs. The changes in backscatter reflect changes in shape, size, and/or density of the scatters in the tissue, which are related to the changes in the constituent concentration and the orientation of the matrix.

Relationship between acoustic and mechanical properties

Both acoustic and mechanical properties of articular cartilage are dependent on the composition and structure of the tissue. It was found that dynamic modulus was positively correlated with PG concentration while reflection coefficient correlated with collagen concentration (Laasanen et al., 2003a). The relationship between acoustic and mechanical properties has been used to assess the composition-level cartilage degeneration using ultrasound indentation as shown in Fig. 2.3 (Toyras et al., 1999, 2002). In recent years, new indexes have been developed to evaluate the cartilage tissue. A cartilage quality index including modulus, degeneration score and water content was proposed and found to negatively correlate with attenuation and ultrasound speed (Nieminen et al., 2004). The reflex echogram of ultrasound signals transformed by wavelet was used to observe the positive correlation between the maximum magnitude and the aggregate modulus (Hattori et al., 2005a). However, there is less investigation on the relationship between acoustic and swelling behavior of articular cartilage.

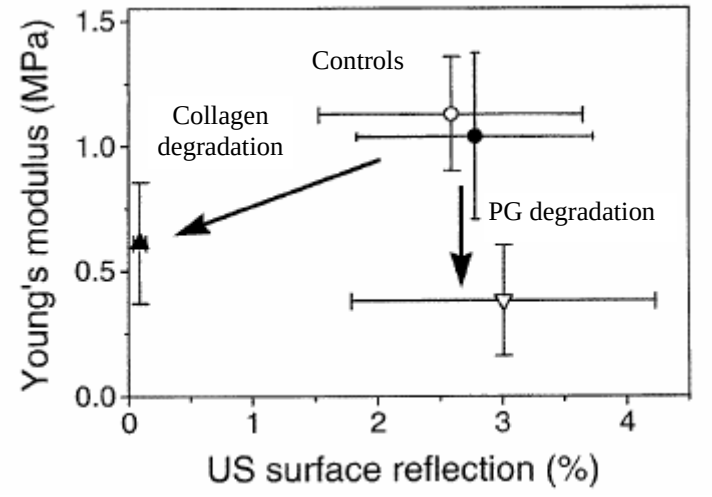

Fig. 2.3 Relationship between Young's modulus and reflection coefficient of normal and degenerated cartilage measured using ultrasound (US) indentation (Toyras et al., 1999).

2.3.3 Other techniques

The conventional clinical approaches, such as x-ray, MRI and B-mode ultrasound imaging, only offer a resolution with the order of millimeter. However, these techniques have been developed rapidly.

Microscopic optical method

Aided by computer and high-resolution charge coupled device (CCD) optical system, microscopic imaging has been applied to monitor the cross-sectioned cutting surface of articular cartilage, so as to extract the non-uniform compressive or free swelling-induced strains of articular cartilage at equilibrium state (Flahiff et al., 2002, 2004; Narmoneva et al., 1999; Schinagl et al., 1996; Setton et al., 1998; Wang et al., 2002). It was also found that the compressive modulus of articular cartilage depth-dependently increased (Chen et al., 2001; Jurvelin et al., 1997; Laasanen et al., 2003b; Wang et al., 2003). However, these studies had to cut cartilage into several sub-layers and only

observed the cutting surface. Properties of the integrated cartilage may not be maintained in the excised specimens, making the *in vivo* or *in situ* measurement difficult. To the best of our knowledge, few *in situ* studies have been reported on the transient swelling behavior of articular cartilage induced by changing the concentration of the bathing saline solution.

Optical coherence tomography (OCT)

Optical coherence tomography (OCT) was first applied in ophthalmology (Fujimoto et al., 1995; Puliafito et al., 1995). With an observation of small animal model, OCT has been proved to have potentials in monitoring the microstructural anatomy and features of OA in comparison with histological assessment (Adams et al., 2006; Patel et al., 2005). To achieve *in vivo* assessment of tissues, the endoscopic OCT facilitated an interstitial imaging for the gastrointestinal and respiratory tracts, the vascular system, and joints (Tearney and Brezinski, 1997). In addition, OCT was applied to measure the displacement of the cartilage surface induced by an external electric field (Youn et al., 2004). However, few studies have been performed on the swelling behavior of articular cartilage.

MRI and μ-MRI (Micro-MRI)

MRI is a powerful tool for assessing joint abnormalities. One advantage is that MRI is capable of directly and non-destructively visualizing the components of joints simultaneously. Therefore, MRI is easy to evaluate the pathological change or anatomical abnormality of articular cartilage in small animal model such as rat and rabbit. The other advantage is that it can provide a panorama view of the knee joint. It

well evaluates cartilage thinning and space narrowing. With the recent developments of MRI technique, MRI has been applied to detect early cartilage degeneration of articular cartilage (Batiste et al., 2004; Jaremko et al., 2006; Laurent et al., 2006; Nissi et al., 2004; Wheaton et al., 2004). Parameters such as magnetization transfer rate, T1 and T2, were used as indexes for assessing the scale of OA (Koff et al., 2005; Laurent et al., 2006; Nieminen et al., 2000). However, one difficult issue for MRI is to be an imaging modality for the measurement of the cartilage stiffness (Nieminen et al., 2000). The other issue is its high cost to monitor the transient change of the tissue. Therefore, the swelling behavior of articular cartilage has seldom been studied using MRI.

μ-MRI provides a relatively high resolution at the macromolecular level for morphologic analysis of articular cartilage (Batiste et al., 2004; Beuf, 2004). However, the resolution of μ-MRI seems still not sufficient for good evaluation of the micro-structural changes of articular cartilage.

CT and μ-CT (Micro-CT)

It has been well known that CT， similar to the conventional x-ray radiography, provides superior details for the bone and calcified tissues. Although μ-CT is improved in resolution and has an ability to show the skeletal structure, it is unable to image soft tissues such as articular cartilage (Batiste et al., 2004; Berquist, 1997). Therefore, this imaging modality is a good evaluation tool for the late-staged OA with the damage or osteophyte development of the bone tissue. In a recent study, μ-CT has been applied to investigate the micro-architectural features of subchondral bone in OA models (Ding,

2005). μ-MRI and μ-CT are potential for assessing OA of the small joints of small animal models (Wachsmuth and Engelke, 2004).

Arthroscope or endoscope

As a transcutaneous approach, arthroscope or endoscope has to invade into the chamber of joints. However, this method can provide the most direct information of tissues, although this information only comes from the surface of tissues. It plays an important role in joint surgery to help doctors observe the condition of the tissue and the progress of surgery. Recent studies have applied arthroscope or endoscope associated with ultrasound technique to observe acoustic parameters (Hattori et al., 2004) or mechano-acoustic properties of articular cartilage (Laasanen et al., 2002). In their studies, an arthroscopic ultrasound probe with a small size was designed as shown in Fig. 2.4. This method could provide not only the video image of joints but also the acoustic and/or mechanical information of the cartilage tissues, which are deeply located inside the joints and difficultly observed using regular clinical B-mode ultrasound imaging. The arthroscopic ultrasound probe tends to be promising for the *in-vivo* assessment of the cartilages (Hattori et al., 2005b). Lyyra et al. (1999) *in vivo* characterized the indentation stiffness of human articular cartilage. However, it seems unsuitable for monitoring the free swelling behavior of articular cartilage due to its progressive nature.

Histological evaluation

Histology, a conventional assessment approach, provides an optical microscopic evaluation of the tissue. It can provide microscopic information including the normal and degenerated structure and composition. However, to achieve the histological images,

the specimen should be removed from the body and processed using the routine tissue processing protocols (Kiernan, 2001), which are time-consuming. Special attention should be paid during each step (e.g. fixation, decalcification, embedding, sectioning, staining) since the operations affect the final staining result (Kiernan, 2001). The histological assessment has been applied as a criterion for evaluating the validity of other aforementioned methods in the studies on the progressive degeneration of articular cartilage (Adams et al., 2006; Hattori et al., 2004; Kuroki et al., 2004; Laasanen et al., 2006; Laurent et al., 2006; Qin et al., 2002; Saied et al., 1997).

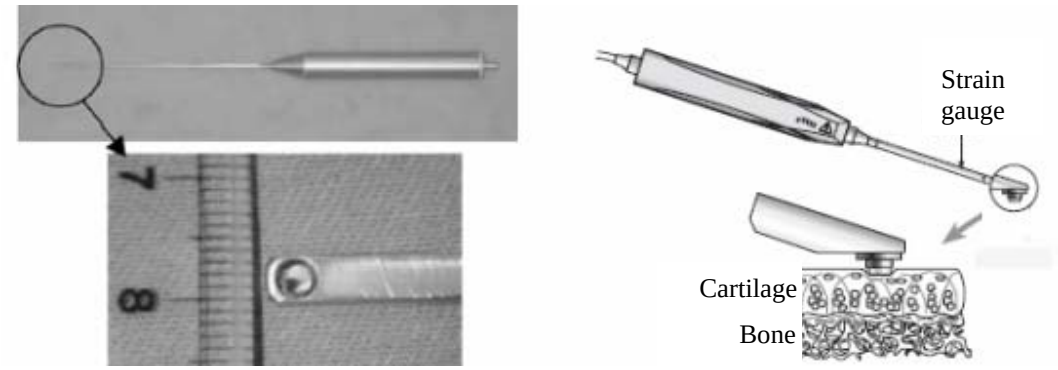

(a) (b)

Fig. 2.4 Two types of arthroscopic ultrasonic probe (a) for acoustic analysis (Hattori et al., 2004) and (b) for indentation (Laasanen et al., 2002).

Radiography

Due to the limitation of differentiating soft tissue, radiography (x-ray) provides less information extracted from the cartilage layer. Therefore, radiographic changes of OA including narrowing of joint space, osteophytosis (or bony spurs), cartilage loss and abnormality of subchondral bone, generally characterize the late stage of OA. However, a magnification radiography method was developed and could provide the bone changes at the early stage of OA (Buckland-Wright and Bradshaw, 1989). At present,

radiographic criteria remain as an assistant evaluation to confirm OA diagnosis (Buckland-Wright, 2004).

In a summary, various imaging methods applied in the assessment of articular cartilage and OA have their individual advantages and disadvantages. Standard radiography (x-ray) remains the primary imaging method for the joint abnormalities. It is believed to be the most economic and direct way to show the fracture and loss of bones and cartilage. However, it is not sensitive to the early stage of the pathological changes of soft tissues. MRI and μ-MRI offer a precise panorama image of the knee joint and thus potentially visualize and analyze the quantification of the degeneration of bone and soft tissues. However, the knees with metallic implants are forbidden from MRI examination. Moreover, obese patients are unsuitable to be examined with MRI, and the examination takes long time. CT and μ-CT can detect fine calcifications but lack information for soft tissues. MRI and CT are both expensive. Ultrasound has been applied to detect the abnormalities of the knee joint and even articular cartilage. UBM imaging could provide a microscopic image of articular cartilage. However, the accuracy and reliability of ultrasonic measurement remain in controversy. Arthroscopy permits direct observation of tissues inside of the joint capsule, but only for the surface morphological information. Optical methods are low-cost but the loss of integrity of articular cartilage is a limitation. From a technique view, OCT is similar to ultrasound. They both can provide an intra-tissular image of the intact tissue. But the light is easily scattered and attenuated by the tissue. It has been noted that whichever OCT or ultrasound combines with arthroscopy can improve the images at the price of losing their non-invasive feature to monitor articular cartilage in joint chamber *in vivo*.

2.4 Effects of Osteoarthritis on Mechano-Acoustic Properties

This section provides a literature review on the effects of OA changes (including composition loss, structure change, and aging) on mechano-acoustic properties of articular cartilage.

2.4.1 Effects on swelling behavior

During OA, the degeneration of articular cartilage occurs in the early stage, including PG depletion, water increase, and collagen damage (Maroudas 1976a; Mow et al., 2005). These changes affect the swelling behavior of articular cartilage (Flahiff et al., 2004; Narmoneva et al., 2002; Wang and Zheng, 2004). Triphasic theories demonstrate that cartilage swelling is related to FCD and PG content (Lai et al., 1991). Using MRI, Calvo et al. (2004) reported that there was a correlation between the swelling (increment of cartilage thickness) and the PG depletion and the cell loss. Meanwhile, the OA cartilage contains a considerable increase of water content and the swelling strains of the superficial zone increase (Narmoneva et al., 2001, 2002). Using ultrasound, it was monitored that the amplitude of the transient cartilage swelling reduced after trypsin digestion in comparison with normal cartilage (Zheng et al., 2004a).

However, it is also well known that collagen network limits the swelling behavior (Eisenberg and Grodzinsky, 1985; Lai et al., 1991; Maroudas, 1976a; Maroudas et al., 1986). Bank et al. (2000) reported that the increased swelling of the full-depth OA cartilage seemed to be related to the amount of degraded collagen molecules, instead of FCD or PGs, probably because the osmotic pressure gradient increased the water

absorption when the restraining force of collagen network was impaired. Other studies also demonstrated that collagen damages gave rise to the increase of osmosis-induced swelling strains (Flahiff et al., 2004) and transient dehydration-induced swelling strain (Wang and Zheng, 2004), and the nonlinearity of the swelling strains was caused by the collagen fibres (Tepic et al., 1983). Therefore, the integrity of the collagen network is important to resist the swelling pressures in the cartilage tissue.

Due to the complexity of the properties of articular cartilage, comprehensive research on this aspect is still expected. With respect to the OA tissue, the quantification for the period of hydration, the speed of the water permeability, and the progressive degeneration are needed. Therefore, more efforts should be put into this research area.

2.4.2 Effects on acoustic properties

Since the acoustic parameters contain rich information of the tissue and thereby reflect the changes in composition and structure, many effects have been made to investigate the changes of the acoustic properties of the OA or OA-like articular cartilage (Table 2.3).

Ultrasound speed

The mean values of ultrasound speed in the bovine or human cartilage measured by previous studies ranged from 1622 m/s to 1765 m/s (Agemuran et al., 1990; Myers et al., 1995; Nieminen et al., 2002; Toyras et al., 1999). It has been reported that sound speed in the PG-depleted tissue decreased. Suh et al. (2001) obtained a sound speed of 1735 ± 35 m/s in the normal cartilage and 1598 ± 28 m/s in the PG-depleted cartilage. It was

found that the sound speed in the trypsin-digested tissue or OA cartilage decreased approximately 7 m/s in comparison with that in the control samples (Myers et al., 1995; Nieminen et al., 2002). Meanwhile, collagen network affects sound speed in articular cartilage in a same pattern, i.e. sound speed decreases with collagen loss (Laasanen et al., 2002; Nieminen et al., 2002; Toyras et al., 1999). Some investigators believed that a constant ultrasound speed in both normal and degenerated cartilage tissues could be accepted in the measurement of the cartilage thickness based on their results that there was mild difference in the average sound speed in the full-thickness cartilage (Nieminen et al., 2002). However, it has been well known that the inhomogeneity and anisotropy of composition and structure (refer to subsection 2.1.1) determine the non-constant sound speed in articular cartilage. Therefore, the determination of sound speed in the tissue has been a concerned issue or a limitation for ultrasound measurement.

Attenuation coefficient

Attenuation coefficient is an index presenting the response of the tissue to ultrasound wave and must be changed by the OA or experimentally induced degeneration of articular cartilage. A significant increase in the attenuation coefficient was discovered during trypsin digestion (Nieminen et al., 2002). This finding consisted with Joiner's study (2001), which reported that the mean attenuation coefficient increased 30% and 20% for the papain-digested bovine and human cartilages with a loss of PGs, respectively, but was different from the earlier study of Toyras et al. (1999), which demonstrated that there was no insignificant increase in attenuation after chondroitinase ABC digestion. In addition, for collagen-digested cartilage samples, a statistically insignificant decrease was found in Nieminen's study (2002), but a statistically

insignificant increase in Toyras' study (1999). The difference of the previous results may be caused by different enzymes and measurement methods. Although the frequency-dependent attenuation in articular cartilage may be sensitive to experimental modification of the PG-collagen matrix, the roles of PGs and collagens in ultrasound attenuation have not been quite clearly characterized.

Reflection coefficient

Previous studies demonstrated that reflection coefficient was more sensitive to the collagen degeneration (Lyyra et al., 1999; Nieminen et al., 2002). Nieminen et al. (2002) found that collagenase digestion caused a significant decrease in ultrasound reflection coefficient from the cartilage surface. Cherin et al. (1998, 2001) demonstrated that reflection variation caused by OA degeneration indicated a change in acoustical impedance of the superficial layer of articular cartilage, which was linked to the change in constituent content of collagen fibres. However, the effect of PGs on reflection coefficient has been in controversy. Nieminen et al. (2002) reported that reflection coefficient significantly positively linearly correlated with the uronic acid concentration or PG content. Meanwhile, Laasanen et al. (2003a) proposed that the reflection coefficient was not associated with GAG concentration. In addition, reflection was also associated with water content (Saarakkala et al., 2003). Generally, it has been proved that this index is primarily determined by the composition and micro-architecture of the tissue, especially of the superficial zone (Pellaumail et al., 2002). But it was noted that enzymatic degeneration did not significantly change reflection while reflection at the surface of the spontaneously repaired tissue was significantly lower than the normal cartilage tissue (Laasanen et al., 2006).

2.4.3 Effects on mechanical properties

Many previous studies investigated the alterations of mechanical properties after articular cartilage was degraded. It was revealed that modulus of the damaged PG-collagen matrix decreased (an averaged 48% decrease from the normal value of 21 MPa, Narmoneva et al., 2002; gradually reduced from 10.1 MPa, Flahiff et al., 2004; ~ 10% reduction from 13.8 MPa, Laasanen et al., 2003a). Using ultrasound indentation technique, the combination of Young's modulus with reflection was applied to diagnose health cartilage from the degenerated cartilage and meanwhile to distinguish collagen damage from PG depletion (Fig. 2.3) (Saarakkala et al., 2003; Toyras et al., 1999). Meanwhile, Laasanen et al. (2003b) suggested the measurements of dynamic and equilibrium modulus could also be applied to diagnose the component degradation because the dynamic and equilibrium properties were determined by collagen fibres and PGs, respectively. In compression test, the equilibrium compressive moduli of the PG-degraded cartilage specimens were significantly lower that those of normal cartilage (Qin et al., 2002; Zheng et al., 2001), and a similar result was obtained for the surgery-induced OA cartilage with a depletion of PG content (LeRoux et al., 2000). In addition, cartilage stiffness decreased while PGs or collagen fibrils in the superficial zone were digested (Laasanen et al., 2002; LeRoux et al., 2000; Lyyra et al., 1999; Nieminen et al., 2002). Furthermore, it was found that there was a direct correlation between the shear modulus and the orientation of collagen fibres in the superficial zone of articular cartilage (LeRoux et al., 2000). And it was found that the creep rate significantly increased after trypsin treatment (Laasanen et al., 2002; Nieminen et al., 2002). A brief

review of the mechanical changes of the degenerated cartilage measured using ultrasound was listed in Table 2.3.

2.4.4 Relationship between mechano-acoustic properties and aging

It is well known that OA is regarded as an age-related disease with a high prevalence in the elderly. Using animal model, it was found that there was no lesion in the articular cartilage of the knee for young adult rat, but with the increase of age the lesions became more severe (Smale et al., 1995). Previous studies have demonstrated that PG content decreases with growth and, in contrast, collagen content increases with maturation (Cherin et al., 2001). Because of the component- and structure-dependence of the mechanical and acoustic properties aforementioned, age-related changes in the composition and morphology of articular cartilage affect the mechanical and acoustic parameters (Cherin et al., 1998, 2001). In animal models, it has been found that both instantaneous and equilibrium Poisson's ratio are significantly higher for adult cartilage compared with fetal and young cartilages, and there was a stronger swelling pressure in the adult cartilage than in the immature cartilage (Wong et al., 2000). Moreover, the thinning of the cartilage thickness of the older people might be a result of aging (Adam et al., 1998; Cherin et al., 2001). Observing the rat cartilage model, Cherin et al. (1998) found that reflection coefficient remained unchanged with aging while backscatter coefficient declined as a function of aging.

2.5 Summary of Literature Review

This chapter has reviewed previous studies covering from the basic component-structure-function knowledge of articular cartilage to the biphasic and triphasic

modeling theories, from the compression, tension and indention properties to acoustic parametric extraction, and from the weighting gain method, the optical method to MRI, OCT, and ultrasound. Based on the broad background, the swelling behavior of articular cartilage, as a special, complex and vital property, has been focused on in this PhD study. The negative charges on the PGs are the origin of swelling pressure. The interaction between PGs and collagen network and water content plays an important role in swelling. Changes in composition and structure will lead to the change in the swelling behavior of articular cartilage. In comparison with other methods and techniques, high frequency ultrasound has more advantages for monitoring and quantifying the swelling behavior of articular cartilage. The transient and inhomogeneous intra-tissular swelling-shrinkage and hydration behaviors and the progressive enzyme-digestion procedure could be displayed by A-mode, M-mode, and B-mode ultrasonic modalities *in situ* and both swelling and acoustic parameters could be obtained for assessing articular cartilage.

CHAPTER 3 METHODS

This chapter systematically introduces the methodology of this study including specimen preparation, the set-up of the ultrasound swelling measurement system (USMS), experimental protocols, and data processing and analysis. The main experiments (Fig. 3.1) are listed as follows.

1. Feasibility studies on the validation and repeatability of the USMS;
2. Dimension-dependence of the swelling behavior using nominal 50 MHz focused ultrasound transducer with a beam diameter of 0.1 mm;
3. Progressive degeneration of the OA-like articular cartilage induced by trypsin digestion;
4. Osmosis-induced swelling and hydration of the normal and degenerated articular cartilage measured using the manually controlled 3D USMS;
5. Extraction of acoustic parameters of articular cartilage;
6. Prediction of mechanical properties using the bi-layered triphasic model based on the ultrasound-measured experimental data;
7. The shrinkage-swelling behavior monitored using the motor-controlled 3D USMS.

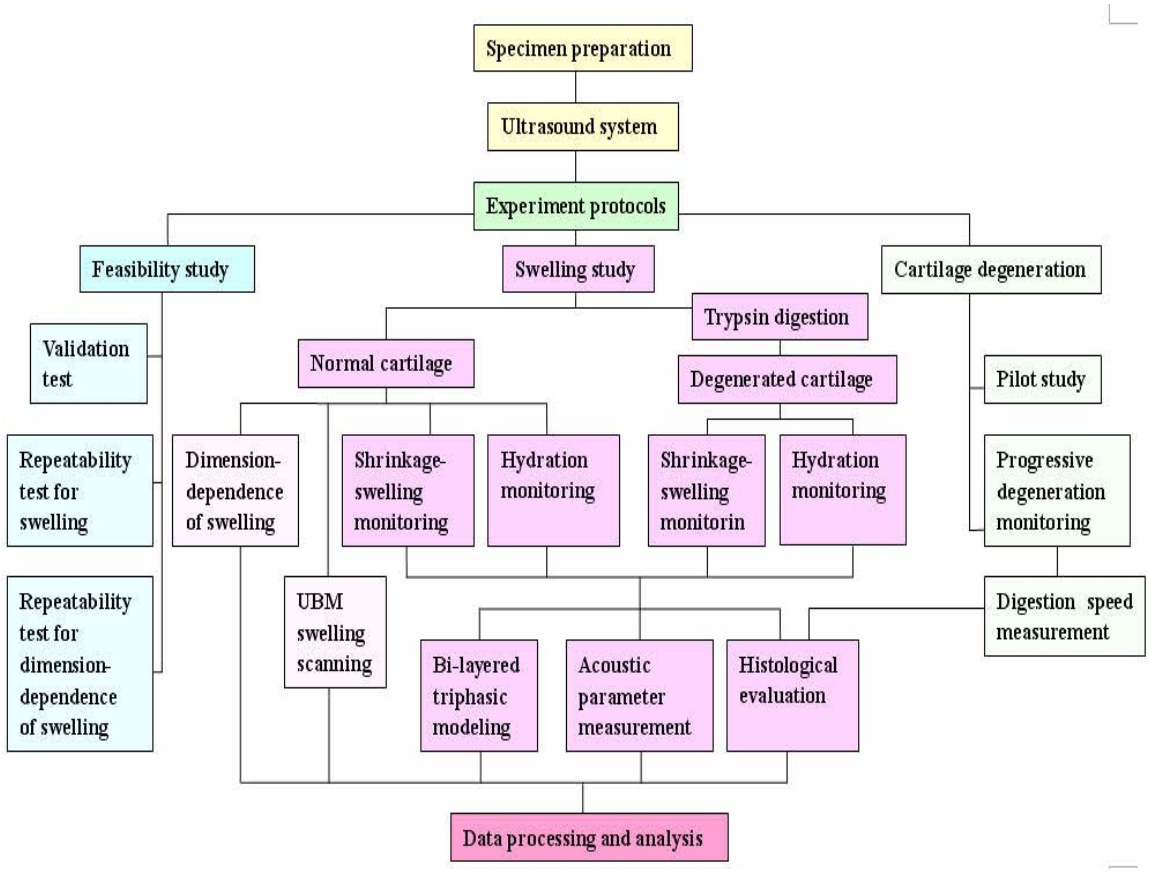

Fig. 3.1 Block diagram of the contents of this study.

3.1 Specimen Preparation

Fresh mature bovine patellae without obvious lesions were obtained within 6 hours of slaughter and stored at -20°C until further specimen preparation. The intact patella was excised into four parts (Fig 3.2) using a band saw machine. The four quadrants were anatomically named according to the medial or lateral side of the patella, i.e. MU (Medial Upper), ML (Medial Lower), LU (Lateral Upper), and LL (Lateral Lower). The extra bone tissues were cut off to make the surface of articular cartilage and the bottom of the bone approximately parallel. During specimen preparation, careful attention was

paid to keep the surface of articular cartilage undamaged and moist with the physiological saline solution.

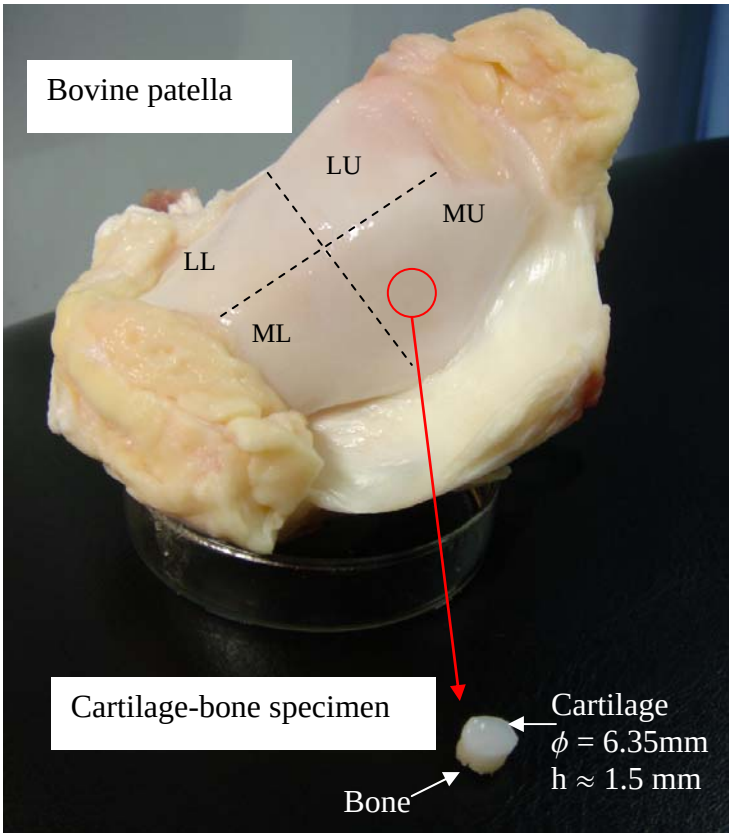

Fig. 3.2 Schematic of specimen preparation. One patella is excised into four parts: MU (Medial Upper), ML (Medial Lower), LU (Lateral Upper), and LL (Lateral Lower). A cartilage-bone sample with a diameter of 6.35 mm and a cartilage layer of ~1.5 mm is prepared from the MU side.

Cartilage-bone plugs with cartilage thickness ranging from 0.8 to 2.7 mm were cored out of the flat area of the MU slab (n = 95) using a metal punch with a diameter of 6.35 mm (Fig. 3.2) (Patil et al., 2004; Wang and Zheng, 2006; Zheng et al., 2001, 2002). 10 plugs were used for the validity test; 9 for the repeatability test; 20 for the shrinkage-swelling of normal specimens; 10 for the dimension-dependence test; 10 for the

progressive degeneration monitoring; 6 for the pilot study on trypsin digestion; and 30 for monitoring the shrinkage-swelling before and after trypsin digestions. Specimens were wrapped in wet gauze soaked with physiological saline, and stored at -20°C until testing. The tested specimen was removed from the -20°C condition to the 3°C condition at night before the test day. In the test day, the specimen was removed from the refrigerator, put into the physiological saline solution, and thawed for one hour at room temperature (21 ± 1°C) to approach equilibrium (Setton et al., 1998; Wang and Zheng, 2006; Zheng et al., 2004a).

It was reported in previous studies that cryopreservation storage and thawing of cartilage specimens would not affect the mechanical and acoustic properties of articular cartilage (Agemura et al., 1990; Dhillon et al., 2001; D'Astous and Foster, 1986; Kim et al., 1995; Kiefer et al., 1989; Kwan et al., 1992).

3.2 Ultrasound Swelling Measurement System (USMS)

In this study, two non-contact 3D ultrasound systems were established. One was a manually controlled 3D USMS, which was designed to monitor the swelling behavior of articular cartilage at one observation site using M-mode ultrasound image. The other was a motor-controlled 3D USMS, which could monitor cartilage swelling along the cross-section of the specimen using UBM B-mode images.

3.2.1 Manually controlled 3D USMS

As shown in Fig. 3.3, the manually controlled 3D USMS mainly includes an ultrasound transducer, an ultrasound pulser/receiver, a 3D translating platform with specimen container, and a computer with an 8-bit analog/digital (A/D) converter and custom-

designed software. It was used to monitor the deformation of cartilage specimen under osmotic loading at one observation site in a non-contact and non-destructive way.

An ultrasound pulser/receiver (Model 5601A, Panametrics, Waltham, MA, USA) was used to drive a nominal 50 MHz focused broadband polymer (PVDF) ultrasound transducer with a focal length of 12.7 mm, a –6 dB focal zone diameter of 0.1 mm and a focal zone depth of 0.95 mm (Panametrics, Waltham, MA, USA). The axial and lateral resolutions of the focused ultrasound beam were approximately 100 μm and 50 μm, respectively. The central frequency of this transducer was 35 MHz, and its –6 dB bandwidth ranged from 24 to 46 MHz. Ultrasound waves radiated via the saline solution and propagated through the tissue. A-mode ultrasound radiofrequency (RF) signals reflected or scattered within articular cartilage were received and amplified by the ultrasound pulser/receiver. The bandwidth of the receiver was set to 5 to 75 MHz. The maximum gain of the pulser/receiver was used in this study to acquire the sufficient amplitude of the ultrasound echoes. The attenuation (unit in dB) of the pulser/receiver was set at zero to obtain the saturated RF signals or at a certain dB value to achieve the unsaturated RF signals with maximum amplitude. The received ultrasound signals were digitized by an 8-bit A/D converter card with a sampling rate of 500 MHz (Model CompuScope 82GPCI, Gage, Canada) installed in the computer. The A/D converter was triggered by the trigger signal out of the pulser/receiver. The resolution for the flight-time measurement was 2 ns. Assuming an average ultrasound speed in articular cartilage of 1675 m/s (Patil et al., 2004), the corresponding displacement resolution in the tissue could approach to approximately 1.7 μm.

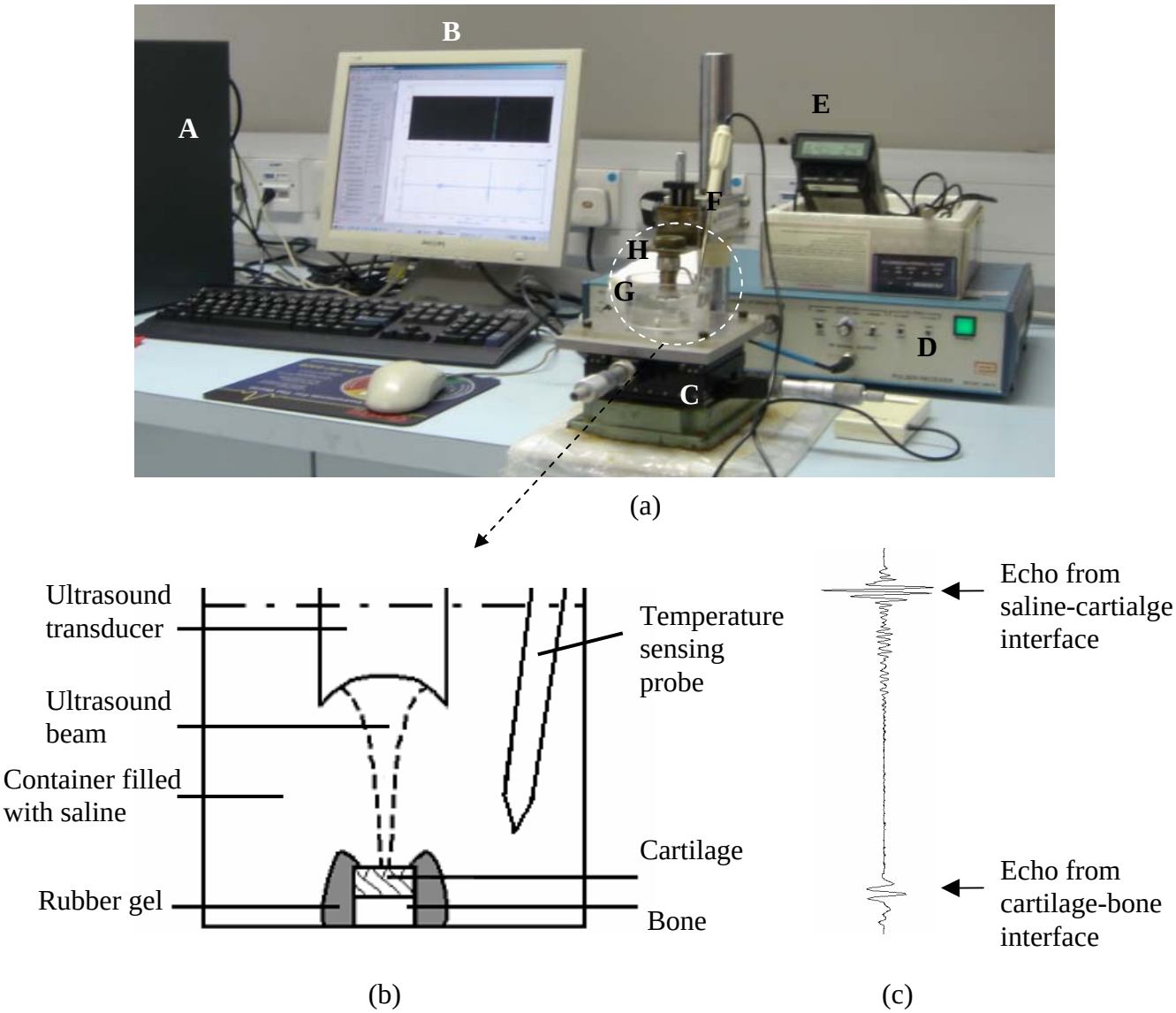

Fig. 3.3 Experimental set-up of the manually controlled 3D USMS. (a) Overall set-up including **A**: computer with A/D card and signal processing software; **B**: computer monitor displaying the software interface; **C**: 3D translating platform; **D**: ultrasound pulser/receiver; **E**: thermo-hygrometer; **F**: probe thermometer; **G**: container filled with saline solution; and **H**: ultrasound transducer. (b) An enlarged view for the essential components. Specimen is installed on the bottom of the container and immerged in the saline solution. (c) A-mode ultrasound echoes were collected from ultrasound transducer.

In fact, articular cartilage can be divided into 4 zones: the superficial zone, the middle zone, the deep zone and the calcified zone (Mankin et al., 2000). The first three zones

compose the uncalcified cartilage (Mankin et al., 2000; Mow et al., 2005). The tidemark can be considered as the interface between the deep zone and the calcified zone (Mankin et al., 2000; Mow et al., 2005). The calcified zone is much stiffer in comparison with other zones. In one of the thickness measurement techniques called "needle punching", the reaction force will have a sudden change when the needle tip reach the tidemark (Jurvelin et al., 1995). Therefore, the ultrasound reflection from the uncalcified-calcified cartilage interface would be very strong because of the large impedance mismatch. In comparison with the optical measurement, it was confirmed that the second ultrasonic reflection used in the thickness measurement was from the tidemark (Jurvelin et al., 1995; Modest et al., 1989). Although it is expected that there is another echo comes from the interface between the calcified zone and the subcondral bone, it is overlapped with the echo from the uncalcified-calcified cartilage interface. This makes it technically difficult to measure the deformation of the calcified region. Moreover, since the calcified zone is much stiffer than the cartilage, its deformation during the swelling process (involving approximately 1% deformation, Eisenberg and Grodzinsky, 1985; Narmoneva et al., 2002; Wang and Zheng, 2006) would be negligible. Therefore, the current study focused on the uncalcified cartilage. To simplify the description, the "uncalcified-calcified cartilage interface" was presented as the "cartilage-bone interface" in this thesis. As shown in Fig. 3.3c, the two large echoes along the echo train (the ultrasound scattering signals through the matrix) were reflected from the saline-cartilage interface and the cartilage-bone interface, respectively.

A-mode signals were continuously recorded at a sampling rate of approximately one frame per 0.6 second. The ultrasound RF signals were displayed on the monitor in real-

time and automatically saved into the hard disk for offline data analysis. Meanwhile, the M-mode image constructed by A-mode signals (Fig. 3.4) demonstrated the shifts of the ultrasound echoes from the cartilage tissues at different depths during the shrinkage and swelling processes. The brightness or colour in the M-mode image represents the amplitude of the ultrasound RF signals.

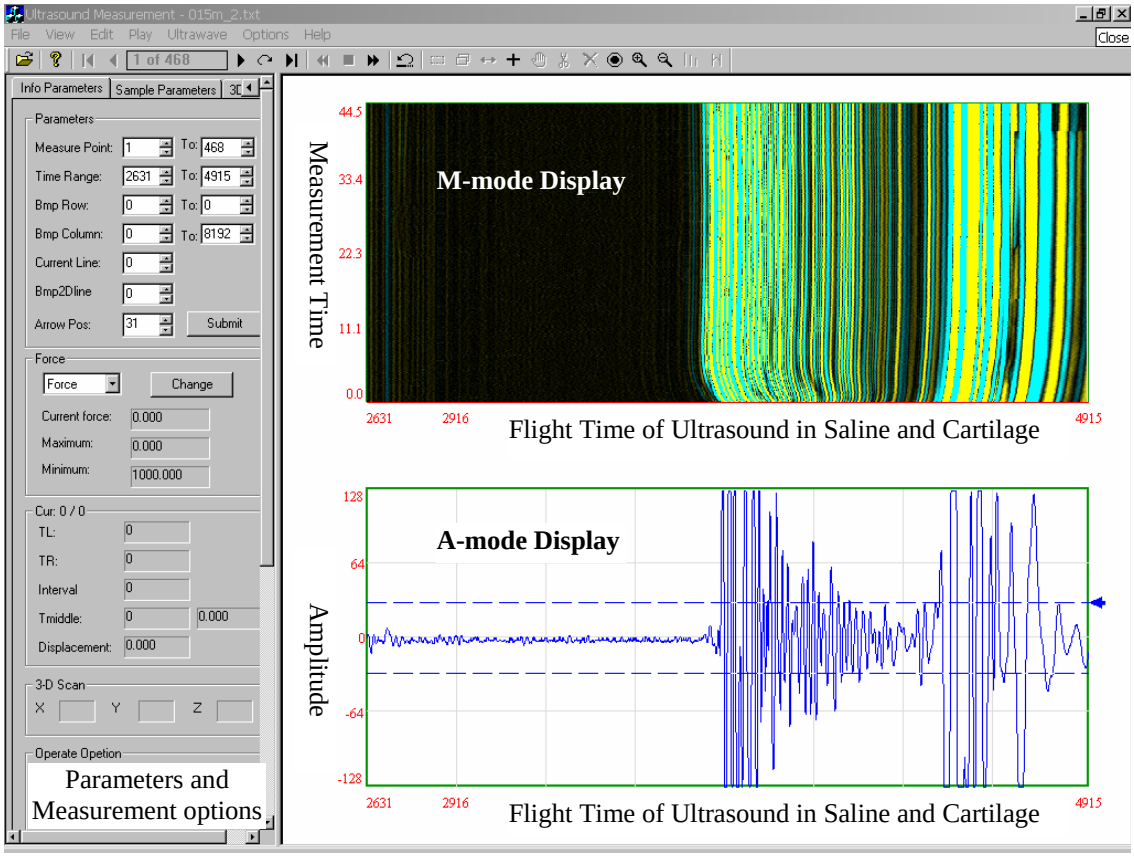

Fig. 3.4 M-mode image and A-mode signals of cartilage swelling were displayed in real-time using the custom-designed program. M-mode image shows the transient depth-dependent deformation of the cartilage specimen at the observed site.

During the test, the cartilage-bone plug was fixed on the bottom of the container, surrounded by rubber gel (Blu-Tack, Australia), and submerged in the saline solution. The outer ring of the surface of the cartilage disc with a width of approximately 0.6 mm

was gently covered by the rubber gel. Therefore, the diffusion of ions and water was not allowed from the sides of the specimen and the free swelling in the central portion of the specimen could be treated as an *in-situ* condition. A 3D translating platform with micrometers (Model R301MMX/2201MMXY, Ball Slide Positioning Stages, Deltron Precision Inc.) was designed to align the focused ultrasound beam into the cartilage specimen. One low-profile micrometer was attached to the ultrasound transducer in the *z* direction to vertically move the ultrasound beam and the other two were fixed in the *x* and *y* directions respectively to horizontally translate the specimen. Using this device, the ultrasound transducer could be moved to the position over the central portion of the cartilage specimen with the focal zone of ultrasound beam located inside the cartilage layer to obtain the maximum echo amplitude. The temperature of the bathing solution was monitored using a digital thermometer with a stainless steel probe (CheckTemp 1, EUROTRONIK, German). The room temperature and humidity were detected using a digital thermo-hygrometer (Model #411, OMEGA Engineering Inc., Stamford, CT, USA).

A custom-designed program developed in our previous study for the ultrasound measurement of motion and elasticity (UMME) of the tissue (Zheng et al., 2001, 2004a) was used for data collection, signal processing and display. The program allowed the user to select a portion of ultrasound signals by setting tracking windows. A cross-correlation algorithm (introduced in section 3.8.2) was used to track the shift of the selected ultrasound echoes so as to calculate the corresponding time of flight, which could be used to obtain the deformation of articular cartilage according to the sound speed in the saline or in the cartilage.

3.2.2 Motor-controlled 3D USMS

The motor-controlled 3D USMS allowed the ultrasound transducer scanning along the diameter direction to investigate the inner section of cartilage specimen during swelling and shrinkage processes in a non-contact and non-destructive way (Fig. 3.5). The same computer, A/D card and ultrasound pulser/receiver were used in this motor-controlled 3D USMS. The 3D translating device (Parker Hannifin Corporation, Irvine, CA, USA) consisted of a compumotor controller, stepper-motor, and a 3D translating frame. A smaller sized focal ultrasound transducer with a central frequency of 42 MHz, the –6 dB bandwidth ranging from 26 to 58 MHz, and a focal length of 12 mm was fixed at the end of the mechanical arm. The movement of the arm was controlled by the compumotor controller. The position of the transducer was adjusted along the *z* direction to maximize the ultrasound signals reflected from the specimen. The motion parameters of the mechanical arm were set using the custom-designed program. And then the transducer could automatically translate along the diameter of the specimen in the *x* direction or the *y* direction to obtain UBM B-mode images. The vertical and horizontal precisions of the 3D translating device were up to 1 μm. Fig. 3.5b shows the elements of the experimental set-up. The control signals were sent from the computer to the motor-controller. The RF ultrasound signals reflected from the cross-section of articular cartilage were received and amplified by the pulser/receiver and digitalized by the A/D converter. The digitalized signals and images were recorded for further offline analysis.

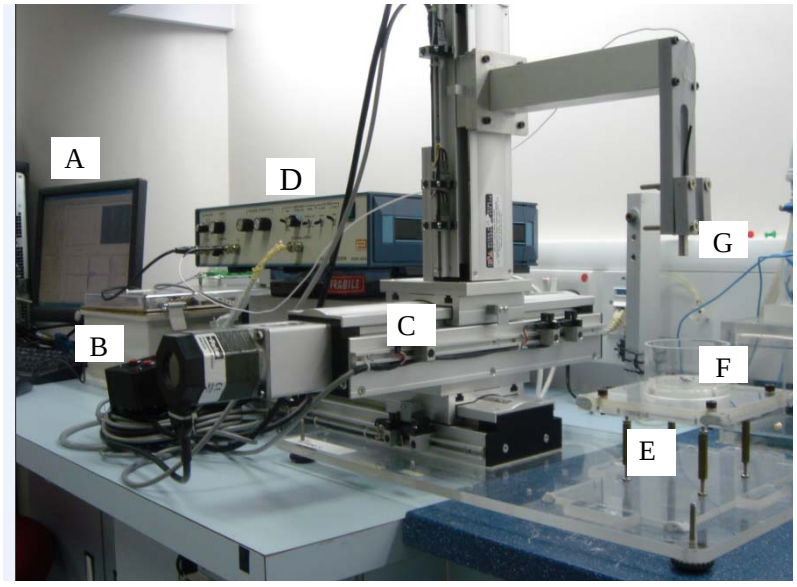

(a)

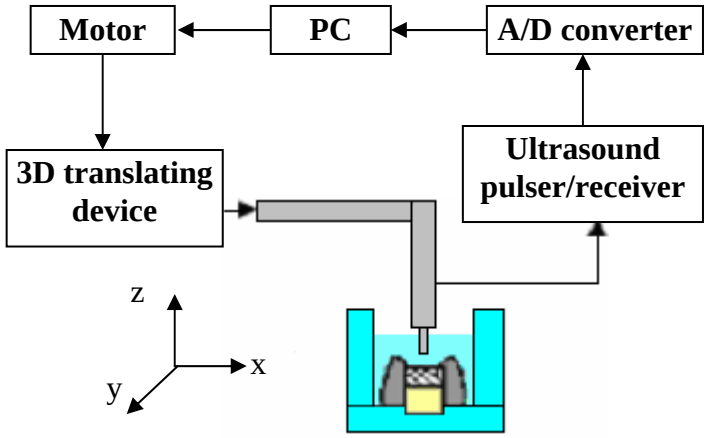

(b)

Fig. 3.5 Experimental set-up of the motor-controlled 3D USMS. (a) Overall set-up. **A**: computer with A/D card and signal processing software; **B**: motor controller; **C**: 3D scanning frame; **D**: ultrasound pulser/receiver; **E**: platform to support container; **F**: container filled with saline solution; and **G**: ultrasound transducer. (b) Block graph of the motor-controlled 3D USMS.

Ultrasound biomicroscopic image reconstructed by A-mode signals (Fig. 3.6) demonstrates the ultrasound echoes from one section of the cartilage tissues at different depths during the shrinkage and swelling processes. M-mode image shows the transient depth-dependent deformation of the cartilage specimen at one observation site with measurement time. One frame of UBM image shows the B-mode image of depth-

dependent sectional deformation of the cartilage specimen. The brightness or colour in the UBM image represents the amplitude of the ultrasound RF signals.

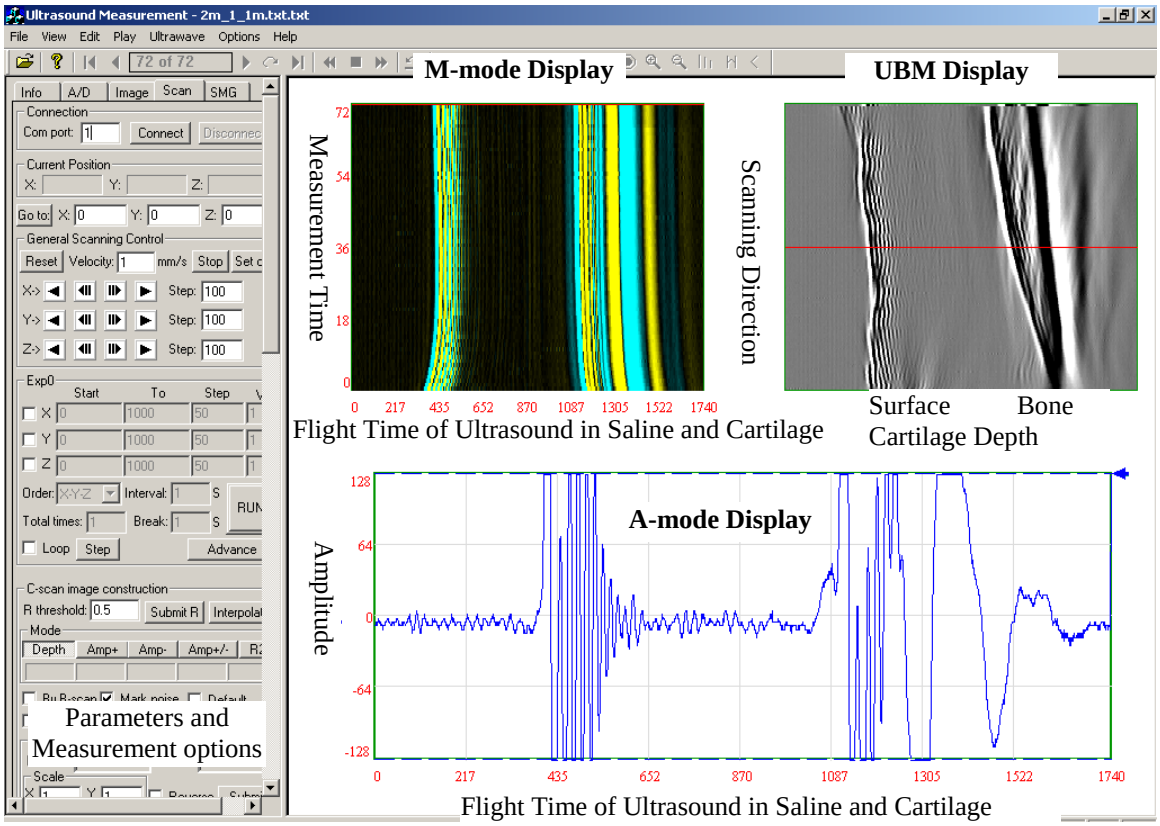

Fig. 3.6 UBM image (upper right), M-mode image (upper left) and A-mode RF signals (lower) of cartilage shrinkage were displayed in real-time using the custom-designed program. The grey levels of the UBM image linearly represent the amplitude of the RF signals.

A custom-designed program similar to that mentioned in the last section was used for 1D and 2D data collection, signal processing and display. A region of interest (ROI) could be outlined by a rectangle in the first frame of the UBM image series to analyze the distribution of the movement of the interstitial tissue at different depths using automatic segmentation and 2D tracking method (Zheng et al., 2004b).

3.3 Feasibility Studies of Ultrasound Swelling Measurement

Previous studies have widely applied ultrasound combined with indentation (Suh et al., 2001; Toyras et al., 1999) and compression (Fortin et al., 2003; Zheng et al., 2001, 2002) to explore the mechanical and acoustic properties of articular cartilage. The preliminary ultrasound-monitored results of cartilage swelling were achieved in our previous study (Zheng et al., 2004a). In this study, ultrasound as a non-contact novel method was used to quantitatively and systematically measure the transient swelling behavior and progressive degeneration of articular cartilage. Therefore, validation test and repeatability test were performed to evaluate the feasibility of the ultrasound swelling measurement.

3.3.1 Validation test

Ten cartilage-bone specimens were prepared. After thawed, the tested specimen was mounted on the bottom of the container and submerged in physiological saline. The ultrasound transducer of the manually controlled 3D USMS was first moved up and down in the *z* axial direction using the micrometer to locate the focal point at the surface of the cartilage specimen by monitoring the amplitude change of the ultrasound signals. This position of the ultrasound transducer was treated as the reference position. The ultrasound transducer was moved vertically from -250 μm to 250 μm at a step of 50 μm. The ultrasound signals were recorded during the movement procedure (Fig. 3.7).

The time shift (*T*) of the echo from the cartilage surface was measured using cross-correlation algorithm. The sound speed in saline was then calculated at each step and the results obtained for the ten specimens were averaged. The mean value of the sound

speed was represented as c_s. The surface displacement (d) of the cartilage was given by Eq. 3-1.

$$d = c_s \frac{T}{2} \tag{3-1}$$

Following the validation test in the physiological saline solution, the specimen was submerged in the hypertonic saline solution (2 M NaCl solution). When the equilibrium was approached, the above procedure was repeated.

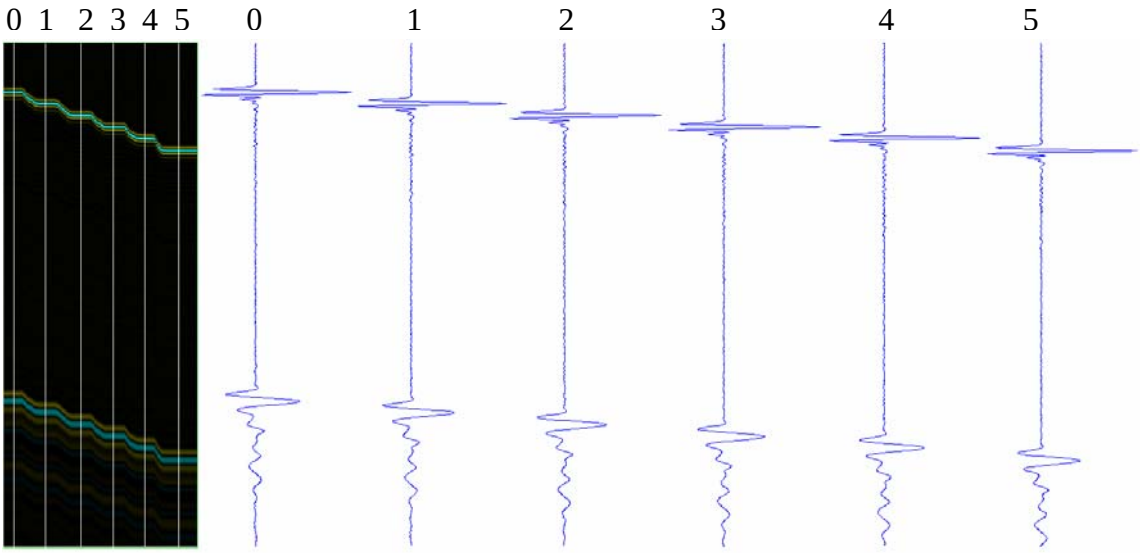

Fig. 3.7 Ultrasound signals were recorded while the ultrasound transducer was moved at a step of 50 μm. "0" represents the reference position of the transducer. Numbers from 1 to 5 indicate 5 steps of transducer movement. RF signals numerically correspond to the positions indicated by the white solid lines in M-mode image.

A similar procedure was adopted for validating the motor-controlled 3D USMS. The specimen was submerged in 0.15 M and 2 M saline solutions, respectively. The ultrasound transducer was first moved up and down in the vertical direction by controlling the motor to locate the same reference point as mentioned above. Then, the ultrasound transducer was moved vertically from 0 μm to 10 μm at a step of 2 μm. The displacement of the surface echoes was calculated using Eq. 3-1.

3.3.2 Repeatability test for shrinkage-swelling measurement

Three specimens were used to test the repeatability of this non-contact ultrasound measurement for the shrinkage and swelling strains of articular cartilage. The specimen was first allowed to reach an equilibrium state in physiological saline. The concentration of the bathing solution was then increased to 2 M (to test shrinkage). After one hour, the concentration was decreased back to 0.15 M (to test swelling). The details of the shrinkage-swelling procedures will be described in section 3.4.2. The process was repeated for three times for each sample under the same controlled environment. The whole shrinkage-swelling process was monitored using the manually controlled 3D USMS. The repeatability of the measurement was assessed by calculating the mean percentage values of coefficient of variation (CV%) (Gluer et al., 1995) and the intraclass correlation coefficient (ICC) for the measurement of the peak shrinkage and swelling strains. The average relative root mean square difference (rRMSD) was also calculated for the transient strains of the full-thickness cartilage layer and the transient time shifts of the cartilage-bone interface.

The peak shrinkage or swelling strain (ε) of the full-thickness cartilage layer was defined as

$$\varepsilon = \frac{d}{h} \tag{3-2}$$

where *d*, the displacement of the cartilage layer, is given by Eq. 3-1. *h* is the thickness of the cartilage layer and given by $h = c_{AC}\frac{T}{2}$, where c_{AC} is the sound speed in the

cartilage tissue (refer to section 3.8.3) and *T* denotes the corresponding flight time of the ultrasound echoes throughout the cartilage matrix during shrinkage or swelling phase.

3.3.3 Repeatability test for dimension-dependence of swelling behavior

Six plugs were divided into two groups: cylindrical (or large) specimens (n = 3) and slim (or small) specimens (n = 3). The slim specimens with a width of 2 mm were obtained by cutting the two sides of the cartilage layer using a surgical scalpel (Fig. 3.8b). Before the test, the specimen was marked in two orthogonal directions using a permanent marker pen. It was then installed onto the container bottom and fixed with rubber gel, on which two dents were correspondingly marked using a blade to match the marks on the specimen (Fig. 3.8a). Then the specimen was submerged in the physiological saline solution to approach equilibrium. The entire monitoring procedure included the shrinkage and swelling phases mentioned in section 3.4.2, which were also induced by changing the concentration of the bathing solution from 0.15 M to 2 M and then back to 0.15 M. In order to test the repeatability of reinstalling the specimen, each specimen was taken out, carefully reinstalled back with the reference of the marks and monitored during the shrinkage and swelling phases. The procedure was repeated for three times. To study the changes of the shrinkage and swelling behavior if the measurement site was moved slightly, each specimen was also tested at three observation sites within a range of –0.5 mm to 0.5 mm, i.e. the distance between the two sites on the left and right and the central position was 0.5 mm (Fig. 3.8b). The three points were selected by manually adjusting the micrometers on the 3D translating platform. The shrinkage and swelling procedure at each site was repeated following the same experimental protocols as mentioned above.

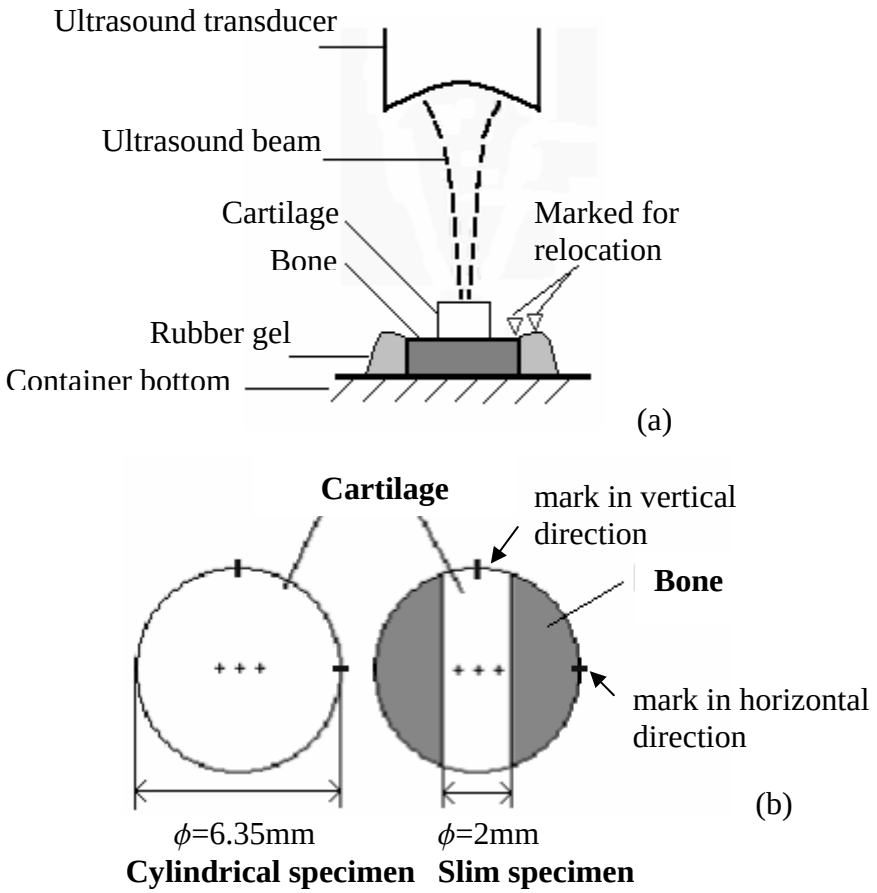

Fig. 3.8 (a) An enlarged schematic of the ultrasound monitoring part. Specimen was installed on the bottom of the container as shown in Fig. 3.3. The width of ultrasound beam in the focal zone is 0.1 mm. Two triangles represent the locations of marks on the specimen and rubber gel, respectively. (b) Platform view of two types of specimens: cartilage-bone cylinder with a diameter of 6.35 mm (left) and cartilage slice with a width of 2 mm attached to the bone (right). Two marks (black short bars) in the horizontal and vertical directions were made to match those on the surrounding rubber gel in (a). Three black spots in the central region represent the different observation sites with an interval distance of 0.5 mm.

3.4 Ultrasonic Characterization of Transient and Inhomogeneous Swelling Behavior of Normal Articular Cartilage

Using the USMS to investigate the swelling behavior of normal bovine articular cartilage, we performed the dimension-dependence test, the dynamic shrinkage-swelling behavior test and the 2D scanning dynamic shrinkage-swelling behavior test.

3.4.1 Study on dimension-dependence of swelling behavior

Ten specimens were prepared to study the dimension-dependence of swelling behavior of articular cartilage. The tested specimen was marked, mounted on the bottom of the container, and tested in the shrinkage and swelling phases as described in section 3.3.3.

After one round of the shrinkage-swelling test, the full-thickness cartilage specimen was removed from the bottom of the container and cut the cartilage tissue using a surgical scalpel from two sides symmetrically (Fig. 3.9). The original cylindrical cartilage-bone specimen was now a slim cartilage-bone specimen with a width of 4 mm. Then the specimen with reduced dimension was reinstalled back to the container. Careful attention was paid to well match the marks on the cartilage and bone with the marks on the rubber gel, so that the specimen could be measured at the approximately same observation point. After the second round of the shrinkage-swelling test was finished, the specimen was taken out and its width was further reduced to approximately 3 mm. This specimen with further reduced dimension underwent a new round of test. This procedure was repeated until the full-thickness cartilage layer (2mm×4mm, Fig. 3.9) was separated from the bone by the scalpel. The cartilage specimen without bone was also monitored for the shrinkage and swelling phases. The same testing protocol was applied to all the specimens with different dimensions (Fig. 3.9).

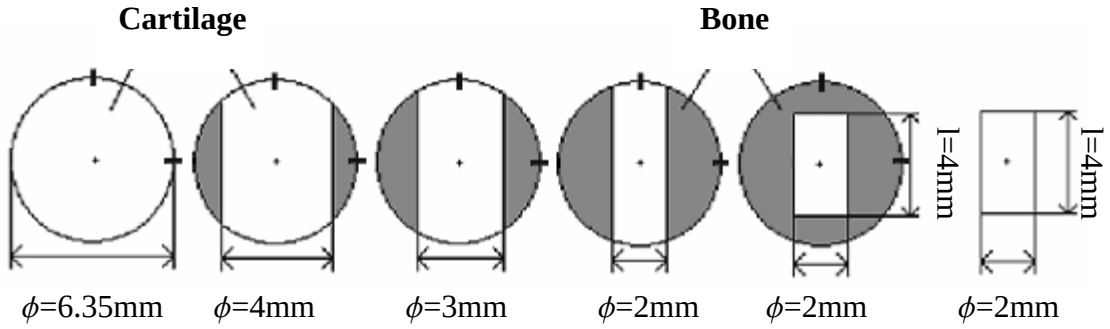

Fig. 3.9 Planform view of the specimens for the dimension-dependence of cartilage swelling measured using ultrasound. Two marks (black short bars) in the horizontal and vertical directions were made to match those on the surrounding rubber gel as shown in Fig. 3.8a. To decrease the dimension of the specimen, the cartilage tissue was cut from two sides using a surgical scalpel. The dimension-decreased cartilage specimens had with a width of 4 mm, 3mm, and 2mm, respectively, and were further reduced to 2mm×4mm (width×length). Finally, the rectangle specimen was separated from the bone. Black spot in the central region represents the observation site.

Three parameters were extracted from the transient swelling and shrinkage behavior. They were the peak strain ($\varepsilon_{\max}$) and the equilibrium strain (ε_{equ}) of the full-thickness cartilage layer and the slope of the linear region of the logarithm of the normalized time shift of the cartilage-bone interface (Tepic et al., 1983). The swelling or shrinkage strain of the full-thickness cartilage layer was calculated using Eq. 3-1 and Eq. 3-2. The slope was used to describe the diffusion speed of ions and water between the cartilage tissue and the bathing saline. The logarithm of the normalized time shift of the cartilage-bone interface ($y(n)$) is defined as

$$y(n) = \log((x_{\max} - x(n)) / x_{\max}) \tag{3-3}$$

where $x(n)$ is the time shift of the cartilage-bone interface measured using cross-correlation algorithm, and x_{max} presents the maximum value of $x(n)$. Then, the slope (β) can be acquired from the linear fitting of the linearly descending part of $y(n)$.

3.4.2 Shrinkage-swelling test

Twenty specimens were prepared to quantify the transient and inhomogeneous shrinkage-swelling behavior of articular cartilage. When the thawed specimen was mounted in the container and reached equilibrium in the physiological saline solution, the bathing saline solution was changed according to the protocol described in Fig. 3.10. The physiological saline solution was rapidly removed using an injection syringe and the container was filled with the 2 M saline. The whole procedure of changing the saline was completed within 30 seconds. Under this condition, the ion concentration inside the cartilage matrix was lower than that of the external bathing solution. This imbalance resulted in a Donnan osmotic loading on the cartilage tissue. With the diffusion of the ions and water, the interstitial swelling pressure generated by the negative charges on the PGs decreased. The dynamic contraction of the cartilage layer at different depths could be observed in the ultrasound signals. The cartilage sample was allowed to equilibrate for approximately one hour. After the new equilibrium was reached, the bathing saline was quickly changed back to 0.15 M NaCl within 30 seconds. Under this condition, the ionic concentration inside the cartilage tissue was higher in comparison with the concentration of the bathing solution. Consequently, the Donnan osmotic pressure with an opposite direction against that during the shrinkage phase caused cartilage swelling. The interstitial swelling pressure generated by the negative charges on the PGs increased. The swelling process was monitored for another hour.

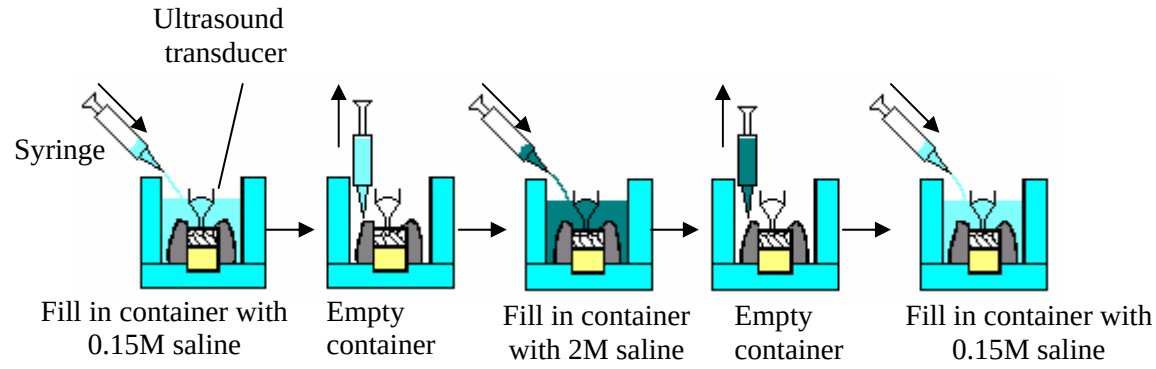

Fig. 3.10 Schematic of the whole procedure of shrinkage and swelling test. A syringe was used to change the bathing solution within 30 seconds.

A-mode signals were sampled in a rate of approximately one frame per 0.6 second during the shrinkage and swelling phases. M-mode image was reconstructed by A-mode signals in real-time. Fig. 3.11 shows the recorded initial and equilibrium A-mode echoes and M-mode image, showing that the full-thickness cartilage tissue swells with the measurement time.

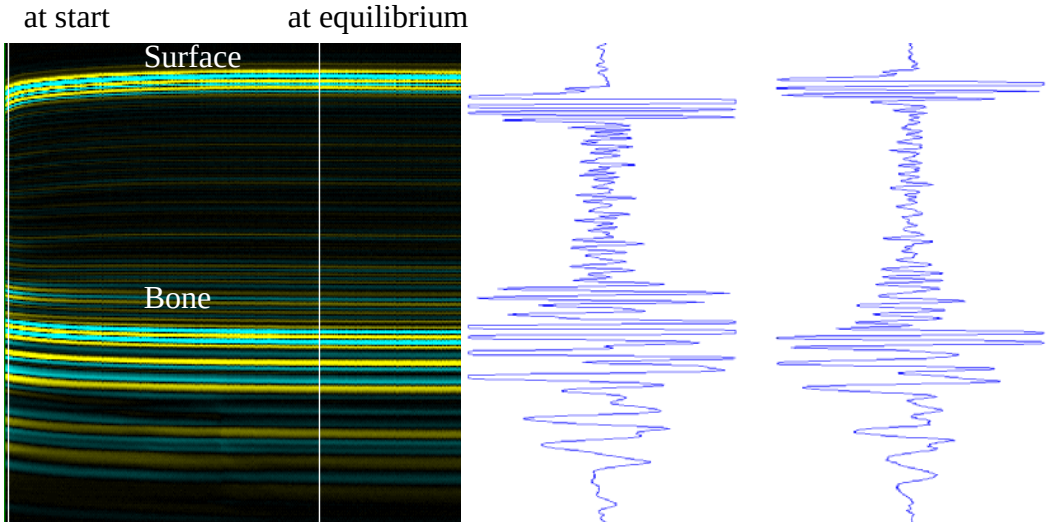

Fig. 3.11 (a) M-mode ultrasound image of swelling; (b-c) A-mode RF signals sampled at the start and equilibrium moments correspond to the positions indicated by the white solid lines in (a), respectively.

In addition to the peak shrinkage and swelling strain (ε) of cartilage layer calculated using Eq. 3-1 and Eq. 3-2, the time to reach the peak value, named as duration, was extracted from the transient swelling and shrinkage behavior.

3.4.3 UBM imaging of swelling behavior

Following the similar protocol described in section 3.4.2, the thawed cartilage-bone plug was mounted in the container, which was installed on the platform of the motor-controlled 3D USMS. The specimen was equilibrated in physiological saline. As shown in Fig. 3.12a, the central section with a length of approximately 5 mm along the diameter direction was selected to be observed. Controlled by the computer and the motor, the transducer could automatically scan from one side (set as the starting point) to the other side (the end point) and then return to the starting point with a higher speed to complete one scanning cycle. The period of one scanning round trip was determined by the speed of transducer translating, step interval, cycle interval and the speed of transducer returning. In this study, it took approximately 48 seconds to collect one frame of UBM imaging. The same protocol of the shrinkage and swelling test described in section 3.4.2 was adopted. The deformation of the intra-cartilage section under the osmotic loading was scanned. Fig. 3.12b shows a frame of UBM image with an image depth of approximately 3 mm and 164 A-mode lines. The number of the sampling lines in the UBM image was determined by the step length.

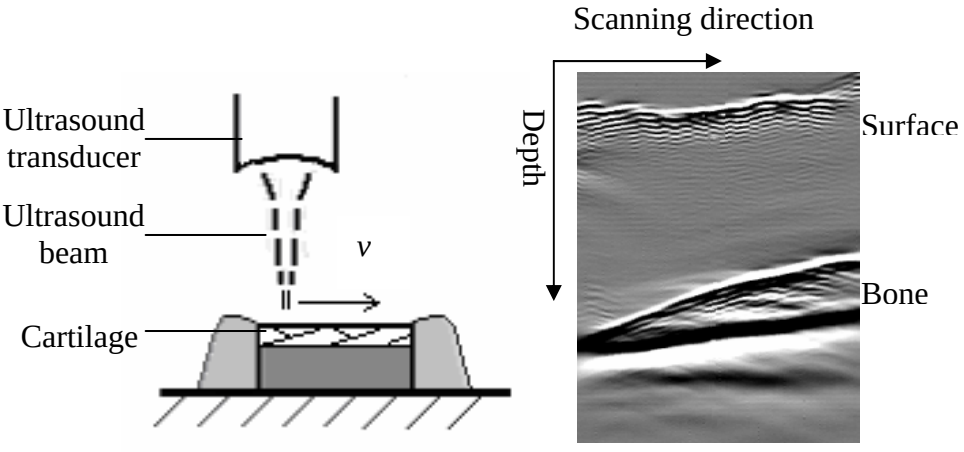

(a) (b)

Fig. 3.12 (a) An enlarged schematic of the ultrasound scanning part. The specimen was mounted on the bottom of the container as shown in Fig. 3.5. The ultrasound transducer was moved along the diameter direction at a speed of *v* set by the software. (b) A frame of UBM image.

3.5 Swelling Behavior of Osteoarthritis-Like Articular Cartilage

In this study, enzyme digestion was used to experimentally induce OA. In comparison with other experimental simulation methods such as surgical method, chemical injection and immobilization, enzyme digestion was relatively easily controlled and less time-consuming (refer to section 2.1.2.2).

3.5.1 Pilot study of degeneration model

Six cylindrical cartilage-bone specimens were divided into three groups, Group A, Group B and Group C. Each group has two specimens. Groups A and B were immersed in trypsin solution (0.25%, GiBco, Canada) for one hour and two hours, respectively, at room temperature (21 ± 1°C). After digestion, the trypsin-treated specimens were washed by physiological saline. Group C served as the control. Half portion of the

surface of the two normal specimens was removed using a surgical scalpel. The digested samples along with the normal specimens were processed (refer to section 3.5.4) for the histological evaluation.

3.5.2 Progressive degeneration of articular cartilage

Ten specimens were prepared for the 3-hour trypsin digestion, which was monitored using the manually controlled 3D USMS. The specimen was mounted on the bottom of the container and allowed reaching equilibrium in the physiological saline solution. Then, the solution was replaced with 0.25% trypsin solution using an injection syringe. According to our preliminary study (Zheng et al., 2004a), the digestion front (echoes from the interface of the digested and undigested tissues) could be monitored. Because the echoes of the digestion front were weak, M-mode image view was set at grey display and a very low saturated brightness level in order to observe the front in real-time.

An interpolation algorithm was used to track the inclined trace formed by the digestion front echoes in the M-mode image. Marks were manually applied along the trace and the software would automatically form the trace line using the linear interpolation. For each specimen, the trace movement was measured for six times and the averaged curve was used to calculate the transient penetration speed of trypsin (the digestion speed).

3.5.3 Swelling behavior of degenerated articular cartilage

Thirty cartilage-bone plugs were prepared (Fig. 3.2) and divided into three groups, Group 10min, Group 20min, and Group 30min. The tested specimen was separated into

two parts (Fig. 3.13). The smaller part (one third of the original dimension) was reserved as the control. The shrinkage-swelling and hydration behaviors of the remained 2/3 portion were tested before and after enzyme digestion.

After thawed in physiological saline, the 2/3 portion sample was tested using the manually controlled 3D USMS. The experiment protocol was as follows.

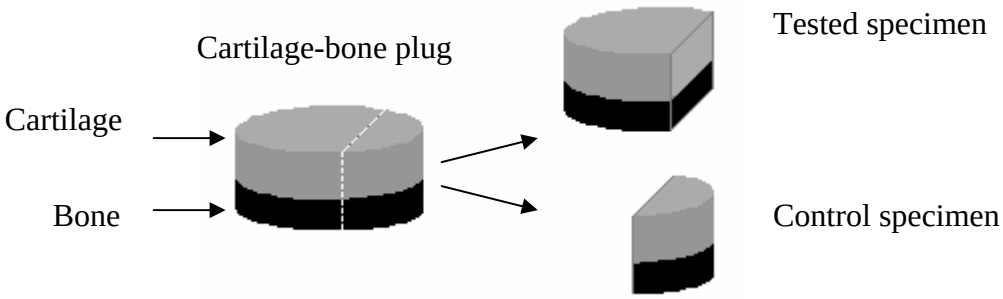

Fig. 3.13 Cartilage-bone plug was cut into two parts. The 1/3 portion was used as the control; the 2/3 portion was measured during the procedures of the shrinkage-swelling, dehydration-hydration tests before and after enzyme digestion.

A. Normal shrinkage-swelling test

The shrinkage and swelling behaviors of all the specimens were examined according to the same protocol as described in section 3.4.2. In addition, at equilibrium of the shrinkage and swelling phases, the saturated and unsaturated echoes were collected for the acoustic parametric analysis, which will be described in section 3.6. In order to obtain the saturated signals, the gain of the ultrasound pulser/receiver was set at maximum and no attenuation (unit: dB) was set. It was found that the echoes from cartilage surface and/or from cartilage-bone interface were saturated while those from the cartilage matrix were unsaturated but with a maximum amplitude. The unsaturated

signals were collected via setting attenuation (unit: dB) by adjusting the knob on the pulser/receiver. The level of attenuation was dependent on the conditions of individual specimens.

B. Normal dehydration-hydration test

After normal shrinkage-swelling test, the physiological saline solution was removed and the specimen surface was exposed to air (humidity = 58±5%, temperature = 21 ± 1°C) and dried using paper tissue. After 45-minute dehydration, the container was refilled with physiological saline. The transient hydration behavior was monitored for 30 minutes. The transient hydration strain of the full-thickness cartilage and the slope of the linear region of the logarithm of normalized hydration strain were calculated using Eq. 3-1, 3-2 and 3-3.

C. Enzyme digestion

Following the dehydration-hydration test, the physiological saline solution was replaced with 0.25% trypsin solution. The specimens of Group 10min, Group 20min and Group 30min were immerged in the enzyme solution for 10 minutes, 20 minutes and 30 minutes, respectively. After the digestion, the enzyme solution was rapidly removed out of the container and the physiological saline solution was refilled in. The residual enzyme digestion lasted for 3 hours and was followed by the post-digestion shrinkage-swelling test.

D. Post-digestion shrinkage-swelling test

After degenerated by trypsin, the PG-degraded specimen remained in the container and the bathing solution was quickly changed with the 2 M NaCl solution. Then, step *A* was repeated, that is, for the degenerated cartilage tissue, the shrinkage and swelling processes and echo collection were performed according to the aforementioned protocol.

E. Post-digestion dehydration-hydration test

Finally, step *B*, the dehydration-hydration test was repeated.

3.5.4 Histological evaluation

After the whole ultrasonic monitoring was completed, both the control (1/3 portion) and the enzyme-digested (2/3 portion) specimens were separated into two halves, respectively. One half was used for histological evaluation; the other was used to measure the layered distribution of the water volume fraction (refer to section 3.7.2).

The safranin O staining contra-stained with fast green and the conventional light microscopy imaging were performed. The specimens for histological evaluation were first preserved and fixed in 10% formalin buffered to pH 7.0 for more than 4 hours at room temperature. Then, the specimens were decalcified in 10% EDTA solution using ultrasound fast decalcificater (Guo et al., 2005) for approximately two days, and the EDTA solution was renewed approximately every 24 hours. The periods of decalcification and EDTA renewal were dependent on the dimension of the individual specimen till the attached bone tissue could be easily cut with a scalpel. The decalcified specimens were infiltrated in Hypercenter Xp tissue processor (Shandon, London, UK)

and embedded into paraffin using Thermolyne Histo-Center II (Shiraimatsu Co. Ltd., Osaka, Japan). Paraffin sections, 4 μm thick, were cut perpendicularly to the cartilage surface using rotary microtome (Leica RM-2135, UK).

The obtained 4 μm thick paraffin sections were immersed in xylene for approximately 15 minutes to clear the wax. Then, the sections were taken into water through a descending series of ethanol (100%, 95%, and 70%). After deparaffinization, the sections were stained with safranin O (SiGMA, CAT NO. F7258, USA) and contra-stained with fast green (SiGMA, CAT NO. S-2255, USA) (Leung et al., 1999). The sections were taken into xylene through an increasing series of ethanol (70%, 95%, 100%, and 100%). After mounting with DPX (BMS Lab supplies, The Hong Kong Polytechnic university), the sections were observed using light microscope imaging system (model FN-S2N, Nikon, Japan). The PG content corresponded to the area fraction of the safranin O-stained zone in the histological image (Leung et al., 1999).

3.6 Extractions of Acoustic Parameters

It has been well known that the ultrasound RF signals result from the interaction between ultrasound waves and tissue structures. Therefore, extraction of the acoustic information (e.g. attenuation, reflection and backscatter coefficient) is an effective method to assess the tissue characteristics. In this study, spectral analysis and extraction of the acoustic parameters were explored via custom-designed MATLAB (V6.5, The MathWorks Inc., USA) programs.

First of all, a series of the unsaturated signals reflected from a steel plate in physiological and hypertonic saline solutions were collected as reference signals to compensate the system-dependent effects (Forster et al., 1990; Fournier et al., 2003). The spectra of these reference signals were used as reference spectra accordingly.

The saturated and unsaturated signals of the tested specimen were recorded as described in section 3.5.3. Using a Hamming window, the central part of the saturated signals and the unsaturated signals from the cartilage surface and the cartilage-bone interface was selected as a region of interest (ROI). The calibrated power spectrum could be written as:

$$S_{cal}(f,z) = \frac{S_T(f,z)}{S_R(f,z)} \tag{3-4}$$

where z is the axial distance of the window centre along the depth direction, $S(f,z)$ is the power spectrum at z. The subscript "*cal*" stands for the calibrated power spectrum, "T" for "Tissue", "R" for "Reference".

Integrated attenuation (IA), attenuation slope (β), and integrated backscatter coefficient (IBS) of the cartilage matrix were calculated based on the spectral analysis of the saturated signals (Forster et al., 1990). Integrated reflection coefficient (IRC) of the cartilage surface and apparent integrated backscatter coefficient (AIB) of the cartilage-bone interface were calculated based on the spectral analysis of the unsaturated signals (Saied and Laugier, 2004). A substitution method (Fink and Cardoso, 1984; Lizzi et al., 1983) and multi-narrowband algorithm (Huisman and Thijssen, 1996; Kuc and

Schwartz, 1979; Roberjot et al., 1996) were used. Moreover, centroid frequency (f_c) and signal amplitude of the echoes reflected from the cartilage surface were calculated. f_c is defined as the frequency weighted by amplitudes divided by the sum of the amplitudes, or Eq. 3-5:

$$f_c = \frac{\sum f_i a_i}{\sum a_i} \tag{3-5}$$

where f_i and a_i present the ith frequency component and its amplitude, respectively. Other aforementioned parameters were introduced in the following subsections.

3.6.1 Attenuation slope (β) and integrated attenuation (IA)

Fig. 3.14 shows the saturated RF signals. The central part of the signals was selected using an ROI window, excluding the saturated signals. Along the depth direction, the selected central part of the saturated signals was divided into narrow bands with a width of 52 points (approximately 0.09 mm) and a 50% overlap. Each gated signal by Hamming window was zero-padded to 512 points and FFT was performed to obtain the power spectrum. The power spectra of the tissue at different depths were the averages from the 40 frames; they were divided by the corresponding reference spectra.

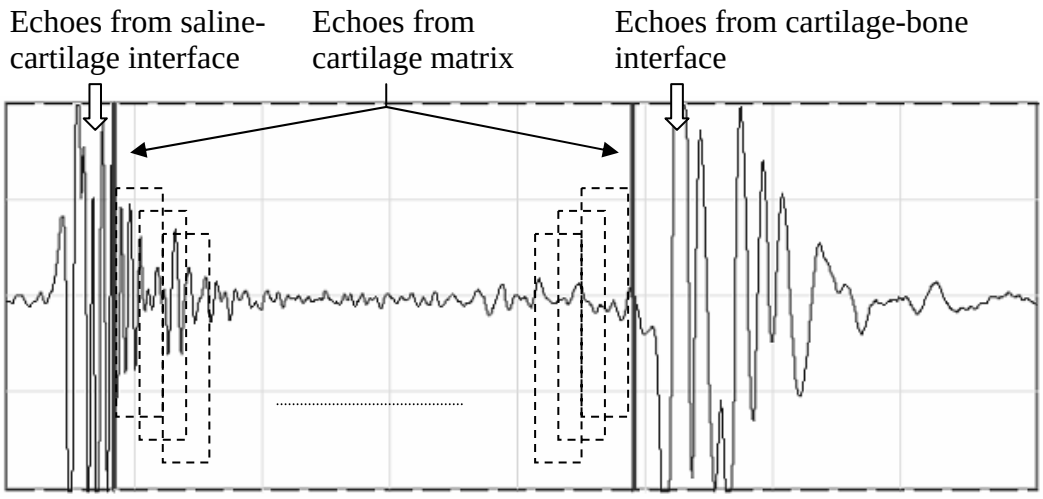

Fig. 3.14 One frame of saturated A-mode RF signals. The echoes from the saline-cartilage interface and the cartilage-bone interface (white arrows) were saturated with the maximum gain used. The unsaturated echoes from the cartilage matrix (black arrows) were selected using ROI window (vertical black bars). Along the depth direction, the signals were divided into narrow bands with a width of 52 points and a 50% overlap.

Assuming that the cartilage was ultrasonically homogeneous, the calibrated power spectrum could be written as:

$$S_{cal}(f,z) = B(f)\cdot 10^{-2\alpha(f)\cdot 2z/20} \tag{3-6}$$

where $B(f)$ is the backscatter transfer function, $\alpha(f)$ is the frequency-dependent attenuation in unit of dB/mm and $2z$ is the whole propagation distance. The relationship between the calibrated spectrum and the propagation distance could be observed more clearly after the logarithm conversion of Eq. 3-6.

$$10\log_{10} S_{cal}(f,z) = 10\log_{10} B(f) - \alpha(f)\cdot 2z \tag{3-7}$$

Attenuation coefficient $\alpha(f)$ was calculated by a regression of the power spectra with respect to the corresponding penetration depth of the cartilage layer. The scope of frequency components was determined based on the central frequency of the transducer. In this study, the central frequency of the transducer was 35 MHz, and the scope of the –6 dB bandwidth ranged from 24 MHz to 46 MHz. A linear frequency dependence of attenuation could be assumed in the cartilage tissue (Forster et al., 1990). It could be expressed as:

$$\alpha(f) = \beta \cdot f + \alpha_0 \tag{3-8}$$

where β is the attenuation slope in unit of dB/mm/MHz, also named as broadband ultrasonic attenuation (BUA) (Langton et al., 1984; Truscott and Strelitzki, 1998). Integrated attenuation (IA, unit: dB/mm) over the frequency bandwidth which characterizes the attenuation coefficient of the tissue was defined here as:

$$\mathrm{IA} = \frac{1}{f_2 - f_1}\int_{f_1}^{f_2} \alpha(f) df \tag{3-9}$$

where $f_1 = 24\,\mathrm{MHz}$ and $f_2 = 46\,\mathrm{MHz}$ according to the –6 dB bandwidth of the transducer.

3.6.2 Integrated backscatter (IBS)

Backscatter coefficient is a quantitative index of the level of acoustic energy backscattered from the cartilage internal structure. In this study, the systemically calibrated spectra were logarithmically transformed to obtain the backscatter spectra $B(f)$ of the cartilage matrix. Integrated backscatter (IBS, unit: dB) was defined as follows:

$$\mathrm{IBS} = \frac{1}{f_2 - f_1}\int_{f_1}^{f_2} B(f)df \qquad (3\text{-}10)$$

where $f_1 = 24\,\mathrm{MHz}$ and $f_2 = 46\,\mathrm{MHz}$ are the lower and upper limits of the frequency range used, respectively. It should be noted that this backscatter was only related to the middle part of the tissue excluding the top superficial zone and the calcified cartilage zone.

3.6.3 Integrated reflection coefficient (IRC) and apparent integrated backscatter (AIB)

While ultrasound waves travel through the saline solution and reach at the saline-cartilage interface, a part of the incident sound will be reflected and the left part transmits through the cartilage superficial zone. Therefore, the reflection coefficient was related to the properties of the surface zone (Adler et al., 1992; Cherin et al., 1998; Jaffre et al., 2003; Nieminen et al., 2002; Toyras et al., 1999, 2002). IRC is a useful index for evaluating the early or slight pathological changes in the cartilage tissue. In this study, the ultrasound beam was perpendicular to the cartilage surface to avoid the measurement errors induced by the oblique incidence. Moreover, during the experiment, the ultrasound transducer was constantly adjusted to the position over the central portion of the specimen with the focal zone of ultrasound beam located inside the cartilage layer to obtain the maximum echo amplitude.

The backscatter coefficient also has been used in the investigation of changes in subchondral bone induced by the chemical injection (Jaffre et al., 2003). In this study, this parameter was defined as apparent integrated backscatter (AIB).

Fig. 3.15 shows the unsaturated ultrasound signals. The echoes from the saline-cartilage and cartilage-bone interfaces were selected using two ROI windows. Hamming windows with a width of 50 points and 100 points were used to gate the signals for the two groups of echoes, respectively. Similarly, the systemically calibrated spectra were logarithmically transformed to obtain the reflection spectra $R(f)$ of the cartilage surface and the backscatter spectra $B(f)$. AIB was calculated using Eq. 3-10, and IRC was obtained by replacing $B(f)$ in Eq. 3-10 with $R(f)$.

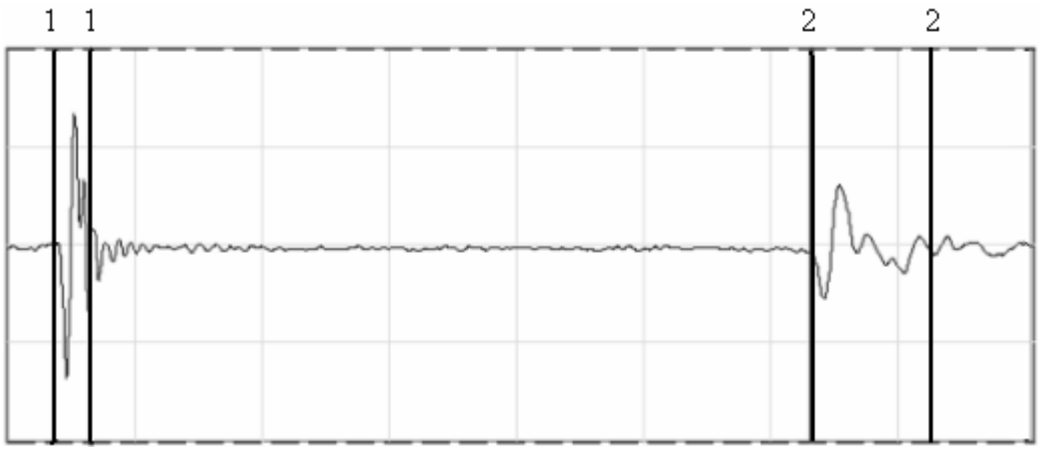

Fig. 3.15 One frame of unsaturated A-mode RF signals. The echoes from the saline-cartilage interface (window 1) and from the cartilage-bone interface (window 2) were selected using two ROI windows.

3.7 Bi-layered Triphasic Model of Swelling Behavior

3.7.1 Triphasic theory

In this study, the cartilage-bone specimen was represented as the cylindrical triphasic material rigidly attached to the bone layer. At the observation site of the central region with a diameter of approximately 0.1 mm, it was assumed that only axial deformations happened due to the osmotic loading. According to the triphasic theory (Lai et al., 1991)

and the extended layered model (Narmoneva et al., 2001), the total stress in the isotropic porous-permeable mixture of the fluid, solid and ion phases in cartilage, σ, was written as follows,

$$\sigma = \sigma^s + \sigma^w + \sigma^+ + \sigma^- = -pI + \lambda_s tr(E)I + 2\mu_s E \qquad (3\text{-}11)$$

where the indices *w*, *s*, +, - denote quantities associated with water, solid, cation and anion, respectively; *E* is the infinitesimal strain tensor induced by decreasing the concentration of the bathing saline from 2 M (the hypertonic reference configuration) to 0.15 M; p is the fluid pressure; λ_s and μ_s are Lame coefficients of the solid matrix. According to Eq. 3-11, the total stress in cartilage at equilibrium under free-swelling conditions consists of two components, the interstitial fluid pressure (*p*) and the elastic stress dependent on the material properties of the solid matrix. The relationship between aggregate modulus (H_A) and the material parameters can be described as $H_A = \lambda_s + 2\mu_s$.

It was assumed in the model that the contribution of the entropic effects to cartilage swelling pressure was zero and there was no externally applied hydrostatic pressure (Narmoneva et al., 2001). Therefore, the fluid pressure (*p*) approximately equalled to the Donnan osmotic pressure π, i.e., all swelling effects arising from the electrostatic interaction between negatively charged PGs and ions. A linear constitutive expression for π can be obtained from the boundary conditions for equivalent chemical potential of water and NaCl ions across the free surface:

$$\pi \approx RT\left(\left[(c_0^F)^2 + (2c^*)^2\right]^{1/2} - 2c^* - tr(E)\cdot(c_0^F)^2/(\phi_0^w[(c_0^F)^2 + (2c^*)^2]^{1/2})\right) \qquad (3\text{-}12)$$

where R is gas constant, T is absolute temperature and c^* is the NaCl concentration; Fixed charge density (c_0^F) and water volume fraction (ϕ_0^w) values of articular cartilage can be measured after equilibration in 2 M NaCl. The essential concept of the theoretical modeling is a principle of balance of forces, i.e., the sum of all forces inside cartilage is zero at equilibrium, including the osmotic pressure, the applied pressure and the tensile stresses in the collagen network.

3.7.2 Inhomogeneous bi-layered model of cartilage swelling

Narmoneva et al. (2001) modeled articular cartilage to be a bi-layered structure in terms of aggregate modulus, Ha, where Ha_2 in the upper layer (near the cartilage surface) linearly increased with depth to Ha_1 constant in the lower layer (Fig. 3.16a). Based on our earlier observation that the modulus in the deep layer also increased with depth (Zheng et al., 2002), we proposed an improved bi-layered model with four parameters (Wang et al., 2006). In this model (Fig. 3.16b), we used three Ha values to describe the bi-layered structure. In the deep region (Layer1), which was attached to the subchondral bone, the aggregate modulus varied linearly from Ha_1 near the cartilage-bone interface to the value Ha_2 at the Layer1-Layer2 interface. In the upper layer (Layer2), the aggregate modulus was also proposed to vary linearly from Ha_2 to Ha_3 at the articular surface. The depth of different cartilage layers from the cartilage-bone interface to the surface is normalized. The parameter h_1 is defined as the normalized depth of Layer 1. Therefore, these four parameters Ha_1, Ha_2, Ha_3 and h_1 are determined by the magnitude and distribution of the axial swelling-induced strain E together with the other parameters including c_0^F, ϕ_0^W, and v_s.

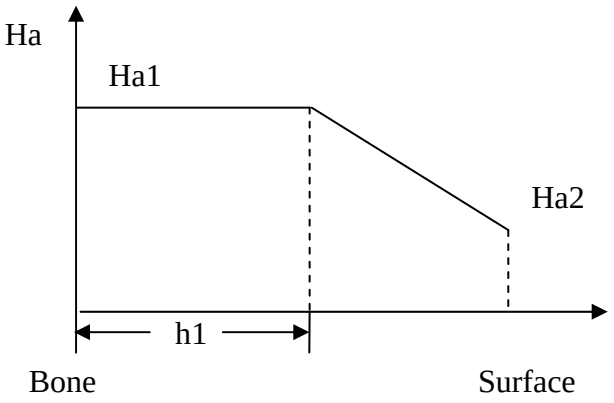

(a)

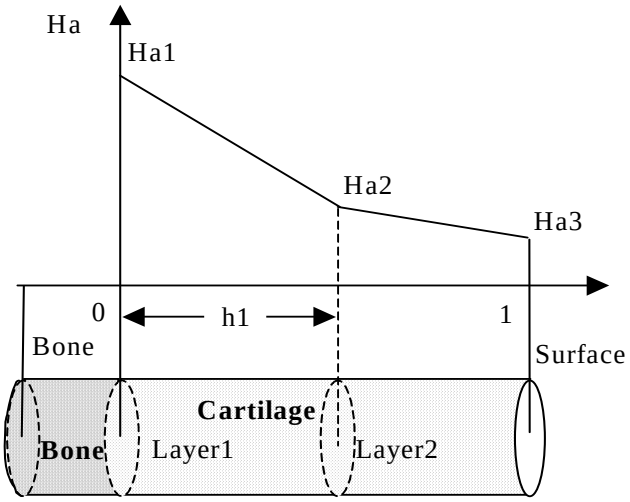

(b)

Fig. 3.16 Bi-layered triphasic model of articular cartilage. (a) Narmoneva's model (2001). (b) Schematic diagram of the inhomogeneous model with four parameters (Ha_1, Ha_2, Ha_3, h_1).

In this study, the remained half samples of the control and degenerated specimens from histological assay were used to calculate the reference values of ϕ_0^W. The full-thickness cartilage layer was separated from the bone and serially sectioned into 5-7 layers with a thickness of approximately 200 μm using microtome. The slices were soaked in 2 M saline solution for one hour and the wet weight (WW_0) of each slice was measured. Then, each slice was equilibrated in 0.15 M saline for one hour, and then dried at 37^o C

in an incubator for 12 hours. The dry weight (DW) of each slice was measured. The reference ϕ_0^W was calculated as (Gu et al., 1996; Narmoneva et al., 1999),

$$\phi_0^w = \frac{WW_0 - DW}{(WW_0 - DW) + DW(\rho_{2M} / \rho_s)} \quad (3\text{-}13)$$

where ρ is the density. The subscript *2M* and *s* represent the 2 M NaCl solution and the cartilage solid matrix, respectively. ρ_s equals to 1.323 g/ml (Gu et al., 1996).

Since the dimethyl-methylene blue (DMMB) dye-binding assay could not be performed in our lab, an indirect method using image processing was designed to obtain the values of c_0^F based on the literature values. The average normalized distribution of hue of hue-saturation-value color map was calculated based on the histological images. Let each value $x_i = a_i x_{\max}$, where x_{max} is the maximum hue value, a is coefficient, and the subscript i represents the number of layer and equals to 1 to 9. Then, the integral area (A) of the hue distribution curve was a function of x, i.e. $A=f(x)$. Using the literature values of c_0^F as the reference (Narmoneva et al., 2001; Wang et al., 2002; Fig. 3.17), the reference integral area was calculated as A_0. Assuming that $A=A_0$, the relationship between the reference c_0^F and the hue values was expressed. Consequently, the calibrated c_0^F values were obtained.

A constant v_s of 0.25 was used for the model (Mow et al., 2005). Using the distribution of the axial component of the ultrasound-measured swelling-induced strain E and the assigned c_0^F, ϕ_0^W and v_s, the four parameters Ha_1, Ha_2, Ha_3 and h_1 were predicted. The least square error (LSE) between the predicted strain values and those measured

experimentally was used as the curve fitting criterion. For comparison purpose, we also calculated the parameters using the bi-layered model proposed by Narmoneva et al. (2001) as well as a homogeneous model (Lai et al., 1991; Setton et al., 1996).

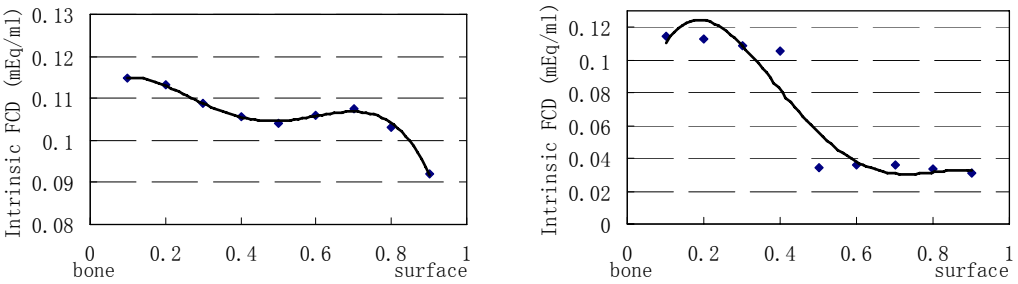

(a) (b)

Fig. 3.17 Depth-dependent distribution of reference FCD c_0^F of (a) the normal cartilage (Wang et al., 2002) and of (b) the degenerated cartilage (Narmoneva et al., 2001; Wang et al., 2002).

3.8 Data Processing

3.8.1 Low pass filtering

Using hardware (filtering circuit) and software (averaging of signals during data acquisition) methods, the efforts of reducing noises from different sources were carried out. However, the noise problem was still unavoidable in signal collection. According to the spectrum of the ultrasound signals from the cartilage tissue, a Butterworth low pass filter with a cutoff frequency of 50 MHz and a filter order of 10 was designed. The effective result of low-pass filtering was clearly shown in Fig. 3.18 by comparing with the spectra of A-mode ultrasound signals before filtering.

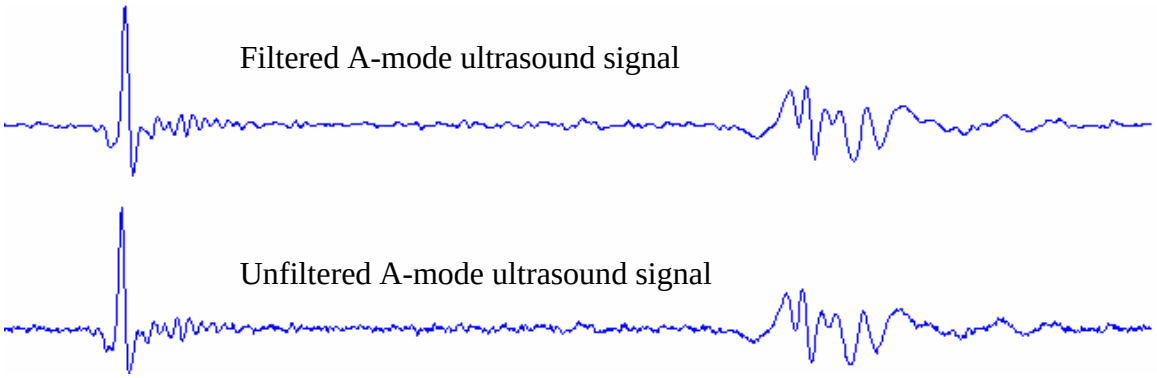

(a)

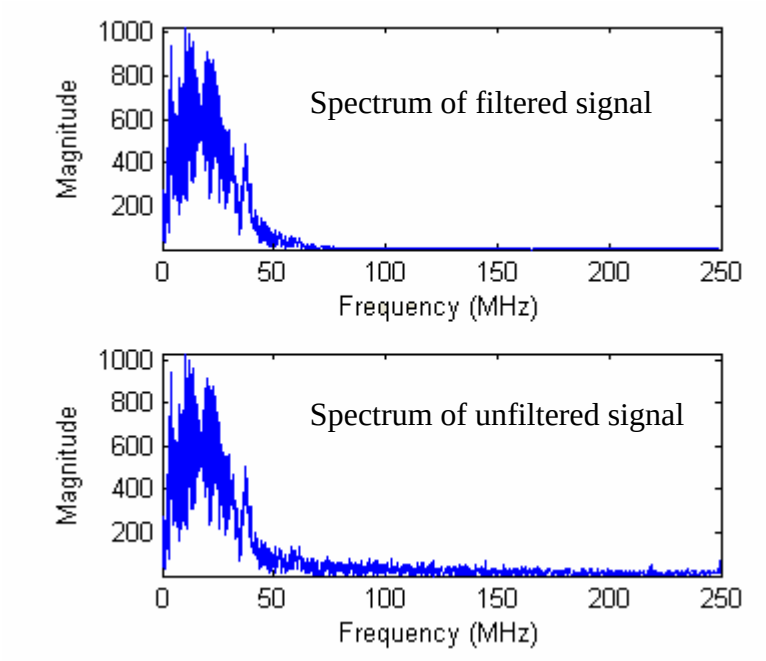

(b)

Fig. 3.18 (a) A-mode ultrasound signals before and after low-pass filtering. (b) Spectra of the filtered and unfiltered ultrasound signals.

3.8.2 Cross-correlation algorithm

To calculate the displacement of the interested echo signals at different depths during the experiments, a cross-correlation echo tracking method (Zheng et al., 2001) was applied. The cross-correlation technique is generally used for the study of the similarity

between two signals. The normalized correlation coefficient of two series of discrete values

$$X = \{x(0), x(1), ..., x(N-1)\} \text{ and}$$

$$Y = \{y(0), y(1), ..., y(N-1)\}$$

can be written as

$$R = \frac{\sum_{i=0}^{N-1}[x(i) - \overline{X}][y(i) - \overline{Y}]}{\sqrt{\sum_{j=0}^{N-1}[x(j) - \overline{X}]^2 \sum_{k=0}^{N-1}[y(k) - \overline{Y}]^2}} \quad (3\text{-}14)$$

where $\overline{X}$ is the mean of X, and $\overline{Y}$ is the mean of Y. If X and Y are exactly the same, then $R = 1$, and, if they have no similarity, then $R = 0$. $R = -1$ indicates that the two signals are exactly inverted in the amplitude. The cross-correlation method provides the time shift value of the selected echoes. Then the displacement is equal to the product of the sound speed and the time shift value (Eq. 3-1). This method has been used for the ultrasound elastography of soft tissues (Ophir et al., 1991; Zheng et al., 2004b) and tracking the movements of the selected tissue portions at different depths within the cartilage layer under mechanical force (Zheng et al., 2001, 2002, 2005) or osmotic pressure (Wang and Zheng, 2006; Zheng et al., 2004a).

3.8.3 Constant ultrasound speed

In our previous study (Zheng et al., 2006b), the ultrasound speeds in the 0.15 M and 2 M saline solutions and the speeds in the cartilage tissue submerged in the 0.15 M and 2 M saline solutions were 1530 ± 5 m/s and 1646 ± 3 m/s, and 1675 ± 51 m/s and 1781 ± 48 m/s, respectively, measured using a non-contact ultrasound approach (Patil et al., 2004) (Fig. 3.19). The effect of the inhomogeneity of the ultrasound speed in articular

cartilage on the final parametric measurements will be discussed in chapter 5. According to the study of Nieminen et al. (2002), 1668 m/s was the ultrasound speed in the degenerated cartilage tissue in physiological saline (99.6% of the speed in the normal tissue).

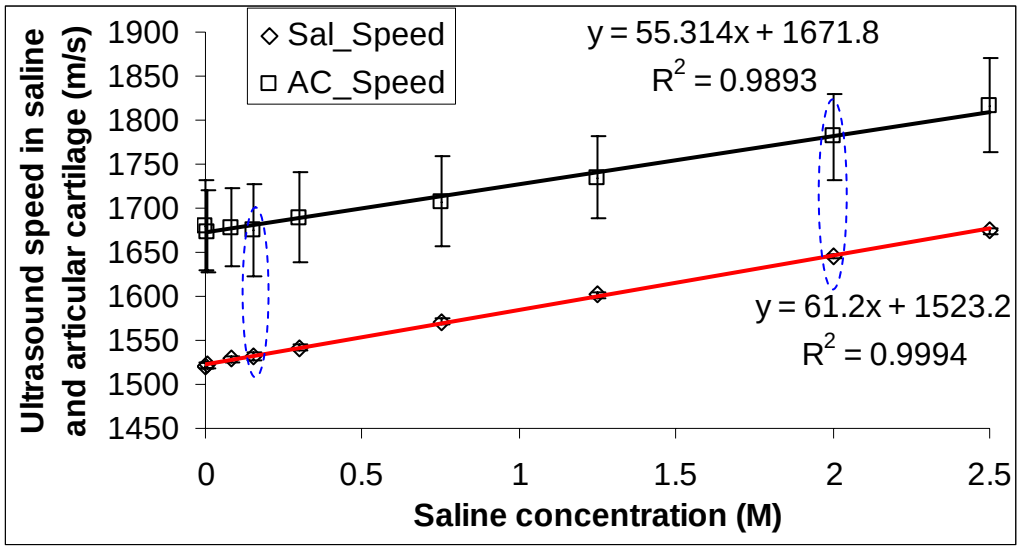

Fig. 3.19 Ultrasound speed in articular cartilage (AC_Speed) and saline solutions (Sal_Speed) with different concentrations. The error bars represent standard deviations (n = 19) (Zheng et al., 2006b).

3.8.4 Compensation for temperature change

It was noted that the temperature in the container varied slightly during the change of saline solution (Zheng et al., 2004a). In this study, the fluctuation of saline temperature was monitored using a fine copper wire, which was attached under the transducer, approximately 1.5 mm from the surface of the cartilage specimen (Fig. 3.20a). The wire blocked a small portion of the ultrasound beam and a calibration echo was generated (Fig. 3.20b). If the sound speed in the saline solution changes due to the temperature fluctuation, the amount of the shift of echoes from the fine wire would be used to compensate the shifts of the echoes from the tissue using ‘autoshiftwave’ algorithm in

the custom-designed program. After this auto-compensation, the slight temperature change in the saline solution would not affect the final measurement results (Fig. 3.20c).

3.8.5 Compensation for period of solution change

As described earlier, the saline solution was changed from one concentration to another in approximately 30 seconds. During this period, no ultrasound signal was recorded, as there was no coupling medium between the ultrasound transducer and the cartilage specimen. According to our previous study (Wang and Zheng, 2006), the cartilage tissue deformed rapidly during the initial period after changing the concentration of the bathing saline. Therefore, the swelling or shrinkage happened during this 30 seconds should be compensated. Although we were not able to obtain the exact transient data for this period, the overall displacement of the cartilage surface happened during this period could be calculated as,

$$\Delta d = c_s' \frac{T_1^{'}}{2} - c_s \frac{T_1}{2} \qquad (3\text{-}15)$$

where Δd is the displacement of the cartilage surface; c_s and c_s' are the sound speeds in the saline before and after the concentration was changed; T_1 and T_1' are the flight times of ultrasound from the transducer to the cartilage surface before and after changing the saline solution.

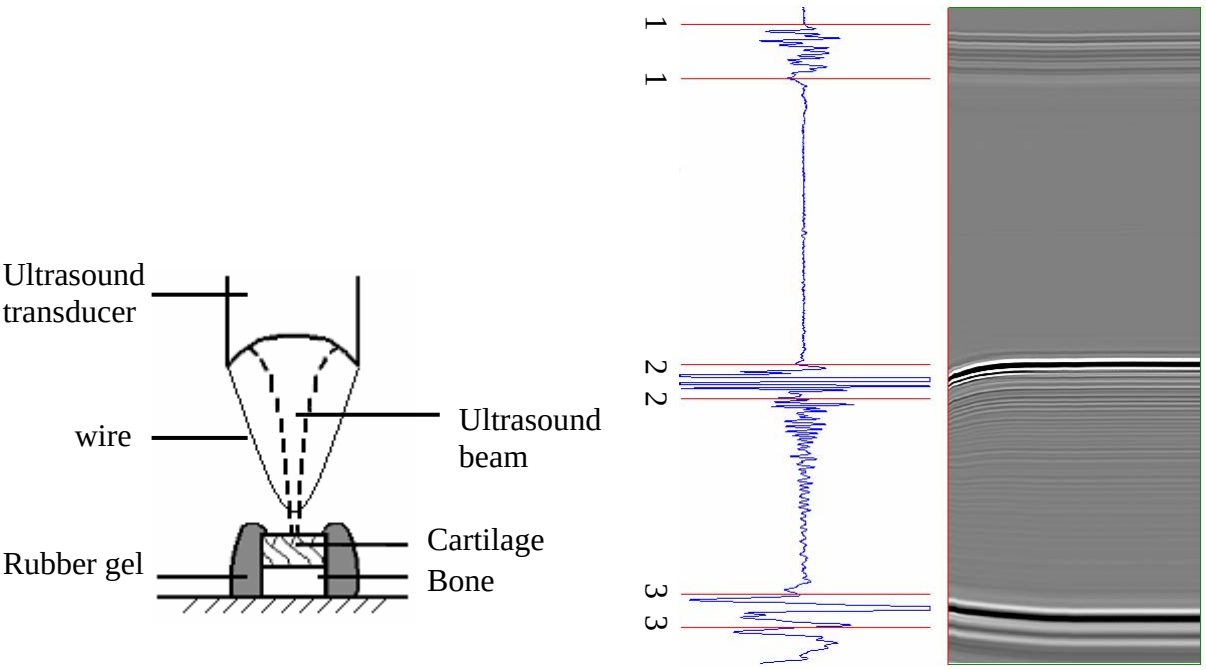

(a) (b)

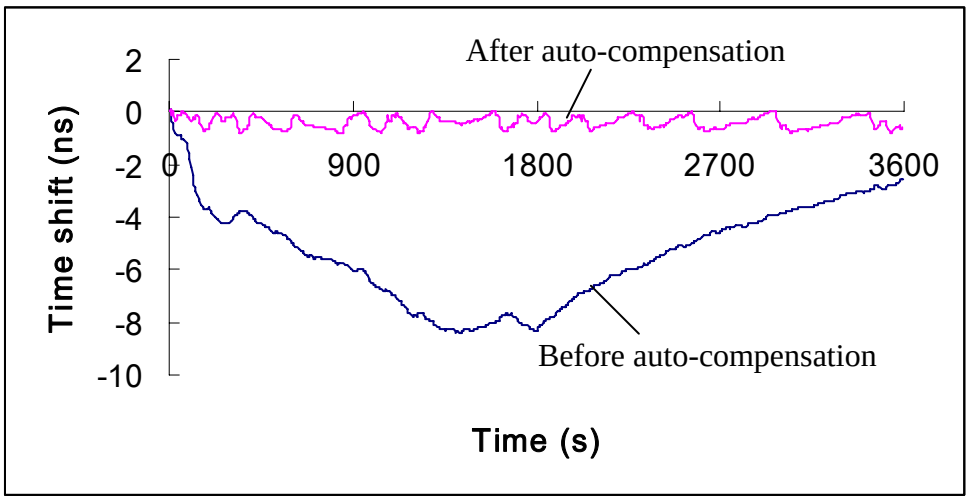

(c)

Fig. 3.20 (a) An enlarged schematic of the ultrasound monitoring part including a wire attached under the transducer. (b) A-mode ultrasound signals reflected from the wire, the cartilage surface and the cartilage-bone interface at the start moment of swelling process (left) and M-mode ultrasound image of swelling process (right). Numbers 1-3 represent the ROI windows for tracking the shift of the selected echoes. (c) The values of time shift of the wire-reflected echoes before and after auto-compensation.

3.8.6 Compensation for depth-dependent displacement in modeling

The depth-dependent displacements of the tissue layers could be calculated from the time shifts of the corresponding echoes at different depths. However, such displacement calculation was associated with the ultrasound speed in the tissue. If the ultrasound speed in the cartilage keeps constant, the measured displacements are the absolute displacements. However, as the salt gradually moved out of the cartilage tissue during the swelling process, the ultrasound speed in the tissue would change accordingly. It was observed that the echoes from the cartilage-bone interface moved during the swelling process though the cartilage layer was attached to the bone tissue. Therefore, the real tissue displacements no longer equalled to the displacements observed in the experiment using a constant ultrasound speed. To measure the proximally real swelling strain at equilibrium, the measured displacement should be corrected according to the change of the ultrasound speed in articular cartilage.

Using the custom-designed software, the shifts of the tissues at different depths were measured. Based on the time shift value (ΔT) of the cartilage-bone interface at equilibrium, the displacement compensation was conducted. As shown in Fig. 3.21, the corrected value of the time shift at depth x is derived as

$$T_x' = T_x - \frac{t_x}{T}\Delta T \qquad (3\text{-}16)$$

where T_x' is the corrected time shift; T_x is the original time shift measured before compensation; t_x denotes the flight time from the surface to the depth x at time 0 (the moment just after the change of the solution); T is the flight time from the cartilage surface to the cartilage-bone at time 0. After the calibrated values of the time shift were

achieved, the strains of sub-layers at different depths could be calculated. The strain ε of the arbitrary layer (from depth x_1 to depth x_2) was calculated by Eq. 3-17.

$$\varepsilon = \frac{T'_{x_2} - T'_{x_1}}{t_{x_2} - t_{x_1}} \tag{3-17}$$

where T'_{x_1} and T'_{x_2} are the corrected time shifts of the echoes from the tissue at depths x_1 and x_2, respectively. t_{x_1} and t_{x_2} are the original flight times of ultrasound at time 0 from the cartilage surface to tissues at depths x_1 and x_2, respectively. It should be noted that the proposed correction was particularly suitable for the equilibrated state of the swelling test, as the salt change in the cartilage tissue was uniformly distributed throughout the depth. During the transient process, there must be a gradient of the salt concentration in the cartilage in the depth direction and more sophisticated correction algorithm should be applied. In this study, only the strains at the equilibrated state were used for the subsequent modelling calculation.

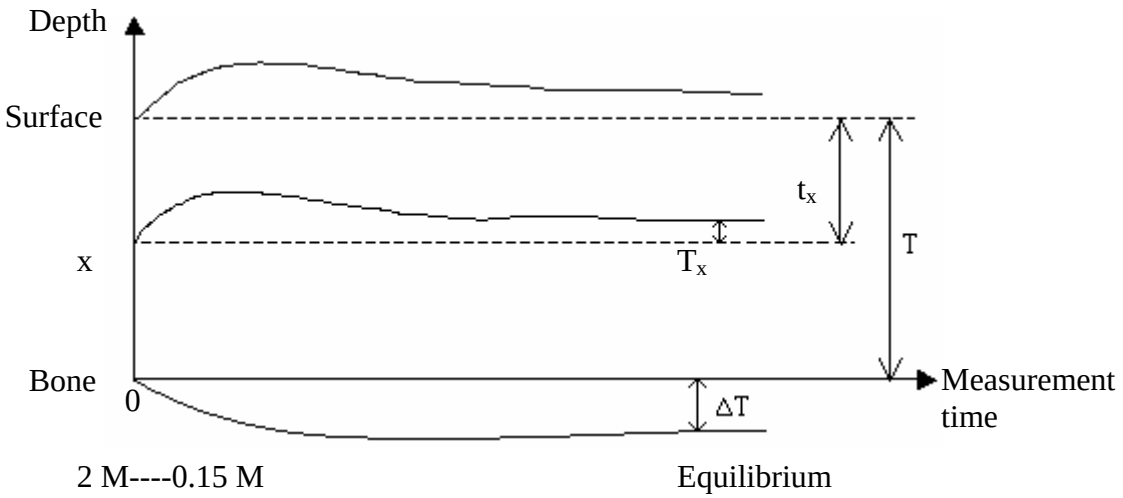

Fig. 3.21 Sketch of the compensation for the time shifts measured at different depths using the time shift (ΔT) of the cartilage-bone interface to correct the error caused by the change of the sound speed in the cartilage tissue.

3.9 Data Analysis

In this study, the results were presented in the form of mean ± SD. Paired t-test was used to test the significance of the difference between the parameters in the shrinkage and swelling phases. One-Way ANOVA was used to test the significance of the differences among the parameters of specimens with different dimensions and among the normal and the degenerated specimens trypsin-treated with different digestion periods. The correlations between different parameters, such as the swelling and shrinkage strains, water contents and FCD, and the acoustic parameters, were conducted for all the normal and degenerated samples. The statistical analysis software SPSS (V11.5, SPSS Inc., Chicago, USA) was used for data analysis.

CHAPTER 4 RESULTS

4.1 Feasibility of Ultrasound Measurement

4.1.1 Validation of ultrasound measurement

Fig. 4.1 shows the results of the validation experiments for the manually controlled 3D USMS. The data of the changes of the distance between the cartilage surface and the ultrasound transducer measured using the USMS and those read from the micrometer agreed very well when the specimens were emerged in 0.15 M saline (slope = 1.0026, R^2 =1, $p < 0.001$, Fig. 4.1a) and 2 M saline (slope = 1.0023, R^2 = 0.9999, $p < 0.001$, Fig. 4.1b), respectively. If the data measured by the micrometer were treated as the real values, the root mean square (RMS) error for the ultrasound measurement was 0.7 μm in 0.15 M saline and 1.2 μm 2 M saline, corresponding to 0.07% and 0.12% strain inaccuracy for a cartilage specimen with a thickness of 1 mm, respectively.

Fig. 4.2 shows the results of the validation experiments for the motor-controlled 3D USMS. The data measured using the USMS and those read from the 3D scanning compumotor agreed very well when the specimens were emerged in 0.15 M saline (slope = 1.0001, R^2 = 0.9941, $p < 0.001$, Fig. 4.2a) and 2 M saline (slope = 0.8646, R^2 = 0.9849, $p < 0.001$, Fig. 4.2b), respectively. If the data controlled by the motor were treated as the real values, the RMS errors for the ultrasound measurement were 1.0 μm in 0.15 M saline and 0.2 μm and 2 M saline, corresponding to 0.1% and 0.02% strain inaccuracy for a cartilage specimen with a thickness of 1 mm, respectively.

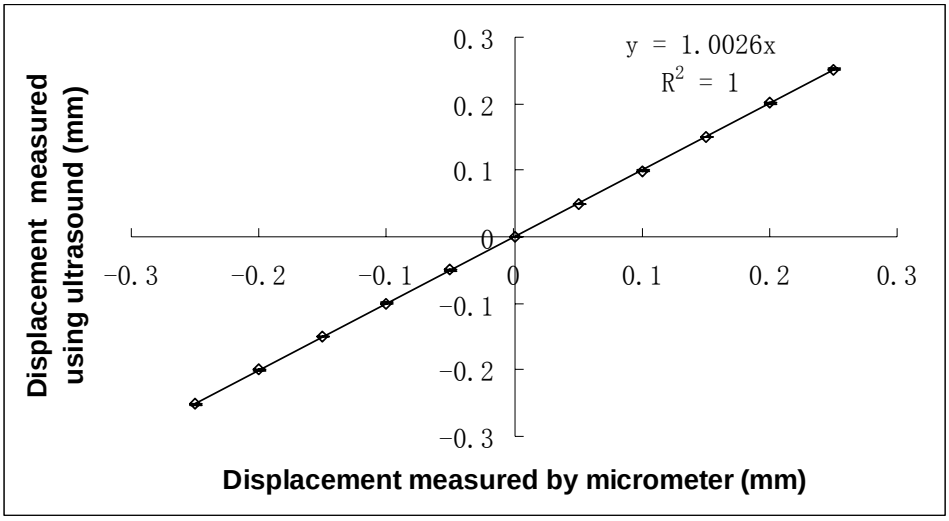

(a)

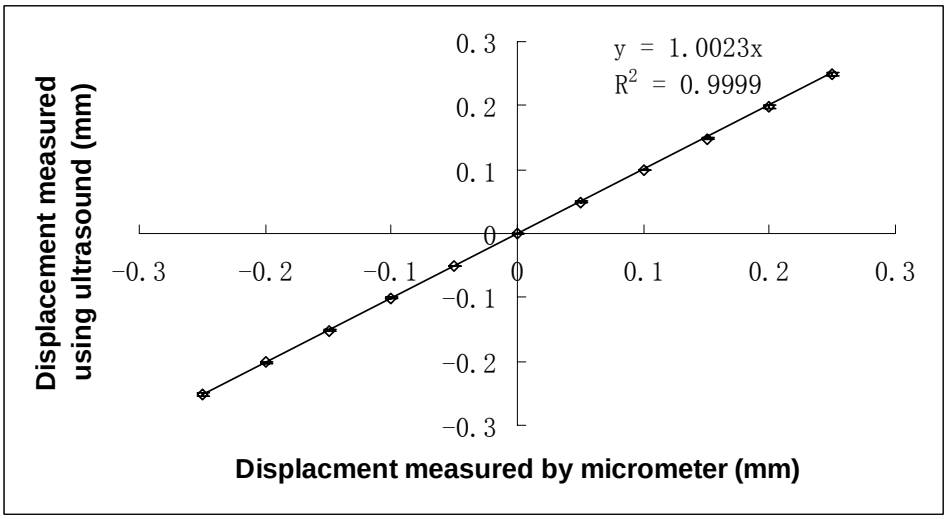

(b)

Fig. 4.1 Linear correlation between the displacements of the echoes measured using the manually controlled 3D USMS and the reference values obtained by micrometer. Specimen was submerged in 0.15 M saline (a) and 2 M saline (b), respectively.

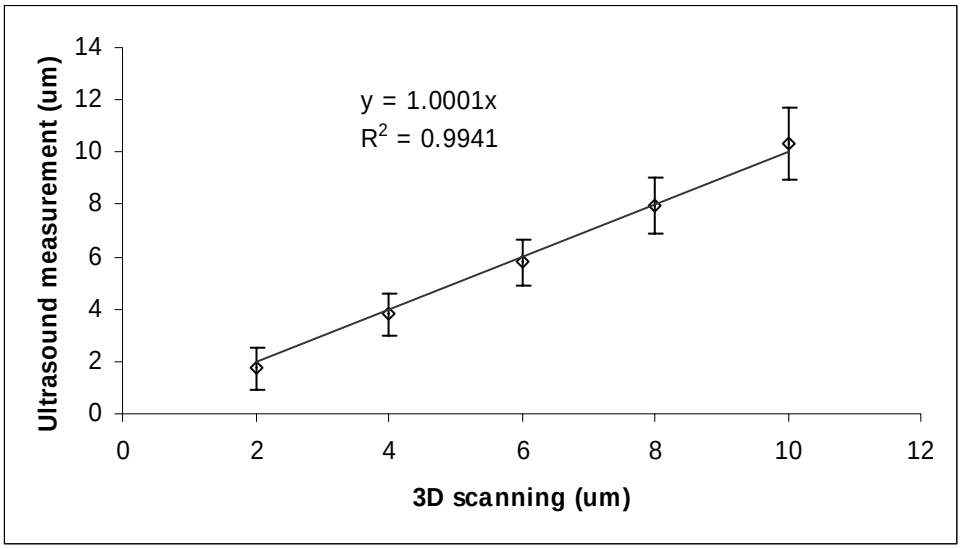

(a)

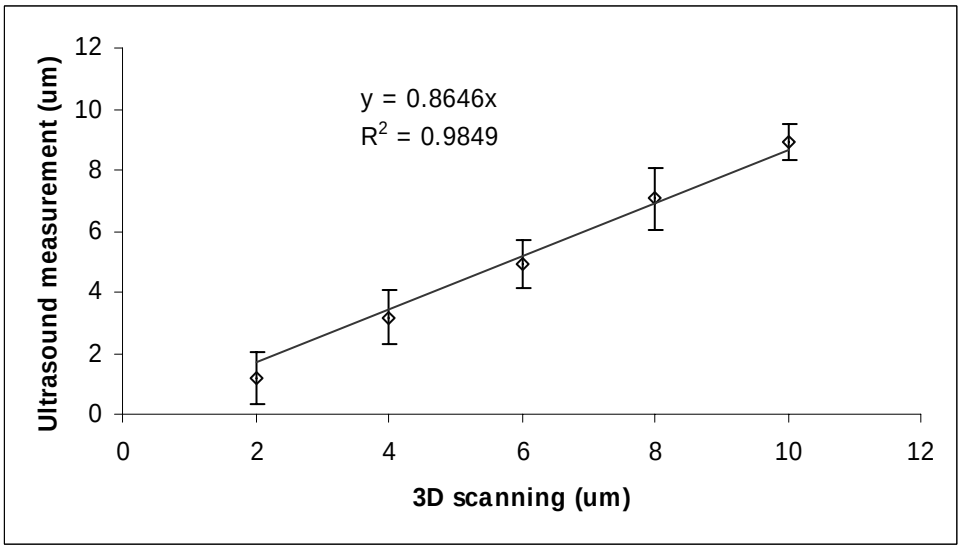

(b)

Fig. 4.2 Linear correlation between the displacements of the echoes measured using the motor-controlled 3D USMS and the reference values obtained by 3D scanning compumotor. Specimen was submerged in 0.15 M saline (a) and 2 M saline (b), respectively.

4.1.2 Repeatability of shrinkage-swelling test

Table 4.1 summarizes the results of the repeatability test. The mean percentage values of CV for the measurement of the peak strains of shrinkage and swelling were less than

10%. The mean rRMSD of the transient shrinkage strains was 9.8%, and the swelling strains 6.9%. As for the time shift of the cartilage-bone interface, the mean rRMSD was 4.1% and 4.4% respectively during the shrinkage and swelling processes. The high correlation (ICC > 0.98) of the maximum strains among the three repeated tests demonstrated that the present ultrasonic measurement had a good repeatability.

Table 4.1 Results of the repeatability experiment including the mean CV% and ICC of the peak shrinkage and swelling strains as well as the mean rRMSD of the transient shrinkage and swelling strains and the time shift of the cartilage-bone interface.

Measurement items	Parameters	Shrinkage	Swelling
CV%	Peak strain	9.6%	7.7%
ICC	Peak strain	0.98	0.99
rRMSD (%)	Transient difference at cartilage surface	9.8%	6.9%
	Transient difference at cartilage-bone interface	4.1%	4.4%

4.1.3 Repeatability of dimension-dependence test

Table 4.2 lists the results of the repeatability parameters including the mean CV%, ICC, and the mean rRMSD for both large and small specimens. In the case of the large specimens with a diameter of 6.35 mm, the CV% values of the peak strains of shrinkage and swelling were less than 10% among the results of the three different sites and three times of reinstallation. For the slim specimens with a width of 2 mm, the CV% values of the peak strains of shrinkage and swelling strain measured at the three sites greatly increased to 18.5% and 16.3%, respectively, higher than those values of the remounting measurements (less than 10%). The ICC values of the two repeatability tests for the peak strains of the cylindrical and slim specimens were both greater than 0.8.

For the cylindrical specimens, the mean rRMSDs of the transient shrinkage and swelling strains were less than 7% among the measurements of reinstallation and three different observation sites. In the case of the slim specimens, similar to the CV% results, the mean rRMSDs among the results obtained from different observation sites were also greater than 10% (shrinkage 12.0%; swelling 10.6%).

Table 4.2 Results of the repeatability experiment including the mean CV%, ICC, and the mean rRMSD for both large and small specimens.

	Large specimen (6.35 mm in diameter)				Small specimen (2 mm in width)			
Measurement items	Shrinkage		Swelling		Shrinkage		Swelling	
	sites	times	sites	times	sites	times	sites	times
CV%	4.3	3.8	8.2	9.4	18.5	6.9	16.3	3.5
ICC	--	0.89	--	0.89	--	0.90	--	0.99
rRMSD (%)	3.6	3.1	5.1	6.3	12.0	6.6	10.6	5.2

4.2 Ultrasonic Characterization of Swelling Behavior

4.2.1 Transient and equilibrium swelling strain

During the shrinkage and swelling processes, the cartilage surface tended to deform rapidly and then moved upwards or downwards gradually close to the equilibrium state in approximately one hour after changing the concentration of the saline solution. This interesting phenomenon observed in the current study demonstrated that the cartilage specimen might experience a “relaxation” state after reaching its maximum shrinkage or swelling amplitude (Fig. 4.3), i.e., the surface moved back towards the original state. The absolute peak value of the shrinkage strain (0.010 ± 0.005) was significantly larger than that of the swelling strain (0.003 ± 0.003) ($p < 0.001$, paired t-test). It was observed

that it took the tested specimens only several minutes to reach the peak shrinkage or swelling amplitude. The shrinkage duration (402 ± 605 s) was insignificantly larger ($p = 0.156$, paired t-test) than the swelling duration (234 ± 485 s). At equilibrium, the shrinkage strains reduced to -0.005 ± 0.005 while the swelling strains was close to zero.

During the diffusion of ions and water between the cartilage tissue and the bathing saline, the compositional and mechanical alteration may lead to a change in the ultrasound speed. This change was represented by the shift of the ultrasound echo from the cartilage-bone interface shown in the M-mode images (Fig. 3.11a). Our study demonstrated that the sound speed in articular cartilage gradually increased when the concentration of the bathing solution was increased from 0.15 M to 2 M. It increased by 5.0% ± 1.5% after one hour. When the concentration of the saline solution was changed back to 0.15 M, the sound speed gradually decreased by up to 5.4% ± 1.2%. It was found that the percentage change of the sound speed in articular cartilage during the shrinkage and the swelling processes both exponentially depended on the measurement time ($R^2 = 0.9920$, $R^2 = 0.9965$, respectively) (Fig. 4.4).

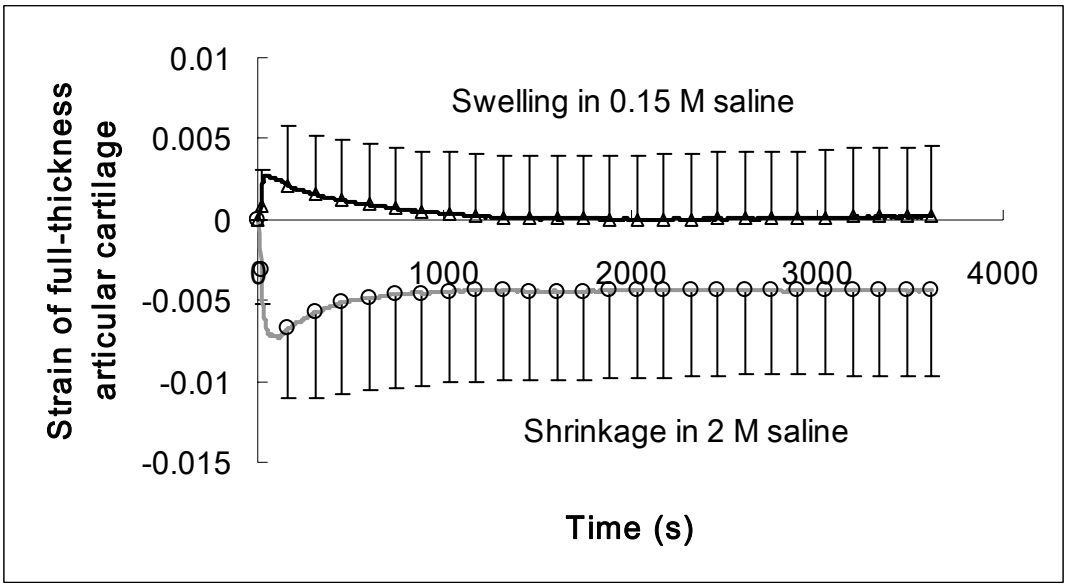

Fig. 4.3 The shrinkage strain (grey line) and the swelling strain (black line) versus the measurement time. The error bars represent standard deviations (n = 50).

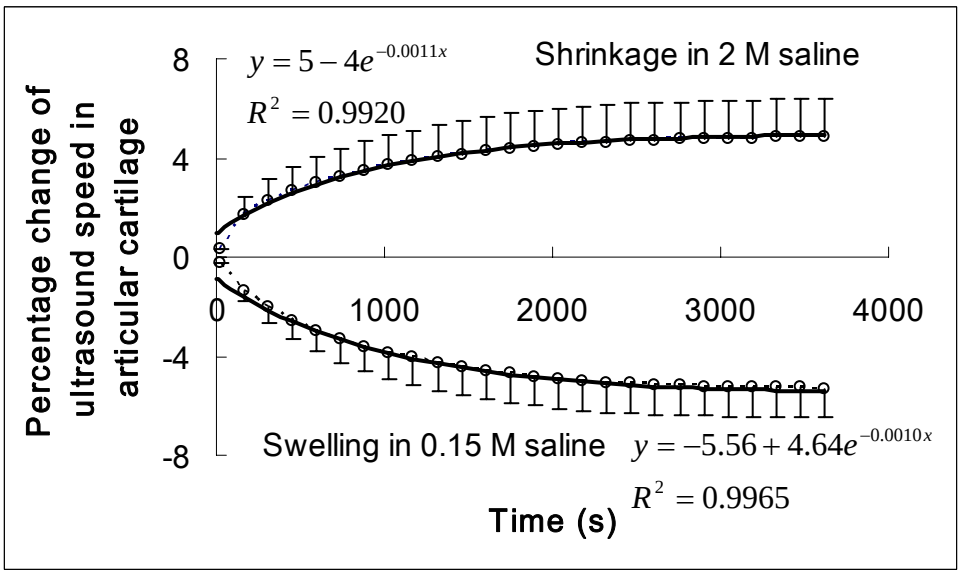

Fig. 4.4 Ultrasound speed in articular cartilage increased during the shrinkage process, but decreased during the swelling process. Experimental data (dashed lines and circle marks) can be well fitted by exponential functions (solid lines). The error bars represent standard deviations (n = 50).

4.2.2 Dimension-dependence of swelling behavior

In pair-wise comparison of the peak strains of cartilage samples with different dimensions, the statistical analysis of LSD Post Hoc Tests of One-Way ANOVA showed that there were significant differences ($p < 0.05$) in the peak shrinkage strains between the small samples (ϕ = 2 mm) and the larger samples (ϕ = 6.35 mm and ϕ = 4 mm) (Fig. 4.5). However, no significant differences ($p > 0.05$) among the peak swelling strains were found for all the cartilage-bone specimens with various sizes (Fig. 4.5). Moreover, it was found that there were significant differences ($p < 0.05$) in the equilibrium swelling strain between the small samples (ϕ = 2 mm) and the larger samples (ϕ = 6.35 mm and ϕ = 4 mm) and significant differences ($p < 0.05$) in the equilibrium shrinkage strain between the cylindrical samples (ϕ = 6.35 mm) and the smaller samples (ϕ = 4, 3, and 2 mm) (Fig. 4.6).

Fig. 4.7 shows the absolute values of the slope k calculated from the linear region of the logarithm of the normalized time shift of the cartilage-bone interface (or the bottom surface for the cartilage samples without bone). From the statistical results of LSD Post Hoc Tests of One-Way ANOVA, the slope values for the cylindrical samples (ϕ = 6.35 mm) and the larger slim specimens (ϕ = 4 and 3 mm) were significantly ($p < 0.05$) smaller than those of the small specimens (ϕ = 2mm).

In addition, in comparison the rectangle (2mm×4mm) cartilage specimens under *in-situ* condition (cartilage tissue attached to the bone) with those under *ex-situ* condition (cartilage tissue without the bone), the statistical results showed that there were significant differences ($p < 0.05$) in the three parameters: the peak strain of shrinkage

and swelling, the equilibrium strain of shrinkage and swelling, and the slope *k* (Fig. 4.5-4.7).

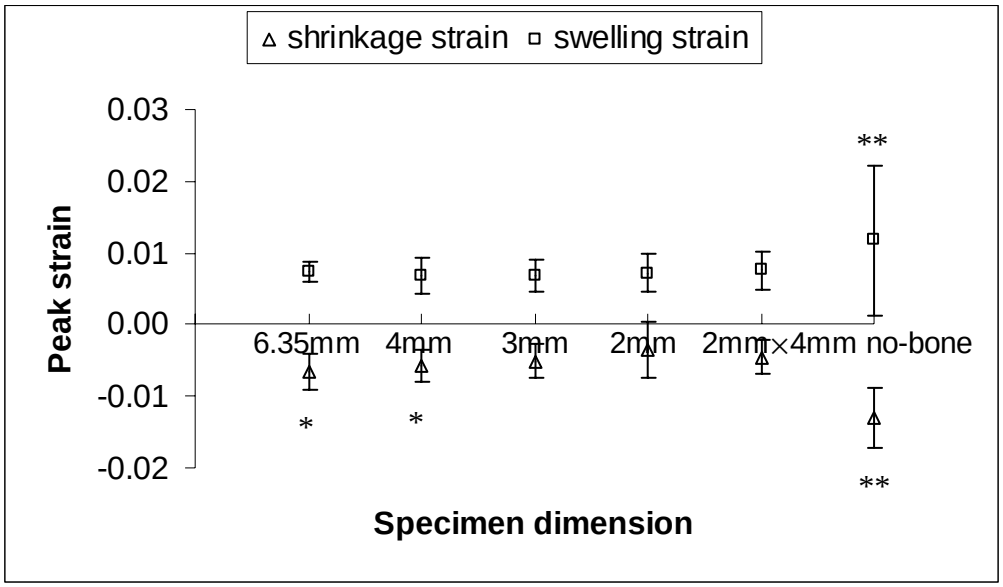

Fig. 4.5 The peak shrinkage and swelling strains of cartilage samples with different dimensions. The error bars represent standard deviations (n = 10). '6.35mm' represents the cylindrical specimens with a diameter of 6.35 mm; '4mm', '3mm', and '2mm' represent the slim cartilage specimens with a width of 4 mm, 3 mm, and 2 mm, respectively. '2mm×4mm' represents the rectangular cartilage layer with a width of 2 mm and a length of 4 mm attached to the bone. 'no-bone' represents the '2mm×4mm' rectangular cartilage layers separated from the bone. * Significant difference ($p < 0.05$ by LSD Post Hoc Tests of One-Way ANOVA) in comparison with the samples with a width of 2 mm. ** Significant difference ($p < 0.05$ by One-Way ANOVA) between the rectangular cartilage specimens attached to the bone and those without the bone tissue.

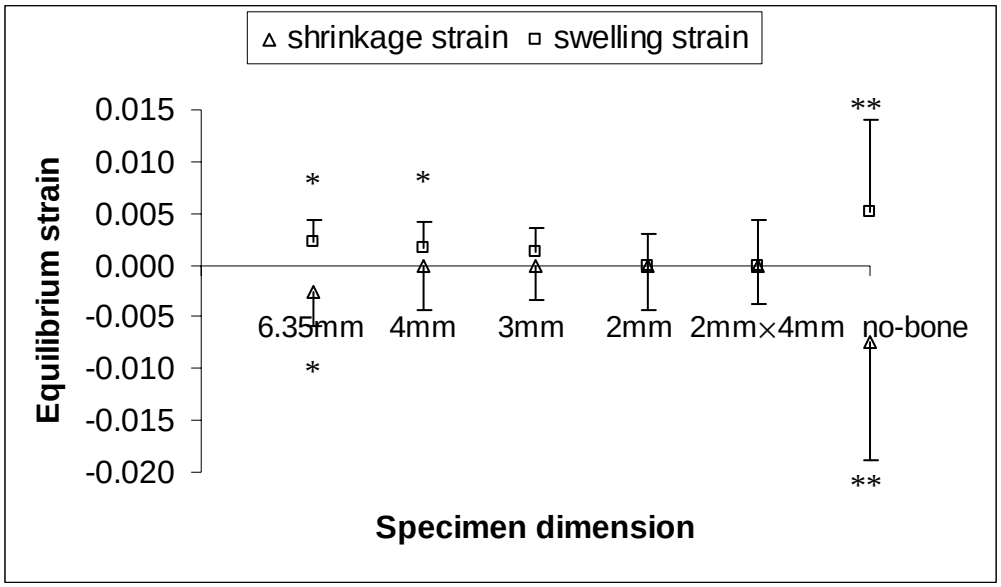

Fig. 4.6 The equilibrium shrinkage and swelling strains of cartilage samples with different dimensions. The error bars represent standard deviations (n = 10). The representations of '6.35mm', '4mm', '3mm', '2mm', '2mm×4mm' and 'no-bone' are same as in Fig. 4.5. * and ** represent the same significant difference as in Fig. 4.5.

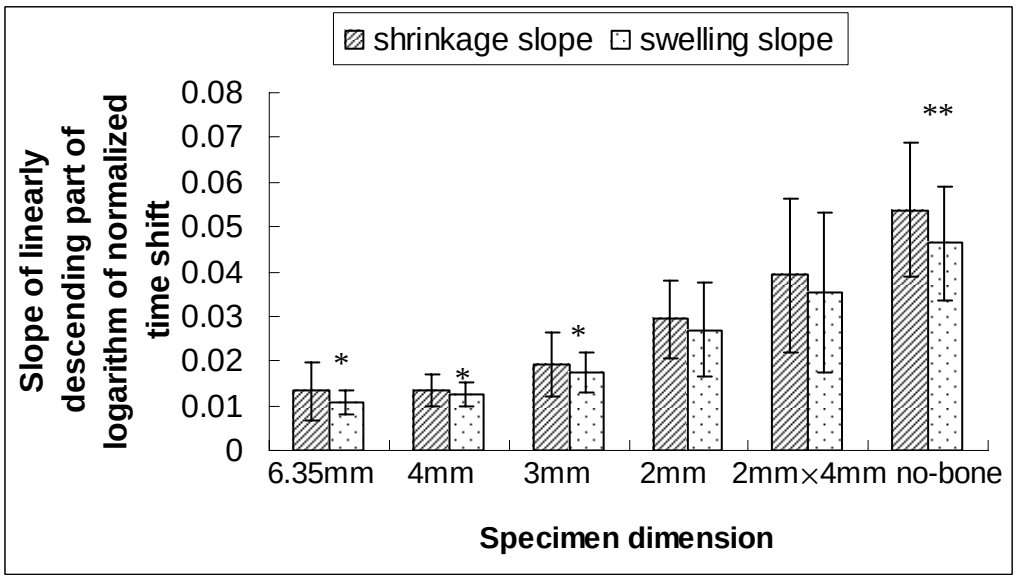

Fig. 4.7 The absolute values of the slope calculated from the linearly descending part of the logarithm of the normalized time shift of the cartilage-bone interface or the bottom surface for the cartilage samples without bone. The error bars represent standard deviations (n = 10). The representations of '6.35mm', '4mm', '3mm', '2mm', '2mm×4mm', and 'no-bone' are same as in Fig. 4.5. * and ** represent the same significant difference as in Fig. 4.5.

4.2.3 Depth-dependence of swelling behavior

In this study, the averaged values of the osmosis-induced swelling strains at the deep (30% of the total thickness), middle (55%), and surface (15%) zones were measured using ultrasound (Fig. 4.8). The non-uniformity of the swelling strains at different zones indicated the depth-dependence of the swelling strain. It was noted that the deep zone had compressive strains (-0.008 ± 0.013) while the tensile strains were observed in the middle and superficial zones (0.009 ± 0.010 and 0.002 ± 0.012, respectively).

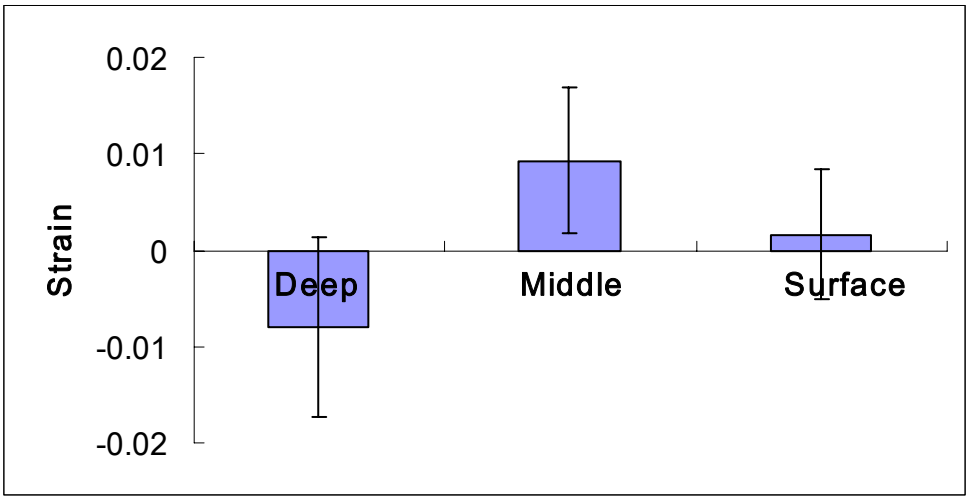

Fig. 4.8 Nonuniform swelling-induced strains at the deep, middle and surface zones. The error bars represent standard deviations (n = 44).

Fig. 4.9 shows the result of a typical 2D scanning during the shrinkage process induced by the change of saline concentration from 0.15 M to 2 M. To analyze the distribution of the movement of the interstitial tissue at different depths, an ROI was outlined by the dashed rectangle in the B-mode image shown in Fig. 4.9a. The ROI area was divided into 15 × 40 segments. The tissue displacement images during the different periods were formed using the automatic segmentation and 2D cross-correlation tracking

method (Zheng et al., 2004b). Fig. 4.9b-d shows the changes in the displacement distribution of the tissue at different moments. They indicated that the movement of the tissue was large during the beginning phase of the swelling and shrinkage processes. As time going, the movements of tissues inside cartilage tended to be zero and approach equilibrium.

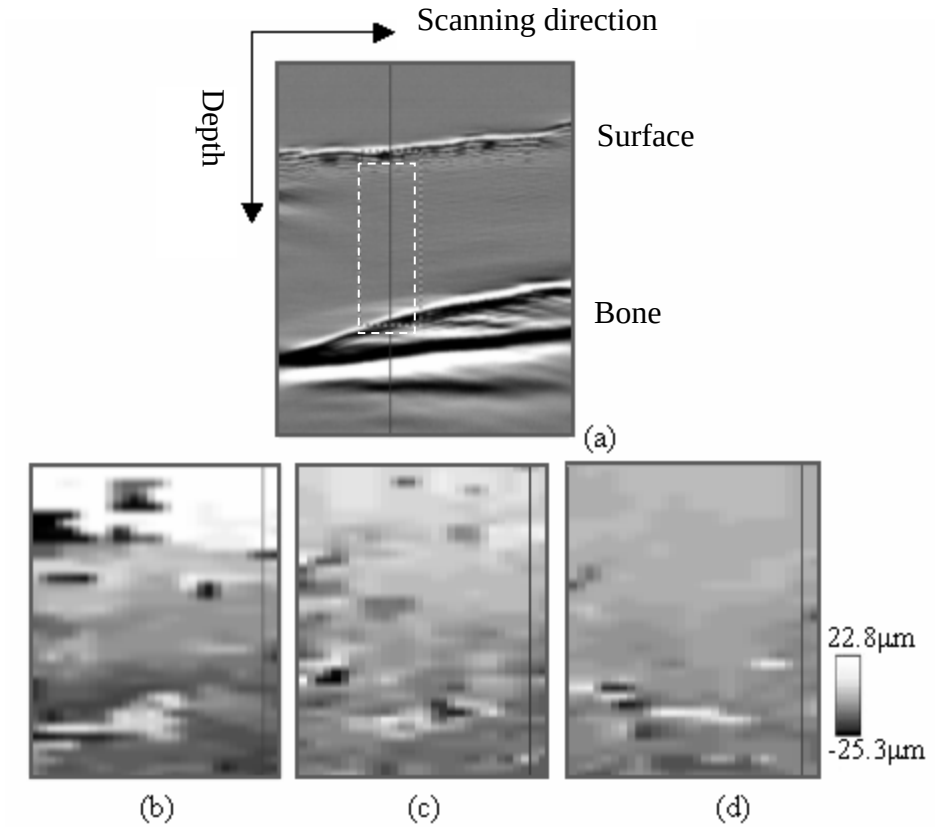

Fig. 4.9 (a) An UBM image of the cartilage cross-section during the shrinkage phase. The images of displacement distribution of articular cartilage extracted from the ROI indicated by the dashed rectangle in (a) were obtained between two moments of 2.5 min and 4.2 min (b), 5.8 min and 7.5 min (c), and 10.8 min and 12.5 min (d), respectively. The grey levels in (b-d) represent the displacement values.

4.2.4 Results of pilot study of enzyme digestion

The results of our pilot study showed that the PG content was more quickly digested by 0.25% trypsin solution at room temperature than we had expected. For Group A, one-

hour digestion depleted approximately 90% of the PG content while the PG content of the specimens in Group B was totally digested by two-hour digestion (Fig. 4.10). Based on this result and in view of the different PG contents and thicknesses of the cartilage specimens, 3-hour digestion was selected to monitor the enzyme penetration during the progressive degeneration procedure, and 10-minute, 20-minute and 30-minute digestions were chosen to obtain the degenerated cartilage with different digested degrees.

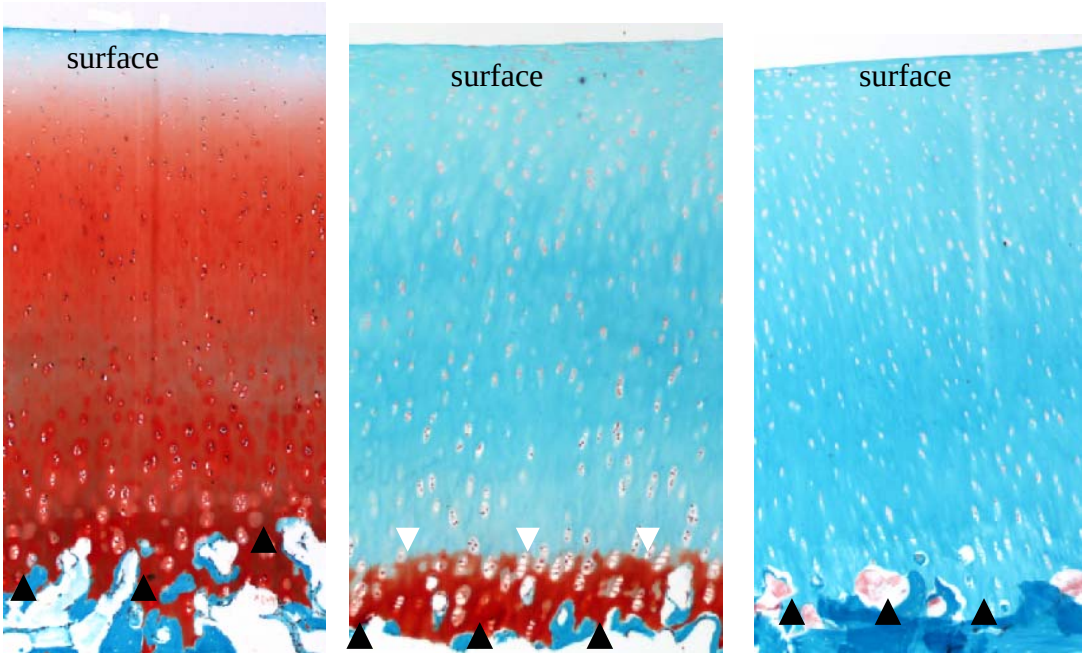

(a) (b) (c)

Fig. 4.10 Histological images of cartilage sections stained with safranin O and fast green. Red color (dark in grey image) indicates the PG content. ▲ represents the cartilage-bone interface. (a) Normal cartilage. (b) A sample digested for 1 hour. White arrows indicate the interface of the undigested and digested tissues. (c) A sample digested for 2 hours.

Fig. 4.11 shows the effect of ultrasonic decalcification on the PG content of articular cartilage. The left part of the histological image shows the full-thickness cartilage tissue

with the original surface while the right side shows the tissue without the surface layer. The observation that the cut section was still stained with red color (dark in grey image) demonstrated that tissue processing including ultrasonic decalcification led to little loss of the PG content. This result guaranteed that ultrasonic decalcification would not affect the histological assessment.

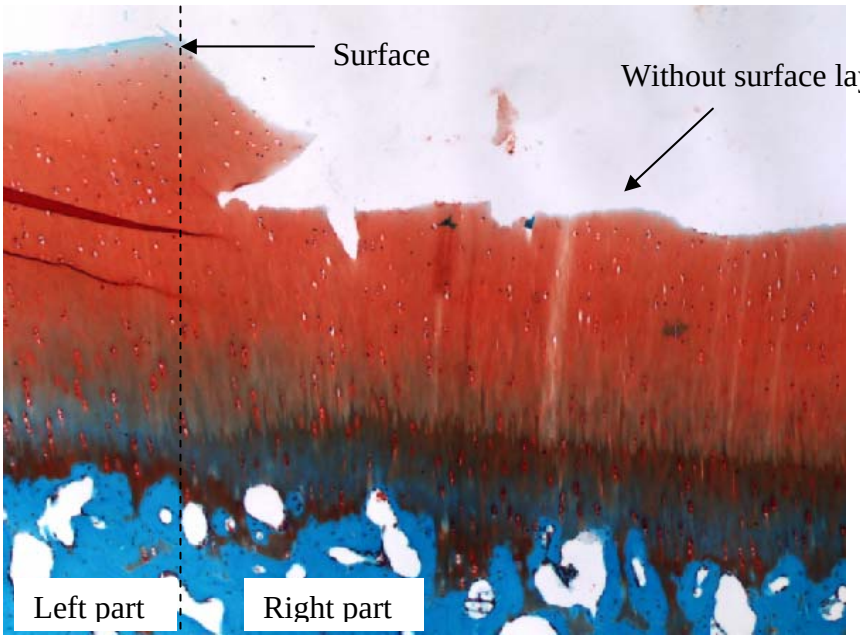

Fig. 4.11 Histological image of cartilage section stained with safranin O and fast green. The left part is the full-thickness tissue. The right part is the tissue without the surface zone.

4.2.5 Progressive degeneration of articular cartilage

Progressive trypsin digestion

Fig. 4.12 shows the ultrasound signals collected from a typical specimen during the process of trypsin digestion, which lasted for 3 hours. Inclined traces as shown in Fig. 4.12 were clearly observed in the M-mode ultrasound images collected from all the specimens. As the trypsin penetrated into the cartilage tissue and broke down the

aggregating PGs, additional echoes were generated from the interface of the digested and undigested cartilage tissues (Fig. 4.12). The small echoes along the echo trains were the ultrasound scattering signals from the matrix, which appeared to be stable during the progressive PG-depleted digestion. In other words, the trypsin digestion might only have little effect on the scatters in the cartilage matrix.

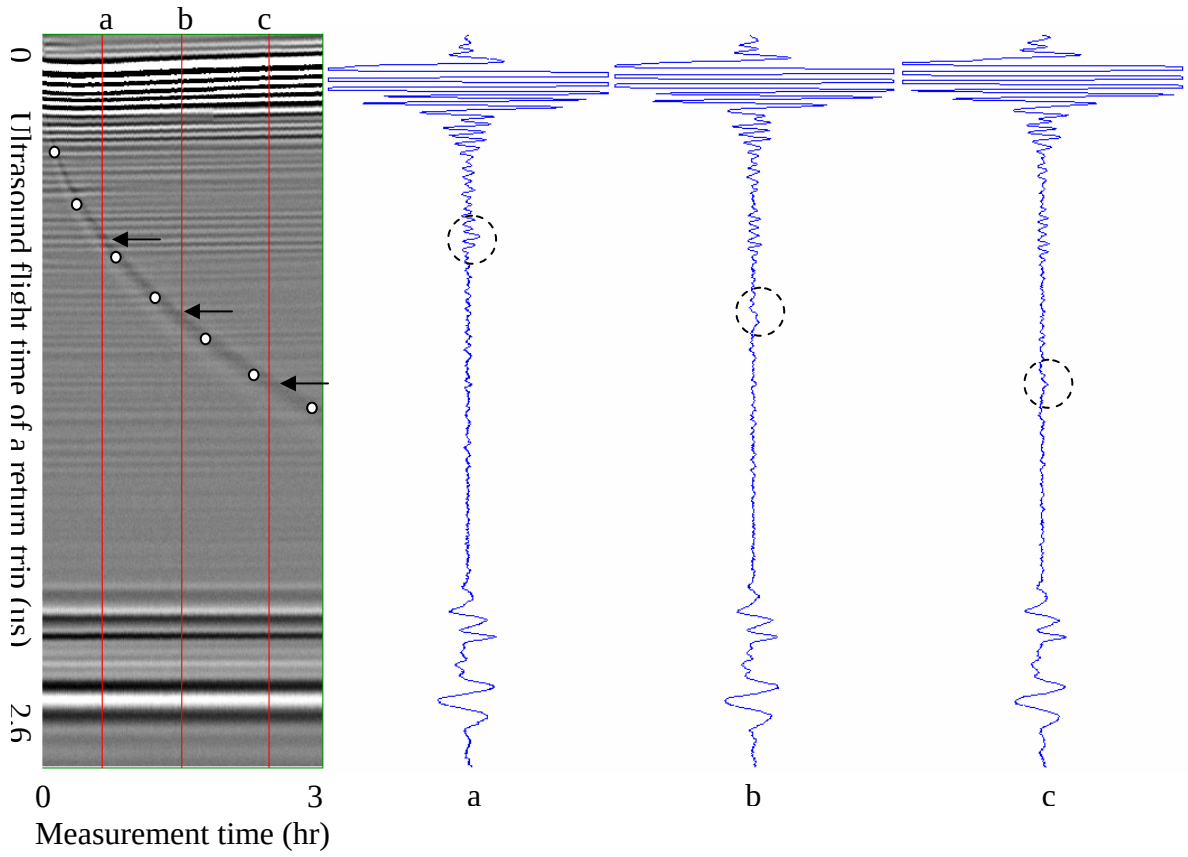

Fig. 4.12 A typical M-mode ultrasound image display shows the progressive degeneration of articular cartilage induced by trypsin enzyme. A clear darker trace is observed. The white dots in M-mode image represent the marks manually applied and used for the interpolation of the inclined digestion trace. To avoid overlapping the trace, fewer marks than required were indicated in the figure. The RF ultrasound echoes (a-c) were collected at the time points indicated by the solid lines (a-c) in M-mode image. The trypsin penetration front and the corresponding additional echoes generated from the interface of the digested tissue and the undigested tissue are indicated with the black arrows in M-mode image and the circles in A-mode RF signal, respectively.

The transient speed of movement of the digestion front echo was calculated during the three hours and the averaged profile is shown in Fig. 4.13a. Fig. 4.13b shows the digestion speed as a function of the tissue depth. It can be clearly demonstrated that the digestion speed slowed down as the increase of the depth. It was found that the digestion speed (0.62 ± 0.16 μm/s) (mean ± SD) at the beginning of digestion was faster than the speed (0.04 ± 0.02 μm/s) in the deeper region of the cartilage tissue (approximately 70% of the full thickness), suggesting that the enzyme may penetrate from the surface into the deeper region of the tissue with a changing speed.

Residual trypsin digestion

After the short-time enzyme digestion, the residual digestion was monitored when the digested sample was immerged in the 0.15 M saline. It was found that the enzyme continuously penetrated through the tissue. The digestion front moved at a speed of 0.31 ± 0.23 μm/s, 0.19 ± 0.08 μm/s, 0.20 ± 0.05 μm/s just after the 10-minute, 20-minute, and 30-minute digestion, respectively (Fig. 4.14a). The digestion speed slowed down to 0.00 ± 0.01 μm/s, 0.01 ± 0.01 μm/s, 0.02 ± 0.00 μm/s in the deeper region of the cartilage tissue (approximately 60% of the full thickness) at the end of the 3-hour residual digestion (Fig. 4.14b). The results demonstrated that the residual digestion could still remain for a long time.

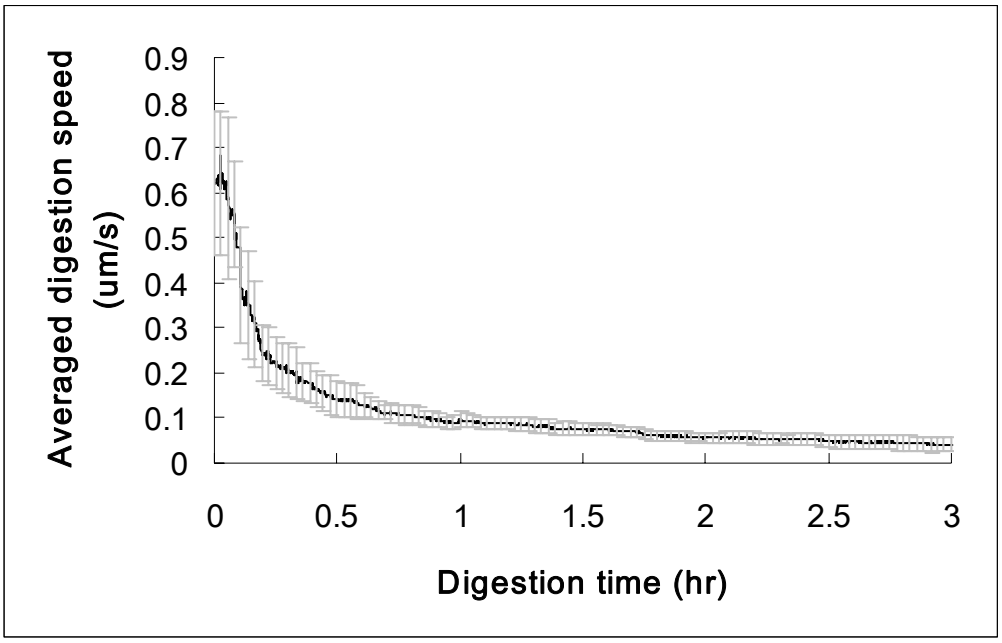

(a)

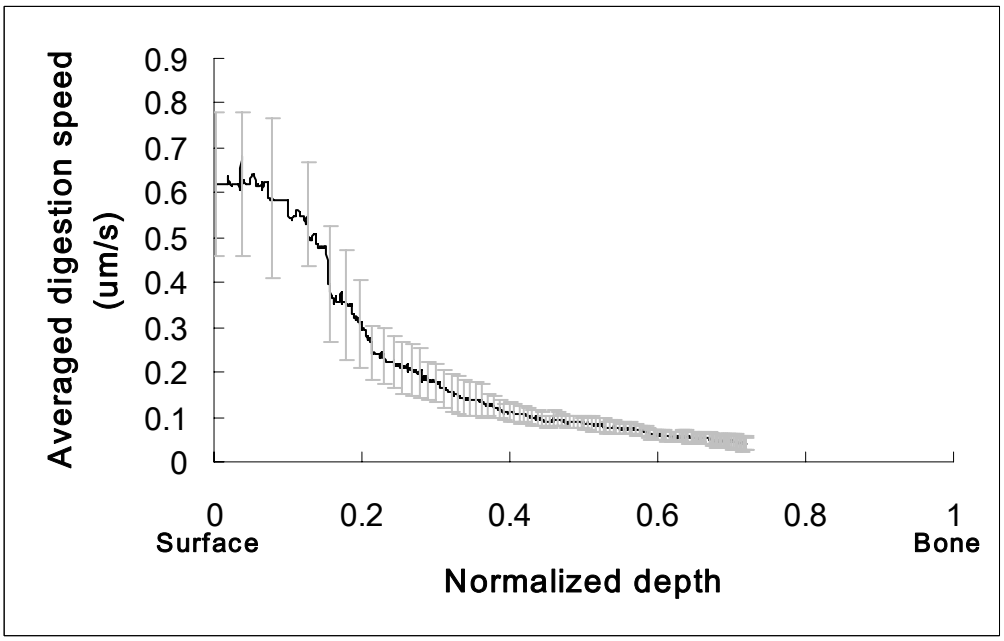

(b)

Fig. 4.13 (a) The profile of the averaged digestion speed as a function of digestion time. (b) The profile of the averaged digestion speed as a function of depth. The error bars represent standard deviations (n = 10).

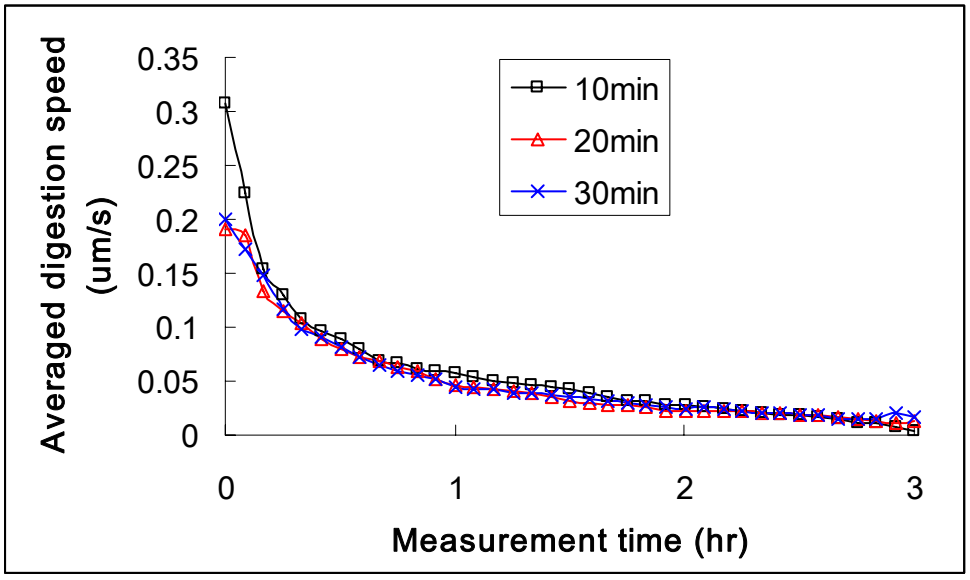

(a)

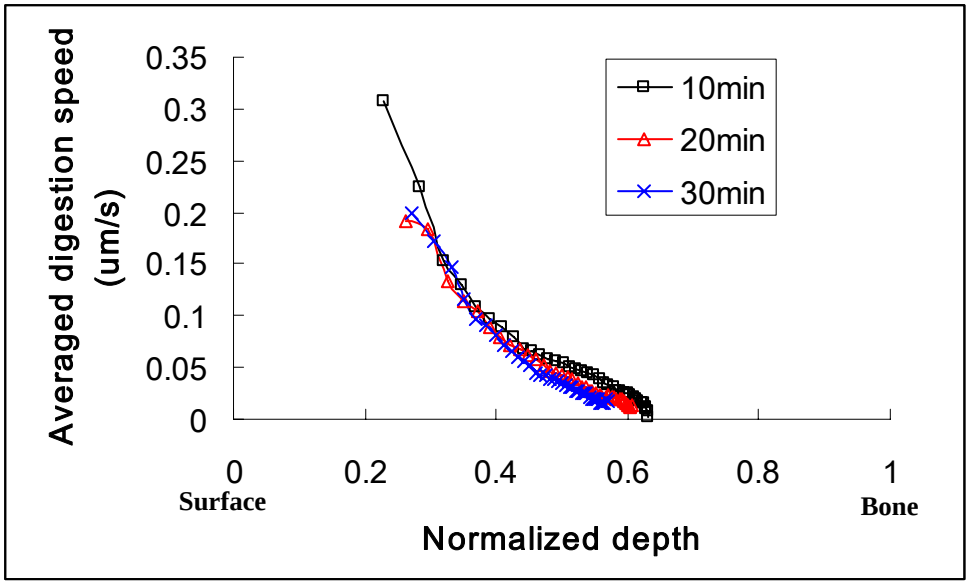

(b)

Fig. 4.14 The profiles of the averaged residual digestion speed as a function of time (a) and as a function of depth (b) when the trypsin-digested specimens were in 0.15 M saline solution after 10-minute (-□-), 20-minute (-Δ-) and 30-minute (-×-) digestions.

4.2.6 Comparison of swelling behavior between normal and degenerated articular cartilage

Fig. 4.15 shows the M-mode ultrasound images collected during different processes. During the shrinkage, swelling and hydration phases, the deformations of the cartilage

at different depths, especially the superficial layer were clearly and dynamically indicated in the ultrasound images.

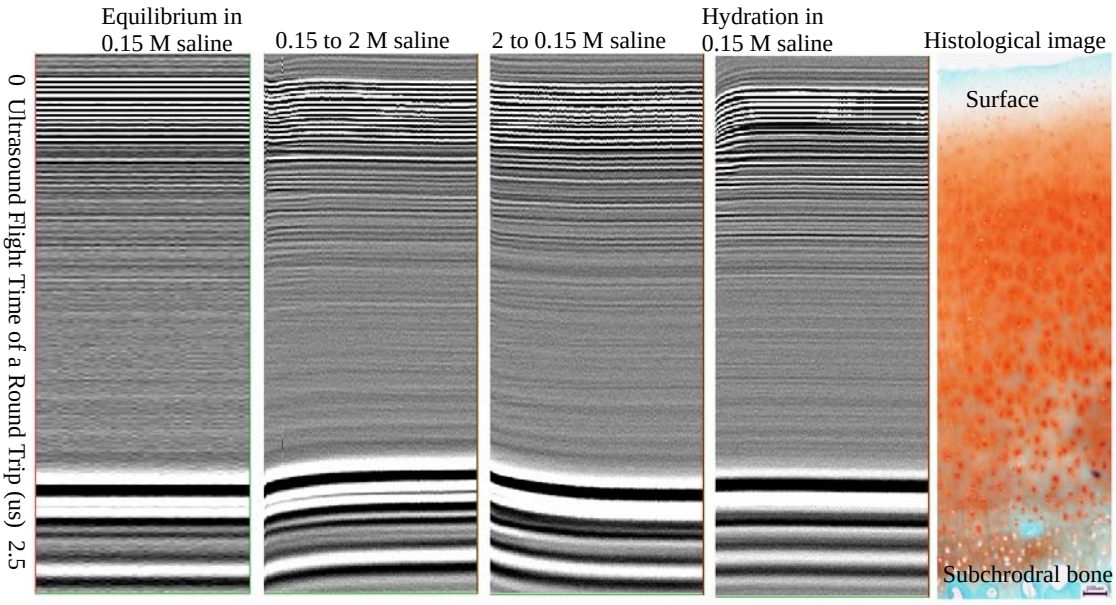

Fig. 4.15 The M-mode ultrasound images collected from a consistent site of one specimen during different monitoring processes: (a) Equilibrium in 0.15 M saline; (b) Shrinkage process after 0.15 M saline was replaced with 2M saline; (c) Swelling process after 2 M saline was replaced with 0.15 M saline; (d) Hydration process in 0.15 M saline after 45-minute dehydration. (e) Histological image of normal cartilage section stained with safranin O and fast green.

The digestion process was clearly shown by the echoes generated at the interface between the digested and undigested tissues (Fig. 4.16). The front echoes shifted with time and depth as an inclined streak during the trypsin digestion and residual digestion phases. The inclined trace was not clear in trypsin digestion due to the high amplitude of the echoes from the cartilage surface. However, it came to be obvious when the middle part of the tissue was digested during the residual digestion in physiological

saline, shrinkage, swelling, and hydration phases. It was demonstrated that the residual digestion came to an proximate end with a quite slow digestion speed (approximately 0.01 μm/s) after the specimen was soaked in physiological saline for 3 hours (Fig. 4.14).

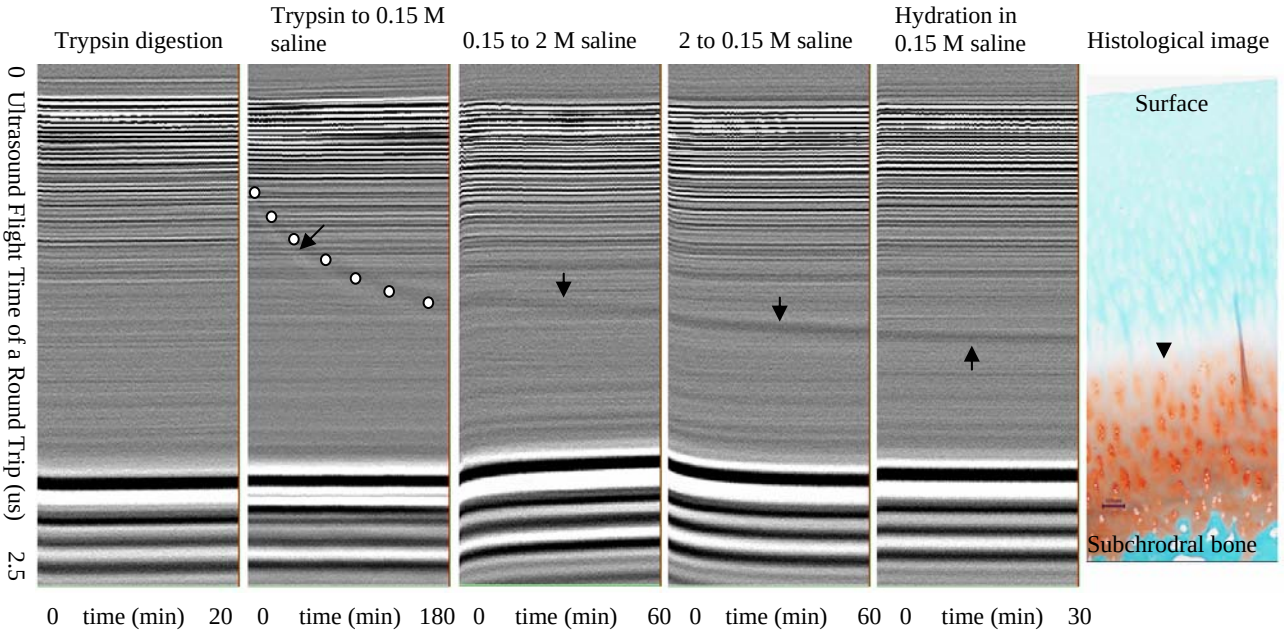

Fig. 4.16 The M-mode ultrasound images collected from the same site as in Fig. 4.15 during trypsin digestion and other post-digestion monitoring processes: (a) Trypsin digestion after 0.15 M saline was replaced with 0.25% trypsin solution; (b) Residual digestion after trypsin solution was replaced with 0.15 M saline; (c) Shrinkage process; (d) Swelling process; (e) Hydration process. (f) Histological image of the degenerated cartilage section. The area stained with red color (dark in grey image) indicates the PG content reduced in comparison with Fig. 4.15e. Black arrows show the digestion trace in (b-e) and the interface of the digested and undigested cartilages in (f). The white dots in (b) represent the marks manually applied and used for the interpolation of the inclined digestion trace as shown in Fig. 4. 12.

After digested with trypsin, the degenerated specimens showed weak shrinkage, swelling and hydration behaviors (Fig. 4.16c-e) in comparison with the normal

specimen without digestion (Fig. 4.15b-d). The results of the parametric measurements will be reported in the following subsections. The final digestion depth in the ultrasound M-mode image was matched with that in the stained histological image (Fig. 4.15e-f). A good correlation in the digestion proportion measured using ultrasound and the histological method was obtained (section 4.2.7, Fig. 4.25).

4.2.6.1 Shrinkage and swelling behavior

Fig. 4.17 demonstrates the comparisons of the transient shrinkage and swelling strains between the normal and degenerated full-thickness cartilage tissues. Overshoot relaxation phenomena during the shrinkage and swelling phases were observed for both normal and degenerated articular cartilage. However, the amplitude of the overshoot decreased after the digestion, especially for the shrinkage behavior of articular cartilage.

Fig. 4.18 shows the comparisons of the peak shrinkage and swelling strains between the normal and degenerated cartilage samples. The absolute values of the peak shrinkage strain significantly ($p < 0.05$, One-Way ANOVA) decreased 45.4%, 42.1% and 50.6% after 10-minute, 20-minute and 30-minute trypsin digestions, respectively (Fig. 4.18a). However, there was no significant difference between the swelling strains of the normal and degenerated samples. It was calculated that the overall mean value of the peak swelling strain also decreased approximately 14% after trypsin digestion (Fig. 4.18b). The statistical results of One-Way ANOVA showed that the overall mean shrinkage duration for the degenerated samples decreased insignificantly ($p > 0.05$) while their overall mean swelling duration increased significantly ($p < 0.05$) (Fig. 4.19). There were large standard deviations in the duration measurement for both the normal and degenerated cartilage tissues.

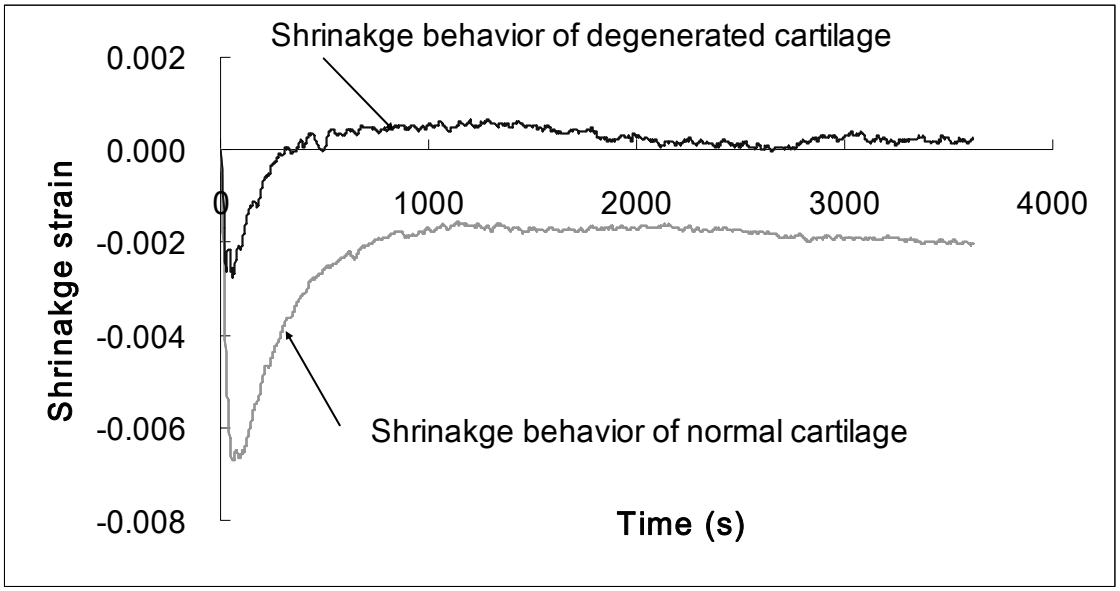

(a)

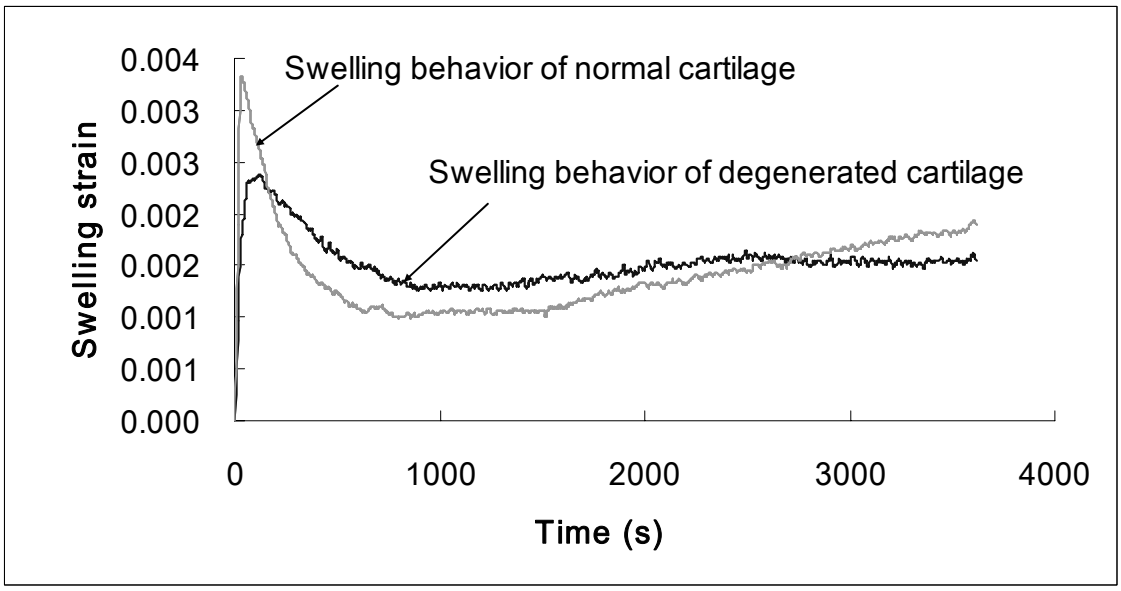

(b)

Fig. 4.17 The comparisons of the transient shrinkage (a) and swelling (b) strains between the normal and degenerated cartilage tissues. The light grey and black solid curves represent the mean transient strains measured before and after trypsin digestion, respectively.

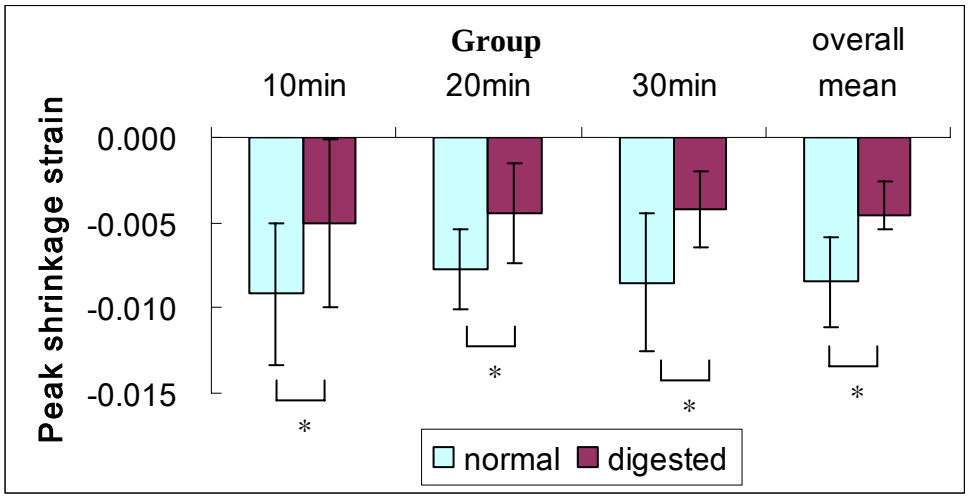

(a)

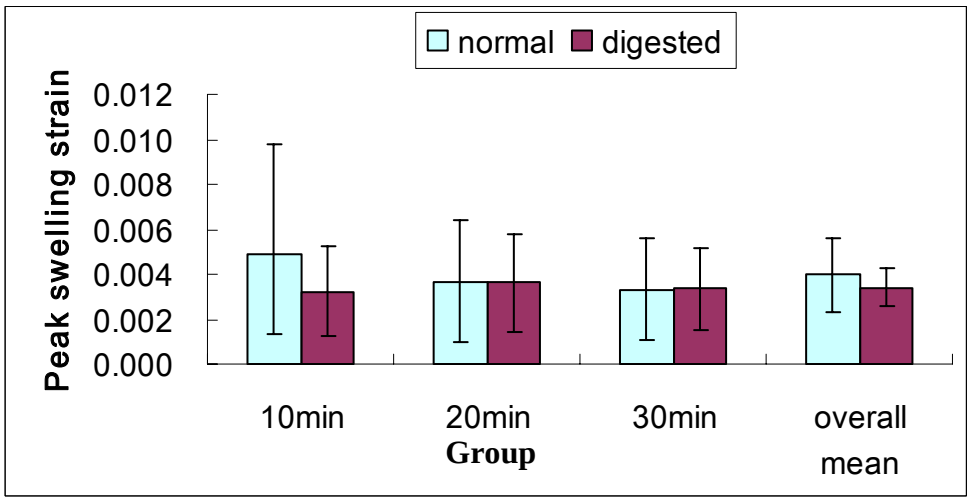

(b)

Fig. 4.18 The comparisons of the peak shrinkage (a) and swelling (b) strains between the normal and degenerated cartilage tissues. The error bars represent standard deviations (n = 10, overall 30 samples). * Significant difference ($p < 0.05$ by One-Way ANOVA) between the normal and degenerated samples.

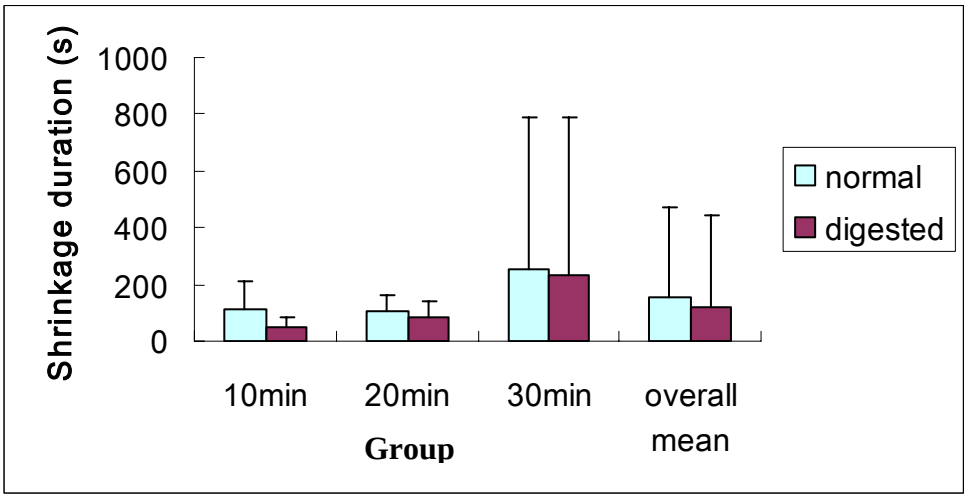

(a)

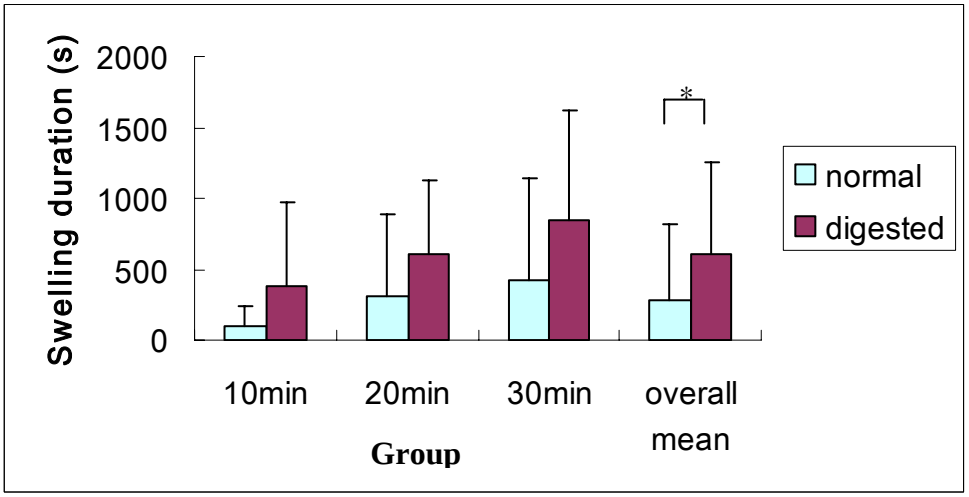

(b)

Fig. 4.19 The comparisons of the shrinkage (a) and swelling (b) duration between the normal and degenerated cartilage tissues. The error bars represent standard deviations (n = 10, overall 30 samples). * Significant difference ($p < 0.05$ by One-Way ANOVA) between the normal and degenerated samples.

After the depletion of the PG content, the percentage change of the sound speed in cartilage during both the shrinkage and swelling processes remained to exponentially depend on the measurement time (Fig. 4.20). The changes can be described by an exponential formula ($y = A + Be^{Cx}$). There was no significant difference among the coefficients of *A*, *B*, and *C* for the samples with different digestion periods. A similar

overall speed change was found between the degenerated cartilage and the normal cartilage for both the shrinkage and swelling processes (5.2 ± 1.5 % and -5.1 ± 1.1 % for normal samples; 5.1 ± 0.8 % and -4.9 ± 1.2 % for degenerated samples, respectively, Table 4.3). Among the three groups, there was no significant difference ($p > 0.05$, LSD Post Hoc Tests of One-Way ANOVA).

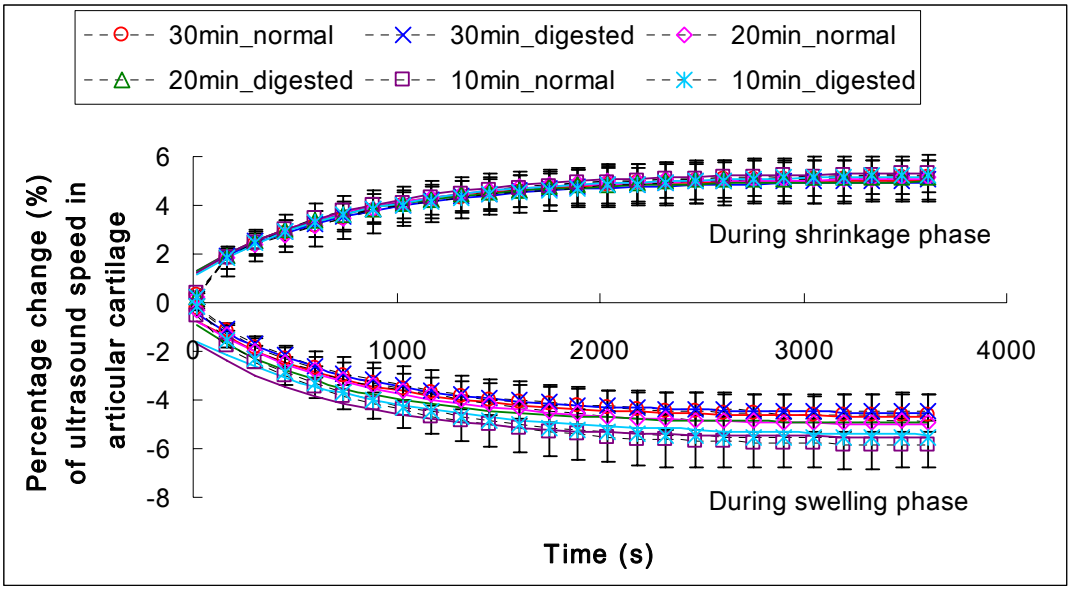

Fig. 4.20 The comparison of the percentage change of ultrasound speed in articular cartilage between the normal and degenerated samples. The error bars represent standard deviations (n = 10).

Table 4.3 The percentage change (mean ± SD) of ultrasound speed in articular cartilage at equilibrium during shrinkage and swelling processes before and after trypsin digestion.

Measurement items	Shrinkage		Swelling	
	Normal	Trypsin-treated	Normal	Trypsin-treated
Group 10min (n = 10)	5.3 ± 2.4	5.2 ± 0.8	-5.8 ± 1.0	-5.5 ± 1.3
Group 20min (n = 10)	5.1 ± 1.0	5.1 ± 0.7	-4.9 ± 1.2	-4.8 ± 1.2
Group 30min (n = 10)	5.1 ± 0.9	5.0 ± 0.8	-4.6 ± 0.8	-4.5 ± 0.9
Overall (n = 30)	5.2 ± 1.5	5.1 ± 0.8	-5.1 ± 1.1	-4.9 ± 1.2

4.2.6.2 Depth-dependence of swelling behavior

Fig. 4.21 shows the depth-dependent swelling strains of the normal and trypsin-treated articular cartilage samples at equilibrium. It was found that in comparison with the overall (n = 44) mean swelling strains of the normal tissues at different depths, the overall (n = 30) mean swelling strain at the superficial layer of the degenerated tissues increased, the strain at the middle layer decreased, and the strain at the deep layer changed little. The swelling strain at the superficial layer of the 30-minute digested samples significantly increased and the swelling strain at the middle layer of the 10-minute digested samples significantly ($p < 0.05$ by LSD Post Hoc Tests of One-Way ANOVA) decreased. However, there was no significant difference ($p = 0.568$) in the strains at the deep layer between the normal and the digested cartilage samples.

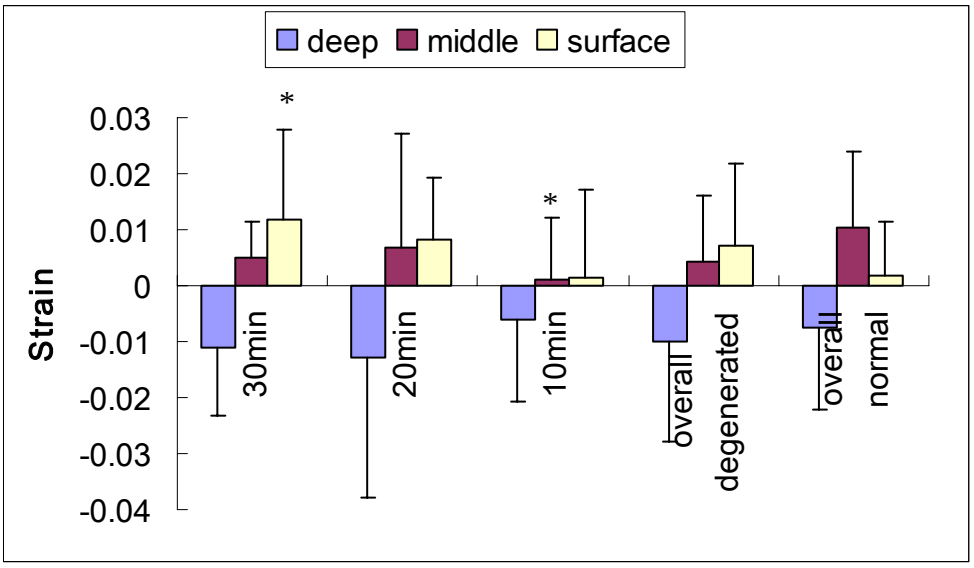

Fig. 4.21 The equilibrium swelling strains at the deep, middle and surface layers of the degenerated cartilage samples in comparison with the overall mean swelling strains of normal samples. * Significant difference ($p < 0.05$ by LSD Post Hoc Tests of One-Way ANOVA) in comparison with the normal samples.

4.2.6.3 Hydration

A more obvious swelling behavior (hydration) was observed when the specimen was re-soaked in physiological saline after dehydrated in the air for 45 minutes. For the normal specimens, the overall value of equilibrium hydration strains (0.037 ± 0.009, $n = 30$) was significantly ($p < 0.001$, One-Way ANOVA) larger than the absolute values of the overall peak strain of swelling (0.004 ± 0.002) and shrinkage (0.009 ± 0.003) induced by osmotic loading.

No overshoot-relaxation phenomenon was observed during hydration. Fig. 4.22 shows the transient hydration strains of the normal and the 10-minute digested articular cartilage during the 30-minute hydration phase. The averaged equilibrium hydration strains decreased significantly ($p < 0.01$, One-Way ANOVA) from 0.038 ± 0.013 to 0.016 ± 0.012 after 10-minute trypsin digestion (Fig. 4.23). A similar significant decrease in the equilibrium hydration strain was obtained for Group 20min (from 0.046 ± 0.019 to 0.026 ± 0.015, $p < 0.02$) and Group 30min (from 0.026 ± 0.013 to 0.013 ± 0.007, $p < 0.01$). However, it was found that the different digestion periods did not cause significant changes ($p > 0.05$, LSD Post Hoc Tests of One-Way ANOVA) in the hydration strains between the normal and degenerated tissues among the three groups. Therefore, the different digestion periods of 10, 20, and 30 minutes selected in this study did not cause a significant difference in the decrease of the hydration strain.

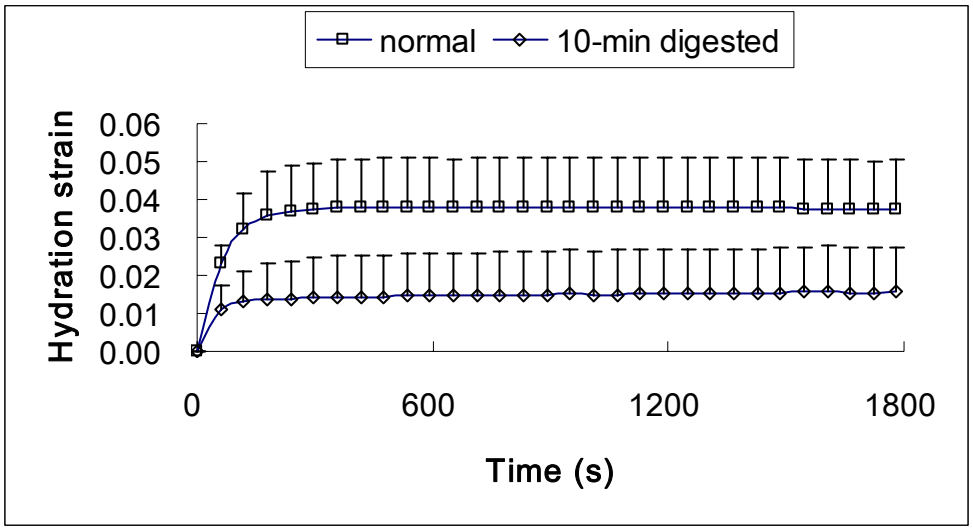

Fig. 4.22 The transient hydration strains of the normal and 10-minute digested cartilage specimens. The error bars represent standard deviations (n = 10).

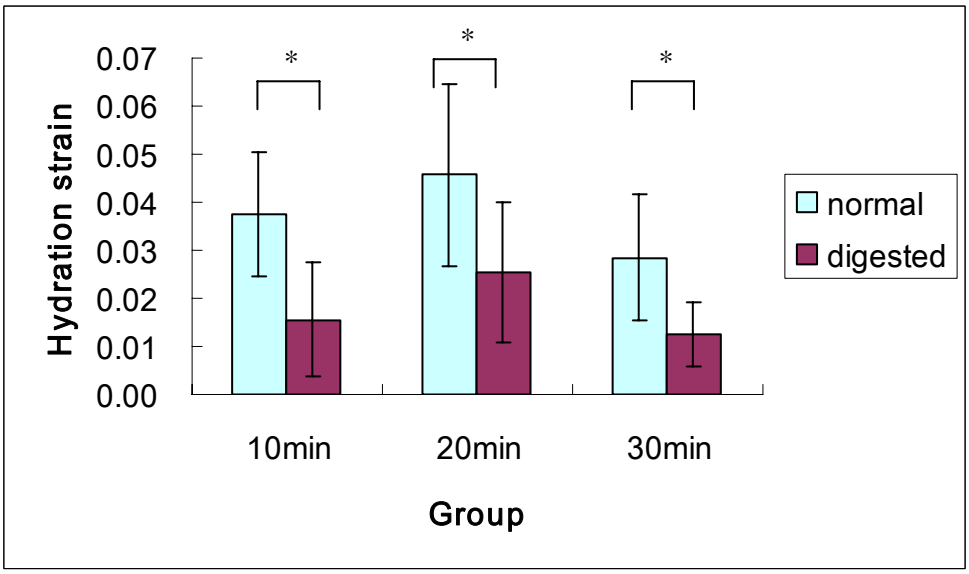

Fig. 4.23 The comparison of equilibrium hydration strain between the normal specimens and their 10-minute, 20-minute and 30-minute trypsin-digested tissues. The error bars represent standard deviations (n = 10). * Significant decrease ($p < 0.05$ by One-Way ANOVA) in comparison with the normal cartilage.

4.2.7 Correlation of results obtained by ultrasonic measurement and histological analysis

Digestion proportion

The digestion proportions induced by 10-minute, 20-minute and 30-minute trypsin digestions were measured using the manually controlled 3D USMS and histology (Fig. 4.24). It was clearly shown that the depth of trypsin penetration increased with the increase of the digestion time. After the 30-minute digestion, averagely 31.4% were digested, which was significantly higher than those after the 10-minute and 20-minute digestions (22.3% and 24.7%, respectively) ($p < 0.05$ by LSD Post Hoc Tests of One-Way ANOVA). However, after the 3-hour residual digestion in 0.15 M saline and shrinkage-swelling and hydration phases, the final digestion proportions were not significantly different among the three groups ($p > 0.6$, LSD Post Hoc Tests of One-Way ANOVA). It was found that the ultrasound-measured results were similar to those measured using histological method (Fig. 4.24), and a good correlation was obtained between these two methods (slope = 0.9896, $R^2 = 0.7993$, Fig. 4.25). Fig. 4.26 indicates the similar digestion proportion showed in M-mode ultrasound images of hydration phase and histological images after the processes of trypsin digestion, residual digestion, shrinkage, swelling and hydration for the specimens from one patella.

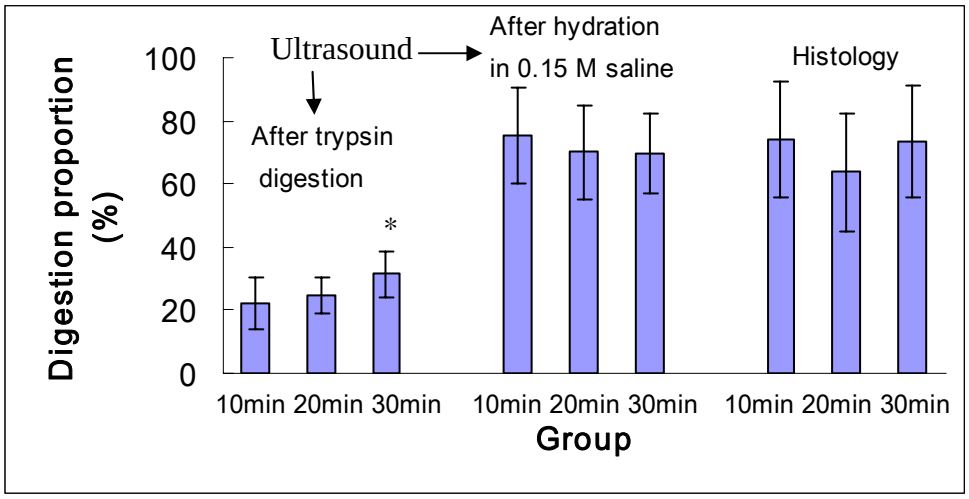

Fig. 4.24 The digestion proportions of the three groups were measured at the end of trypsin digestion and hydration phases measured by ultrasound, respectively, in comparison with the final digestion proportions measured by histology. The error bars represent standard deviations (n = 10). * Significant increase ($p < 0.05$ by LSD Post Hoc Tests of One-Way ANOVA) in comparison with the 10-minute and 20-minute digestions.

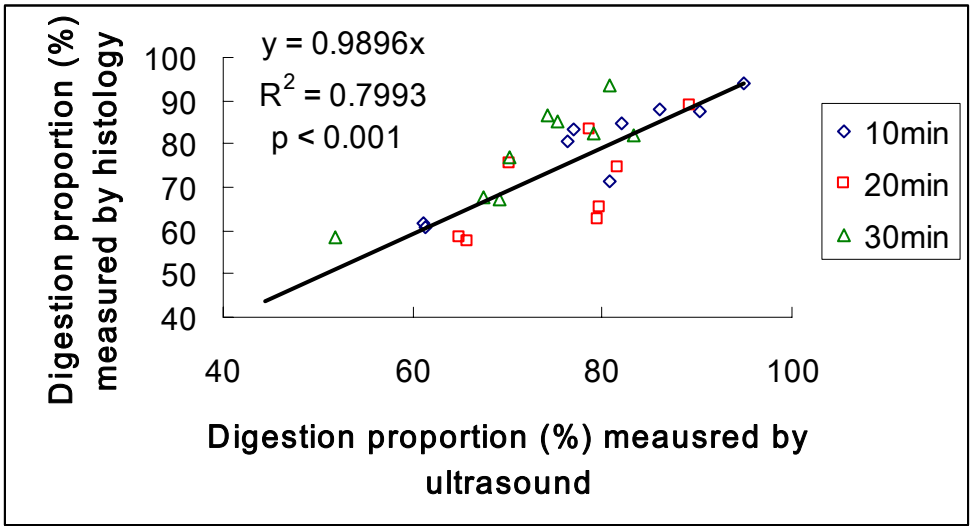

Fig. 4.25 A significant correlation of the digestion proportions measured using ultrasound and histological methods (n = 30).

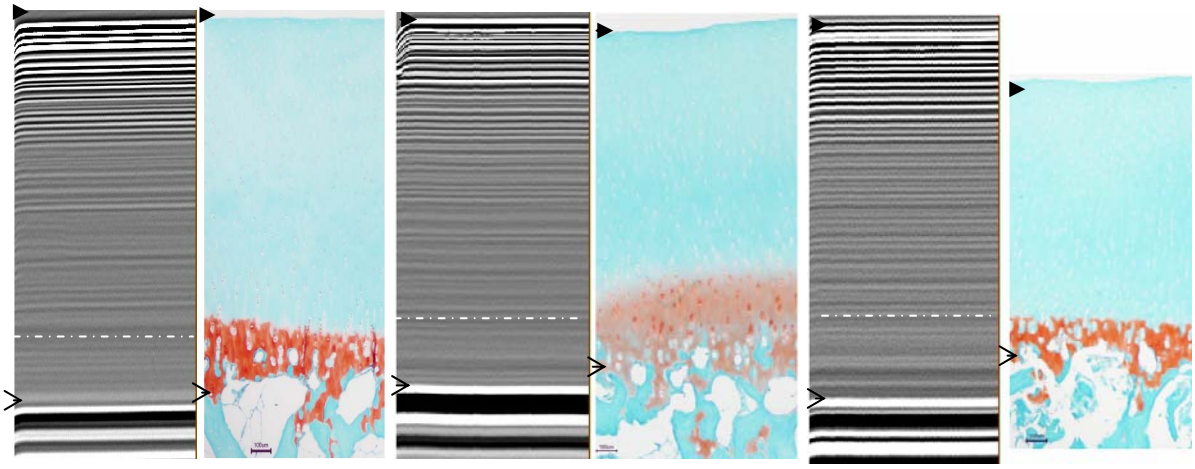

(a) (b) (c) (d) (e) (f)

Fig. 4.26 M-mode ultrasound images (a, c, e) of hydration process and histological images (b, d, f) of specimens from one patella. (a-b): the 10-minute digested specimen; (c-d): the 20-minute digested specimen; and (e-f): the 30-minute digested specimen. The dashed line in M-mode ultrasound images represents the location of the digestion depth. The solid arrowheads indicate cartilage surface and the line arrowheads indicate cartilage-bone interface.

Thickness

Meanwhile, the thickness of the cartilage layer was measured using ultrasound, histology and digital caliper, respectively. The results that the thickness measured by ultrasound was well correlated with that measured by histology and caliper ($p < 0.001$, Fig. 4.27), respectively, demonstrated that it is feasible to use ultrasound to measure the thickness of articular cartilage with the assumed ultrasound speed. In addition, no obvious change was found in the thickness of the cartilage layer before and after trypsin digestion.

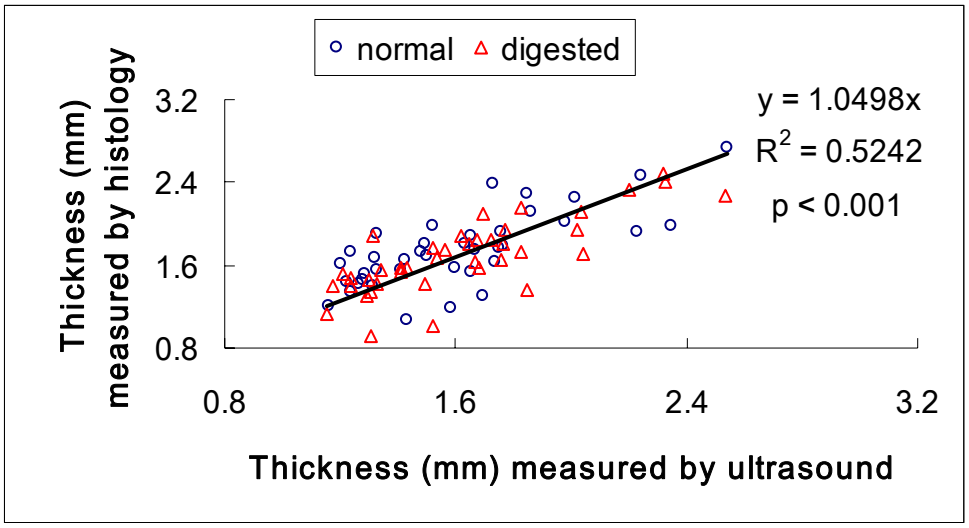

(a)

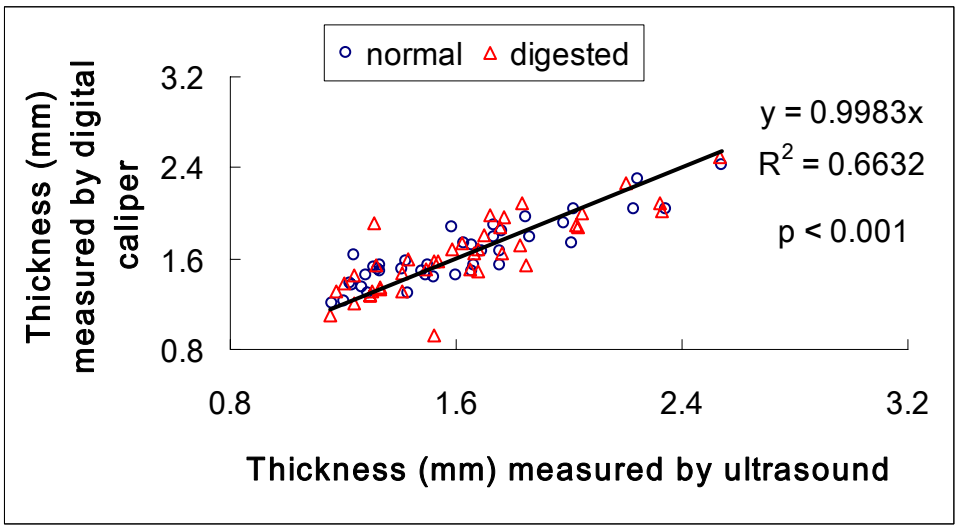

(b)

Fig. 4.27 The thickness of the cartilage layer measured using ultrasound well correlates with that measured using the histological method (a) and digital caliper (b), respectively.

4.3 Parametric Prediction Based on Bi-layered Triphasic Modeling

4.3.1 Measurement of water fraction of articular cartilage

It was found that there was no significant difference ($p > 0.5$, One-Way ANOVA) in the distribution of water content between the degenerated cartilage tissues with 10-minute and 20-minute digestions and their normal tissues, respectively (Fig. 4.28a-b). However,

the water content of the cartilage tissue digested 30 minutes decreased significantly ($p < 0.01$, One-Way ANOVA), especially for the 50% upper cartilage layer (Fig. 4.28c).

4.3.2 Measurement of FCD of articular cartilage

Based on the reference FCD distribution of the normal and degenerated cartilage tissues (Fig. 3.17), the real FCD distributions of the normal and the 10-minute, 20-minute, and 30-minute digested specimens in this study were calculated using our indirect method. The FCD significantly decreased at the trypsin-digested cartilage layer ($p < 0.001$, One-Way ANOVA) in comparison with that of the normal tissue for all the three groups (Fig. 4.29). The values of FCD at the deep layer, however, were close to the normal value due to the non-full-thickness digestion used in this study.

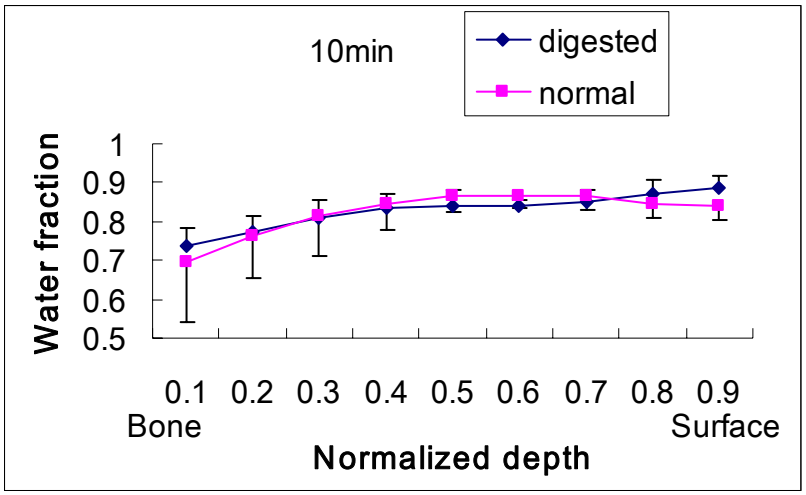

(a)

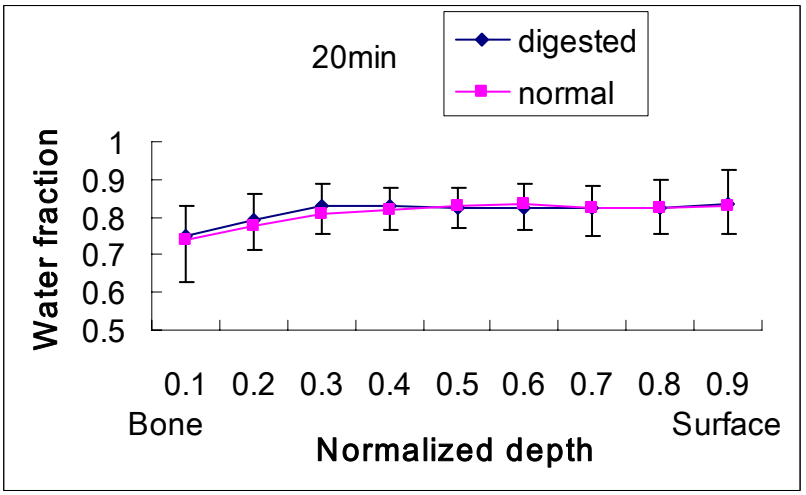

(b)

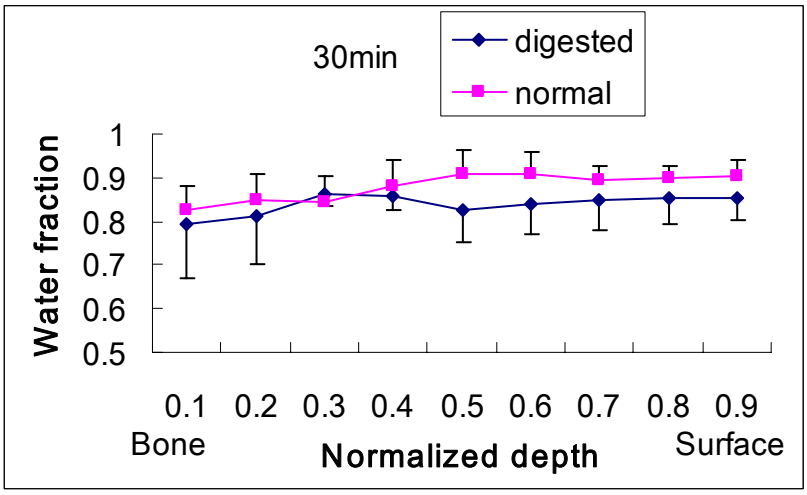

(c)

Fig. 4.28 The depth-dependent distribution of water fraction of articular cartilage before and after the 10-minute (a), 20-minute (b) and 30-minute (c) trypsin digestions. The error bars represent standard deviations (n = 10).

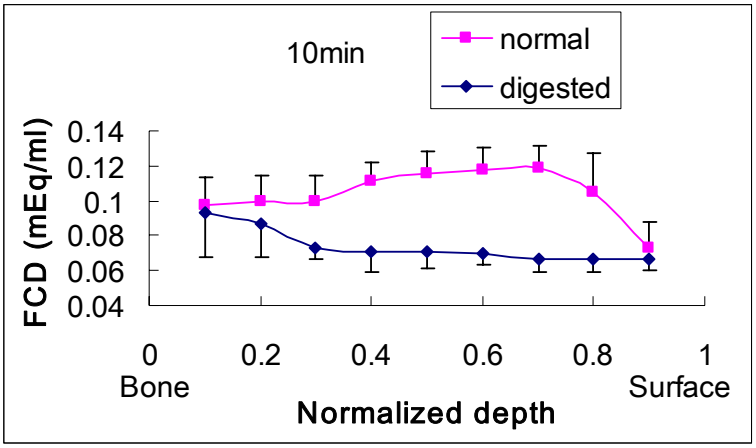

(a)

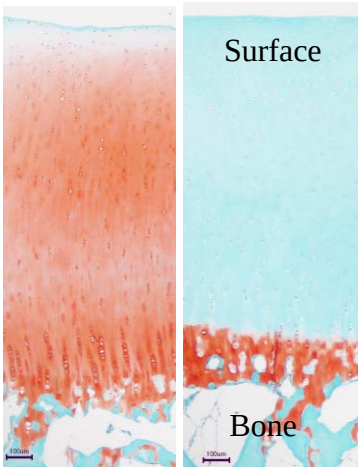

(b) (c)

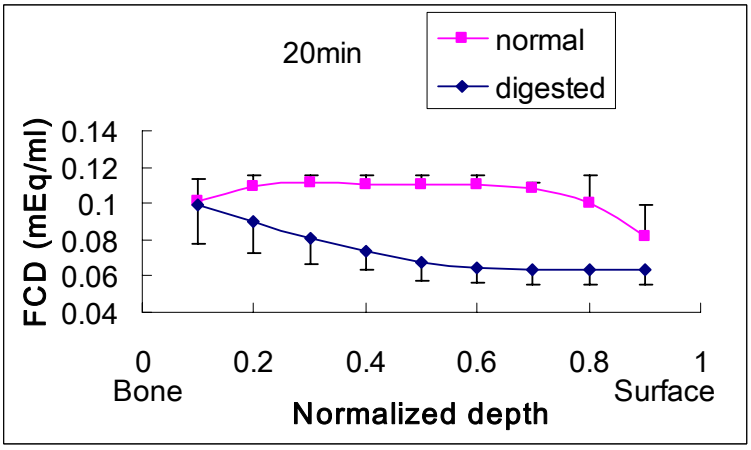

(d)

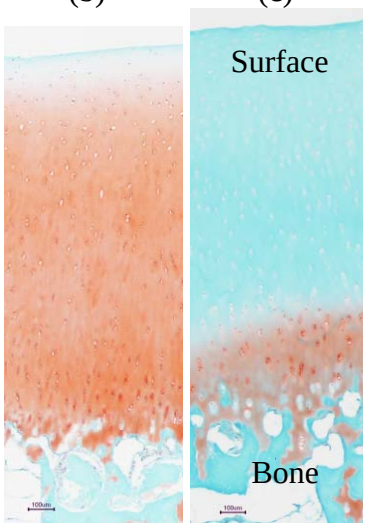

(e) (f)

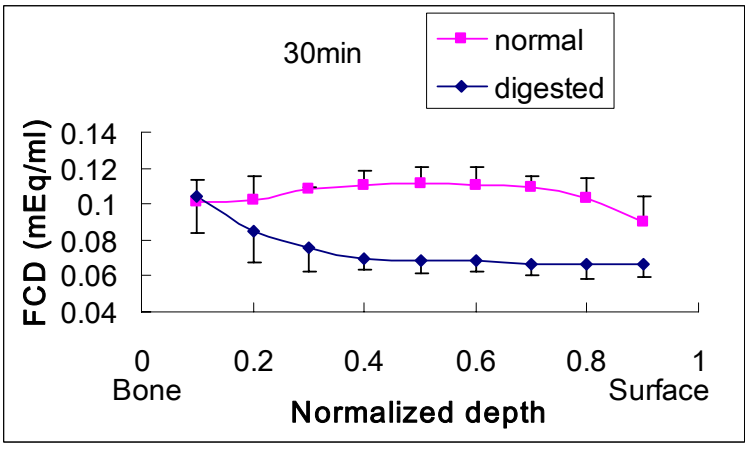

(g)

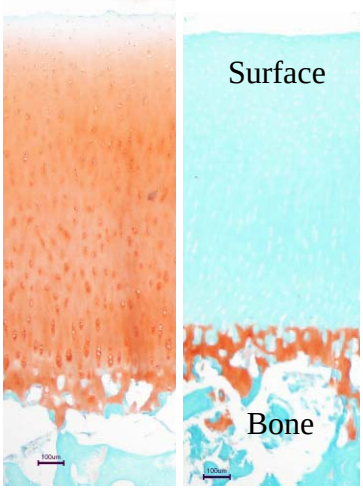

(h) (i)

Fig. 4.29 The depth-dependent distribution of FCD and histological images of articular cartilage before and after the 10-minute (a-c), 20-minute (d-f), and 30-minute (g-i) trypsin digestions. (b, e, h): histological images of normal cartilage; (c, f, i): histological images of degenerated cartilage. The error bars represent standard deviations (n = 10).

4.3.3 Theoretical prediction of cartilage swelling

The newly-developed bi-layered triphasic model was used to describe the nonuniform swelling-induced strains of both normal and trypsin-digested articular cartilage (Fig. 4.30). It was observed that the interface of Layer1 and Layer2 moved towards the bone and thus the distribution pattern of the strains was changed depth-dependently after the PGs were depleted. For all the specimens, the mean values of the 4 parameters predicted using three different models were listed in Table 4.4. The region near the bone, for the normal specimens, had a significantly higher modulus (Ha_1 = 18.5 ± 15.5 MPa) in comparison with the middle zone and the surface layer (Ha_2 = 7.6 ± 11.6 MPa and Ha_3 = 3.6 ± 3.3 MPa, respectively) ($p < 0.001$, LSD Post Hoc Tests of One-Way ANOVA). The predicted normalized thickness of the deep layer (Layer1) h_1 was 0.67 ± 0.22, which indicates the separating location of the two layers (Fig 3.16). With the increase of the digestion time from 10 minutes to 30 minutes, the mean *Ha* and *h1* values of the three groups of the degenerated cartilage samples decreased gradually and insignificantly ($p > 0.2$, LSD Post Hoc Tests of One-Way ANOVA). For the 30-minute trypsin-digested specimens, the averaged values were *Ha1* = 11.1 ± 10.1 MPa, *Ha2* = 6.7 ± 16.9 MPa, *Ha3* = 1.9 ± 2.8 MPa, *h1* = 0.55 ± 0.24. Fig. 4.31 shows the *Ha* distribution of the normal samples and the changes of the parameters after the 30-minute digestion. However, no significant changes were found among the parameters predicted between the normal and the digested samples ($p > 0.1$, LSD Post Hoc Tests of One-Way ANOVA) probably due to the large variance. Similar results were obtained using the 3-parameter model (Table 4.4). The overall aggregate modulus of the normal samples obtained using the homogeneous model was significantly higher than those of

the degenerated specimens ($p < 0.05$, One-Way ANOVA). It was also found that the aggregate modulus of the degenerated specimens exponentially decreased with the increase of digestion time in comparison with the normal specimens ($R^2 = 0.968$, $p < 0.05$).

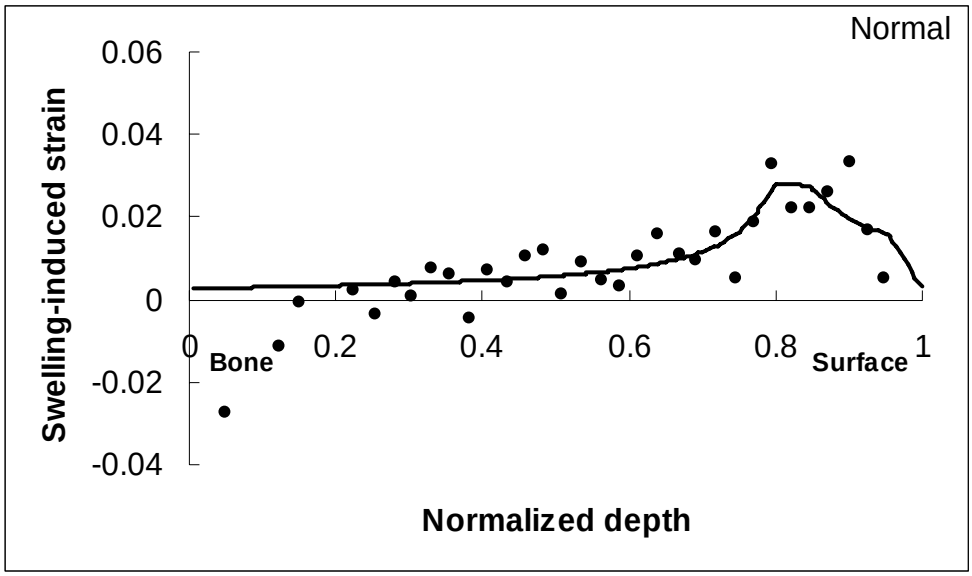

(a)

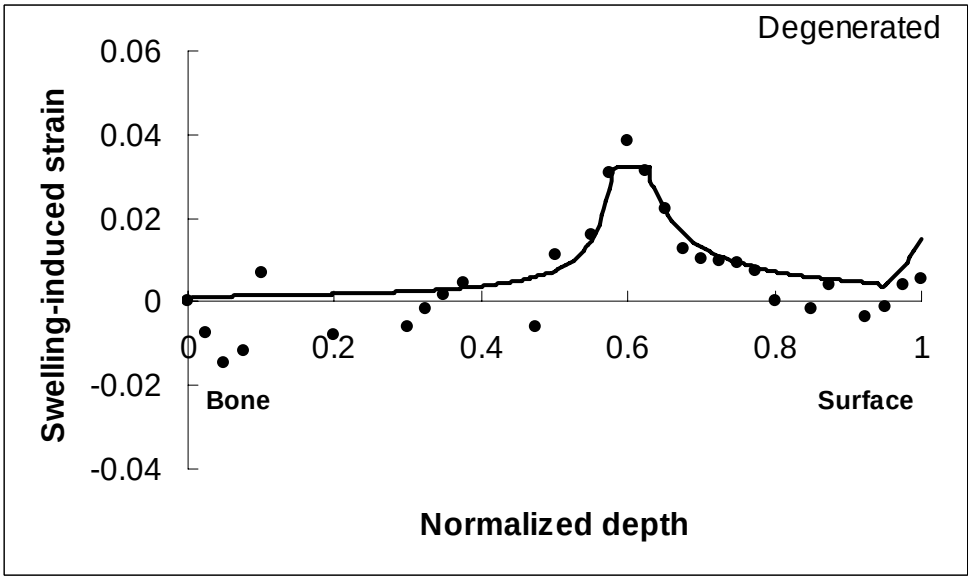

(b)

Fig. 4.30 The nonuniform distribution of the swelling-induced strains before (a) and after (b) 10-minute trypsin digestion for a typical cartilage specimen. The solid line represents the theoretical prediction of the strain distribution obtained using the new bi-layered triphasic model.

Table 4.4 The predicted parameters (mean ± SD) of the new bi-layered model (4 parameters) in comparison with the results of the 3-parameter bi-layered model and the homogeneous model.

Parameters	**4-parameter layered model**		**3-parameter layered model**		**Homogenous model**	
			Normal (n = 44)			
Aggregate modulus (MPa)	Ha_1	18.5 ± 15.5*	Ha_1	9.3 ± 12.6	*Ha*	7.1 ± 6.1**
	Ha_2	7.6 ± 11.6	Ha_2	3.5 ± 3.7		
	Ha_3	3.6 ± 3.3				
Thickness of Layer1 (mm)	h_1	0.67 ± 0.22	h_1	0.56 ± 0.29		
			After 10-minute trypsin digestion (n = 10)			
Aggregate modulus (MPa)	Ha_1	17.9 ± 11.8	Ha_1	15.3 ± 18.5	*Ha*	4.0 ± 1.9
	Ha_2	12.9 ± 14.2	Ha_2	3.4 ± 4.0		
	Ha_3	2.9 ± 3.2				
Thickness of Layer1 (mm)	h_1	0.69 ± 0.19	h_1	0.54 ± 0.25		
			After 20-minute trypsin digestion (n = 10)			
Aggregate modulus (MPa)	Ha_1	13.6 ± 10.4	Ha_1	7.9 ± 10.6	*Ha*	3.3 ± 2.1
	Ha_2	9.3 ± 12.2	Ha_2	2.9 ± 3.6		
	Ha_3	2.2 ± 2.9				
Thickness of Layer1 (mm)	h_1	0.57 ± 0.31	h_1	0.58 ± 0.32		
			After 30-minute trypsin digestion (n = 10)			
Aggregate modulus (MPa)	Ha_1	11.1 ± 10.1	Ha_1	5.4 ± 11.8	*Ha*	2.2 ± 0.6
	Ha_2	6.7 ± 16.9	Ha_2	1.5 ± 2.5		
	Ha_3	1.9 ± 2.8				
Thickness of Layer1 (mm)	h_1	0.55 ± 0.24	h_1	0.45 ± 0.24		

* Significant difference ($p < 0.001$ by LSD Post Hoc Tests of One-Way ANOVA)

** Significant difference ($p < 0.05$ by One-Way ANOVA)

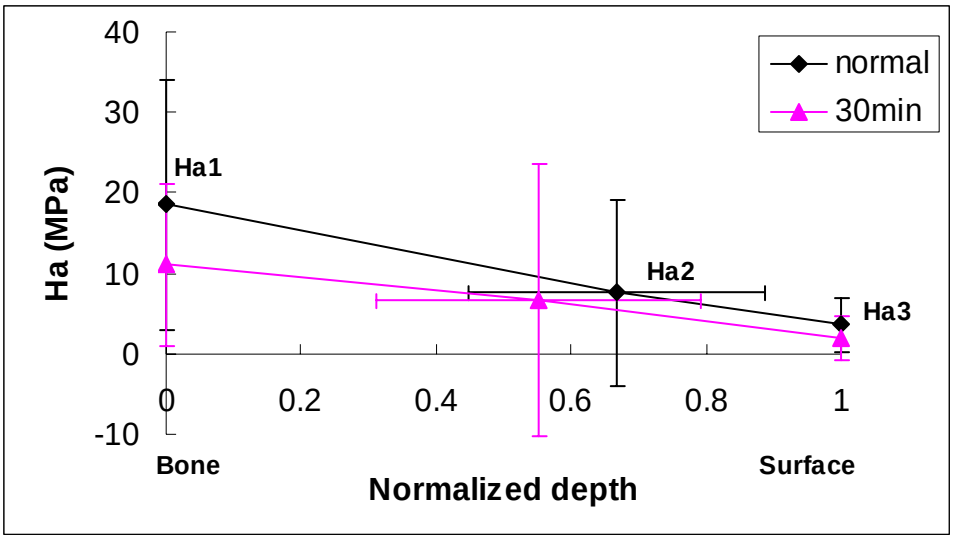

Fig. 4.31 The parameters Ha_1, Ha_2, Ha_3, h_1 (mean ± SD) of the 30-minute trypsin-digested samples (n = 10) estimated by the new bi-layered triphasic model in comparison with the normal specimens (n = 44).

According to the calculation of LSE, the predicted strain values using the three models were evaluated. It was obvious that the new model used in this study could achieve better curve fitting for the strains, as the percentage LSE value for the new model (0.23 ± 0.10) was significantly ($p < 0.05$, LSD Post Hoc Tests of One-Way ANOVA) smaller than that for Narmoneva's model (0.30 ± 0.16) and the homogeneous model (0.31 ± 0.15).

4.4 Comparison of Acoustic Properties between Normal and Degenerated Articular Cartilage

Amplitude of the reflection echo

The attenuation dB value of the cartilage samples was set using the ultrasound pulser/receiver to guarantee the peak of the signals nicely unsaturated during the experiments. In comparison with the normal specimens, the amplitude of the ultrasonic

echoes of the trypsin-digested cartilage decreased with the increase of the digestion time (Group 10min: 18.7±7.5 dB; Group 20min: 15.3±3.6 dB; Group 30min: 13.3±4.9 dB, Fig. 4.32). The dB value of the digested specimens insignificantly ($p > 0.2$, One-Way ANOVA) decreased 1.5, 1.7 and 2.8 dB from that of their normal specimens, respectively. Meanwhile, the maximum amplitude of the echoes reflected from the cartilage surface was measured in Table 4.5. The peak value of the amplitude of the digested specimens slightly and insignificantly decreased 0.003~0.006 dB with the time of trypsin digestion for the three groups.

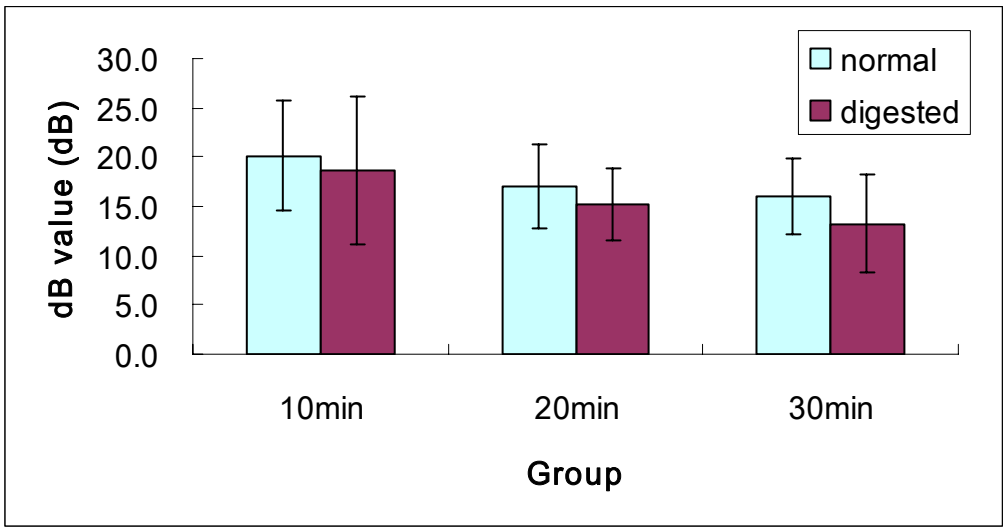

Fig. 4.32 The attenuation dB values of the 10-minute, 20-minute, and 30-minute digested specimens in comparison with their normal cartilage specimens before trypsin digestion. The error bars represent standard deviations (n = 10).

Table 4.5 Centroid frequency and maximum amplitude of the echoes from the cartilage surface before and after trypsin digestion.

	Centroid frequency (MHz)			Max amplitude (dB)		
	normal	digested	Δ	normal	digested	Δ
Group 10min	32.39	34.07	1.68	0.033	0.030	-0.003
	±3.43	±4.92		±0.021	±0.021	
Group 20min	31.82	31.92	0.10	0.021	0.018	-0.003
	±3.14	±3.52		±0.018	±0.007	
Group 30min	29.78	30.38	0.60	0.023	0.017	-0.006
	±2.69	±2.08*		±0.014	±0.002	

∗ Significant difference ($p < 0.05$ by LSD Post Hoc Tests of One-Way ANOVA) from the value of Group 10min.

Centroid frequency

The centroid frequency of the echoes from the cartilage surface averagely increased 1.68 MHz, 0.10 MHz, and 0.60 MHz after the 10-minute, 20-minute, and 30-minute trypsin digestion, respectively (Table 4.5). The increase of the centroid frequency indicates that the low-frequency content of the echoes reduced and high-frequency content increased due to the trypsin digestion. A significant difference ($p < 0.05$, LSD Post Hoc Tests of One-Way ANOVA) in the centroid frequency was found between Group 30min (30.38 ± 2.08 MHz) and Group 10min (34.07 ± 4.92 MHz) samples after digestion.

Reflection coefficient

The integrated reflection coefficient (IRC) of the cartilage surface decreased approximately 1~4 dB for all the three groups (Table 4.6). However, no significant difference was found between the mean values of the normal and the digested samples

($p > 0.05$, One-Way ANOVA), except the comparison between the 10-minute and 30-minute digested groups ($p < 0.05$, LSD Post Hoc Tests of One-Way ANOVA).

Backscatter coefficient

In this study, the integrated backscatter coefficients including AIB of the cartilage-bone connection zone and IBS of the middle cartilage tissue were calculated. The AIB values decreased approximately 2~3 dB after the trypsin digestions for all the three groups (Table 4.6). Also, no significant decrease ($p > 0.05$, LSD Post Hoc Tests of One-Way ANOVA) in AIB was found between the digested groups and the normal samples before digestion. Similarly, the IBS values of the middle matrix of the degenerated cartilage tissue insignificantly differ from those obtained before digestion ($p > 0.05$, LSD Post Hoc Tests of One-Way ANOVA, Table 4.7).

Table 4.6 Reflection coefficient of the cartilage surface and the integrated backscatter coefficient of the cartilage-bone interface before and after trypsin digestion.

	IRC (dB)			AIB (dB)		
	normal	digested	Δ	normal	digested	Δ
Group 10min	-31.70	-35.36	-3.66	-49.10	-51.13	-2.03
	±8.47	±11.82		±7.10	±7.74	
Group 20min	-30.42	-31.02	-0.60	-52.63	-55.35	-2.72
	±10.08	±10.31		±5.53	±5.06	
Group 30min	-22.29	-23.89	-1.60	-52.00	-54.49	-2.49
	±11.86	±12.11*		±6.15	±6.87	

* Significant difference ($p < 0.05$ by LSD Post Hoc Tests of One-Way ANOVA) from the value of Group 10min.

Attenuation

The integrated attenuation (IA) coefficient increased approximately 4 dB/mm after the 20-minute and 30-minute trypsin digestion, which was larger than that of the 10-minute digested samples (0.16 dB/mm) (Table 4.7). The increases were not statistically significant ($p > 0.05$, One-Way ANOVA) from those of the corresponding normal samples before digestion.

IA coefficient changes as a function of frequency were showed in Fig. 4.33. An obvious increase in the value of the IA curve of the 30-minute digested samples was indicated, which is located outside the IA range (mean ± SD) of the normal specimens. However, the difference was not significant ($p > 0.05$, LSD Post Hoc Tests of One-Way ANOVA). In addition, it was found that the IA slope of the digested cartilage insignificantly decreased approximately 0.1~0.3 dB/mm/MHz in comparison with the normal cartilage ($p > 0.05$, LSD Post Hoc Tests of One-Way ANOVA, Table 4.8).

Table 4.7 Attenuation coefficient and the integrated backscatter coefficient of the middle cartilage tissue before and after trypsin digestion.

	IBS (dB)			IA (dB/mm)		
	normal	digested	Δ	normal	digested	Δ
Group 10min	-70.62	-71.84	-1.22	15.40	15.56	0.16
	±4.30	±3.39		±14.27	±8.15	
Group 20min	-75.43	-74.06	1.37	20.42	25.29	4.87
	±4.30	±2.42		±8.26	±12.23	
Group 30min	-72.34	-70.98	1.36	22.09	26.39	4.30
	±5.57	±5.26		±15.48	±17.17	

In summary, the results indicated that the tendency of the change in the acoustic parameters was similar for all the three groups. The changes of the samples digested for 30 minute were more obvious than those of the samples digested for 10 and 20 minutes. However, not all the parameters changed with a statistical significance after trypsin digestion. It was found that parameters such as the amplitude, centroid frequency of the echoes from the cartilage surface, and IRC were more sensitive to the change in the PG content of the cartilage tissue induced by trypsin digestion.

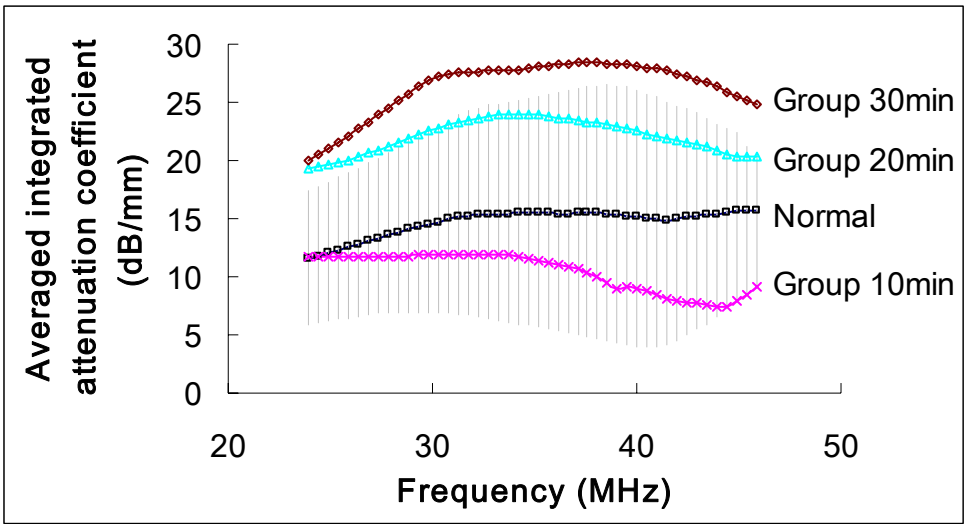

Fig. 4.33 The profiles of the averaged integrated attenuation coefficient as a function of frequency. The degenerated samples from Group 10min, Group 20min, and Group 30min were compared with all the normal samples. The error bars represent standard deviations (n = 30).

Table 4.8 IA slope of the middle cartilage tissue before and after trypsin digestion.

	IA slope β (dB/mm/MHz)		
	normal	digested	Δ
Group 10min	0.39 ± 0.30	0.16 ± 0.25	-0.23
Group 20min	0.25 ± 0.32	0.15 ±0.24	-0.10
Group 30min	0.33 ± 0.60	0.21 ± 0.55	-0.12

4.5 Analysis and Correlation of Swelling, Acoustic and Biochemical Parameters

Correlations between swelling and shrinkage parameters

Besides the swelling behavior of articular cartilage, the shrinkage behavior was also investigated in this study. It was found that a linear correlation existed between two phases (Fig. 4.34). For the normal specimens, the peak swelling strain correlated with the peak shrinkage strain ($R = -0.45$, $p < 0.05$), while such a correlation did not exist between the shrinkage duration and the swelling duration. Although with a decrease in the mean amplitude of the peak strains (Fig. 4.18), a similar correlation ($R = -0.51$, $p < 0.01$) was obtained for the trypsin-digested cartilage samples.

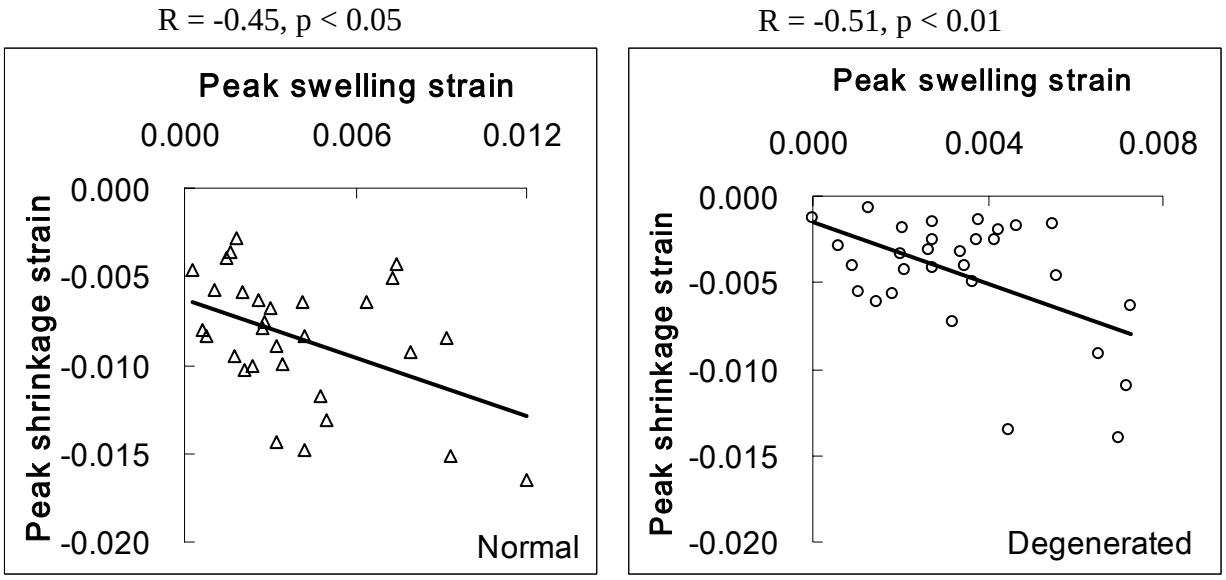

(a) (b)

Fig. 4.34 Correlations between the peak shrinkage strain and the peak swelling strain for the normal (a) and degenerated (b) specimens.

Correlations between swelling and acoustic parameters

Fig. 4.35 shows a relatively good correlation between the peak swelling strain and IA slope (β) for both the normal and degenerated specimens. However, no significant correlation was found between swelling strains and other acoustic parameters.

R = 0.343, p = 0.068 R = 0.39, p < 0.05

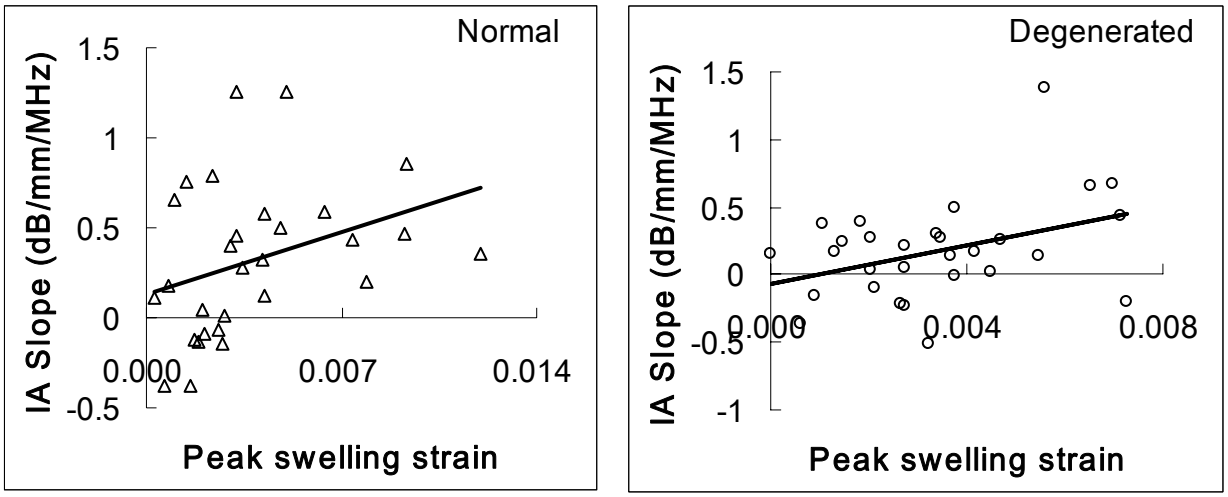

(a) (b)

Fig. 4.35 Correlations between the peak swelling strain and IA slope β for the normal (a) and degenerated (b) samples.

Correlations between acoustic and biochemical parameters

The IRC of the cartilage surface was significantly related to the water fraction of the normal cartilage tissue (Fig. 4.36a). After the PG content was depleted, this linear correlationship became insignificantly (Fig. 4.36b). Meanwhile, it was found that the IBS of the cartilage matrix was significantly negatively correlated with the FCD (representing the PG content) of the normal cartilage tissue (Fig. 4.36c). No such correlation was found after the samples were digested (Fig. 4.36d).

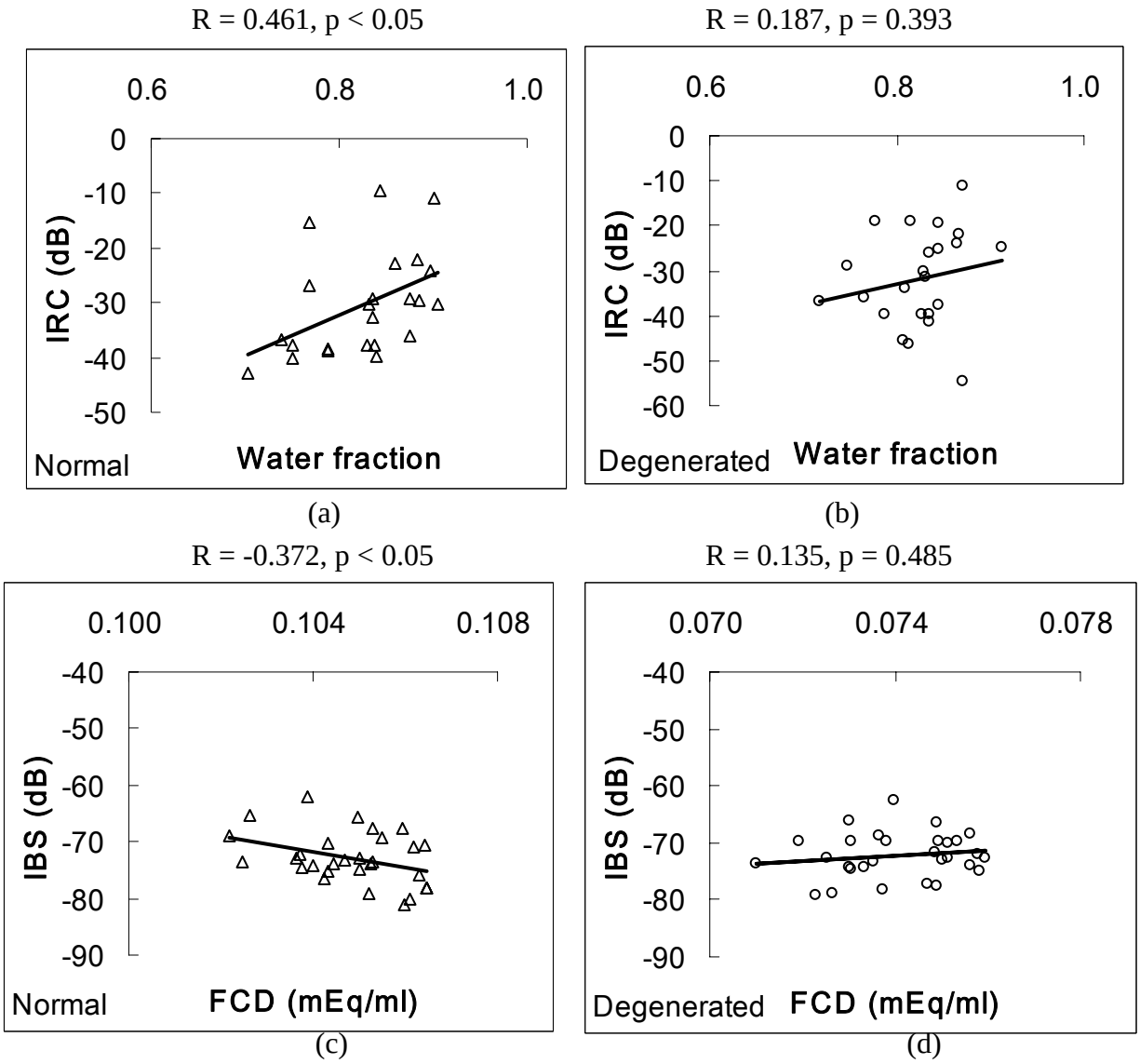

Fig. 4.36 Correlations between IRC and water fraction for the normal (a) and degenerated (b) samples. And correlations between IBS and FCD for the normal (c) and degenerated (d) samples.

Correlations between aggregate moduli and other parameters

The result of this study indicated that the overall aggregate modulus *Ha* of the full-thickness degenerated matrix obtained using the homogeneous triphasic model negatively correlated with IRC (R = -0.525, p < 0.05, Fig. 4.37b). No significant correlation was found between *Ha* and other acoustic parameters, or between *Ha* and the biochemical parameters, including water fraction and FCD. Moreover, the

correlations between the aggregate moduli (*Ha1*, *Ha2* and *Ha3*) obtained using the new bi-layered triphasic model and the acoustic and biochemical parameters were also calculated. However, no significant correlations were found.

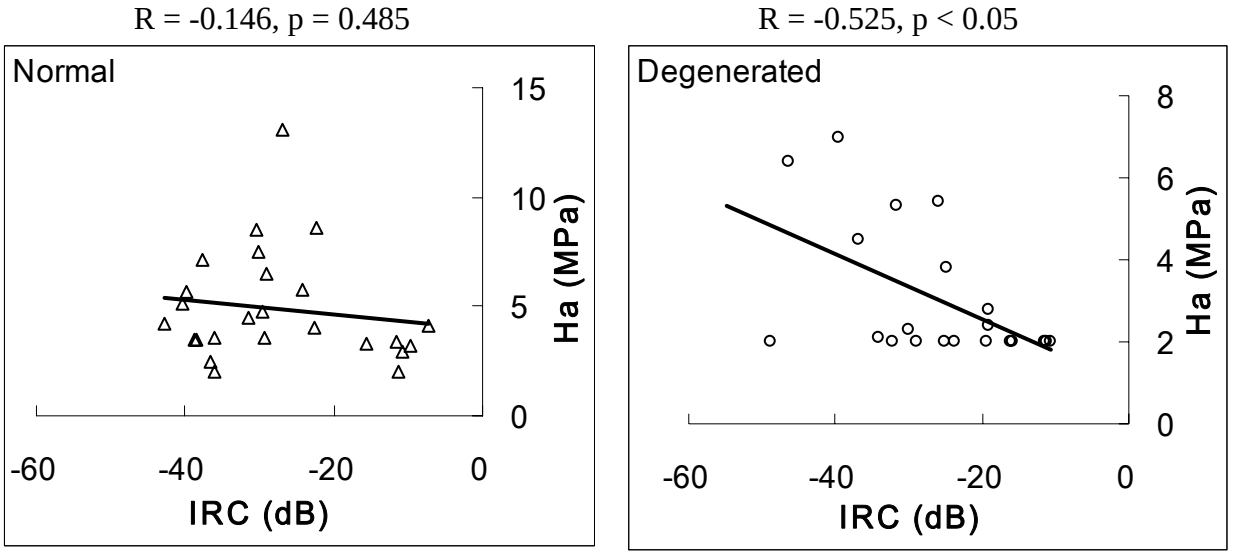

(a) (b)

Fig. 4.37 Correlations between the aggregate modulus predicted by the homogeneous triphasic model and IRC for the normal (a) and degenerated (b) samples.

CHAPTER 5 DISCUSSION

5.1 Ultrasound Swelling Measurement System

5.1.1 Validation and repeatability of USMS

The results of the validity test showed that for both the 0.15 M and 2 M saline solutions the simulated subtle displacements of the cartilage surface measured by the manually controlled and motor-controlled 3D USMS were linearly correlated with the reference values read by the micrometer ($R^2 > 0.99$) and by the 3D scanning motor ($R^2 > 0.98$), respectively. It was demonstrated that the uncertainty of the strain measurement (approximately 0.7 μm) caused by the experimental system could be acceptable in comparison with the swelling strain of articular cartilage (approximately 0.3%) tested in this study. The high reliability score (ICC > 0.98) demonstrated that the ultrasound measurement system had a good reliability according to a general guideline (Shoukri and Edge, 1996). The CV% values of the measured peak strains and the averaged rRMSD of the transient data were both less than 10%, indicating that the repeatability of the measurements was acceptable using the current measurement systems (Laasanen et al., 2002).

Similarly, either for the large (6.35 mm in diameter) or small (2 mm in width) specimens, the high reliability score of ICC of the peak strains (> 0.8) also demonstrated that the ultrasonic measurements of the shrinkage and swelling behavior of articular cartilage had a good reliability according to the general guideline of assessment (Shoukri and Edge, 1996) for both mounting-remounting and measuring at different sites. However, the CV% values of the measured peak strains and the averaged

rRMSD values of the transient data among the three tested sites were all greater than 10% for the small specimens. In contrast, the two parameters were much smaller in the case of mounting-remounting for both the large or small specimens. The results indicated that the variation caused by mounting-remounting was within an acceptable range for both the small and large specimens tested in this study. However, the site dependence (0.5 mm apart) of the measurement needs to be considered for the specimens with a width of 2 mm. Therefore, the results of this repeatability test suggested that the specimen dimension should not be too small. One possible reason for the stronger site-dependence in the small specimens may be the obvious edge effect, as the exchange of water and ions across the sides of the small specimens could significantly affect the swelling-shrinkage behavior. The other potential reasons are elaborated in next section.

5.1.2 Effect of specimen dimension on swelling measurement

In view of nano-structure, the collagen fibrils are made of the staggered arrays of the triple helixes and the PG aggregates are bounded together to form macromolecular complexes that are immobilized with the collagen network (Mow et al., 2005). The negative charges on the PGs generate the swelling pressure balanced by the limitation of the fibril network (Mankin et al., 2000; Mow et al., 2005). Cutting the cartilage tissue to reduce dimension at macro-scale tends to destroy the original nano-structure of the proximity of the cutting section. It was found that the cartilage tissue on the edge protruded slightly during our specimen preparation. This phenomenon might be caused by the loss of the constraining force of the damaged collagen network. The excised strips in such a ‘destructive’ way may not provide the same material properties of

articular cartilage as those in its natural intact state. Therefore, the boundary condition is one possible reason for the significant changes in the transient osmosis-induced swelling behavior of the cartilage samples with different dimensions. The other possible reason might be the increased diffusion of ions and water with the reduced sample dimension. It has been well accepted that articular cartilage is widely regarded as a triphasic material (Mow et al., 2005). Based on the ideal osmotic pressure law, the Donnan osmotic pressure π is related with the difference of ion concentrations between the interstitium and the external bathing solution. It is demonstrated that the dynamic cartilage swelling depends on the transient alterations in the ion concentration and the fixed charge density in the interstitium (Lai et al., 1991; Maroudas, 1976a), which are affected by the diffusion of ions and water during the shrinkage and swelling phases. Furthermore, our results demonstrated that the ion exchange after changing the concentration of the bathing solution was correlated with the specimen dimension. Therefore, the study on the transient cartilage swelling must consider the size of the cartilage sample. Smaller specimens might have a stronger dimension-dependence of cartilage swelling in consideration of the edge effect. Relatively large specimens remaining an *in-situ* condition with little edge effect might less depend on the dimension. If specimens are prepared with enough large dimension, the ultrasonic approach (the ultrasound beam width of 0.1 mm) may well secure the *in-situ* conditions of the cartilage samples with a large size (ϕ > 3 mm) and can be used to investigate the dynamic responses of the intact cartilage layer to electrochemical or mechanical stimulations.

Ultrasound technique has been regarded as a potential approach for the study on the swelling behavior of articular cartilage. High frequency ultrasound with a high resolution has been applied to monitor a relatively small specimen (Fortin et al., 2003; Wang and Zheng, 2005). The results of our experiments suggested that the width of the specimen should not be too small in comparison with the focal zone diameter of the ultrasound beam when ultrasound is used to detect the swelling behavior of articular cartilage. It is believed that the geometry of the specimen should be taken into account when studying the biomechanical properties of articular cartilage as well as other materials.

5.1.3 *In-situ* measurement

Since the cartilage samples were attached to the bone, the obtained results reflected the swelling behavior and the material properties of articular cartilage *in situ* (Narmoneva et al., 1999). In order to demonstrate the differences between cartilage specimens with and without the bone tissue, the swelling behavior of the full-thickness cartilage layer without bone was monitored as well. The statistical results of the pair-wise comparison showed that the absolute peak shrinkage and swelling strains of the cartilage samples without bone were significantly larger than those of the cartilage-bone specimens. It was consistent with the results of Mow and Schoonbeck's study (1984). Setton et al. (1998) reported that the cartilage layer without the support or limitation of the bone behaved in curling and swelling. Their findings indirectly provided evidences for the difference between cartilage specimens in *in-situ* and *ex-situ* conditions.

Without applying any external mechanical stress, we studied the responses of articular cartilage to the change of the ion concentration of the bathing solution. The osmosis-induced shrinkage and swelling behaviors observed at the central portion (ϕ = 0.1mm) of the cartilage plugs (ϕ = 6.35mm) could closely approximate the *in situ* behavior of the intact tissue without edge effect. In comparison with other methods such as wet-weighting, mechanical (indention, tension, compression), and optical methods, the ultrasonic method provides a non-contact and non-destructive way to observe the swelling behavior inside the cartilage without removing the cartilage layer from the bone or cutting the cartilage into slices. Therefore, it is potential to become a more acceptable method to measure the *in-situ* material properties of articular cartilage.

5.1.4 Correlation between ultrasonic evaluation and histological analysis

The histological assessment has been applied as a criterion in the studies on the degeneration of articular cartilage (Adams et al., 2006; Hattori et al., 2004; Kuroki et al., 2004; Laasanen et al., 2006; Laurent et al., 2006; Qin et al., 2002; Saied et al., 1997). In this study, trypsin digestion was used to break down the PGs without inducing a macroscopic damage on the cartilage surface. The histological assessment was performed not only for the measurement of FCD but also for assessing the PG depletion in comparison with the ultrasonic evaluation. The result that the digestion proportion and the thickness of the cartilage layer measured by the USMS highly correlated with the histological analysis indicated the validity of the ultrasonic measurement of the cartilage thickness and the progressive degeneration of the tissue.

5.2 Ultrasonic Characterization of Swelling Behavior of Articular Cartilage

5.2.1 'Overshoot-relaxation' transient swelling behavior

This study demonstrated that the shrinkage and swelling behavior of articular cartilage experienced an 'overshoot-relaxation', similar to the "salt-induced stress relaxation" behavior of articular cartilage earlier observed using a confined configuration (Eisenberg and Grodzinsky, 1987). However, the transient stress in this earlier study showed a monotonic decrease after the saline concentration was increased. One possible reason for this overshoot-relaxation may be the interactions between the PGs and the collagen fibres in the cartilage surface zone. According to the conventional theories, the Donnan osmotic pressure plays a dominant role in the free swelling behavior of cartilage (Lai et al., 1991; Maroudas et al., 1986; Narmoneva et al., 2001). With the decreased saline concentration, swelling stress in articular cartilage increased and the sample was allowed to swell. However, it was soon balanced with the constraining force of the stretched collagen network, particularly the reinforced collagen fibrils in the cartilage superficial zone. The cartilage sample had a tendency to be compressed back to its initial state. In contrast, swelling stress in articular cartilage decreased when the saline concentration was increased. The total pressure squeezed on the cartilage and allowed the cartilage to shrink. Also balanced by the tensile force of collagen fibres and their interaction within the PG-collagen matrix, the cartilage surface moved backwards after the strain reached the peak. Another possible reason for the phenomenon may be due to the ion redistribution. During the shrinkage process, the cartilage tissue at certain depths might absorb more ions than required for balancing the fixed charges at that

region. This may cause a temporary overshoot of the shrinkage followed by a relaxation phase as the ions are redistributed. Similar explanation could be applied to the overshoot phenomenon of the swelling. Other possible explanations for this overshoot phenomenon could include the depth-dependent distribution of fixed charge density (Narmoneva et al., 2001) and the interaction between ions and collagen matrix (Eisenberg and Grodzinsky, 1987). Triphasic theory (Lai et al., 1991) provides a model to explain the electrochemomechanics of cartilage at equilibrium or non-equilibrium states. By applying the triphasic model, further investigations on the transient free-swelling behavior of cartilage are necessary to better understand the causes of this phenomenon.

The mean peak shrinkage strain (1%) and the mean peak swelling strain (0.3%) of bovine cartilage obtained in this study were much smaller than the 3% swelling strain reported by Mow and Schoonbeck using the water-weight-gain method (Mow and Schoonbeck, 1984), but appeared to agree with Eisenberg and Grodzinsky's result, which was less than 1% measured by a uniaxial confined compression method (Eisenberg and Grodzinsky, 1985). Narmoneva et al. (2002) found that the mean swelling strain of the canine cartilage strips was approximately 1%. The inconsistency of the swelling strains reported in the literature as well as in this study could be due to individual variations of the specimen location, joint, species, age, degeneration status, specimen configuration, and measurement technique. This study also provided evidence that the cartilage disc detached from the subchondral bone tended to swell more in comparison with *in-situ* intact condition (Mow and Schoonbeck, 1984).

This study investigated not only the swelling strain but also the shrinkage strain (or de-swelling strain). We found that the swelling behavior of cartilage correlated with its shrinkage behavior. However, there was a significant change between the transient responses during these two processes in the strain amplitude, i.e., they are not reversible. This phenomenon might be caused by the anisotropic mechanical properties and ion diffusion rates of articular cartilage. Further explanation to this finding requires more theoretical and experimental studies.

5.2.2 Depth-dependence of swelling strain

From the M-mode images (Fig. 3.11), it is clearly shown that the ultrasound signals at different depths shift differently. Our results for bovine articular cartilage showed that the swelling-induced strain was depth-dependent (Fig. 4.8). This was similar to the results of the canine and human cadaver cartilage (Narmoneva et al., 1999, 2001). It has been known that most of the PGs are located in the middle zone of articular cartilage and the fixed negative charges on the PGs play a primary role in swelling (Maroudas, 1976a; Mow et al., 2005). Therefore, the swollen middle layer may cause a compressive stress on the deep zone. In addition, the *in-situ* configuration that the deep zone was attached to the bone might give a rigid support to place the cartilage matrix in a state of compression. It is also known that collagen fibre organization in cartilage is highly nonuniform and anisotropic. Fibres are oriented tangential to the surface at the superficial zone to confine the swelling stress (Eisenberg and Grodzinsky, 1985; Lai et al., 1991; Maroudas et al., 1986). This may explain why the tensile strain of the surface layer is lower than that of the middle zone. Further studies are definitely needed to

better understand the reasons for the compressive strains in the deep zone while the full-thickness cartilage experienced an overall tensile strain during the free swelling test.

This study not only provided the transient swelling strains, but also successfully used dynamic 2D images of cartilage to image the displacement distribution of the tissues. Using 2D tracking method (Zheng et al., 2004b), the tissue displacement images during the different periods of the swelling and shrinkage processes could be obtained automatically after an ROI in the B-mode ultrasound image was selected (Fig. 4.9b-d). From the changes in the brightness of the images, the deformations inside of the tissue were detected. It was found that the movements of tissues inside articular cartilage were intensive gradually reducing as time going, and finally equilibrium was approached.

It was noted that under the external compression loading, the superficial layer of the sample incurred most of the deformation applied on the specimen while the strains in the middle zone were relatively much smaller using ultrasound compression system (Zheng et al., 2002) and optical microscopic methods (Guilak et al., 1995; Schinagl et al., 1996, 1997). In comparison with the mean equilibrium compressive strains, the osmosis-induced swelling strains at cartilage sub-layers were found to distribute in a different way as shown in Fig. 4.8. Therefore, further studies on the non-uniform deformations induced by the osmotic loading are necessary.

In our modeling, the predicted swelling strain also indicated a corresponding heterogeneity along the depth (Fig. 4.30), with the upper middle zone having a higher strain. However, the current model could not predict the compressive strains. Thus, the

theoretically predicted strain data approached to zero in the deep layer. In this study, the theoretically predicted strain data of the bi-layered cartilage tissue were calculated based on the experimentally measured strain data acquired using ultrasound in the free-swelling test by replacing the hypertonic saline (2 M NaCl) with the physiological saline (0.15 M NaCl). These strain data and the reference values of c_0^F and ϕ_0^W were used to estimate the material properties of articular cartilage based on a triphasic eletromechanochemical theory (Lai et al., 1991). The prediction of the swelling-induced strain fields in the cylindrical cartilage layer was performed as a function of the material properties of the solid matrix (aggregate modulus *Ha* and Poisson's ratio v_s) and the reference c_0^F and ϕ_0^W (Setton et al., 1996). Since the swelling prediction was a weak function of Poisson's ratio v_s (Athanasiou et al., 1991; Narmoneva et al., 1999), a constant value for v_s was assumed throughout the depth direction in this study. The results showed that our model could better fit the measured strain distribution for the bovine articular cartilage.

5.2.3 Progressive degeneration of articular cartilage

High frequency ultrasound technology provides a unique tool for real time monitoring of the progressive degeneration process. Our earlier study has addressed the possibility of using ultrasound to monitor the progressive depletion of PGs of articular cartilage induced by trypsin digestion (Zheng et al., 2004a). A similar study has been reported using ~30 MHz ultrasound to measure the dynamic acoustic parameters with a time interval of 5 minutes (Nieminen et al., 2002). However, no further parametric quantification was obtained. In this study, the RF signals were recorded at a sampling rate of one frame per 0.6 second. Therefore, the transient trypsin penetration front was

more clearly observed in the ultrasound M-mode image and its transient penetration speed was calculated. Our results demonstrated that this ultrasonic approach could effectively track the alteration in the structure of the PG macromolecular induced by trypsin enzyme, simulating the natural degeneration of articular cartilage. The good correlation of the digestion proportion measured using USMS with that of the histological assessment was consistent with previous studies (Nieminen et al., 2002; Qin et al., 2002; Zheng et al., 2001).

Our study successfully tracked the progressive degeneration of articular cartilage *in situ*. It was found that the enzyme solution with the trypsin concentration of 0.25% penetrated into the tissue and digested the PGs at an average speed of 0.62 μm/s. After approximately three-hour digestion, the digestion speed decreased to a very low level. One possible reason might be the activity decrease of trypsin enzyme as time going since the digested PGs might lead to an alteration in the condition inside the cartilage tissue, such as pH, resulting in the difficulty of the trypsin molecules to reach the deep zones. Consequently, the non-constant concentration of trypsin during the digestion should be considered. The inhomogeneous distribution of the PG content may be another possible reason for this phenomenon. It took enzymes less time to digest the PGs in the superficial zone where the content is low and enzymes are easy to reach. Correspondingly, more PGs in the middle and deep zones need more time to be broken down. The individual variance in PG content among different samples may explain why there was a relatively large variance during digestion process among individual specimens.

The digestion process is complex, so further studies are required. The method of turning the cartilage layer upside down tends to be useful to confirm the effects of the possible factors in the future studies. This ultrasound method provides a feasible approach to observe the dynamic digestion process inside the tissue.

The observation and quantification of the residual trypsin digestion indicated that the residual enzymes inside the tissue digested PGs at lower speed but still remained a relatively strong activity. It was found that after the 30-minute trypsin digestion, the enzyme penetrated into approximately 1/3 of the full thickness of the cartilage layer, which was significantly ($p < 0.05$, One-Way ANOVA) larger than the penetration depth after the 10-minute and 20-minute digestions. However, after the specimens rested for 3 hours in physiological saline for residual digestion, the digested proportions measured by both USMS and histology were insignificantly different among the three groups ($p > 0.05$, LSD Post Hoc Tests of One-Way ANOVA). The results suggested that the residual digestion must be carefully considered in the enzyme digestion of articular cartilage. To stop the residual digestion, enzyme inhibitors could be used (Nieminen et al., 2002; Qin et al., 2002). Therefore, future studies may investigate the property changes of the degenerated cartilage tissue with a certain digestion depth with the use of enzyme inhibitors.

5.2.4 Swelling behavior of the OA-like articular cartilage

This study systematically investigated the osmosis-induced shrinkage-swelling and hydration behavior of the degenerated cartilage using ultrasound. Firstly, it was found that the magnitude of the transient strains of the full-thickness cartilage layer decreased

after the trypsin digestion, i.e. the absolute values of the peak strain of both shrinkage and swelling decreased after trypsin digestion (Fig. 4.17-18). Narmoneva et al. (2001) reported that the swelling strain of the mild degenerated cartilage changed less in comparison with that of the normal tissue. However, other previous studies reported that the increase in cartilage volumetric swelling (or water gain) would be regarded as one of the early signs of OA (Maroudas et al., 1986; Torzilli et al., 1990). The damage and loss of collagen fibres might result in the stronger swelling behavior (Narmoneva et al., 2001). The difference between these previous studies and this study might be related to the PG depletion and the minor extent of the damaged collagen network. It is known that trypsin not only digests the PGs but also affects the collagen fibrils. However, Harris et al. reported that trypsin only cleaved a minor amount of collagen (Harris et al., 1972). In this study, the collagen network in the surface zone was directly submerged in the enzyme solution, so it was easily affected. However, the short-time trypsin digestion applied in this study tended to induce no significant change in the collagen network of the trypsin-digested cartilage using polarized light microscopy, consistent with previous study (Nieminen et al, 2002). Moreover, the results of water volume fraction measurement indicated that there was no significant difference between the normal and the degenerated cartilage for Group 10min and Group 20min but showed a significant decrease for Group 30min. The loss of PGs resulting in a decrease of swelling pressure might cause a loss of water, and meanwhile, the collagen network limited the gain in water (Mankin et al., 2000). In addition, previous studies reported that the enzyme-induced PG depletion did not significantly affected the cartilage density (Gu et al., 1999) and only resulted in a minor change in cartilage structure and composition (Lyyra et al., 1999). Besides the inclined trace of the additional echoes from the interface of the

digested and undigested cartilage tissue, the echoes from the cartilage matrix shifted slightly, indicating that the progressive PG-depleted digestion did not obviously affect the ultrasound scattering signals from the tissue. Thus it could be suggested that the depletion of PGs in this study did not change the structure of the tissue. Therefore, the trypsin-digested OA-like articular cartilage specimens obtained from the normal cartilage without visual surface lesions showed a different swelling behavior from the spontaneous OA or collagen-damaged articular cartilage. It is expected that chondroinase ABC will be used to only digest the PGs and collagenase to digest collagen fibrils. The further results must demonstrate the roles of the PGs and collagens in the various properties of articular cartilage and provide an insight explanation for the results obtained in this study.

Secondly, it was found that the current result of the depth-dependence of the swelling-induced strains for the degenerated samples was consistent with the result of a previous study that the swelling strain of the superficial zone for the damaged cartilage increased (Narmoneva et al., 2001). The least content of the PGs and the minor alterations of the collagen network at the surface zone as discussed above may explain this finding. With the loss of PGs, the swelling strain at the middle zone reduced while the swelling strain at the surface zone increased. The strain at the deep zone changed insignificantly probably because the deep zone was not digested by trypsin, which was confirmed by both the histological and ultrasound measurements.

Thirdly, the hydration induced by the process of dehydration and re-immersion showed more obvious osmotic swelling behavior of articular cartilage compared with the

swelling induced by changing the concentration of the bathing saline solution. According to a previous study that an 1-hour exposure to air did not change the water content of intervertebral disc (Pflaster et al., 1997), the 45-minute exposure to air (humidity = 58±5%; temperature 21 ± 1°C) was applied in this study. Because this relatively short dehydration and the large drag forces preventing the interstitial water to flow from the deep zone upwards to the surface (Mankin et al., 2000; Mow et al., 2005), an alteration was induced only at the superficial layer and the condition of the deeper zones kept unchanged. These are the possible reason for explaining the difference in behavior of concentration-induced swelling and dehydration-induced hydration. After water evaporation, the loss of fluid content resulted in the top zone of the PG-collagen solid matrix more densely (Mankin et al., 2000; Mow et al., 2005) and thus generated an osmotic pressure gradient between the cartilage superficial zone and the bathing solution causing cartilage swelling. After trypsin digestion, the broken-down PGs might cause changes in material properties of the matrix and consequently result in a decrease of the osmotic pressure induced by dehydration and re-immersion in comparison with their normal counterparts. An earlier study using ultrasound to probe the hydration process of the partially dehydrated normal cartilage reported that the interaction between collagen network and PGs affected this hydration behavior of articular cartilage (Tepic et al., 1983).

However, the spontaneous OA was a more complex process related to a multi-composition change of the cartilage while the experimentally enzyme-treated OA-like cartilage could only lose a single composition. Thus further studies are required to

investigate the swelling behavior of the spontaneous OA articular cartilage using our ultrasound method.

5.3 Bi-layered Triphasic Modeling

5.3.1 Prediction of aggregate moduli

In the earliest model of articular cartilage, the tissue was modeled as linearly elastic, isotropic and homogeneous material. In that single-phased model, a uniform Young's modulus (E) was determined by the ratio of axial stress and strain. With the increasing knowledge of articular cartilage, an inhomogeneous triphasic model with non-uniform modulus was developed to study the swelling behavior (Narmoneva et al., 2001), based on the triphasic theory (Lai et al., 1991). In that study, two aggregate moduli *Ha* were used to describe articular cartilage, assuming that *Ha* changed linearly with the depth in the layer near the cartilage surface and *Ha* was a constant in the deep region. In the current study, the inhomogeneous model was extended by including an additional aggregate modulus *Ha*. We assumed that *Ha* in the deep region would also vary with the depth as shown in Fig. 3.16. Our results (Table 4.4) were in general consistent with the modulus values of the patellar articular cartilages of human cadavers (the average modulus of the deeper layer equaled to 12.4 ± 9.3 MPa; the superficial region 1.7 ± 2.3 MPa; the normalized thickness of the deeper zone was 0.6 ± 0.1) (Narmoneva et al., 2001), and this demonstrated the reliability of our new method. According to our results, using a single *Ha* to describe the deep region appeared to be not accurate enough for the specimen that we tested, as there was a significant difference ($p < 0.05$) between the aggregate moduli in the surface and

middle regions (Ha_3 *and* Ha_2) and the aggregate modulus in the region towards the bone (Ha_1).

The results of this study indicated that the aggregate moduli of the cartilage tissue at different depths from the deep region to the surface decreased insignificantly after trypsin digestion (Table 4.4, Fig. 4.31) using both the 3-parameter model proposed by Narmoneva (Narmoneva et al., 2001) and our new 4-parameter model. The insignificance might result from the minor change in the density (Gu et al., 1999) and in collagen network (Nieminen et al., 2002) after trypsin digestions. The stiffness of the cartilage matrix highly depends on the collagen fibres and the PGs, which are the major components to form the matrix. Narmoneva et al. (2001) found that the breakdown of collagen fibrils could induce a decrease of the modulus. In this study, the results showed that the trypsin-induced PG depletion without the damage of collagen fibrils could cause an insignificant change in the stiffness of the matrix. Further experiments using collagenase to digest collagen fibrils are required to demonstrate the significant reduction of the aggregate moduli in the degenerated cartilage. It should also be noted that there were very large individual variations of the parameters even for the normal specimens. More specimens may be required.

Moreover, our bi-layered 4-paramerter triphasic model measured the minor changes in the cartilage matrix structure caused by the PG depletion by calculating the normalized thickness of the deep layer (h_1). The value of 1-h_1 represented the thickness of the degenerated region (Narmoneva et al., 2001). In this study, the value of h_1 gradually decreased from 0.69 ± 0.19 to 0.55 ± 0.24 with the digestion time from 10 to 30

minutes. However, it was found that these modeling results were larger than the measurements of the undigested portion using histology (0.25 ± 0.18 for Group 10min, 0.36 ± 0.18 for Group 20min, 0.27 ± 0.18 for Group 30min) and ultrasound (0.24 ± 0.15, 0.30 ± 0.15, and 0.30 ± 0.13 for the three groups, respectively). This difference tended to provide evidence that h_1 was related to the trypsin-induced PG depletion but not equal to the real value of the thickness of the undigested region. The possible reasons may be the insensitivity of the model to the changed material properties of the matrix (refer to the following section) and the insignificantly changed swelling strain data used for theoretical parametric extraction.

The comparison among the predicted results of the three models showed that the parametric prediction of articular cartilage using the new 4-parameter model had the lowest errors. The homogeneous model might not be able to well predict the alteration in the swelling-induced strains and the aggregate modului of articular cartilage at different depths, especially for the degraded cartilage (Narmoneva et al., 2001). However, it was demonstrated that the overall aggregate modulus obtained using the homogeneous triphasic model was significantly affected by the trypsin digestion, indicating the reduction of overall stiffness of cartilage after digestion. Further studies are necessary to improve the model for obtaining better parametric prediction of articular cartilage.

5.3.2 Effect of c_0^F and ϕ_0^W distribution

For the triphasic model, the reference water volume fraction ϕ_0^W and fixed charge density c_0^F are important compositional indices of the model, which affect the

swelling strain fields and the prediction of Ha of cartilage (Lai et al., 1991; Narmoneva et al., 2001). To test the effects of the distributions of ϕ_0^W and c_0^F on the estimation of the parameters including Ha_1, Ha_2, Ha_3 and h_1, we compared the results of Ha predicted using the reported values of c_0^F and ϕ_0^W of bovine cartilage (Shapiro et al., 2001; Wang et al., 2002) with the Ha values obtained using the other two extreme distributions of c_0^F and ϕ_0^W, i.e., a constant value throughout the depth (Fig. 5.1c-d) and a reverse distribution (Fig. 5.1e-f) contrary to the literature one (Fig. 5.1a-b). A similar approach for parametric studies has been reported for studying depth dependent strains induced by compressive loading (Wang et al., 2001).

By comparing the results obtained using the three types of ϕ_0^W and c_0^F distributions, we found that the estimated parameters were relatively insensitive to the assigned distributions. That is to say, there was insignificant interaction ($p > 0.05$, Two-Way Repeated ANOVA) between the distributions of c_0^F and ϕ_0^W and the estimated Ha_1, Ha_2, Ha_3 and h_1, with the exception that Ha_2 was significantly affected by the ϕ_0^W distribution ($p < 0.05$), but not c_0^F ($p > 0.05$). Although it was found that the ϕ_0^W distribution affected the prediction of mechanical properties of articular cartilage, its effects on the estimation of Ha_2 might be smaller in real situation, as the ϕ_0^W distribution in the normal cartilage may not be so extreme as used for comparison in this study from specimen to specimen.

Previous studies had demonstrated the inhomogeneous distributions of the fixed negative charges (Flahiff et al., 2002; Narmoneva et al., 1999, 2001, 2002; Wang et al.,

2002) and the water volume fraction (Narmoneva et al., 1999, 2001, 2002; Shapiro et al., 2001) in articular cartilage. Consequently, the distribution of the swelling-induced strains (Narmoneva et al., 1999, 2001, 2002; Wang et al., 2002) is different at different depths as well as for tissues with different moduli (Chen et al., 2001; Wang et al., 2002). Therefore, it will be very useful if the ϕ_0^W and c_0^F distributions can be measured for each specimen in our studies, particularly for the study on the degenerated cartilage, where the ϕ_0^W and c_0^F distributions can vary significantly from case to case.

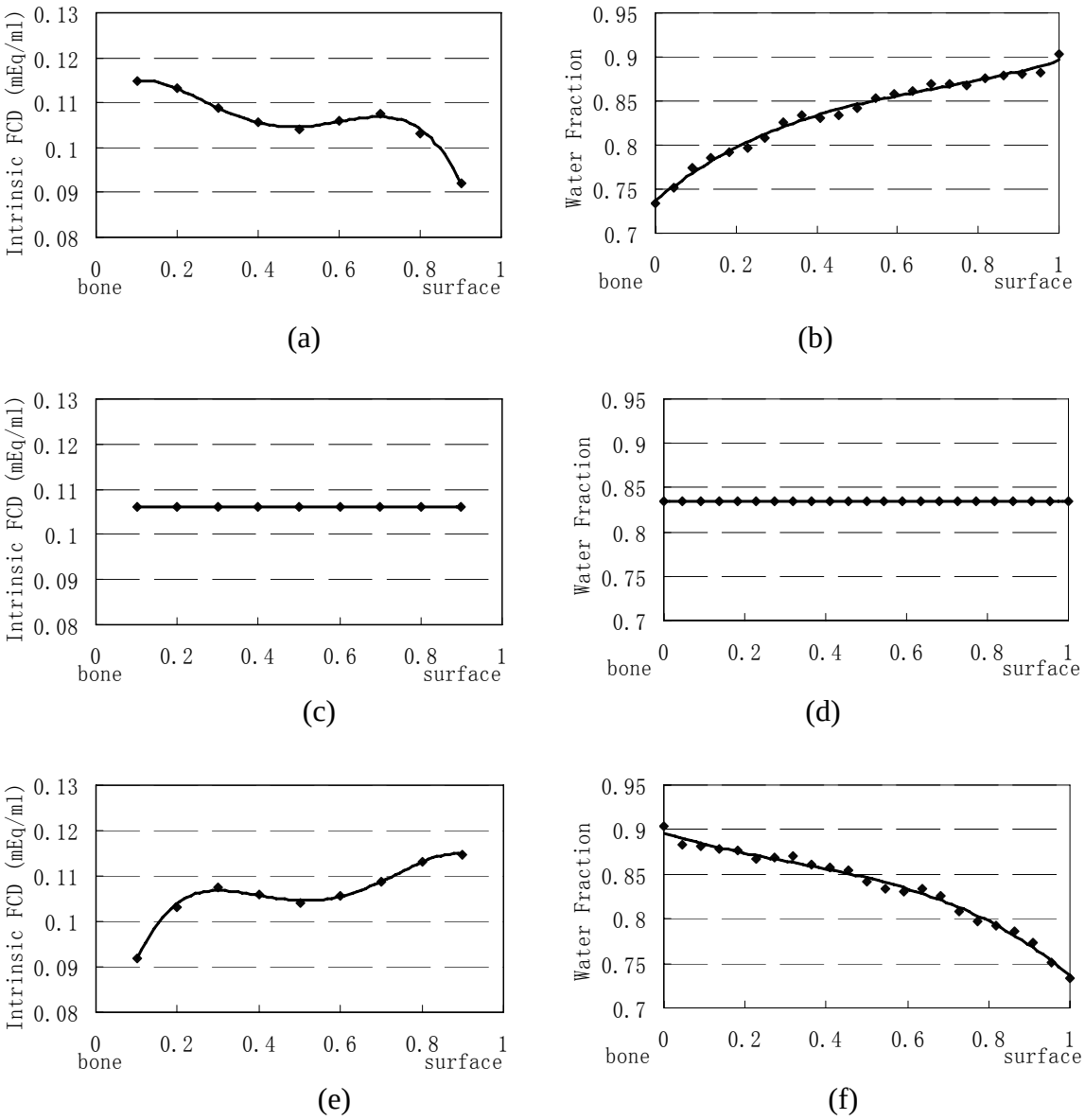

Fig. 5.1 Depth-dependent distribution of (a) fixed charge density c_0^F and (b) water volume fraction ϕ_0^W of bovine cartilage reported in the literature (Shapiro et al., 2001; Wang et al., 2002). Two other types of distributions of c_0^F and ϕ_0^W were also assumed in this study: constant distributions of c_0^F and ϕ_0^W in (c-d) and varying distributions of c_0^F and ϕ_0^W in (e-f) reverse to those in (a-b), respectively.

5.4 Acoustic Assessment of Articular Cartilage

In this study, high frequency ultrasound was used to characterize the alteration in the acoustic properties of the PG-degenerated articular cartilage. It was first found that the amplitude of the echoes from the articular surface appeared to be correlated with the digestion time. The amplitude of the echoes for the specimens digested for 30 minutes decreased greatly in comparison with the specimens of Group 10min, i.e. digested for 10 minutes. It might suggest that the longer the trypsin digestion lasted, the more effect of trypsin on the tissue. Since the cartilage surface was set perpendicular to the beam, the reflection was dependent on the properties of the surface such as the impedance and the roughness (Adler et al., 1992, Cherin et al., 1998). The finding that IRC of all the PG-degenerated specimens showed different levels of insignificant decrease suggested that the PG depletion could induce a minor change in the properties of the articular surface without macroscopic damage. Similarly, a slight change in the reflection coefficient was obtained in previous studies (Laasanen et al., 2002; Pellaumail et al., 2002; Toyras et al., 1999). It has been well known that the PG content is lower but the collagen content is highest in the surface layer (Mow et al., 2005; Shapiro et al., 2001; Wang et al., 2002). Therefore, the alteration in collagen fibrils for the collagenase-digested samples resulted in a significant decrease in the reflection of the surface (Cherin et al., 2001; Jaffre et al., 2003; Nieminen et al., 2002; Saarakkala et al., 2004).

The backscatter coefficients, IBS of the middle cartilage matrix and AIB of the cartilage-bone interface were evaluated in this study. The values of IBS changed insignificantly between the normal and the trypsin-digested specimens for all the three groups. The result consisted with that of the control and OA-like cartilage of the mature

rat (Jaffre et al., 2003). It was suggested that the incomplete trypsin-digestion (i.e. approximately 70% of PGs was removed.) induced in this study tended to be insufficient to generate a significant change in the major structure of the cartilage matrix. With respect to AIB, the decrease of approximately 2-3 dB was caused by the PG depletion. AIB could be affected by not only the regularization of the cartilage-bone interface but also the thickness and attenuation of the full-thickness cartilage layer (Jaffre et al., 2003). In this study, the trypsin enzymes in general did not reach the deepest region of the cartilage layer. Therefore, the slight change of the cartilage-bone interface may explain why the values of AIB decreased insignificantly for the three groups. Our findings may provide evidence for a previous conclusion that the PG content plays a minor role in the backscatter (Pellaumail et al., 2002).

The evaluation of attenuation and attenuation slope was performed using a multi-narrowband algorithm (Huisman and Thijssen, 1996; Kuc and Schwartz, 1979; Roberjot et al., 1996), FFT (512 points) and a substitution method (Fink and Cardoso, 1984; Lizzi et al., 1983). The mean values of IA for the normal cartilage ranged from 11.5 to 15.8 dB/mm at 24 to 46 MHz, which suggested the frequency-dependence of attenuation (Agenura et al., 1990; Joiner et al., 2001; Nieminen et al., 2002; Senzig et al., 1992). An insignificant increase of IA of the trypsin-digested samples was found in this study, probably due to the extra interface of the digested-undigested tissue induced by the uncompleted PG-depletion, which was similar to the result of Toyras' study (1999). However, a significant increase of attenuation was found in other studies (Joiner et al., 2001; Nieminen et al., 2002). With investigation on the spontaneous OA cartilage, an inconsistent result of IA was recently reported (Nieminen et al., 2004). The

difference may be caused by the involvement of collagen damage, which decreases the attenuation coefficient (Nieminen et al., 2002). Moreover, this study also found that the PG depletion resulted in the insignificant decrease of the attenuation slope, which agreed with Nieminen's study (2004).

5.5 Correlation between Swelling, Acoustic and Biochemical Parameters

Previous studies usually used the condition of articular cartilage in 2 M saline solution as the reference configuration and did not regard it as a tested phase. In the current study, not only the swelling behavior but also the shrinkage behavior was investigated. The result of the correlation between the peak swelling and shrinkage strains demonstrated that articular cartilage tended to swell with larger amplitude if it shrank more strongly (Fig. 4.34). However, it was also found that there was a significant change between the transient responses during the shrinkage and swelling processes in the strain amplitude. This difference may be caused by the special 'overshoot-relaxation' phenomenon. The surface layer of articular cartilage may significantly limit cartilage swelling (Setton et al., 1998), but it may have slight limitation on shrinkage behavior due to the osmotic pressure generated by the hypertonic bathing solution and applied on articular cartilage in an opposite direction in comparison with that in the swelling process. In addition, there are two experimental factors, the equilibrating time after the bathing saline solution is changed and the time of changing solution. It was appeared that cartilage specimens from different patella required different during the free swelling. Complicated by these two experimental factors, we were not able to make a solid conclusion on such properties in this study. Further studies are required to obtain a better understanding of the relationship between these two phases.

One advantage of using ultrasound to investigate the swelling behavior of articular cartilage is that both the swelling and acoustic parameters can be obtained simultaneously. Fig. 4.35 shows a relatively good correlation between the peak swelling strains and IA slope (β) for both the normal and degenerated specimens. With the decrease of the peak swelling strain, the value of β decreased. That is to say, the sensitivity of IA to frequency reduced. However, no significant correlation was found between swelling strains and other acoustic parameters, or between the aggregate moduli predicted using the new triphasic model and the acoustic parameters. It was found that only the overall aggregate modulus obtained using the homogeneous model correlated with IRC for the degraded specimens. Recent studies used ultrasound and indention to obtain significantly linear correlation between the dynamic modulus and ultrasound reflection (Saarakkala et al., 2003) and between the aggregate modulus and the maximum magnitude of the echoes (Hattori et al., 2005a).

Similar to Saarakkala's result (Saarakkala et al., 2003), the IRC of the echoes from the cartilage surface significantly correlated with the water fraction of the normal cartilage tissue. Meanwhile, it was found that the IBS of the cartilage matrix was significantly negatively correlated with the FCD of the normal cartilage tissue. No such a significant correlation was obtained with the degenerated samples. Previous studies found that the uronic acid concentration correlated with both ultrasound reflection coefficient (Saarakkala et al., 2003) and integrated attenuation (Nieminen et al., 2004). However, this study did not obtain a significant correlation between acoustic parameters (IRC and IA) and FCD, which was measured using an indirect method based on the reference data.

In addition, Laasanen et al. also found that the PG content was not related with the reflection coefficient (Laasanen et al., 2003a). Therefore, further research is required to explain the controversial findings.

Although this study demonstrated that the modeling-predicted aggregate moduli decreased with the PG depletion, no correlation between the aggregate moduli and the PG content was obtained. However, a previous study reported that the PG content linearly correlated with both Young's modulus and dynamic modulus (Laasanen et al., 2003a). Since the depth-dependent distributions of c_0^F for the cartilage specimens were measured based on the literature data due to the limitation of our experimental facilities, the technique of histological assay in this study has to be improved, or techniques for directly measuring PG content should be used in the future studies.

5.6 Limitations of Ultrasound Swelling Measurement

5.6.1 Limitations of experimental set-up

In this study, it took approximately 30 seconds to change the saline solution in the container. Since there was no coupling medium between the ultrasound transducer and the cartilage specimen, no ultrasound signal was recorded during this period. It was observed that the cartilage deformed rapidly during the initial period after changing the concentration of saline (Wang and Zheng, 2006). Therefore, this period of solution change should play an important role in the measurement of the transient swelling or shrinkage strains. Although compensation for the time used for the change of the saline solution was carried out in this study (refer to section 3.8.5), it is still necessary to

improve the experiment setup for recording the entire swelling and shrinkage progresses in future studies.

With regard to the motor-controlled 3D USMS, one of its advantages is to obtain the UBM image of the internal section of the cartilage tissue when the transducer is scanning the specimen along the diameter direction. However, it took approximately 48 seconds to collect one frame of UBM image in this study. The interval between two sequent UBM images depends on several factors including the number of the sampling data, the velocity of the transducer movement and the duration of data acquisition. This relatively long interval would cause some dynamic information missed. In the future study, we may use a high-resolution UBM with higher scanning speed. Anyway, ultrasonic scanning in this study is feasible to investigate the two-dimensional anisotropic, heterogeneous map of the swelling strains of articular cartilage. Therefore, it may have potentials to obtain the 2D predicted distribution of the material properties from free swelling tests in further studies.

5.6.2 Limitations of the modeling

One main drawback of this study was that we had not directly measured the depth-dependent distributions of c_0^F for the cartilage specimens. The FCD of articular cartilage is known to be determined by the amount of PGs or GAGs. Previous studies used the DMMB dye-binding assay to determine the cartilage GAGs and FCD (Narmoneva et al., 1999; Wang et al., 2002). Due to the limitation of our experimental facilities, an indirect method using image processing was designed to obtain the values of FCD based on the literature DMMB-measured values. In this study, an average

normalized hue-saturation-value distribution curve as a function of depth was calculated based on the safranin O-fast green stained histological images. The relationship between the reference c_0^F (Narmoneva et al., 2001; Wang et al., 2002) and the hue values was expressed. Consequently, the calibrated c_0^F values were obtained. In addition, it should be noted that only the colour intensity but not true optical density might increase the uncertainty of the quantitative estimate of FCD. Although the PG depletion could be quantified using safranin O-fast green staining (Kiviranta et al., 1987; Leung et al., 1999; Rosenberg, 1971), the effect of contra-staining with fast green on the optical measurement of GAGs should be investigated in future study.

The water fractions (ϕ_0^W) at different depths were measured using a traditional method of weighting. The full-thickness cartilage layer was separated from the bone and serially sectioned into several thin slices. The accurate measurement of ϕ_0^W from the thin slices is demanding. Thus a special attention should be paid during the measurement. To investigate the effect of ϕ_0^W and c_0^F, the sensitivity of the model to the distributions of these two parameters was studied using the assumed extreme configurations in section 5.3.2. The results indicated that the model was generally insensitive to the assigned distributions, with only an effect on Ha_2.

Another drawback was that only the equilibrium state was in consideration. Most of the recent studies for cartilage swelling focused on the equilibrated state due to the computing simplification or the difficulty in detecting the dynamic process. The triphasic theory can be applied to the transient swelling process (Lai et al., 1991).

More efforts are needed to take advantage of the ability of the ultrasound technique to measure the transient displacements of the tissues at different depths.

5.6.3 Effect of ultrasound speed

Ultrasound techniques have been applied in the research of articular cartilage for decades. The ultrasonic signals provide the inside information of the tissue with high resolution. However, the change of ultrasound speed with environmental factors or specimen compositions and structures (Agemura et al., 1990; Cherin et al., 1998; Joiner et al., 2001) has been a controversial issue since ultrasound was used in the quantitative assessment. The reliability of ultrasound measurement was still questioned by some researchers because of the wide variation of ultrasound speed in articular cartilage (Jurvelin et al., 1995; Yao and Seedhom, 1999). The variations of ultrasound speed under various conditions, such as at different observation sites, under different temperatures, in the external solutions with different concentrations and in various degenerated cartilage tissues, were investigated (Patil et al., 2004; Zheng et al., 2006b).

In this study, the mean sound speeds in the tissue and in the saline solutions were used with a reference of our previous study (Zheng et al., 2006b). The sound speeds in the saline solutions were relatively stable (1530 ± 5 m/s in 0.15 M NaCl; 1646 ± 3 m/s in 2 M NaCl) since the temperature of the experimental environment was controlled. Moreover, in order to eliminate the effect of the temperature fluctuation, the software provided an automatic compensation method. The characteristic mean values of ultrasound speed in the full-thickness cartilage while immerged in 0.15 M and 2 M saline were 1675 ± 51 m/s and 1781 ± 48 m/s, respectively, which agreed with the

earlier mean values of 1622 to 1765 m/s for bovine or human cartilage (Agenura et al., 1990; Joiner et al., 2001; Kolmonen et al., 1995; Myers et al., 1995; Nieminen et al., 2002; Suh et al., 2001; Toyras et al., 1999; Youn et al., 1999). It has been found that the sound speed in the PG-depleted cartilage only decreased 0.4% to 1.5% (Nieminen et al., 2002; Toyras et al., 1999) though a greater decrease (4.6%) was found in the OA cartilage (Myers et al., 1995). The ultrasound speed in the cartilage tissue might be insensitive to degeneration of the tissue (Nieminen et al., 2002). In this study, the ultrasound-measured thickness was well validated using the digital caliper and histological method (slope ≈ 1, $R^2 > 0.9$). The results demonstrated that the change of ultrasound speed in the degraded tissue was minor and the literature values were acceptable. It might suggest that the depletion of PGs induced by trypsin digestion did not significantly change the structure of the matrix, which is framed by collagen fibres. This agreed with the previous studies (Gu et al., 1999; Lyyra et al., 1999; Nieminen et al., 2002).

However, the ultrasound speed in articular cartilage is not a constant. First, it was found that the change of the mean ultrasound speed in articular cartilage could be approximately represented by an exponential function of the measurement time during the swelling or shrinkage phase. Secondly, the variation of the speed at different depths depends on the inhomogeneity, heterogeneity, or anisotropy of articular cartilage. According to our previous study on the depth-dependence and anisotropy of the ultrasound speed in articular cartilage (Patil et al., 2004), there was an approximately 10% increase of the speed from the superficial layer to the deep layer. If the changes of the sound speed at different tissue depths caused by the change of saline concentration

have the same ratio, the depth-dependent ultrasound speed would not affect the calculation of the strains at different depths. However, considering the depth-dependent distribution of FCD, it is reasonable for us to assume that the absorption and release of salt ions during shrinkage (0.15 to 2 M) and swelling process (2 to 0.15 M) respectively would be depth-dependent as well. Since the change of ultrasound speed in articular cartilage under different saline solutions is mainly due to the change of the salt ion concentration in the cartilage tissue, it is reasonable to expect that the changing factor of the ultrasound speed would be depth-wise. The depth-dependent strain data obtained by the optical method using the three-parameter bi-layered model (Narmoneva et al., 2001) were matched with those obtained by our ultrasound method using the same model. Although the compensation for this depth-dependence at equilibrium was carried out in this study, future studies are required to quantitatively investigate this depth-wise changing of ultrasound speed in articular cartilage during the dynamic shrinkage and swelling processes.

CHAPTER 6 CONCLUSIONS AND FUTURE RESEARCH

6.1 Conclusions

The complex compositions, structures and functions of articular cartilage determine the material, mechanical and acoustic properties of articular cartilage. In this study, the osmosis-induced swelling behavior and progressive degeneration of the cartilage tissue were investigated using nominal 50 MHz focused ultrasound. According to the systematic and parametric comparisons of the electrochemomechanical, acoustic and histological properties of articular cartilage before and after trypsin digestion, the findings of this study are summarized as follows.

1. Potentials of USMS

It was demonstrated that the USMS developed in this study was reliable and the results were reproducible for the quantitative analysis of the free swelling behavior of articular cartilage under an osmotic loading. This ultrasonic technique can well secure the *in-situ* condition of the tissue and thus has potentials for the investigations on the dynamic and depth-dependent responses of the tissue to the electrochemical or mechanical stimulations.

2. Dimension-dependence of cartilage swelling

The results of our experiments suggested that the width of the specimen should not be too small in comparison with the focal zone diameter of the ultrasound beam when ultrasound is used to detect the swelling behavior of articular cartilage. To the best of our knowledge, there has been no research on the dimension-dependence of the

cartilage swelling. Thus, the results achieved in this study can provide a reference for the specimen preparation in further studies using ultrasound or other methods, such as OCT and laser.

3. Depth-dependence of cartilage swelling

In this study, the transient swelling behavior of the full-thickness cartilage at one observation site was recorded in M-mode image and the sectional deformation was mapped in ultrasonic elasticmicroscopic image using the manually controlled and motor-controlled 3D USMS, respectively, in a non-destructive way. The results demonstrated the nonuniformity of the swelling-induced alterations inside the cartilage tissue, which is related with the layered structure and heterogeneous distribution of the compositions.

4. Progressive degeneration of articular cartilage

The inclined trace of the additional echoes from the interface of the digested and undigested tissues was clearly observed in M-mode image. The nonlinear speed of trypsin penetration through the cartilage tissue as a function of time or depth was obtained using an interpolation algorithm.

5. Swelling behavior of normal and degenerated cartilage

The transient “overshoot-relaxation” swelling and creep hydration were observed during the shrinkage-swelling phase and hydration phase, respectively. The former was induced by changing the concentration of the bathing solution while the later was by dehydration. For the normal specimens, the absolute peak strains of shrinkage and

swelling were 0.010 ± 0.005 and 0.003 ± 0.003, respectively, and the hydration strain was 0.037±0.009. After the trypsin digestion for 10 to 30 minutes, the amplitudes of these behaviors of the degenerated specimens were decreased significantly in the peak shrinkage strain and the hydration strain but insignificantly in the peak swelling strain. In addition, no significant difference in the percentage change of the ultrasound speed during shrinkage and swelling phases was found. The results demonstrated that the PG depletion affected the amplitude of the swelling behaviors remarkably but had less effect on ultrasound speed in articular cartilage.

6. Correlation between ultrasonic evaluation and histological analysis

The good correlation (slope ≈1, R^2 > 0.5) between ultrasonic evaluation and histological analysis in digestion proportion and cartilage thickness demonstrated that the USMS can be a valid tool for the degeneration assessment and parametric measurement.

7. Parametric prediction using triphasic modeling

Using the newly-developed bi-layered triphasic model, the aggregate moduli of the normal cartilage from the region near the bone to the surface were 18.5 ± 15.5 MPa, 7.6 ± 11.6 MPa and 3.6 ± 3.3 MPa, respectively. The predicted normalized thickness of the deeper layer h_1 was 0.67 ± 0.22. With the increase of the digestion time from 10 minutes to 30 minutes, the mean *Ha* values of the three groups of the degenerated cartilage samples decreased gradually and insignificantly. For the 30-minute trypsin-digested specimens, the averaged values were *Ha1* = 11.1 ± 10.1 MPa, *Ha2* = 6.7 ± 16.9 MPa, *Ha3* = 1.9 ± 2.8 MPa, *h1* = 0.55±0.24, correspondingly. The results showed

that the degenerated tissue became softer with a decreased stiffness and the thickness of the deeper layer reduced. The results demonstrated that this model achieved a better prediction in comparison with the earlier models.

8. Acoustic analysis of normal and degenerated cartilage

The acoustic parameters of both the degenerated and the normal cartilage specimens including the surface, the matrix body, and the cartilage-bone interface were evaluated. It was found that the PG depletion resulted in insignificant changes in the acoustic parameters of the degenerated cartilage, including a decrease of approximately 1~3 dB in dB value, an increase of less than 2 MHz in centroid frequency, a decrease of approximately 1~4 dB in IRC, a decrease of less than 0.3 dB/mm/MHz in IA slope, a decrease of approximately 2 dB in AIB, etc. Further experiments are expected to make a solid conclusion on the relationship between the alterations of acoustic parameters and the digestion times.

9. Correlation between swelling, acoustic and biochemical parameters

This study observed that there were correlations between swelling, acoustic and biochemical parameters. The peak swelling strains positively correlated with the peak shrinkage strains and IA slope (β) for both the normal and degenerated specimens. The IRC of the cartilage surface and the IBS of the cartilage matrix significantly correlated with the water fraction and FCD of the normal cartilage tissue, respectively. Only the overall aggregate modulus correlated with IRC for the degraded specimens.

6.2 Directions of Future Research

Based on the findings of the present study, a number of further studies can be carried out to improve the USMS and to extend its applications as follows:

1. The PG-collagen matrix is framed by collagen fibres. It has been reported that the collagens at the surface layer play an important role in the balance of the swelling pressure. Therefore, the role of collagen fibrils in the swelling behavior of articular cartilage is worthy to be studied. Experimentally, the collagenase enzyme may be used to induce the damage of the fibrils. In comparison with the present results, it is believed that the roles of the different compositions in cartilage swelling will be better understood.

2. The site-dependence of swelling should be studied in the future by collecting depth-dependent strain profile at multiple locations (e.g. cartilage specimens prepared from femur and tibia) may be performed to study. The relationship between swelling and anatomical sites may help explain the role of swelling in the mechanical functions of articular cartilage at different sites.

3. Further efforts should be focused on the investigation on the swelling behavior of articular cartilage using the motor-controlled 3D USMS. One advantage is that a series of the sequent UBM images with high resolution can perfectly describe a two-dimensional anisotropic, heterogeneous map of the swelling strains of the internal tissue. The other advantage is that ultrasonic scanning can be performed along the directions parallel or perpendicular to the split-line to test the effect of orientation on the swelling behavior. However, the

limitation of the low image sampling rate as discussed earlier will lead to the loss of the rapidly changing information during the "overshoot-relaxation" swelling behavior. The USMS should be further improved in future studies by taking this problem in consideration.

4. Similar to most of the recent studies on cartilage swelling, this study focused on the equilibrated state in order to simplify the computing. The ultrasound technique introduced in this study can measure the transient displacements of the tissues at different depths. Therefore, the combination of the ultrasound with the triphasic theory may provide a potential way for the study of the dynamic swelling behavior of articular cartilage. However, the dynamic change of ultrasound speed in the tissue with time and depth should be taken into account. It is not an easy task.

5. Further experiments on human cartilage specimens should be performed *in situ* to demonstrate the potentials of the USMS in the clinical diagnosis of the earlier signs of cartilage degeneration. Ultimately, it is expected that the USMS combined with arthroscope will be used in the *in-vivo* assessment of the swelling behavior of articular cartilage.

6. This ultrasound approach can be applied for the dynamic evaluation of the electromechanochemical behavior of other biological or bioengineered tissues, biomaterials and nonbiomaterials, such as intervertebral disc, cartilage-like explant, and thermo-responsive polymers.

REFERENCES

Adam C, Eckstein F, Milz S, Putz R. 1998. The distribution of cartilage thickness in the knee-joints of old-aged individuals-measurement by A-mode ultrasound. Clin Biomech. 13, 1-10.

Adams SB Jr, Herz PR, Stamper DL, Roberts MJ, Bourquin S, Patel NA, Schneider K, Martin SD, Shortkroff S, Fujimoto JG, Brezinski ME. 2006. High-resolution imaging of progressive articular cartilage degeneration. J Orthop Res. 24(4), 708-715.

Adler RS, Dedrick DK, Laing TJ, Chiang EH, Meyer CR, Bland PH, Rubin JM. 1992. Quantitative assessment of cartilage surface roughness in osteoarthritis using high frequency ultrasound. Ultrasound Med Biol. 18(1), 51-58.

Agemura DH Jr, O'Brien WD, Olerud JE, Chun LE, Eyre DE. 1990. Ultrasonic propagation properties of articular cartilage at 100 MHz. J Acoust Soc Am. 87(4), 1786-1791.

Alexopoulos LG, Williams GM, Upton ML, Setton LA, Guilak F. 2005. Osteoarthritic changes in the biphasic mechanical properties of the chondrocyte pericellular matrix in articular cartilage. J Biomech. 38(3), 509-517.

Armstrong CG, Mow VC. 1982. Variations in the intrinsic mechanical properties of human cartilage with age, degeneration and water content. J Bone Joint Surg. 64A, 88-94.

Arokoski JP, Hyttinen MM, Lapvetelainen T, Takacs P, Kosztaczky B, Modis L, Kovanen V, Helminen H. 1996. Decreased birefringence of the superficial zone collagen network in the canine knee (stifle) articular cartilage after long distance running training, detected by quantitative polarised light microscopy. Ann Rheum Dis. 55(4), 253-264.

Athanasiou KA, Rosenwasser MP, Buckwalter JA, Malinin TI, Mow VC. 1991. Interspecies comparisons of *in situ* intrinsic mechanical properties of distal femoral cartilage. J Orthop Res. 9(3), 330-340.

Bank RA, Soudry M, Maroudas A, Mizrahi J, TeKoppele JM. 2000. The increased swelling and instantaneous deformation of osteoarthritic cartilage is highly correlated with collagen degradation. Arthritis Rheum. 43(10), 2202-2210.

Basser PJ, Schneiderman R, Bank RA, Wachtel E, Maroudas A. 1998. Mechanical properties of the collagen network in human articular cartilage as measured by osmotic stress technique. Arch Biochem Biophys. 351(2), 207-219.

Batiste DL, Kirkley A, Laverty S, Thain LM, Spouge AR, Holdsworth DW. 2004. *Ex vivo* characterization of articular cartilage and bone lesions in a rabbit ACL transection model of osteoarthritis using MRI and micro-CT. Osteoarthr Cartilage. 12(12), 986-996.

Berquist TH. 1997. Imaging of articular pathology: MRI, CT, arthrography. Clin Anat. 10, 1–13.

Beuf O. 2004. High-resolution MRI techniques for studies in small-animal models. In: Cartilage and osteoarthritis (Volume 2). Ceuninck FD, Sabatini M, Pastoureau P. eds. Humana Press Inc. Totowa, New Jersey. USA. pp. 219-229.

Brooks P. 2003. Inflammation as an important feature of osteoarthritis. In: Bulletin of the World Health Organization. 81(9), 689-690.

Buckland-Wright JC, Bradshaw CR. 1989. Clinical applications of high-definition microfocal radiography. Br J Radiol. 62(735), 209-217.

Buckland-Wright C. 2004. Subchondral bone changes in hand and knee osteoarthritis detected by radiography. Osteoarthr Cartilage. 12 Suppl A, S10-19.

Calvo E, Palacios I, Delgado E, Sanchez-Pernaute O, Largo R, Egido J, Herrero-Beaumont G. 2004. Histopathological correlation of cartilage swelling detected by magnetic resonance imaging in early experimental osteoarthritis. Osteoarthr Cartilage. 12, 878-886.

Chen AC, Bae WC, Schinagl RM, Sah RL. 2001. Depth- and strain-dependent mechanical and electromechanical properties of full-thickness bovine articular cartilage in confined compression. J Biomech. 34(1), 1-12.

Cherin E, Saied A, Laugier P, Netter P, Berger G. 1998. Evaluation of acoustical parameter sensitivity to age-related and osteoarthritic changes in articular cartilage using 50-MHz ultrasound. Ultrasound Med Biol. 24(3), 341-354.

Cherin E, Saied A, Pellaumail B, Loeuille D, Laugier P, Gillet P, Netter P, Berger G. 2001. Assessment of rat articular cartilage maturation using 50-MHz quantitative ultrasonography. Osteoarthr Cartilage. 9, 178-186.

Cohn NA, Emelianov SY, Lubinski MA, O'Donnell M. 1997a. An elasticity microscope. Part I: Methods. IEEE Trans Ultrason Ferroelectr Freq Control. 44(6), 1304-1319.

Cohn NA, Emelianov SY, O'Donnell M. 1997b. An elasticity microscope. Part II: Experimental results. IEEE Trans Ultrason Ferroelectr Freq Control. 44(6), 1320–1331.

D'Astous FT, Foster FS. 1986. Frequency dependence of ultrasound attenuation and backscatter in breast tissue. Ultrasound Med Biol. 12, 795-808.

Dhillon N, Bass EC, Lotz JC. 2001. Effect of frozen storage on the creep behavior of human intervertebral discs. Spine. 26, 883-888.

Ding M. 2005. Microarchitectural adaptations of osteoarthrotic subchondral bone. In: Proceedings of 2005 International Symposium on Quality of Bone and Scaffold

Biomaterials Evaluated by microCT, pQCT and MRI. Hong Kong, China. October 17-18, 2005. pp. 125-130.

DiSilvestro MR, Suh JK, 2002. Biphasic poroviscoelastic characteristics of proteoglycan-depleted articular cartilage: Simulation of degeneration. Ann Biomed Eng. 30(6), 792-800.

Disler DG, Raymond E, May DA, Wayne JS, McCauley TR. 2000. Articular cartilage defects: *in vitro* evaluation of accuracy and interobserver reliability for detection and grading with US. Radiology. 215, 846-851.

Eisenberg SR, Grodzinsky AJ. 1985. Swelling of articular cartilage and other connective tissues: Electromechanochemical forces. J Ortho Res. 3, 148-159.

Eisenberg SR, Grodzinsky AJ. 1987. The kinetics of chemically induced nonequilibrium swelling of articular cartilage and corneal stroma. J Biomech Eng. 109, 79-89.

Fenter TC, Naslund MJ, Shah MB, Eaddy MT, Black L. 2006. The cost of treating the 10 most prevalent diseases in men 50 years of age or older. Am J Manag Care. 12(4 Suppl), S90-98.

Fink MA, Cardoso JF. 1984. Diffraction effects in pulsed-echo measurement. IEEE Trans Sonics Ultrason. 31, 313-329.

Flahiff CM, Narmoneva DA, Huebner JL, Kraus VB, Guilak F, Setton LA. 2002. Osmotic loading to determine the intrinsic material properties of guinea pig knee cartilage. J Biomech. 35, 1285-1290.

Flahiff CM, Kraus VB, Huebner JL, Setton LA. 2004. Cartilage mechanics in the guinea pig model of osteoarthritis studied with an osmotic loading method. Osteoarthr Cartilage. 12, 383-388.

Flores RH, Hochberg MC. 2003. Definition and classification of osteoarthritis. In: Osteoarthritis. Brandt KD, Doherty M, Lohmander LS. eds. Oxford University Press, Oxford, New York. pp.1-8.

Fortin M, Soulhat J, Shirazi-Adl A, Hunziker EB, Buschmann MD. 2000. Unconfined compression of articular cartilage: nonlinear behavior and comparison with a fibril-reinforced biphasic model. J Biomech Eng. 122(2), 189-195.

Fortin M, Buschmann MD, Bertrand MJ, Foster FS, Ophir J. 2003. Dynamic measurement of internal solid displacement in articular cartilage using ultrasound backscatter. J Biomech. 36, 443-447.

Forster FK, Olerud JE, Riederer-Henderson MA, Holmes AW. 1990. Ultrasonic assessment of skin and surgical wounds utilizing backscatter acoustic techniques to estimate attenuation. Ultrasound Med Biol. 16(1), 43-53.

Foster FS, Pavlin CJ, Harasiewicz KA, Christopher DA, Turnbull DH. 2000. Advances in ultrasound biomicroscopy. Ultrasound Med Biol. 26(1), 1-27.

Fournier C, Bridal SL, Coron A, Laugier P. 2003. Optimization of attenuation estimation in reflection for *in vivo* human dermis characterization at 20 MHz. IEEE Trans Ultrason Ferroelect Freq Contr. 50, 408-418.

Fujimoto JG, Brezinski ME, Tearney GJ, Boppart SA, Bouma B, Hee MR, Southern JF, Swanson EA. 1995. Optical biopsy and imaging using optical coherence tomography. Nat Med. 1(9), 970-972.

Fung YC. 1993. Bone and Cartilage. In: Biomechanics Mechanical Properties of Living Tissues. 2nd edition. Springer-Verlag New York Inc. pp. 500-544.

Gluer CC, Blake G, Lu Y, Blunt BA, Jergas M, Genant HK. 1995. Accurate assessment of precision errors: How to measure the reproducibility of bone densitometry techniques. Osteoporosis Int. 5, 262-270.

Grodzinsky AJ, Roth V, Myers E, Grossman WD, Mow VC. 1981. The significance of electromechanical and osmotic forces in the nonequilibrium swelling behavior of articular cartilage in tension. J Biomech Eng. 103, 221-231.

Gu W, Lewis B, Lai WM, Ratcliffe A, Mow VC. 1996. A technique for measuring volume and true density of the solid matrix of cartilaginous tissues. ASME Advances in Bioengineering BED-33, 88-90.

Gu WY, Lai WM, Mow VC. 1998. A mixture theory for charged-hydrated soft tissues containing multi-electrolytes: passive transport and swelling behaviours. J Biomed Eng. 120, 169-180.

Gu JD, Mao WY, Lai WM, Mow VC. True density of normal and enzymatically treated bovine articular cartilage. In: Proceedings of 45th Annual Meeting of Orthopaedic Research Society. Anaheim, CA. February 1–4, 1999. pp. 642.

Guilak F, Ratcliffe A, Lane N, Rosenwasser MP, Mow VC. 1994. Mechanical and biochemical changes in the superficial zone of articular cartilage in canine experimental osteoarthritis. J Orthop Res. 12, 474-484.

Guilak F, Ratcliffe A, Mow VC. 1995. Chondrocyte deformation and local tissue strain in articular cartilage: A confocal microscopy study. J Orthop Res. 13, 410-421.

Guilak F, Mow VC. 2000. The mechanical environment of the chondrocyte: a biphasic finite element model of cell-matrix interactions in articular cartilage. J Biomech. 33(12), 1663-1673.

Guo X, Lam WL, and Zheng YP, Rapid and quantified decalcification of bone: apparatus and methods. No. 10/510,450. Oct 2005 (PolyU IP174A). US Patent pending.

Harris ED Jr, Parker HG, Radin EL, Krane SM. 1972. Effects of proteolytic enzymes on structural and mechanical properties of cartilage. Arthritis Rheum. 15, 497-503.

Hattori K, Takakura Y, Ishimura M, Habata T, Uematsu K, Ikeuch K. 2004. Quantitative arthroscopic ultrasound evaluation of living human cartilage. Clin Biomech (Bristol, Avon). 19(2), 213-216.

Hattori K, Ikeuchi K, Morita Y, Takakura Y. 2005a. Quantitative ultrasonic assessment for detecting microscopic cartilage damage in osteoarthritis. Arthritis Res Ther. 7(1), R38-46.

Hattori K, Takakura Y, Ishimura M, Tanaka Y, Habata T, Ikeuchi K. 2005b. Differential acoustic properties of early cartilage lesions in living human knee and ankle joints. Arthritis Rheum. 52(10), 3125-3131.

Hayes WC, Keer LM, Herrmann G, Mockros LF. 1972. A mathematical analysis for indentation tests of articular cartilage. J Biomech. 5, 541-551.

Hayes WC, Bodine AJ. 1978. Flow-independent viscoelastic properties of articular cartilage matrix. J Biomech. 11, 407-419.

Huisman HJ, Thijssen JM. 1996. Precision and accuracy of acoustospectrographic parameters. Ultrasound Med Biol. 22, 855-871.

Hunziker EB, Michel M, Studer D. 1997. Ultrastructure of adult human cartilage matrix after cryotechnical processing. Microsc Res Technol. 37, 271-284.

Huyghe JM, Janssen JD. 1997. Quadriphasic mechanics of swelling incompressible porous media. Int J Eng Sci. 35 (8), 793-802.

Jaffre B, Watrin A, Loeuille D, Gillet P, Netter P, Laugier P, Saied A. 2003. Effects of antiinflammatory drugs on arthritic cartilage: a high-frequency quantitative ultrasound study in rats. Arthritis Rheum. 48(6), 1594-1601.

Jaremko JL, Cheng RW, Lambert RG, Habib AF, Ronsky JL. 2006. Reliability of an efficient MRI-based method for estimation of knee cartilage volume using surface registration. Osteoarthr Cartilage. 14(9), 914-922.

Joiner GA, Bogoch ER, Pritzker KP, Buschmann MD, Chevrier A, Foster FS. 2001. High frequency acoustic parameters of human and bovine articular cartilage following experimentally-induced matrix degradation. Ultrason Imaging. 23, 106-116.

Jurvelin JS, Rasanen T, Kolmonen P, Lyyra T. 1995. Comparison of optical, needle probe and ultrasonic techniques for the measurement of articular cartilage thickness, J Biomech. 28(2), 231-235.

Jurvelin JS, Buschmann MD, Hunziker EB. 1997. Optical and mechanical determination of Poisson's ratio of adult bovine humeral articular cartilage. J Biomech. 30(3), 235-241.

Kuc R, Schwartz M. 1979. Estimating the acoustic attenuation coefficient slope for liver from reflected ultrasound signals. IEEE Trans Sonics Ultrason. 26, 353-362.

Kiefer GN, Sundby K, McAllister D, Shrive NG, Frank CB, Lam T, Schachar NS. 1989. The effect of cryopreservation on the biomechanical behavior of bovine articular cartilage. J Orthop Res. 7, 494-501.

Kiernan JA. 2001. Histological and histochemical methods: theory and practice, 3rd edition. London, Arnold. pp. 11-164.

Kim HKW, Babyn PS, Harasiewicz KA, Gahunia HK, Pritzker KPH, Foster FS. 1995. Imaging of immature articular cartilage using ultrasound backscatter microscopy at 50MHz. J Orthop Res. 13, 963-970.

Kiraly K, Hyttinen MM, Lapvetelainen T, Elo M, Kiviranta I, Dobai J, Modis L, Helminen HJ, Arokoski JP. 1997. Specimen preparation and quantification of collagen birefringence in unstained sections of articular cartilage using image analysis and polarizing light microscopy. Histochem J. 29(4), 317-327.

Kiviranta I, Jurvelin J, Tammi M, Saamanen AM, Helminen HJ. 1987. Weight bearing controls glycosaminoglycan concentration and articular cartilage thickness in the knee joints of young beagle dogs. Arthritis Rheum. 30(7), 801-809.

Koff MF, Amrami KK, Kaufman KR. T2 values of patellar cartilage in patients with osteoarthritis. In: Proceedings of ISB XXth Congress - ASB 29th Annual Meeting. Cleveland, Ohio, USA. July 31 - August 5, 2005. pp. 486.

Kolmonen P. Lyyra T, Jurvelin JS. 1995. Experimental comparison of acoustic and mechanical properties of bovine knee articular cartilage. Trans. Orthop. Res. Soc. 20, 513.

Kremkau FW. 1998. Diagnostic ultrasound principles and instruments. W.B. Saunders Company, USA.

Kuroki H, Nakagawa Y, Mori K, Ohba M, Suzuki T, Mizuno Y, Ando K, Takenaka M, Ikeuchi K, Nakamura T. 2004. Acoustic stiffness and change in plug cartilage over time after autologous osteochondral grafting: correlation between ultrasound signal intensity and histological score in a rabbit model. Arthritis Res Ther. 6(6), R492-504.

Kwan MK, Hacker SA, Woo SLY, Wayne JS. 1992. The effect of storage on the biomechanical behavior of articular cartilage - A large strain study. J Biomech Eng. 114(1), 149-153.

Laasanen MS, Toyras J, Hirvonen J, Saarakkala S, Korhonen RK, Nieminen MT, Kiviranta I, Jurvilin JS. 2002. Novel mechano-acoustic technique and instrument for diagnosis of cartilage degeneration. Physiol Meas. 23, 491-503.

Laasanen MS, Saarakkala S, Toyras J, Hirvonen J, Rieppo J, Korhonen RK, Jurvelin JS. 2003a. Ultrasound indentation of bovine knee articular cartilage *in situ*. J Biomech. 36, 1259-1267.

Laasanen MS, Toyras J, Korhonen RK, Rieppo J, Saarakkala S, Nieminen, MT, Hirvonen J, Jurvelin JS. 2003b. Biomechanical properties of knee articular cartilage. Biorheology. 40, 133-140.

Laasanen MS, Saarakkala S, Toyras J, Rieppo J, Jurvelin JS. 2005. Site-specific ultrasound reflection properties and superficial collagen content of bovine knee articular cartilage. Phys Med Biol. 50(14), 3221-3233.

Laasanen MS, Toyras J, Vasara A, Saarakkala S, Hyttinen MM, Kiviranta I, Jurvelin JS. 2006. Quantitative ultrasound imaging of spontaneous repair of porcine cartilage. Osteoarthr Cartilage. 14(3), 258-263.

Lai WM, Hou JS, Mow VC. 1991, A triphasic theory for the swelling and deformation behaviors of articular cartilage. J Biomech Eng. 113, 245-258.

Langton CM, Palmer SB, Porter RW. 1984. The measurement of broadband ultrasonic attenuation in cancellous bone. Eng Med. 13(2), 89-91.

Laurent D, Wasvary J, Rudin M, O'Byrne E, Pellas TC. 2003. *In vivo* assessment of macromolecular content in articular cartilage of the goat knee. Magn Reson Med. 49, 1037–1046.

Laurent D, O'byrne E, Wasvary J, Pellas TC. 2006. *In vivo* MRI of cartilage pathogenesis in surgical models of osteoarthritis. Skeletal Radiol. 35(8), 555-564.

Lee D, Bouffard JA. 2001. Ultrasound of the knee. Eur J Ultrasound. 14(1), 57-71.

Lefebvre F, Graillat N, Cherin E, Berger G, Saied A. 1998. Automatic three-dimensional reconstruction and characterization of articular cartilage from high-resolution ultrasound acquisitions. Ultrasound Med Biol. 24(9), 1369-1381.

LeRoux MA, Arokoski J, Vail TP, Guilak F, Hyttinen MM, Kiviranta I, Setton LA. 2000. Simultaneous changes in the mechanical properties, quantitative collagen organization, and proteoglycan concentration of articular cartilage following canine meniscectomy. J Orthop Res. 8, 383–392.

Leung KS, Qin L, Leung MCT, Fu LLK, Chan CW. 1999. Decrease in proteoglycans content of the remaining patellar articular cartilage after partial patellectomy in rabbits. J Clin Exp Rheumatol. 17, 597–600.

Lizzi FL, Greenebaum M, Feleppa EJ, Elbaum M, Coleman DJ. 1983. Theoretical framework for spectrum analysis in ultrasonic tissue characterization. J Acoust Soc Am. 73, 1366-1373.

Lu MH, Zheng YP, Huang QH. 2005. A novel noncontact ultrasound indentation system for measurement of tissue material properties using water jet compression. Ultrasound Med Biol. 31(6), 817-826.

Lyyra T, Kiviranta I, Vaatainen U, Helminen HJ, Jurvelin JS. 1999. *In vivo* characterization of indentation stiffness of articular cartilage in the normal kuman knee. J Biomed Mater Res. 48, 482-487.

Mak AF. 1986. The apparent viscoelastic behavior of articular cartilage - the contributions from the intrinsic matrix viscoelasticity and interstitial fluid flows. J Biomech Eng. 108, 123-130.

Mak AF, Lai WM, Mow VC. 1987. Biphasic indentation of articular cartilage—I. theoretical analysis. J Biomech. 20(7), 703-714.

Mankin HJ, Mow VC, Buckwalter JA, Iannotti JP, Ratcliffe A. 2000. Articular cartilage structure, composition, and function. In: Orthopaedic basic science. 2nd edition. Buckwalter JA, Einhoun TA, Simnon SR. eds. American Academy of Orthopaedic Surgeons. pp. 444-470.

Mann RW. 2001. Comment on 'Ultrasonic measurement of the thickness of human articular cartilage *in situ*' by Yao and Seekhom. Rheumatology. 40, 829-831.

Maroudas A. 1976a. Balance between swelling pressure and collagen tension in normal and degenerate cartilage. Nature. 260, 808-809.

Maroudas A. 1976b. Transport of solutes through cartilage – permeability to large molecules. J Anat. 122, 335-347.

Maroudas A. 1979. Physicochemical properties of articular cartilage. In: Adult articular cartilage. Freeman MAR. ed. Petman Medical. Kent, UK. pp. 215-290.

Maroudas A, Mizrahi J, Katz EP, Wachtel EJ, Soudry M. 1986. Physicochemical properties and functional behavior of normal and osteoarthritic human cartilage. In: Articular cartilage biochemistry. Kuettner KE, Schleyerbach R, Hascall VC. eds. Raven Press, New York. pp. 311-329.

Martini FH. Fundamentals of anatomy and physiology (6th Edition), Upper Saddle River, NJ: Prentice Hall, 2004.

Meire HA, Farrant P. 1995. Basic Ultrasound, John Wiley & Sons, Ltd., Chichester, England. pp. 8-17.

Mente PL, Lewis JL. 1994. Elastic modulus of calcified cartilage is an order of magnitude less than that of subchondral bone. J Orthop Res. 12(5), 637-647.

Modest VE, Murphy MC, Mann RW. 1989. Optical verification of a technique for *in situ* ultrasonic measurement of articular cartilage thickness. J Biomech. 22, 171-176.

Mow VC, Kuer SC, Lai WM, Armstrong CG. 1980, Biphasic creep and stress relaxation of articular cartilage in compression: Theory and experiments. J Biomech Eng. 102, 73-84.

Mow VC, Schoonbeck JM. 1984. Contribution of Donnan osmotic pressure towards the biphasic compressive modulus of articular cartilage. Trans Orthop Res Soc. 9, 262.

Mow VC, Ateshian GA, Lai WM, Gu WY. 1998. Effects of fixed charges on the stress-relaxation behavior of hydrated soft tissues in a confined compression problem. Int J Solids Struct. 35, 4945-4962.

Mow VC, Wang CC, Hung CT. 1999. The extracellular matrix, interstitial fluid and ions as a mechanical signal transducer in articular cartilage. Osteoarthr Cartilage. 7(1), 41-58.

Mow VC, Hung CT. 2001. Biomechanics of articular cartilage. In: Basic biomechanics of the musculoskeletal system. 3rd edition. Nordin M, Frankel VH. eds. Lea & Feviger Philadelphia, London. pp. 60-101.

Mow VC, Guo XE. 2002. Mechano-electrochemical properties of articular cartilage: their inhomogeneities and anisotropies. Annu Rev Biomed Eng. 4, 175-209.

Mow VC, Gu WY, Chen FH. 2005. Structure and function of articular cartilage and meniscus. In: Basic orthopaedic biomechanics and mechano-biology. 3rd edition. Mow VC, Huiskes R, eds. Lippincott Williams & Wilkins: Philadelphia, PA, USA. pp. 181-258.

Murphy JM, Boynton RE, Kraus KH, Cole JC, Hunziker EB, Pellas T, O'Byrne E, Barry FP. 1999. An experimental model of osteoarthritis in goats. Trans Orthop Res Soc. 24, 435.

Murray CJL, Lopez AD. 1996. The global burden of disease: a comprehensive assessment of mortality and disability from disease, injury and risk factors in 1990 and projected to 2020. Harvard University Press. Cambridge, MA.

Myers ER, Lai WM, Mow VC. 1984. A continuum theory and an experiment for the ion -induced swelling behavior of articular cartilage. J Biomech Eng. 106, 151-158.

Myers SL, Dines K, Brandt DA, Brandt KD, Albrecht ME. 1995. Experimental assessment by high frequency ultrasound of aticular cartilage thickness and osteoarthritic changes. J Rheumatol. 22, 109-116.

Narmoneva DA, Wang JY, Setton LA. 1999. Nonuniform swelling-induced residual strains in articular cartilage. J Biomech. 32, 401-408.

Narmoneva DA, Wang JY, Setton LA. 2001. A noncontacting method for material property determination for articular cartilage from osmotic loading. Biophys J. 81, 3066-3076.

Narmoneva DA, Cheung HS, Wang JY, Howell DS, Setton LA. 2002. Altered swelling behavior of femoral cartilage following joint immobilization in a canine model. J Orthop Res. 20, 83-91.

Nieminen MT, Toyras J, Rieppo J, Hakumaki JM, Silvennoinen J, Helminen HJ, Jurvelin JS. 2000. Quantitative MR microscopy of enzymatically degraded articular cartilage. Magn Reson Med. 43(5), 676-681.

Nieminen HJ, Toyras J, Rieppo J, Nieminen MT, Hirvonen J, Korhonen R, Jurvelin JS. 2002. Real-time ultrasound analysis of articular cartilage degradation *in vitro*. Ultrasound Med Biol. 28(4), 519-525.

Nieminen HJ, Saarakkala S, Laasanen MS, Hirvonen J, Jurvelin JS, Toyras J. 2004. Ultrasound attenuation in normal and spontaneously degenerated articular cartilage. Ultrasound Med Biol. 30(4), 493-500.

Nissi MJ, Toyras J, Laasanen MS, Rieppo J, Saarakkala S, Lappalainen R, Jurvelin JS, Nieminen MT. 2004. Proteoglycan and collagen sensitive MRI evaluation of normal and degenerated articular cartilage. J Orthop Res. 22(3), 557-564.

Ophir J, Cespedes I, Ponnekanti H, Yazdi Y, Li X. 1991. Elastography: a quantitative method for imaging the elasticity of biological tissues. Ultrason Imaging. 13, 111-134.

Ophir J, Alam SK, Garra B, Kallel F, Konofagou E, Krouskop T, Varghese T. 1999. Elastography: ultrasonic estimation and imaging of the elastic properties of tissues. Proc Inst Mech Eng. 213, 203-233.

Parsons JR, Black J. 1977. The viscoelastic shear behavior of normal rabbit articular cartilage. J Biomech. 10, 21-29.

Patel NA, Li X, Stamper DL, Fujimoto JG, Brezinski ME. 2005. Using optical coherence tomography to guide articular cartilage ablation. Am J Orthop. 34(3), 111-115.

Patil SG, Zheng YP, Wu JY, Shi J. 2004. Measurement of depth-dependency and anisotropy of ultrasound speed of bovine articular cartilage *in vitro*. Ultrasound Med Biol. 30(7), 953-963.

Pellaumail B, Watrin A, Loeuille D, Netter P, Berger G, Laugier P, Saied A. 2002. Effect of articular cartilage proteoglycan depletion on high frequency ultrasound backscatter. Osteoarthr Cartilage. 10(7), 535-541.

Pflaster DS, Krag MH, Johnson CC, Haugh LD, Pope MH. 1997. Effect of test environment on intervertebral disc hydration. Spine. 22(2), 133-139.

Puliafito CA, Hee MR, Lin CP, Reichel E, Schuman JS, Duker JS, Izatt JA, Swanson EA, Fujimoto JG. 1995. Imaging of macular diseases with optical coherence tomography. Ophthalmology. 102, 217–229.

Qin L, Zheng YP, Leung CT, Mak AFT, Choy WY, Chan KM. 2002. Ultrasound detection of trypsin-treated articular cartilage: its association with cartilaginous proteoglycans assessed by histological and biochemical methods. J Bone Miner Metab. 20(5), 281-287.

Roberjot V, Bridal SL, Laugier P, Berger G. 1996. Absolute backscatter coefficient over a wide range of frequencies in a tissue-mimicking phantom containing two populations of scatterers. IEEE Trans Ultrason Ferroelect Freq Contr. 43, 970-978.

Rosenberg L. 1971. Chemical basis for the histological use of safranin O in the study of articular cartilage. J Bone Joint Surg Am. 53(1), 69-82.

Roth V, Mow VC. 1980. The intrinsic tensile behavior of the matrix of bovine articular cartilage and its variation with age. J Bone Joint Surg. 62, 1102-1117.

Saarakkala S, Laasanen MS, Jurvelin JS, Torronen K, Lammi MJ, Lappalainen R, Toyras J. 2003. Ultrasound indentation of normal and spontaneously degenerated bovine articular cartilage. Osteoarthr Cartilage. 11, 697-705.

Saarakkala S, Toyras J, Hirvonen J, Laasanen MS, Lappalainen R, Jurvelin JS. 2004. Ultrasonic quantitation of superficial degradation of articular cartilage. Ultrasound Med Biol. 30(6), 783-792.

Saarakkala S, Laasanen MS, Jurvelin JS, Toyras J. 2006. Quantitative ultrasound imaging detects degenerative changes in articular cartilage surface and subchondral bone. Phys Med Biol. 51(20), 5333-5346.

Saied A, Cherin E, Gaucher H, Laugier P, Gillet P, Floquet J, Netter P, Berger G. 1997. Assessment of articular cartilage and subchondral bone: Subtle an progressive changes in experimental osteoarthritis using 50 MHz echography *in vitro*. J Bone Miner Res. 12(9), 1378-1386.

Saied A, Laugier P. 2004. High-resolution ultrasonography for analysis of age- and disease-related cartilage changes. Methods Mol Med.101, 249-265.

Saladin KS. 2005. Human anatomy. McGraw-Hill, New York. USA.

Sandy JD. 2003. Proteolytic degradation of normal and osteoarthritic cartilage matrix. In: Osteoarthritis. Brandt KD, Doherty M, Lohmander LS. eds. Oxford University Press, Oxford, New York. pp. 82-92.

Schinagl RM, Ting MK, Price JH, Sah RL. 1996. Video microscopy to quantitate the inhomogeneous equilibrium strain within articular cartilage during confined compression. Ann Biomed Eng. 24, 500-512.

Schinagl RM, Gurskis D, Chen AC, Sah RL. 1997. Depth-dependent confined compression modulus of fullthickness bovine articular cartilage. J Orthop Res. 15, 499-506.

Senzig DA, Forster FK, Olerud JE. 1992. Ultrasonic attenuation in articular cartilage. J Acoust Soc Am. 92, 676-681.

Setton LA, Mow VC, Muller FJ, Pita JC, Howell DS. 1994. Mechanical properties of canine articular cartilage are significantly altered following transection of the anterior cruciate ligament. J Orthop Res. 12(4), 451-463.

Setton LA, Gu W, Lai MW, Mow VC. 1996. Predictions of swelling-induced pre-stress in articular cartilage. In: Mechanics of Poroelastic Media. Selvadurai APS. ed. Dordrecht: Kluwer Academic Publishers, pp. 299-320.

Setton LA, Tohyama H, Mow VC. 1998. Swelling and curling behaviors of articular cartilage. J Biomech Eng. 120, 355-361.

Shapiro EM, Borthakur A, Kaufman JH, Leigh JS, Reddy R. 2001. Water distribution patterns inside bovine articular cartilage as visualized by ^{1}H magnetic resonance imaging. Osteoarthr Cartilage. 9, 533-538.

Shoukri MM, Edge VL. 1996. Statistical analysis of measurements reliability. In: Statistical methods for health sciences. Shoukri MM, Edge VL. eds. CRC Press, Boca Raton, Florida. pp. 18-40.

Skaggs DL, Warden WH, Mow VC. 1994. Radial tie fibers influence the tensile properties of the bovine medial meniscus. J Orthop Res. 12(2), 176-185.

Smale G, Bendele A, Horton WE Jr. 1995. Comparison of age-associated degeneration of articular cartilage in Wistar and Fischer 344 rats. Lab Animal Sci. 45(2), 191-194.

Song Y, Greve JM, Carter DR, Koo S, Giori NJ. 2006. Articular cartilage MR imaging and thickness mapping of a loaded knee joint before and after meniscectomy. Osteoarthr Cartilage. 14(8), 728-737.

Suh JKF, Youn I, Fu FH. 2001. An *in situ* calibration of an ultrasound transducer: a potential application for an ultrasonic indentation test of articular cartilage. J Biomech. 34, 1347-1353.

Sun DN, Gu WY, Guo XE, Lai WM, Mow VC. 1999. A mixed finite element formulation of triphasic mechano-electrochemical theory for charged, hydrated biological soft tissues. Int J Numer Meth Eng. 45, 1375-1402.

Tearney GJ, Brezinski ME. 1997. *In vivo* endoscopic optical biopsy with optical coherence tomography. Science. 276, 2037–2039.

Tepic S, Macirowski T, Mann RW. 1983. Mechanical properties of articular cartilage elucidated by osmotic loading and ultrasound. In: Biophysics, Proceedings of the National Academy Sciences, June, USA. 80, 3331-3333.

Torzilli PA, Askari E, Jenkins JT. 1990. Water content and solute diffusion properties in articular cartilage. In: Biomechanics of diarthrodial joints (Volume 1). Mow VC, Ratcliffe A, Woo SLY. eds. Springer-Verlag New York Inc. pp. 363-390.

Toyras J, Rieppo J, Nieminen MT, Helminen HJ, Jurvelin JS. 1999. Characterization of enzymatically induced degradation of articular cartilage using high frequency ultrasound. Phys Med Biol. 44, 2723-2733.

Toyras J, Nieminen HJ, Laasanen MS, Nieminen MT, Korhonen RK, Rieppo J, Hirvonen J, Helminen HJ, Jurvelin JS. 2002. Ultrasonic characterization of articular cartilage. Biorheology. 39(1-2), 161-169.

Toyras J, Laasanen MS, Saarakkala S, Lammi MJ, Rieppo J, Kurkijarvi J, Lappalainen R, Jurvelin JS. 2003. Speed of sound in normal and degenerated bovine articular cartilage. Ultrasound Med Biol. 29(3), 447-454.

Treppo S, Koepp H, Quan EC, Cole AA, Kuettner KE, Grodzinsky AJ. 2000. Comparison of biomechanical and biochemical properties of cartilage from human knee and ankle pairs. J Orthop Res. 18(5), 739-748.

Truscott JG, Strelitzki R. 1998. Challenges in the ultrasonic measurement of bone. In: Ultrasound in medicine. Duck FA, Baker AC, Starritt HC. eds. Institute of Physics Publishing, London. pp. 287-306.

Verteramo A, Seedhom BB. 2004. Zonal and directional variations in tensile properties of bovine articular cartilage with special reference to strain rate variation. Biorheology. 41(3-4), 203-213.

Wachsmuth L, Engelke K. 2004. High-resolution imaging of osteoarthritis using microcomputed tomography. In: Cartilage and osteoarthritis (Volume 2). Ceuninck FD, Sabatini M, Pastoureau P. eds. Humana Press Inc. Totowa, New Jersey. USA. pp. 231-248.

Wang CC, Hung CT, Mow VC. 2001. An analysis of the effects of depth-dependent aggregate modulus on articular cartilage stress-relaxation behavior in compression. J Biomech. 34(1), 75-84.

Wang CC, Guo XE, Sun DN, Mow VC, Ateshian GA, Hung CT. 2002. The functional environment of chondrocytes within cartilage subjected to compressive loading: A theoretical and experimental approach. Biorheology. 39(1-2), 11-25.

Wang CC, Chahine NO, Hung CT, Ateshian GA. 2003. Optical determination of anisotropic material properties of bovine articular cartilage in compression. J Biomech. 36(3), 339-353.

Wang Q, Zheng YP. Study on transient osmotic-induced hydration of articular cartilage by high-frequency ultrasound. In: Proceedings of Biomedical Engineering Conference on Integrating Science and Technology in the Healthcare Industry. Hong Kong, China. September 23-25, 2004. pp.135-140.

Wang Q, Zheng YP. Evaluation of osmosis-induced deformation of articular cartilage using ultrasound biomicroscopy imaging. In: Proceedings of ISB XXth Congress - ASB 29th Annual Meeting. Cleveland, Ohio, USA. July 31 - August 5, 2005. pp. 440.

Wang Q, Zheng YP. 2006. Non-contact evaluation of osmosis-induced shrinkage and swelling behavior of articular cartilage *in situ* using high-frequency ultrasound. Instrument Sci Technol. 34(3), 317 – 334.

Wang Q, Zheng YP, Niu HJ, Mak AFT. 2007. Extraction of mechanical properties of articular cartilage from osmotic swelling behavior monitored using high-frequency ultrasound. J Biomech Eng. 129(3), 413-422.

Wells PNT. 1993. Advances in ultrasound techniques and instrumentation, Churchill Livingstone Inc. pp. 109-123.

Wheaton AJ, Borthakur A, Shapiro EM, Regatte RR, Akella SV, Kneeland JB, Reddy R. 2004. Proteoglycan loss in human knee cartilage: quantitation with sodium MR imaging--feasibility study. Radiology. 231(3), 900-905.

Wilson W, van Donkelaar CC, van Rietbergen B, Ito K, Huiskes R. 2004. Stresses in the local collagen network of articular cartilage: a poroviscoelastic fibril-reinforced finite element study. J Biomech. 37(3), 357-66. Erratum in: J Biomech. 2005 Oct;38(10), 2138-2140.

Wong M, Ponticiello M, Kovanen V, Jurvelin JS. 2000. Volumetric changes of articular cartilage during stress relaxation in unconfined compression. J Biomech. 33(9), 1049-1054.

Woo SLY, Akeson WH, Jemmott GF. 1976. Measurements of nonhomogeneous, directionalmechanical properties of articular cartilage in tension. J Biomech. 9, 785.

Yao JQ, Seedhom BB. 1999. Ultrasonic measurement of the thickness of human articular cartilage *in situ*. Rheumatology. 38, 1269-1271.

Youn JI, Akkin T, Milner TE. 2004. Electrokinetic measurement of cartilage using differential phase optical coherence tomography. Physiol Meas. 25(1), 85-95.

Youn I, Fu FH, Suh JK. 1999. Determination of the mechanical properties of articular cartilage using a high-frequency ultrasonic indentation technique. Trans Orthop Res Soc. 24, 162.

Zheng YP, Ding CX, Bai J, Mak AFT, Qin L. 2001. Measurement of the layered compressive properties of trypsin-treated articular cartilage: an ultrasound investigation. Med Biol Eng Comput. 39, 534-541.

Zheng YP, Mak AFT, Lau KP, Qin L. 2002. An ultrasonic measurement for *in vitro* depth-dependent equilibrium strains of articular cartilage in compression. Phys Med Biol. 7, 3165-3180.

Zheng YP, Shi J, Qin L, Patil SG, Mow VC, Zhou KY. 2004a. Dynamic depth-dependent osmotic swelling and solute diffusion in articular cartilage monitored using real-time ultrasound. Ultrasound Med Biol. 30, 841-849.

Zheng YP, Bridal SL, Shi J, Saied A, Lu MH, Jaffre B, Mak AFT, Laugier P. 2004b. High resolution ultrasound elastomicroscopy imaging of soft tissues: System development and feasibility. Phys Med Biol. 49, 3925-3938.

Zheng YP, Niu HJ, Mak AFT, Huang YP. 2005. Ultrasonic measurement of depth-dependent transient behaviors of articular cartilage under compression. J Biomech. 38, 1830-1837.

Zheng YP, Lu MH, Wang Q. 2006a. Ultrasound elastomicroscopy using water jet and osmosis loading: Potentials for assessment for articular cartilage. Ultrasonics. 44(Supplement 1), e203-209.

Zheng YP, Patil S, Wang Q. 2006b. Ultrasound speed in articular cartilage under different bathing saline concentration. Key Eng Mater. 321-323, 972-977.

Zhu W, Mow VC, Koob TJ, Eyre DR. 1993. Viscoelastic shear properties of articular cartilage and the effects of glycosidase treatments. J Orthop Res. 11(6), 771-781.